Biochemical and Molecular Analysis of Chlorophyll Degradation in Higher Plants

Dissertation zur
Erlangung der naturwissenschaftlichen Doktorwürde
(Dr. sc. nat.)
Vorgelegt der
Mathematisch-naturwissenschaftlichen Fakultät
Der Universität Zürich

von
Sylvain AUBRY
aus Frankreich

Promotionskomitee
PD Dr. Stefan Hörtensteiner
Prof. Dr. Enrico Martinoia
Prof. Dr. Beat Keller
Prof. Dr. Howard Thomas

Zürich, 2008

Biochemical and Molecular Analysis of Chlorophyll Degradation in Higher Plants

Dissertation zur
Erlangung der naturwissenschaftlichen Doktorwürde
(Dr. sc. nat.)
Vorgelegt der
Mathematisch-naturwissenschaftlichen Fakultät
Der Universität Zürich

von
Sylvain AUBRY
aus Frankreich

Promotionskomitee
PD Dr. Stefan Hörtensteiner
Prof. Dr. Enrico Martinoia
Prof. Dr. Beat Keller
Prof. Dr. Howard Thomas

Zürich, 2008

Die vorliegende Arbeit wurde von der Mathematisch-naturwissenschaftlichen Fakultät der Universität Zürich im Frühjahrsemester 2008 auf Antrag als Dissertation angenommen.
Promotionskomitee: PD Dr. Stefan Hörtensteiner (Leitung der Dissertation), Prof. Dr. Beat Keller, Prof. Dr. Enrico Martinoia, Prof. Dr. Howard Thomas

Pour Adèle et les mauvaises herbes du jardin.

Table of Contents

1. Abbreviations

ABA	Abscicic acid
Acd	Accelerated cell death
AOH	ABC1 homolog
ATH	ABC2 homolog
ATM	ABC transporter of the mitochondria homolog
BSA	Bovine serum albumin
BV	Biliverdin IXα
CAB	Chl *a/b* binding protein
CAO	Chlorophyll a oxygenase
CER	*Eceriferum*
CFTR	Cystic fibrosis transmembrane conductance regulator
Chl	Chlorophyll
Chlide	Chlorophyllide
CLH/chlase	Chlorophyllase
CMO	Choline monooxygenase
Coi	Coronatine insensitive
CPIII	Coproporphyrin III
CPOX	CPIII oxidase
DMSO	Dimethylsulfoxide
EDTA	Ethylenediaminetetraacetic acid
ELIP	Early light induced protein
EMS	Ethyl methane sulfonate
EST	Expressed sequence tag
FCC	Fluorescent chlorophyll catabolite
Fd	Ferredoxin
FNR	Ferredoxin-NADPH-oxidoreductase
FPN1	Ferroportin 1
FW	Fresh weight
G6P	Glucose-6-phosphate
GCN	Yeast general control nonrepressible homolog
GSH	Glutathione reduced
HCP1	Heme carrier protein 1
HO	Heme oxygenase
HPLC	High pressure liquid chromatography
HR	Hypersensitive response
HY	Long hypocotyl
JA	Jasmonic acid
Kb	Kilo base
kDa	Kilo Dalton
LHC	Light harvesting complex
Lls1	Lethal leaf spot 1
MCS	Metal chelating substance
MDR	Multi-drug resistance
MeJA	Methyl jasmonate
MRP	Multidrug resistance associated protein
MS	Mass spectrometry
NAP	Nonintrinsic ABC protein

NBF	Nucleotide binding fold
NBT	Nitroblue tetrazolium
NCC	Non-fluorescent chl catabolite
NDO	Naphtalene dioxygenase
nptII	Neomycin phosphotransferase II
NYC	Non yellowing colour
PAGE	Polyacrylamide gel electrophoresis
PCD	Programmed cell death
PAO	Pheophorbide a oxygenase
Pchlide	Protochlorophyllide
PDR	Pleiotropic drug resistance
PEG	Polyethylene glycol
Pheide	Pheophorbide
PMP	Peroxisomal membrane protein
PMSF	Phenylmethyl sulphonyl fluoride
PPOX	Protoporphyrinogen IX oxidase
PS	Photosystem
PTC52	Protochlide dependent translocon 52
PΦB	Phytochromobiline
RBCS	RubisCO small subunit
RCC	Red chlorophyll catabolite
RCCR	Red chlorophyll catabolite reductase
RFF	RCC forming factor
RNAi	RNA interference
ROS	Reactive oxygen species
RubisCO	Ribulose-1,5-biphosphate carboxylase-oxygenase
SA	Salicylic acid
SAG	Senescence associated gene
Scp	Small Cab protein
SDS	Sodium dodecyl sulphate
SGR/SGN/NYE	Staygreen
Sid	Senescence induced degradation
SMC	Structural maintenance of chromosomes homolog
SUR	Sulfonylurea receptor
TAP	Transporter associated with antigen processing homolog
TAPa	Tandem affinity purification
TF	Transcription factor
TIC	Translocon of the inner envelope of chloroplast
TMD	Transmembrane domain
Tris	Tris(hydroxymethyl)aminomethane
VTE	Vitamin E mutant
WBC	White brown complex
WSCP	Water soluble chl-binding protein
WT	Wild type

2. Abstract

During senescence, chlorophyll (chl) is degraded through a well described pathway to be detoxified and to allow remobilization of nitrogen from the photosystems. One of the major steps in chl breakdown is the opening of the porphyrin ring via the coupled reaction of pheophorbide *a* oxygenase (PAO) and the red chl catabolite reductase (RCCR). Product of this reaction, a fluorescent catabolite (pFCC) is occurring in the chloroplast, whereas, the final products, non fluorescent catabolites of chl are located in the vacuole. The first objective of this work was to identify the transporter involved in pFCC export out of the chloroplast. A primary active ATP dependent transporter, *At*WBC23 was shown to be one of the major transporters involved in this process.

Most of enzymatic steps of degradation of chl are well known, however, regulation of the pathway is still only partially described. We characterized the stay-green factor (SGR, *At*4g22920) as a key element of chl degradation regulation. Moreover, intensive characterization of SGR mutants allowed to identify and characterize one of Mendel's pea lines as being defective in SGR. In addition, major advances in SGR function in relation to the PAO pathway were achieved. In summary, these investigations demonstrate that SGR functions upstream and independent of PAO.

In a third part, I was more interested in characterizing the PAO/RCCR reaction. Thereby an additional protein required in the known reaction was molecularly identified and characterized. This factor could contribute to substrate channelling through PAO/RCCR by detoxifying reactive oxygen species formed in the PAO reaction.

During my PhD thesis, I worked on several aspects of chl breakdown, *i.e.* transport, regulation and catabolism, which considerably improved our understanding of how important proper chl degradation is to avoid phototoxic lesion formation. Further work will be required to show whether such a chl metabolic process is also responsible for chl turnover in green mature leaves.

3. Zusammenfassung

Chlorophyll wird während der Seneszenz abgebaut, um mit seiner Entgiftung der Pflanze Stickstoff aus den Fotosystemen zu Verfügung zu stellen. Im wichtigsten Schritt des Chlorophyllabbaus öffen die Enzyme Pheophorbid *a* Oxygenase (PAO) und „Roter Chlorophyll Katabolit“ Reduktase (RCCR) den Porphyrinring des Chlorophyllmoleküls. Während sich das fluoreszierende Produkt dieser Reaktion (pFCC) im Chloroplasten befindet, werden nicht fluoreszierende Endprodukte in der Vakuole gelagert. Ein Ziel dieser Arbeit war die Identifizierung eines möglichen Transporters, der pFCC aus dem Chloroplasten transportieren könnte. Dabei konnte das ATP abhängige Transporterprotein *At*WBC23 (*At*5g06530) als Haupttransporter von pFCC identifiziert werden.

Der Ablauf des enzymatischen Chlorophyllabbaus ist gut beschrieben, jedoch über die Regulation dieses Prozesses ist noch wenig bekannt. Ich charakterisierte den „Stay-Green“ Faktor (SGR, *At*4g22920), eines der Schlüsselenzyme in der Chlorophyllabbauregulation. Durch diese Untersuchung wurde herausgefunden, dass eine der von Mendel benutzten Erbsensorten (*i*) einen Defekt in der Produktion von SGR aufweist. Weiter konnte die Funktion von SGR im Zusammenhang mit dem PAO-abhängigen Abbauweg besser beschrieben werden. SGR funktioniert unabhängig und vor PAO im Chlorophyllabbau.

Im letzten Teil dieser Arbeit wurde die PAO/RCCR Reaktion genauer untersucht. Es wurde ein zusätzliches Protein identifiziert, das für diese Reaktion benötigt wird. Es handelt sich um eine Peroxidase, die den durch PAO produzierten reaktiven Sauerstoff entgiftet.

Während meiner Dissertation interessierten mich verschiedene Aspekte des Chlorophyllabbaus, vor allem der Transport, die Regulation und der Abbau selbst. Diese Arbeit zeigt, wie wichtig ein gut funktionierender Chlorophyllabbau ist, um durch die Entgiftung der phototoxischen Abbauprodukte die Bildung von Lesionen zu verhindern. Zukünftige Forschung muss zeigen, ob der Chlorophyllabbau via PAO/RCCR nur während der Seneszenz geschieht oder auch schon in den grünen Blättern der Pflanze.

4. Introduction

Chlorophyll (chl) is the key pigment of photosynthesis, responsible for the most predominant carbon fixation process in living organisms. Chl is the most abundant pigment with estimated more than one billion tons synthesized and destroyed every year (Hendry et al., 1987). The most visual demonstration of chl degradation is taking place in forests of temperate climate areas with their splendid autumn scenery. At the end of their life cycle, annual plants and deciduous trees are entering in the last stage of their development: senescence. They start relocating nutrients by degrading photosynthetic complexes as well as the pigments they contain. Bright autumn colours are due to simultaneous chl degradation and synthesis of carotenoids and anthocyanins (Ougham et al., 2005). The plant senescence process as well as chl degradation are tightly regulated mechanisms. Along senescence, chloroplasts are converted to gerontoplasts, they lose volume and density, accumulate plastoglobules and slowly lose photosynthetic capacity. This transition could however be reversed (Parthier, 1988). Physiological relevance for an enzymatic degradation of chl is mainly explainable by the necessity for the plant to recycle fixed nitrogen from photosystem protein complexes. Indeed one mole of chl contains four moles of nitrogen, but chl nitrogen represents only 2% of the cellular nitrogen (Hörtensteiner, 2006). Plants disposing chl aim to recycle photosystem apoproteins gathering 20% of the cellular nitrogen. Chl degradation can be considered as a detoxification process. In green tissues, chl is always bound in protein complexes and chl never gets released. If chl would be released, light activation of free chl or free chl derivatives would lead to a dramatic uncontrolled reactive oxygen species (ROS) accumulation, such as production of singlet oxygen, and would provoke premature cell death, like in the *pao1* (pheophorbide *a* oxygenase 1) mutant (Pružinská et al., 2003). Therefore plants get rid of this potential phototoxin as soon as chloroplast dismantling begins (Hörtensteiner, 2004, 2006).

A biochemical pathway for the degradation of chl was almost not documented until the beginning of the eighties, whereas chl biosynthesis has been extensively studied (Tanaka and Tanaka, 2006). A first hint showing the existence of a pathway for chl degradation in higher plants was the description of the first non-fluorescent chl catabolite (NCC) (Kräutler et al., 1991). Since then, the chl degradation pathway became a better and better described detoxification process, with the help of mutants

impaired in different steps of the pathway. Mutant studies allowed the recent cloning of three of its key enzymes: PAO, red chl catabolite reductase (RCCR) and chl *b* reductase (Wüthrich et al., 2000; Pružinská et al., 2003; Kusaba et al., 2007). Green chl is converted in a multistep pathway to linear colourless and nonfluorescent tetrapyrroles, NCCs (Fig. 1). The earliest step of removing chl from antennas and photosystem cores is still unclear. In algae and higher plants, an important number of reports attempted to characterize the involvement of chl binding proteins and proteases in photosystem degradation, but the overall picture is difficult to sum up in one clear pathway.

The porphyrin degradation itself starts with the consecutive removal from chl of both phytol and the Mg atom by chlorophyllase and a metal-chelating substance, respectively. However, molecular identification of chlorophyllase (CLH) (Tsuchiya et al., 1999) has recently been questioned in *Arabidopsis* (Schenk et al., 2007). Loss of the green colour occurs during the subsequent opening of the porphyrin macrocycle of pheophorbide (pheide) by the coupled action of PAO and RCCR (Fig. 2). This yields a primary fluorescent catabolite (pFCC), which is exported from the plastid by a primary active transporter (Matile et al., 1992). Further steps in the pathway are reminiscent of detoxification processes widely occurring in plants (Kreuz et al., 1996). Thus, pFCCs are activated by hydroxylation and after modifications are imported into the vacuole by a further primary active transport system (Hinder et al., 1996). Due to the acidic vacuolar pH, FCCs eventually tautomerize non-enzymatically to NCCs (Oberhuber et al., 2003; Hörtensteiner, 2006). While the earliest steps of chl degradation are common to all higher plants, the later stages of modification and conjugation are species-specific.

Additional characterization of mutants retaining chl during senescence has recently provided more information on the regulation of the pathway. The SID/SGR/SGN/NYE protein depleted in an important set of mutants in *Festuca*, *Arabidopsis* and rice is a promising regulator of chl degradation, but its physiological function is yet unknown despite the recent increasing interest (Armstead et al., 2007; Park et al., 2007; Ren et al., 2007).

My work attempted to shed light on several issues in the characterization of chl breakdown. Namely, the identification of the export process of the FCC out of the chloroplast, the regulation of the degradation by the so-called staygreen factor (SGR) and additional characterization of the PAO/RCCR coupled reaction.

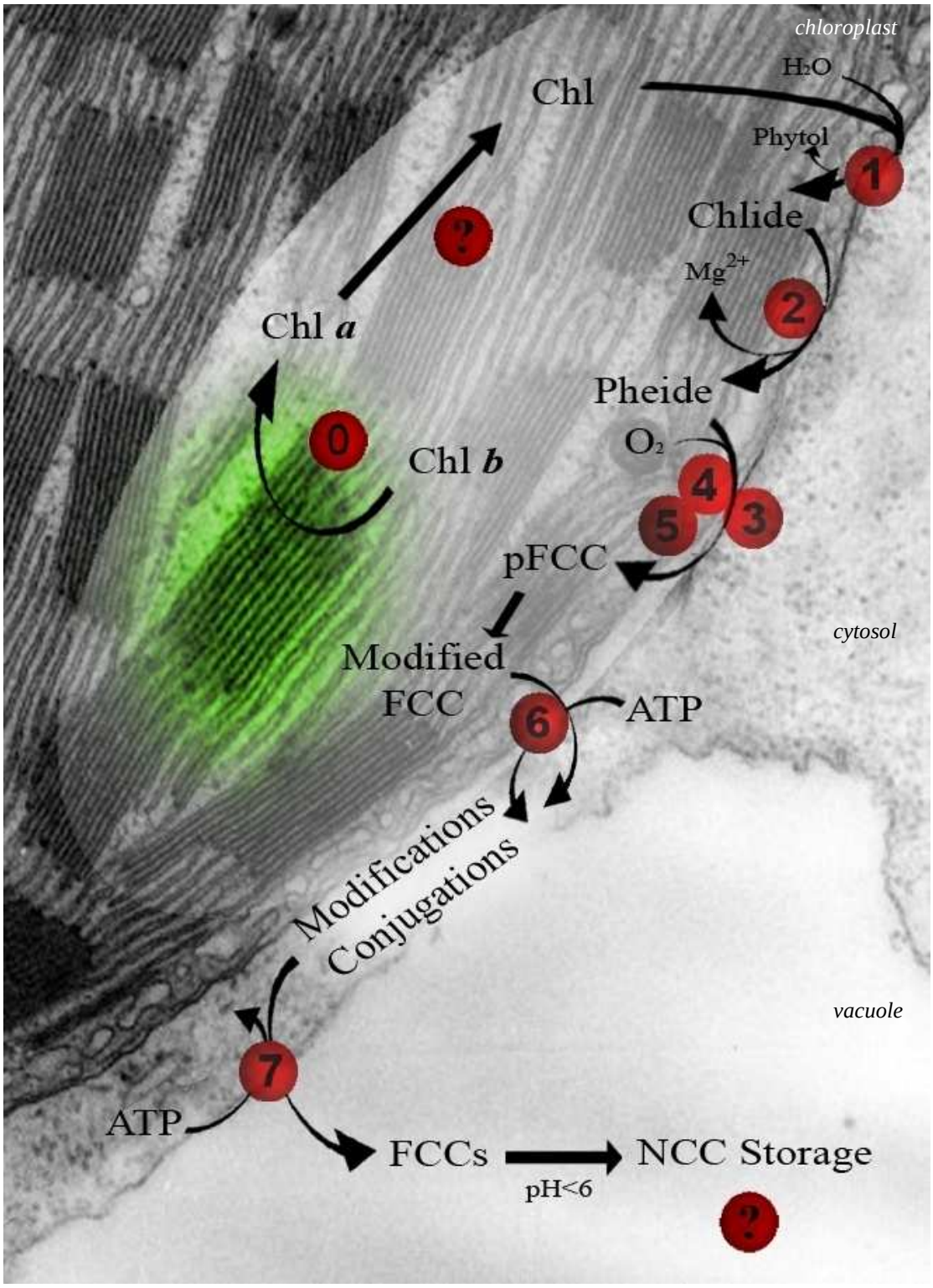

Figure 1. Model of the chl breakdown pathway in higher plants. All steps are labelled with numbers, putative reactions are indicated with a question mark. 0: chl *b* reductase, 1: chlorophyllase, 2: metal chelating substance, 3: red chlorophyll catabolite reductase, 4: pheophorbide *a* oxygenase, 5: putative RFF activity, 6: ABC transporter WBC23, 7: ABC transporter MRP. See Figure 2 for catabolite structures.

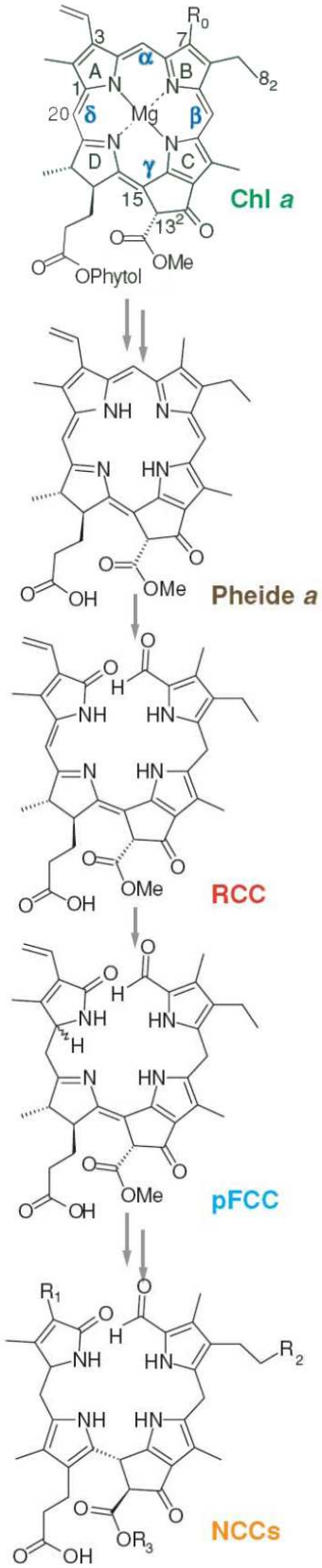

Figure 2. Chemical structures of chlorophyll and chlorophyll catabolites. Labelling of pyrrole rings (A-D), methine bridges (α-δ) and relevant carbon atoms can be seen on chl. R_0= CH_3, chl *a*, R_0= CHO, chl *b*; R_1-R_3 in NCCs indicate possible modification sites. (Adapted from Hörtensteiner, 2006).

4.1 Chlorophyll breakdown pathway

4.1.1 Removing of chlorophyll from the photosystems

Even if extensive literature is covering the assembly of photosystems (PS) and the assembly of their subunits (Baena-Gonzalez and Aro, 2002), degradation processes of the PS supercomplexes are remaining largely unknown, neither concerning the turnover during the life of the plant, nor concerning the senescence-specific degradation. Upon light exposure protochlorophyllide is converted to chl (von Wettstein et al., 1995) and chl binding proteins (D1, CP43 and 47) are synthesized, enabling a final stable assembly of PSII (Kim et al., 1994). Soon after synthesis, as the water splitting chemistry is going on, various reactive and radical oxygen species are produced which cause irreversible damage to PSII. An efficient and rapid mechanism avoids accumulation of damaged PSII. A rapid turnover of the reaction centre D1 protein prevents the whole structure from being further damaged by the oxidative stress (Baena-Gonzalez and Aro, 2002). A highly specific proteolysis of D1 and phosphorylation of PSII proteins allows an efficient recycling of the reaction centre. Other PSII core subunits, as well as other chl binding proteins turnover more slowly (Komenda et al., 2006). During D1 recycling in *Synechocystis*, it is thought that some proteins of the CAB (chl binding protein) family should interact with chl, allowing an efficient recycling (Vavilin and Vermaas, 2007). Interestingly, it has been shown that some small chl binding proteins, such as SCPd, interact with PSII and FTSH proteases, suggesting an involvement of this protease family in PSII dismantling (Yao and Greenberg, 2006). SCP's would bind chl and avoid chl to be converted to chlorophyllide (chlide) by chlase. This would allow a quick recycling of D1 in the complex (Vavilin et al., 2007). However, turnover of D1 in the *Festuca* SGR mutant Bf993 is processing normally, suggesting SGR might not regulate D1 degradation (Hilditch et al., 1986).

In plants, the precise function of CAB proteins is unclear. Plastid encoded chl *a/b* binding proteins are part of the PSI and II reaction centre heterodimers and internal PSII antennas CP43 and 47. The second group are the nuclear encoded LHC (light harvesting complex) proteins binding chl *a* and *b*. This group contains around 30 distant relatives such as PSBs (CP22), known to be involved in non photochemical quenching (Ballottari et al., 2007), or the early light-inducible proteins (ELIPs) (Adamska et al., 1996; Tzvetkova-Chevolleau et al., 2007). ELIP and PSBs

accumulate in thylakoids during high light stress and are proposed to be involved in quenching activity (Horton et al., 1996; Heddad and Adamska, 2002). ELIP contribution to photoprotection has been questioned in *Arabidopsis* (Rossini et al., 2006), although ELIP1 and 2 have been co-isolated with LHCb's (Heddad et al., 2006). ELIP2 has been shown recently to regulate chl synthesis in *Arabidopsis* by sensing thylakoid chl content (Tzvetkova-Chevolleau et al., 2007). However, no function of ELIP during chl degradation has been demonstrated so far.

A large part of chl is located in the antennas of the photosystems (Nelson and Yocum, 2006). Antenna degradation processes in higher plants have been thought to involve proteases such as FTSH6 (Zelisko et al., 2005). However recycling mechanism of the antenna and the mechanism by which antennas are degraded during senescence are largely unknown processes and a real involvement of FTSH in this mechanisms is still under discussion (A. Pruzinska and C. Funk, personal communication). Serine/cystein-type proteases are involved in LHC degradation during light stress (Tziveleka and Argyroudi-Akoyunoglou, 1998). Some reports show endopeptidase and metalloprotease involvement in, respectively, LHCb1 and 3 degradation (Forsberg et al., 2005; Zelisko et al., 2005). Other types of proteases were thought to be involved as well, such as stromal CLP or thylakoid DEGp and SPPa (Adam and Clarke, 2002).

However, it is reasonable to think that removing of chl might be a prerequisite for degradation of chl-binding proteins. This raises the question of specific chl binding mechanisms responsible for chl removal from the complexes. SGR factor has been shown to interact with LHCb and has been proposed to be involved in such mechanism even if no physiological activity has been shown so far for this factor (see section 7) (Park et al., 2007). Chl is believed to turnover rather fast at the steady-state level (Stobart and Hendry, 1984; Thomas et al., 1997). None of the mechanisms or the factors involved in chl removal has been elucidated and there is plenty of room for further investigations in this direction. Recently, the Vermaas lab published a few papers about ^{15}N and ^{13}C pigment labelling in *Synechocystis*, and estimate chl half-life to be around 200 h (Vavilin et al., 2005; Vavilin and Vermaas, 2007; Vavilin et al., 2007).

4.1.2 Catabolic steps of the porphyrin ring

4.1.2.1 Chl *b* reductase

All but one of the NCCs isolated so far from higher plants have been shown to derive from chl *a* (Hörtensteiner, 2006; Müller et al., 2006). One reason for this is the substrate-specificity of PAO for pheide *a*, with pheide *b* being a competitive inhibitor (Hörtensteiner et al., 1995). Furthermore, reduction of chl *b* to chl *a* within the chl-protein complexes of the photosystems has been suggested to be a prerequisite for chl degradation, leading to the destabilization of these chl-protein complexes (Hörtensteiner, 2006). Chl *b* is a component of the antenna complexes in the photosystems. The so called "chl cycle" describes the interconversion of chl/chlide *b* and *a*. The oxidative part of the cycle acts mainly on chlide and is catalyzed by chlide *a* oxygenase, a Rieske-type iron sulphur oxygenase. Thereby the C_7 methyl group of chl is oxidized to a formyl group via a C_7-hydroxy chlide intermediate (Rüdiger, 2002). The opposite reductions are catalyzed by an NADPH-dependent chlide *b* reductase and a ferredoxin-dependent hydroxy-chlide *a* reductase.

Interestingly, chl(ide) *b* reductase is the only enzyme of chl breakdown so far localized in the thylakoid membrane, as probably the first enzyme of the pathway. It is known that chl *b* removal from the antennas leads to lower accumulation of LHCbs (Tanaka and Tanaka, 2005) and chl *b* is needed in a certain stoichiometry to chl *a* in order to stabilize chl-protein complexes (Horn and Paulsen, 2004; Hoober et al., 2007).

4.1.2.2 Chlorophyllase

Chlorophyllase (chlase) is the enzyme responsible for the hydrolysis of the ester bond between ring D of chl and the phytol tail, to yield chlide. A large amount of biochemical literature has accumulated about this enzyme since its discovery in 1913, as it was thought to be the first key enzyme of the pathway (Willstätter and Stoll, 1913). This intriguing enzyme has been purified from *Chenopodium album*, *Citrus sinensis*, *Phaeodactylum tricurnutum* and *Arabidopsis* (Terpstra, 1981; Jacob-Wilk et al., 1999; Tsuchiya et al., 1999). In 1999, two groups independently cloned chlase genes in *C. sinensis* (*Cs*CLH1), *C. album* (*Ca*CLH) and *Arabidopsis* (*At*CLH1 and 2) (Jacob-Wilk et al., 1999; Tsuchiya et al., 1999). All these enzymes are presenting a serine lipase domain mediating the de-esterification. Surprisingly, a rather low

homology has been found between CLH proteins and some were even missing a chloroplast targeting signal.

Recently, CLHs from *Arabidopsis* have been shown to localize outside the chloroplast (Schenk et al., 2007). Moreover, *Arabidopsis* CLH1 and CLH2 are predicted to be soluble, raising questions about their substrate accessibility in the thylakoid membranes (Takamiya et al., 2000). Expression patterns of both genes are not correlated to each other or to senescence (Liao et al., 2007). CLH1 is responsive to methyl jasmonate, wounding and pathogen treatment, which might be an indication of a different function despite of the *in vitro* shown chlase activity (Benedetti et al., 1998; Kariola et al., 2005). Following this new conflicting reports, it might be reasonable to distinguish between chl dephytylation in fruits and in leaves. Indeed *Citrus* chlase cloned from fruits has been located in the chloroplast in two heterologous expression systems in tobacco protoplasts and in squash (*Cucurbita pepo*). *Cs*CLH has also been shown to have an *in vivo* activity with increasing chl degradation when overexpressed (Harpaz-Saad et al., 2007). As identification of the leaf chlase may be missing, it is not known if chlide is formed in the thylakoid membrane or whether chl is taken over by a carrier to be transported to the envelope, as suggested some 10 years ago by Matile's group (Matile, 1997). In this hypothesis the carrier system might involve water soluble chl proteins (WSCPs), which have been shown to remove chl from pigment-protein complexes (Satoh et al., 1998). Plastoglobules could also function as a carrier system, as they have been shown to be contiguous with the thylakoid membranes and contain large amounts of phytol and some predicted chl binding proteins (Brehelin et al., 2007).

4.1.2.3 Phytol recycling

The fate of the phytol tail after its cleavage from the porphyrin ring has only recently been studied. An *Arabidopsis* mutant impaired in tocopherol biosynthesis (*vte5-1*) shows accumulation of free phytol. Once the phytol is released, especially in seeds, it is phosphorylated by two kinases to give phytyldiphosphate, which is converted to tocopherol (Ischebeck et al., 2006; Valentin et al., 2006). Fatty acid phytyl esters derived from chl phytol were also shown to accumulate in thylakoids and plastoglobuli under nitrogen starvation (Gaude et al., 2007). Physiologically, phytol

recycling in tocopherol adds a so far unknown advantage in degrading chl, to protect against oxidative stress via tocopherol.

4.1.2.4 Mg-dechelation

Two processes are thought to be responsible for Mg^{2+} dechelation. The first implicates a low-molecular weight compound named MCS (magnesium chelating substance). A second factor has been described whose activity might be associated with MCS. Whether MCS is working as a co-factor of a dechelatase protein is not known, and sizes vary from species to species. It can just be speculated that dechelation is probably catalyzed by low molecular weight compounds whose structures are not known (Suzuki and Shioi, 2002).

It is of interest to see that opening of the porphyrin ring from heme needs the presence of a ferrous iron and oxygen with formation of an peroxo intermediate and CO emission (Unno et al., 2007). The heme porphyrin ring however is cleaved in biliverdin at the same position like in the pheide/RCC reaction. Obviously there is no need for a dechelation step in heme metabolism, and heme oxygenase is clearly not able to open the chlide ring, *i.e.* there is no cross-talk between heme and chl degradation.

4.1.2.5 PAO: loss of green colour

- PAO reaction

The first detectable linear tetrapyrrole of the chl degradation pathway is the primary fluorescent catabolite (pFCC). pFCC is obtained by the oxidative cleavage and reduction of pheide *a* by the activity of two enzymes: pheide *a* oxygenase and RCC reductase (Fig. 3). Opening of the chlorine cycle can be considered as the most important step in chl catabolism, as it is the first absolutely irreversible step giving raise to colourless catabolites. PAO/RCCR identification and cloning (Wüthrich et al., 2000; Pružinská et al., 2003) followed the establishment of an *in vitro* assay in which pheide *a* is converted in pFCC (Hörtensteiner, 1998). PAO is introducing one molecule of dioxygen at the α-methine bridge on ring B of pheide to form RCC. The second lactam oxygen atom of ring A is probably derived from water (Hörtensteiner et al., 1998).

Pheide *a* has been shown *in vitro* to be an exclusive substrate for PAO with pheide *b* inhibiting in a competitive manner (Hörtensteiner et al., 1995), although discovery of the C_7 hydroxylated *At*-NCC-3 suggests that pheide *b* might be converted by PAO as well (Müller et al., 2006). In *Chlorella protothecoides*, PAO is less specific, causing occurrence of Chl *a* and *b* derived degradation products (Hörtensteiner, 1999).

- PAO and related monooxygenases

PAO is expressed specifically during senescence even if a basic activity level has been shown in non-senescent tissues (Hörtensteiner et al., 1995; Yang et al., 2004). Regulation of PAO at the posttranscriptional level (phosphorylation) has been suggested in oil-seed rape (Hörtensteiner, 2004; Chung et al., 2006). Microarray data show expression of *PAO* in flowers, and partial flowering phenotype of the *pao1* mutant might highlight an additional function of PAO in these organs (Pružinská et al., 2005). *PAO* is also overexpressed during wounding (Yang et al., 2004) and is thought to be a major trigger of the hypersensitive response for light dependent pathogens (H. Ougham and L. Mur, personal communication).

PAO is a Rieske-type iron sulphur monooxygenase which is associated with the envelope of the chloroplast (Matile and Schellenberg, 1996) and contains two transmembrane domains. In *Arabidopsis* it belongs to a five member family of LLS1 (lesion leaf spot) related non heme iron oxygenases containing chl *a* oxygenase (CAO), choline monooxygenase (CMO), PTC52 and TIC55 (Gray et al., 2004). PTC52 is the closest homolog of PAO and was suggested to catalyze the conversion of protochlorophyllide (pchlide) *a* to pchlide *b* (Gray et al., 2004; Reinbothe et al., 2004). TIC55 has been isolated as a member of the chloroplast envelope protein import machinery together with TIC62, a dehydrogenase binding FNR (Stengel et al., 2008). Besides a proposed regulation function in the envelope import machinery, no other function has yet been shown for TIC55 (Küchler et al., 2002).

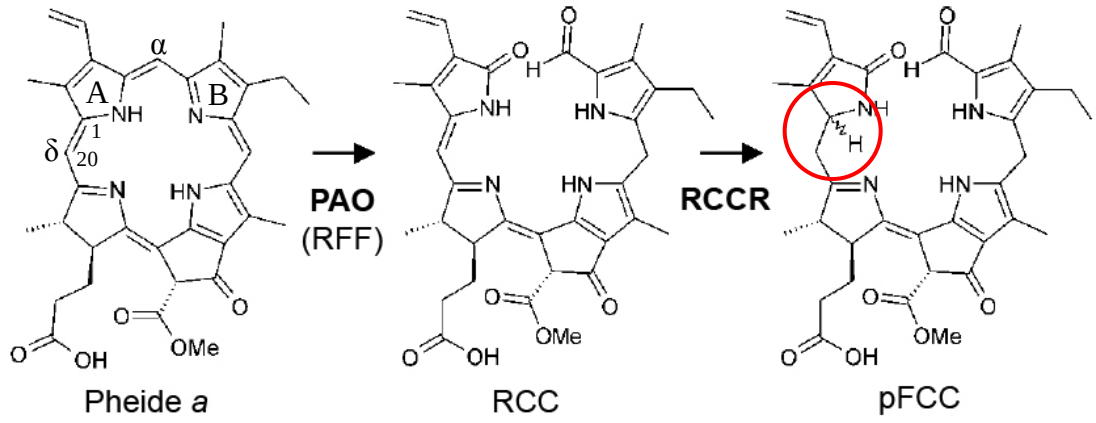

Figure 3. Opening of the porphyrin ring is the key step of chl degradation. PAO is opening the chlorin cycle on the α-methine bridge and adds an oxygen to the ring B. A second atom of oxygen is added on ring A from water. This reaction requires Fd. Subsequent reaction is the reduction of the C_{20}/C_1 δ-methine bridge by RCCR, creating a stereocenter in C_1 (circled in red). Adapted from Hörtensteiner, 2006.

4.1.2.6 RCCR

- A classical bilin reductase

RCCR is a soluble stromal protein catalyzing the reduction of the C_{20}/C_1 bond of RCC to pFCC. RCCR is related to a family of Fd-dependent bilin reductases which reduce biliverdin IX (BV). This family includes HY2, responsible for BV conversion to phytochromobilin, and other photosynthetic bacteria BV reductases converting BV into phycobilins (Frankenberg et al., 2001).

As a consequence of the reduction a stereospecific center is formed (Rodoni et al., 1997). Depending on the source of RCCR, one of two C1 isomers of pFCC is formed (Fig. 3). For example, in *Arabidopsis* RCCR, pFCC-1 is formed, whereas in tomato, pFCC-2 is exclusively formed. Identification of the RCCR gene and chimeric construction of the two isoforms have shown that in *Arabidopsis*, an exchange of Phe_{218} to Val was sufficient to change the specificity of the protein from pFCC-1 to pFCC-2 (Pružinská et al., 2007). However a modelled crystal structure from RCCR based on the biliverdin reductase PCYa from *Synechocystis* hardly shows a specific location of this residue in the substrate pocket of the protein (S. Hörtensteiner, personal communication). Crystallization of both versions of RCCR might bring some more clues concerning the mechanism of RCC formation. When chemically synthesized RCC is incubated with pure RCCR both stereoisomers are formed,

suggesting an influence of PAO or an other factor in the stereospecificity (Rodoni et al., 1997).

- Other potential function

RCCR is expressed constitutively and no proof of any regulation has been shown (Wüthrich et al., 2000). *RCCR* expression is not particularly upregulated during senescence and is thought to have several functions in addition to the protective activity against cell death by removing RCC, such as providing pathogen resistance upon *Pseudomonas syringae* infection (Mach et al., 2001). In addition to the reduction of RCC in pFCC, contradictory reports show a protoporphyrin IX (PPIX) detoxifying activity (Yao et al., 2004). Recent localization of RCCR in non-photosynthetic tissues and at a subcellular level in mitochondria may highlight an other unknown function for this enzyme (Yao and Greenberg, 2006).

4.1.3 Export, modification and storage

The PAO pathway of degradation of chl is leading to an ultimate storage of linear colourless NCCs in the vacuole. This process requires that catabolites cross the envelope of the chloroplast and the tonoplast. Attempts to identify such transporters are hindered by the problem of the exact nature of the substrate which is translocated at every step.

- Chloroplastic export of pFCC

Chloroplastic export of chl catabolites has been shown to require ATP in isolated senescing chloroplasts from barley (Matile et al., 1992). In this fundamental experiment, FCC was exported out of the chloroplast when ATP were applied. Moreover, in *pao1*, where a large amount of pheide is accumulated, no pheide is observed to accumulate outside the chloroplast during senescence (S. Aubry and S. Hörtensteiner, unpublished results) suggesting a rather good specificity of the transporter. We have shown that in *acd2* depleted in RCCR, RCCs are found outside the chloroplast (Pružinská et al., 2007). This might be explained by the similar conformation of RCC and FCC, thought to be the natural substrate. RCC and FCC are both linear tetrapyrroles. RCCs are absorbing in red, pFCC is blue fluorescing and both never accumulate in WT.

A knockout mouse depleted in an ABC transporter, ABCG2 (BCRP1), has been shown to accumulate in the blood and bile large amounts of pheide when fed with chl derived diet. This accumulation lead to a "porphyria" like phenotype, with phototoxic lesions on most light exposed organs, like the ears (Jonker et al., 2002). Fed with pheide, mice were no longer able to detoxify the porphyrin back to the gut and accumulated chl derivatives in their body. The mechanism by which pheide is incorporated as well as its conversion to a linear RCC is still unknown. However ABCG2 has been shown, besides an impressive set of diverse substrates also to transport pheide (Robey et al., 2004; Krishnamurthy and Schuetz, 2005).

Resorption of chl in the mouse gut may be compared to incorporation of heme (Fig. 4). A large part of iron is resorbed in heme-bound form through a facilitator (HCP-1) (Shayeghi et al., 2005; Latunde-Dada et al., 2007). Incorporated heme is either further translocated to the blood or converted by heme oxygenase to free iron and biliverdin. Free iron is further transported by ferroportin (FPN) to the blood, but data are missing concerning the open tetrapyrrole. The porphyria research field is classically concentrated on different enzymatic steps of heme biosynthesis, but accumulation of biliverdin or further degradation products of heme might be responsible for some unexplained porphyria-type disorders.

The accumulation of RCC-like compounds in mice depleted in ABCG2 (see section 6.4) lets imagine a probable chelation of iron on free pheide and subsequent ring opening via heme oxygenase to give raise to a mouse-type RCC (which would have lost the C_5 carbon). Transporters most closely homologous to ABCG2, like WBC23 and 28 in *Arabidopsis*, might be able to transport porphyrins as well.

A.

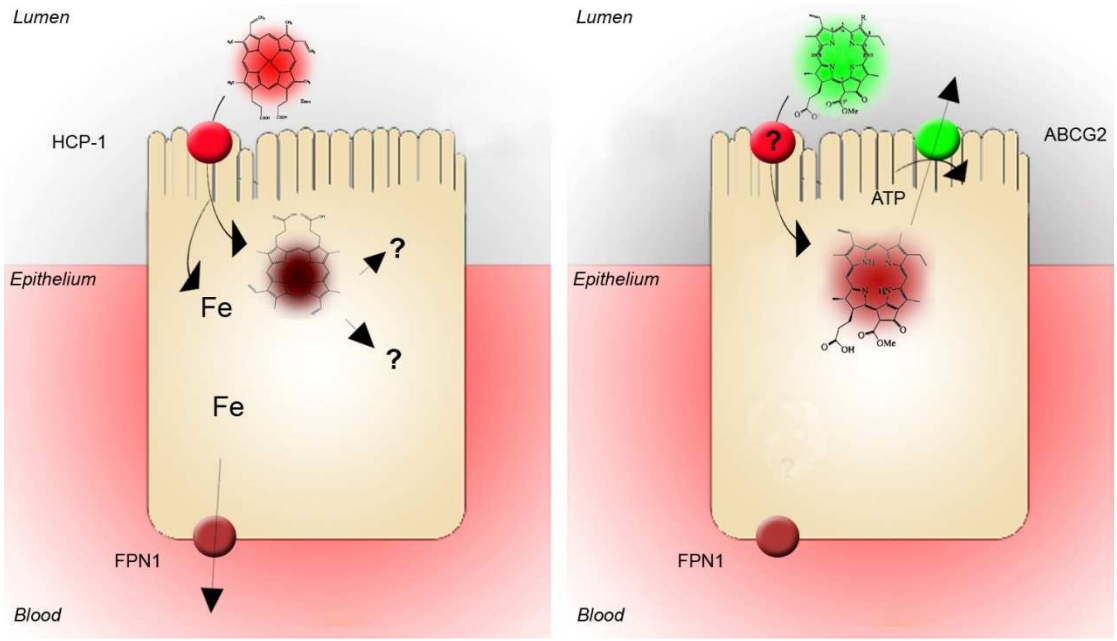

B.

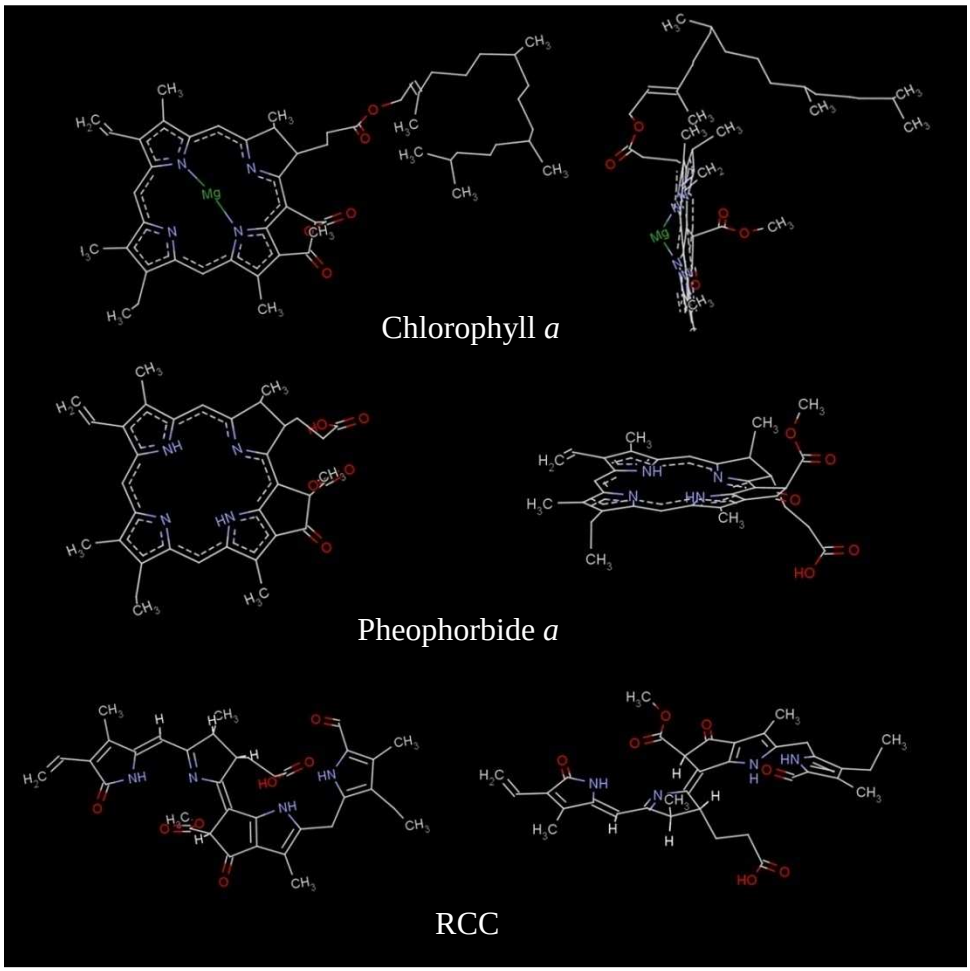

Figure 4. A. Schematic representation of heme and chlorophyll uptake in mammal intestine. Heme is taken up by HCP-1 and cleaved into biliverdin by heme oxygenase. The iron is then imported into the blood by ferroportin (FPN1). Further degradation of biliverdin is not reported. Chlorophyll derivatives are imported by the gut cells by an unknown mechanism. Pheide is exported to the lumen via an active ABC transporter ABCG2. Modified from Latunde-Dada et al, (2006). **B.** 3D representation of chl, pheide *a* and RCC. Designed with MarvinSketch software.

- Export of other porphyrins from the chloroplast

Necessity of porphyrin export out of the chloroplast has been suggested in other context (Tanaka and Tanaka, 2006). Indeed, the earlier steps of biosynthesis of heme and chl are common, and a heme precursor, probably coproporphyrinogen III (CPIII), is translocated to the mitochondria. Plastid to nucleus signalling might also involve PPIX export (Tanaka and Tanaka, 2006; Ankele et al., 2007). The exact nature of the export process(es) is still missing, and identification of transporters for chl derivatives was one of the main objectives of this work. A linear tetrapyrrole transporter is moreover needed for the export from the chloroplast of phytochromobilin as the co-factor needed for phytochrome biosynthesis (Terry et al., 2002).

- Vacuolar transport

A primary active transport system for *Bn*-NCC-1 has been described in barley vacuoles with a surprisingly high affinity for a FCC (Hinder et al., 1997). This suggested the import of FCCs into the vacuole prior to their tautomerization due to pH acidification (Oberhuber et al., 2003). Although two full-size ABC transporters, *At*MRP2 and *At*MRP3, have been shown two transport *Bn*-NCC-1 after expression in yeast, the identity of the *in vivo* transporters is still unknown. As many MRP or other members of the ABC transporter multigenic family are localized to the tonoplast, several transporters may be able to import FCC into the vacuole.

-NCC storage and further modifications

On the way to the vacuole pFCC might be modified by different reactions: dihydroxylation of the vinyl group of pyrrole A, hydroxylation at C_8 followed by a glucosylation and/or malonylation and C_{13} demethylation (for review see Hörtensteiner, 2006). NCCs are derived from either pFCC-1 or -2 and are consequently divided into two stereospecific groups. All but one NCC (*At*-NCC-3) are derived from chl *a*. The exception might be due to chl cycle interconnection of chlide *b* and *a*, even if PAO is specifically acting on pheide *a* in higher plants (Müller et al., 2006).

Due to the acidic condition in the vacuole, FCCs are spontaneously tautomerized to NCCs. Once in the vacuole, storage or further degradation of NCCs is species-specific. Indeed some species keep a ratio of final catabolites equivalent to chl which have been degraded (like in *Arabidopsis* or barley). On the other hand in tobacco or

radish NCC amounts decrease with time (Suzuki and Shioi, 1999; Hörtensteiner, 2006).

Physiological relevance for late modifications and hypothetical controlled degradation of NCC chains is hard to show, as it may occur after the loss of cellular integrity. Conjugations and modifications might allow a better solubility in the vacuole (Oberhuber et al., 2003).

4.2 Significance of detoxifying porphyrins

4.2.1 Leaf senescence

Chl degradation is part of a larger process, leaf senescence. Leaf senescence is not a passive and unregulated degeneration process, such as necrosis, leading to the disruption of the cell in an uncontrolled manner. Conflicting nomenclature in the literature leads to wrong comparison between plant senescence and animal senescence (Ougham et al., 2005). In fact plant senescence is a reversible process of remobilization of nutrients. It takes place every year in annual plants, such as wheat, soybean, corn or rice during grain filling and maturation stage. In *Arabidopsis*, senescing leaves loose 85% of their nitrogen content, as well as large quantities of carbon, sulphur, phosphate, potassium and micronutrients (Himelblau and Amasino, 2001). Similar results have been observed in deciduous *Populus tremula* (Keskitalo et al., 2005).

The earliest and more significant changes in cell structure during senescence is the breakdown of (mesophyll) chloroplasts, containing 70% of the leaf protein (Hörtensteiner and Feller, 2002; Lim et al., 2003). The overall senescence process includes more than 800 genes (Buchanan-Wollaston et al., 2005) and only a small fraction of these senescence associated genes (SAG) has a described function. Part of them, such as NAP or WRKY53 are transcription factors (TF) which have been shown to act positively on senescence. Out of 1500 predicted TF in *Arabidopsis*, microarray data show a more than three-fold overexpression of 96 TF and more than two fold overexpression of 303 TF (Buchanan-Wollaston et al., 2005). On the other side 81 TF were down-regulated during dark-induced senescence (Lin and Wu, 2004). The observed complexity of the senescence TF network allows thinking of a complex and multifactorial regulation of the process, with probably a large redundancy in TF function.

It is not surprising to see a major part of upregulated SAG participating in relocalization processes, such as lipases, nucleases and different types of proteases (Buchanan-Wollaston et al., 2005). Hormones, like ABA, SA, JA and ethylene have been shown to positively regulate leaf senescence whereas cytokinins delay the senescence start (Gan and Amasino, 1997). Cytokinin and ethylene have antagonistic effects. Overexpression of the isopentenyl transferase in tobacco led to the accumulation of cytokinin and delay of senescence (Gan and Amasino, 1995).

Ethylene insensitive mutants such as *Arabidopsis etr1* and *ore3* are also delayed in the senescence process (Woo et al., 2004). However direct involvement of ethylene in the regulation of senescence is not shown (Lim et al., 2003). The interconnection of the different hormone pathways and several internal and external factors involved in their regulation, lead to a complex picture of the overall senescence regulation.

At a cellular level, chloroplasts are converted to gerontoplasts, with dismantling of grana stacks and formation of large plastoglobules (Brehelin et al., 2007). As all photosynthetic genes are down-regulated, breakdown and remobilization processes are initiated. The nucleus and mitochondria remain intact much longer than chloroplasts, to allow SAG gene expression and respiration. However, as photosynthetates are no longer produced, cells start respiration using fatty acids. β-oxidation genes are indeed upregulated during senescence (Buchanan-Wollaston et al., 2003).

4.2.2 Photosensitivity of mutants impaired in the chl degradation pathway

Mutants defective in several steps of chl breakdown have been used to build a scheme of the pathway (Hörtensteiner, 2004). Two types of phenotypes could be distinguished: staygreen mutants, often delayed in the earlier steps of the pathway, avoiding the chl-photosystem complexes to be dismantled, and lesion mimic mutants, accumulating excess chl catabolites and showing dramatic consequences of these phototoxins.

-Lesion mimic mutants

All chl biosynthetic and catabolic intermediates from uroporphyrin III onwards and towards RCC are phototoxic. Accumulation of free porphyrins in plants or animals causes cell death, usually because of light-dependent oxidative stress. The conjugated electron system of the pyrrole ring scavenges photons and produces singlet oxygen which is lethal for the cell in high amounts or which causes a cell death signalling cascade (Wagner et al., 2004). The maize mutant *les22* is defective in uroporphyrinogen III decarboxylase and accumulates free uroporphyrinogen III in leaves which causes formation of light-dependent lesions (Hu et al., 1998). Interestingly, the defect in the same enzyme in human is responsible for a disease called *porphyria cutanea tarda* (PCT) an autosomal dominant trait which is clinically

characterized by a photosensitive dermatosis (Ajioka et al., 2006). When this character is found homozygously, the disease is called *hepatoerythropoietic porphyria* (HEP) and shows more severe symptoms. Porphyrins might accumulate when a step in synthesis or breakdown of any porphyrin is impaired. In plants, absence of coproporphyrinogen oxidase, plastidic ferrochelatase or protoporphyrinogen oxidase leads to the accumulation of their respective phototoxic substrates and subsequently to the formation of necrotic lesions (Kruse et al., 1995; Mock and Grimm, 1997; Molina et al., 1999; Papenbrock et al., 2001). This phenotype is called lesion mimic phenotype, due to its similarity to the localized necrosis during the hypersensitive (HR) response (Lorrain et al., 2003). 37 different lesion mimic phenotypes have been isolated to date, classified in initiation or propagation mutants (Lorrain et al., 2003).

-*pao1* and *acd2*

Mutants depleted in PAO and RCCR have been isolated from an EMS mutagenized screen for plants presenting HR-like symptoms earlier than WT upon pathogen infection (Greenberg and Ausubel, 1993; Greenberg et al., 1994). Both mutant have high content of ROS, proposed to contribute to the propagation of the lesions (Gray et al., 2002). Characterization of these two mutants did not fully answer some of the phenotype features, such as partial flowering impairment in *pao1* or the pathogen hypersensitivity of *acd2* (Greenberg et al., 1994; Pružinská et al., 2005).

-*pao1* and phototoxicity

The *PAO* gene has only recently been cloned in the maize mutant *lls1* and in the *Arabidopsis pao1* mutant (Pružinská et al., 2003). In both mutants accumulation of the PAO substrate, pheide, provokes formation of a light-dependent cell death phenotype. None of the further catabolites of pheide could be isolated in those mutants suggesting a unique enzyme responsible for the ring opening. These mutants are also shown to stay green upon dark incubation (Pružinská et al., 2003; Pružinská et al., 2005) and recently it has been shown that SGR, a factor involved in early chl degradation regulation (see section 7.3) was down-regulated in *pao1* (Park et al., 2007). Authors speculate about retrograde signalling of pheide inhibiting SGR expression. But further work on SGR function is required to determine the real PAO-SGR interaction.

- *acd2* and phototoxicity

Analysis of mutants lacking RCCR (*acd2*) in *Arabidopsis* has shown accumulation of RCC during senescence. A major difference to *pao1* is the accumulation of further catabolites of the pathway (FCC and NCC). However these catabolites appear in both stereoisomeric forms, suggesting a non-enzymatic conversion of RCC, probably after its export out of the plastid (Pružinská et al., 2007). It is of interest to observe that *C. protothecoides* does not contain any RCCR, and chl catabolites accumulating during heterotrophic nitrogen-limiting conditions are excreted into the surrounding medium (Engel et al., 1991).

4.2.3 Heme trafficking

The present study focussed on membrane trafficking of chl catabolites, but a complete view should also include a description of the homeostasis regulation of the structurally close related heme. The early steps of chl and heme biosynthesis, up to the chelation of either Mg or Fe, are common. All subsequent biosynthetic steps as well as catabolism are different. In plants, biosynthesis is taking place in the chloroplast, at least up to CPIII (Moulin and Smith, 2005; Tanaka and Tanaka, 2006). The intriguing presence in the mitochondria of coproporphyrinogen oxidase (CPOX) and protoporphyrinogen IX oxidase (PPOX) raises the question of mitochondrial iron chelation. Import in the mitochondria of precursors of heme would be needed. In mammals, it has been shown that an ABC transporter from the ABCB family, ABCB6, is responsible for trafficking of porphyrins across the outer and probably the inner envelope of mitochondria (Krishnamurthy and Schuetz, 2006; Paterson et al., 2007). Diseases such as cerebrallar ataxia and X-linked sideroblastic anemia are associated with ABCB6 and 7 defects (Csere et al., 1998). Coproporphyrinogen III (CPIII) is thought to be the imported substrate, which is directly oxidised in the mitochondria intermembrane space (Ajioka et al., 2006). It could be speculated that also in plants CPIII might be exported from the chloroplast and imported into the mitochondria, where it would be oxidised and converted to heme.

The closest homologs to *Hs*ABCB6 are the ABC transporters from the ATM family, which has three members in *Arabidopsis*. All three proteins are containing a mitochondria transit peptide and have recently been shown to be localized in the mitochondria (Chen et al., 2006). Historically, the yeast homolog ATM1 was the first

ATM to be localized in the inner envelope of the mitochondria, and has been shown to be involved in synthesis of iron sulphur cluster. A yeast *atm1* mutant shows a *petite* colony phenotype, a low respiration rate and an over-accumulation of mitochondrial iron (Lill et al., 1999). *At*ATM mutants, initially called *starik* (old man in Russian) have been shown to have an important function in iron homeostasis. *At*ATM3 is able to complement the yeast *atm1* mutant (Kushnir et al., 2001). Moreover, *At*ATM3 has been shown to be involved in heavy metal resistance in *Arabidopsis* (Kim et al., 2007). More recently, Chen et al. have proposed a Fe/S cluster export activity out of the mitochondria (Chen et al., 2007). As data on the *in vivo* topology are not available and because structure and localization are similar to ABCB6, ATMs in plants might be good candidates for heme precursor import in the mitochondria. Accumulation of free porphyrins outside the mitochondria might explain the chlorosis phenotype observed in the *starik* mutants. Moreover, as iron is not incorporated into heme anymore, free iron would accumulate inside the mitochondria and become toxic. ATM mutants show an hypersensitivity to cadmium and lead (Kim et al., 2007). The mechanism proposed is a detoxification of the metals out of the mitochondria, probably with conjugated metals. One could also think of an indirect effect. As iron is not properly incorporated into PPIX, the apparent lack of iron would be compensated by an increase in iron incorporation as well as Cd and Pb incorporation. Hypothetical accumulation of CPIII in ATM mutants might be worth being investigated.

4.2.4 Heme degradation

It is commonly accepted that heme is degraded from the moment where its porphyrin cycle is opened (Fig. 5). Nevertheless, once the porphyrin ring is opened by heme oxygenase and biliverdin IX (BV) reduced to phytochromobilin, this forthcoming product is used in phytochromes as the chromophore (Terry et al., 2002). In *Arabidopsis*, 4 genes encode heme oxygenase, but a major one (HO1) encoded by *HY1* has been shown to play a predominant role in heme conversion, with however a contribution of other isoforms (HO2, HO3 and HO4) (Emborg et al., 2006). *hy1* and *hy2* (defective in phytochromobilin synthase) mutants have both been identified as allelic of the genome uncoupled (*gun*) mutants *gun2* and *gun3* respectively (Mochizuki et al., 2001) affecting plastid signalling pathways by interrupting proper plastid to nucleus signalling.

An interesting parallel exists in phytochromobilin and FCC production. Both are products of a coupled reaction of an oxygenase (HY1, PAO) and a specific reductase (HY2, RCCR). However, a large proportion of FCCs is detoxified and exported to the vacuole, whereas the phytochromobilin has an important physiological function. It might be interesting to analyze the mechanism by which heme degradation is regulated to synthesize an appropriate amount of chromophore used in phytochrome, as well as the fate of unused phytochromobilin, like an eventual vacuolar storage. It is interesting to observe that nothing is known about plant mitochondrial heme degradation, in absence of known mitochondrial biliverdin reductase.

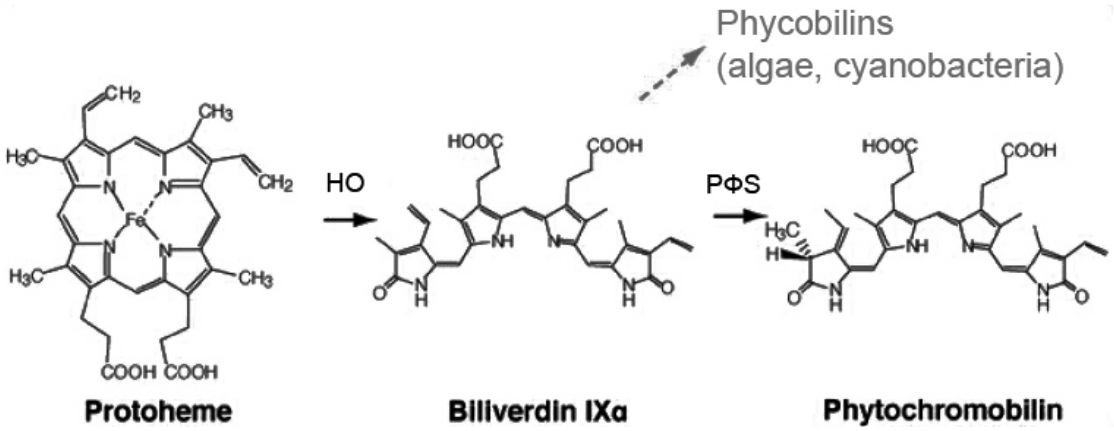

Figure 5. Heme degradation pathway in plants. Protoheme is degraded through two steps, one oxygenolytic, producing biliverdin IX followed by a reduction by phytochromobilin synthase. Degradation is described in the chloroplast. Phytochromobilin is exported from the plastid to participate in phytochrome synthesis. Adapted from Tanaka and Tanaka, 2007.

4.3 Chlorophyll retention and staygreenness

-Cosmetic stay-green

Staygreenness is a well described character found in several genetic variants. Delayed leaf senescence is mainly responsible for retention of chl, with partial or total absence of degradation of the photosynthetic apparatus (Thomas and Howarth, 2000). Increasing of plant productivity by increasing leaf carbon fixation was thought to be possible by delaying the start and the rate of senescence. Moreover, keeping plant material green throughout the senescence process might be of agricultural and economical interest, for example avoiding yellowing in broccoli (Funamoto et al., 2006) or on the other hand hastening the degreening process in canola or soybean seed maturation (Bahmaei et al., 2005). Thomas and Howarth proposed a classification of different staygreen mutants with variation in initiation or rate of senescence (Fig. 6). A large majority of mutants described belong to the so called type C staygreens, "cosmetic" staygreens, showing retention of pigment, but a normal initiation and decrease in the photosynthetic capacity. Study of these mutants allows a better understanding of the regulation between pigment degradation *sensu stricto* and the degradation of the photosynthetic apparatus, which is partially uncoupled in these mutants.

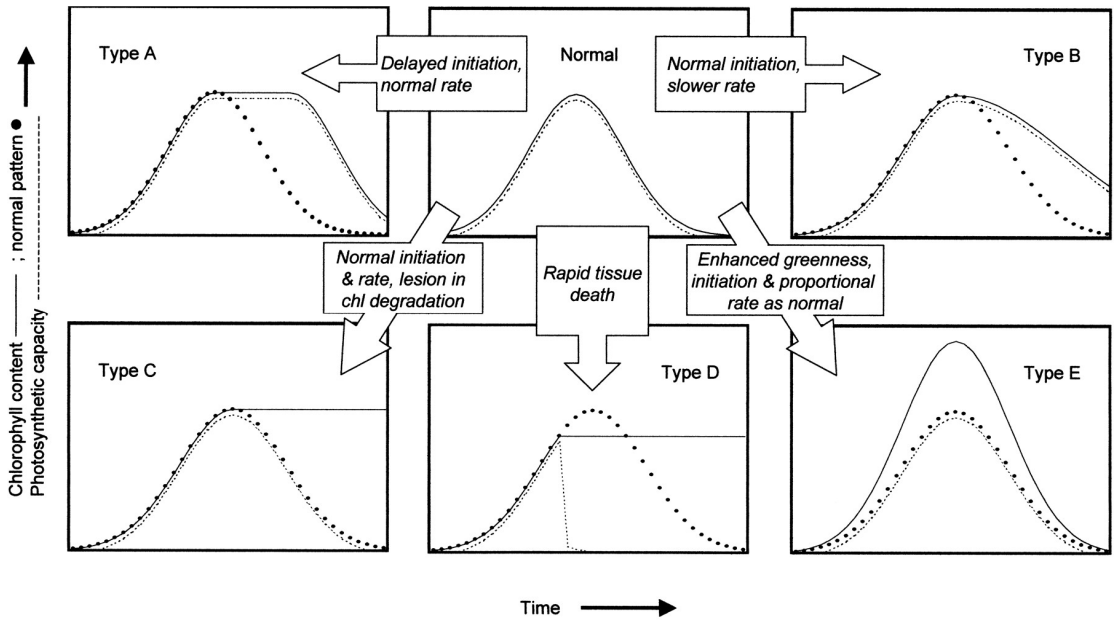

Figure 6. Five ways to stay green. Classification of different types of known staygreen mutants. Most of the staygreens described so far belong to type C, so called "cosmetic" staygreens. This cosmetic mutants are retaining green colour but show a

normal senescence process with normal decrease of their photosynthetic activity during senescence. From Thomas and Howarth, (2000).

-Chl *b* reductase

Cloning of NYC1 from rice (Kusaba et al., 2007) and analysis of respective mutant, *nyc1*, showed retention of chl *a* and *b* as well as retention of light harvesting complex from photosystem II (LHCII). NYC1 activity remains elusive, but is thought to be responsible for reduction of chl *b*, localized mainly in LHCII. NYC1 might be a primary element of the regulation of chl breakdown.

-Chlorophyllase mutant: need for a staygreen ?

Arabidopsis chlase mutants (*clh1-1* and *clh2-1*) have been initially studied in respect of biotic and abiotic stress response rather than during senescence (Benedetti et al., 1998). Study of one insertion mutant of either *At*CLH1, CLH2 and a double mutant did not show any obvious phenotype during dark incubated senescence (Schenk et al., 2007). Moreover, FCC and NCC were accumulating in these lines like in WT (Schenk et al., 2007). Absence of chlase is expected to cause either retention of chl within the LHC complexes or of free chl release. This was not observed in *clh1-1* and *2-1* mutants. These data question the relevance of CLH function as chlase *in vivo*. Preliminary experiments indicate that a mutant depleted in a chloroplastic esterase tentatively called CFC1 (candidate for chlorophyllase) show a type C staygreen phenotype during senescence. Experiments are currently made for confirming CFC1 function as chlorophyllase (S. Hörtensteiner and S. Schelbert, personal communication).

-PAO1 and SGR

Another staygreen mutant (in dark) is the *pao1* mutant depleted in PAO. Due to the accumulation of phototoxic pheide *a*, *pao1* plants show a light-dependent lesion mimic phenotype. It was thought that pheide accumulation induces feedback inhibition of the degradation, but this remains to be shown (Pružinská et al., 2005).

The majority of the type C mutants were thought to be impaired directly in enzymatic steps of the chl degradation pathway, such as *nyc1* and *pao1* (Pružinská et al., 2005; Kusaba et al., 2007), but recently, a further type of stay-green mutants has become a major focus in plant senescence research. These mutants are defective in a gene

originally identified in the Bf993 mutant of *Festuca pratensis* (Thomas, 1987). In this mutant, it has been shown that even when photosynthetic activity was reduced, a large proportion of the photosynthetic proteins remained stable, although their mRNA expression decreased, suggesting a decrease of protein turnover (Thomas et al., 1992). Excess of chl in Bf993 has been shown to induce an increase of non-cyclic electron transport, leading to an increase photorespiration in the mutant without any significant oxidative stress observed (Kingston-Smith et al., 1997). The gene was termed *SID* (*senescence-induced degradation*), but orthologous genes from rice, pea and *Arabidopsis* have now been designated *SGR* (*STAY-GREEN*) (Jiang et al., 1993; Park et al., 2007; Sato et al., 2007), *SGN* (Park et al., 2007) or *NYE1* (*nonyellowing*) (Ren et al., 2007). Introgression of the *sid* locus into *Lolium* species allowed the molecular tagging of the gene (Thomas et al., 1997). By exploiting the high micro synteny between *Lolium-Festuca* and rice, it was possible to identify the candidate locus in a *Lolium* staygreen mapping population that corresponded to a staygreen locus (*sgr*) in rice (Armstead et al., 2006). Silencing of the orthologous gene, *Atsgr1* (At4g22920) of *Arabidopsis*, caused the same staygreenness as in *Festuca* or *Lolium* (Armstead et al., 2007). Along with the retention of chl, chl-binding proteins were shown to be retained in the mutants (Hilditch et al., 1989; Jiang et al., 2007; Park et al., 2007; Sato et al., 2007). Recently, it was demonstrated that rice SGR is able to specifically interact with LHCII subunits (Park et al., 2007). This together with the retention of proteins in the mutants, suggested that SGR might be involved in dismantling chl-protein complexes as a prerequisite for both chl and apoprotein degradation.

4.4 ABC transporters

Part of this work was the characterization of primary active porphyrin transporters involved in chl degradation (see section 6). Here, I provide some basic overview on this major family of translocators. First obvious discrepancy observed is the number of genes present in different organisms. In *Arabidopsis* and rice more than 120 ORF may encode an ABC transporter, whereas in human or mouse, only 50-60 predicted genes are found (Sanchez-Fernandez et al., 2001). ABC transporters are primary active pumps using MgATP to drive transport of substrates. A common feature is the inhibition of their transport activity by vanadate. ABC transporters in plants are classified in some 13 families according to the topology of their domains. An active transporter unit is comprised of at least two transmembrane domains (TMD) and two nucleotide binding folds (NBF). Positioned in opposite symmetry, these domains could be gathered on a single polypeptide (full-size transporters, MDR, MRP, PDR, PMP and AOH family) or on two polypeptides (half-size transporters, ATH, ATM, WBC, TAP) working as dimers. Some bacterial ABC transporters (archaic) are acting with a single domain on each polypeptide, like BtuCD, a vitamin B12 carrier (Di Bartolo et al., 2006). The NBF contains three highly conserved features comprised of around 200 amino acids, the Walker A, Walker B, and the ABC signature (Rea, 2007). Some of the proteins containing the Walker motifs are also soluble and classified as ABC proteins (RLL, GCN, SMC and NAP family), but their function is unclear.

In this section I will focus only on three families which have been shown or thought to transport porphyrins in plants or mammals, MRPs and WBCs. The probable involvement of ATM transporters in porphyrin transport has already been discussed in section 4.2.3. Porphyrin transport might not be restricted to these families, as major redundancy in substrate specificity has been suggested many times (Rea, 2007).

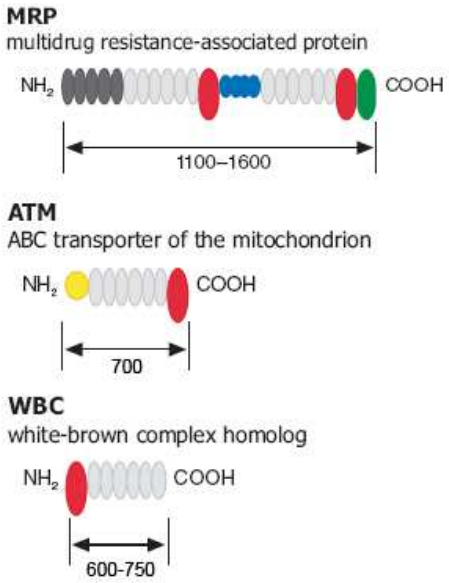

Figure 7. Topology of the domains of three families of ABC transporters: MRP, ATM and WBC. Different domains have been coloured: NBFs in red, linker in blue, C-term extension in green, N-term signal peptide in yellow, N-term extension in dark gray. Adapted from Rea, 2007.

- MRP family (ABCC)

MRP stands for multidrug resistance protein and is the second largest family of full-size transporters with 15 members in *Arabidopsis* (Klein et al., 2006) and 17 in *rice* (Garcia et al., 2004). MRPs differ from MDRs by the presence of an additional transmembrane domain (TMD0) of around 220 amino acids and are mostly found at the tonoplast (Fig. 7). Plants MRPs are showing a low similarity with the yeast or animal MRPs, suggesting a plant specific transport system.

*At*MRP1 to 5 are responsible for detoxifying processes by storing glutathione S-conjugated compounds (like GS-anthocyanin) in the vacuole, and are able to complement the yeast *ycf1* mutant depleted in a vacuolar yeast MRP (Rea et al., 1998). But they are also able to transport glucuronate conjugates (Klein et al., 2004), and the final chl catabolite *Bn*-NCC-1 (Lu et al., 1998; Tommasini et al., 1998).

*At*MRP3 has been shown to have a wide spectrum of substrates, such as glucuronated 17-β-estradiol (Klein et al., 1998), the herbicide metolachlor-GS conjugate, GSH and oxidised GSH (GSSG) as well as *Bn*-NCC-1, with high affinity (Km of 15 µM, (Tommasini et al., 1998). *At*MRP2 but not *At*MRP1 has also been shown to transport *Bn*-NCC-1 in yeast (Lu et al., 1998). Involvement of MRP in chl degradation helped to classify this pathway as a detoxification process. In fact, not NCC itself but FCC is the natural substrate to be imported to the vacuole (Hinder et al., 1996). RCC, FCC

and NCC are sharing similar features in their chemical structure as all are linear plane tetrapyrroles, supposing they could all be transported. Depending on the species, FCCs are however showing different sets of modifications on their side chains which are changing their polarity. MRPs may be involved *in vivo* in the tonoplastic import of FCC and MRP2 is expressed at high level in senescence (Genevestigator). High redundancy in transport processes is making single mutant studies difficult, as plants might compensate the absence of a single transporter. As a consequence, the *in vivo* vacuolar transporter has not yet been identified. Additional features to the MRP's primary transporter function are the possibility of modulating other transporters, like ABCC transporters in human are known to regulate their own activity. *Hs*ABCC7, the cystic fibrosis transmembrane conductance regulator (CFTR), has a chloride channel activity and regulates potassium channels (Gadsby et al., 2006). Likewise, the sulfonylurea receptor (SUR, ABCC8) is a regulatory subunit of the ATP sensitive potassium channel IKATP, with no transport function being described so far (Vila-Carriles et al., 2007). In plants, the plasma membrane transporters, *At*MRP4 and 5, have been shown to regulate guard cell movement by regulating S-type anion channels (Klein et al., 2004).

- WBC family (ABCG)

The *Arabidopsis* genome contains 28 transporters of the White Brown Complex family, characterized by a reverse-oriented domain organisation (Fig. 7). WBCs were first identified in *Drosophila* eyes, where heterodimers of white and scarlet or white and brown are responsible for the transport of OH-kynurenine or drosopterine, respectively (Mackenzie et al., 2000). WBCs are homologous to the mammalian ABCG family, which comprises 5 members. ABCG5/8 heterodimers are responsible for sterol uptake (Mannucci et al., 2007), whereas ABCG1 and ABCG4 are responsible for cholesterol and desmosterol efflux to high density lipoproteins in the brain (Wang et al., 2007). The most studied member, ABCG2, is responsible for drug resistance in a lot of cell lines and extruding a variety of substrates (Krishnamurthy et al., 2007). Among others, it is able to transport heme, pheide and other tetrapyrroles, but not monopyrroles (Krishnamurthy and Schuetz, 2005).

In *Arabidopsis*, only three WBC/ABCGs have been described so far, and only one, *At*WBC12, was shown to transport a natural substrate. The *eceriferum* 5 (*cer5*) mutant depleted in WBC12 accumulates cytoplasmic laminates, containing long chain fatty

acids. Wax components are not able to be secreted and the major wax components (alkanes, ketones and alcohols) are missing (Pighin et al., 2004). Recently, a close homolog, *At*WBC11 has been shown to export wax elements, such as cutin (Panikashvili et al., 2007). The phenotype of respective mutants is resembling the phenotype seen in cells of humans suffering adenoleukodystrophy (Kemp and Wanders, 2007). Another transport activity has been shown for a putative vacuolar *At*WBC19, involved in kanamycin resistance, as a *wbc19* mutant is hypersensitive to the antibiotic treatment (Mentewab and Stewart, 2005). This transporter is supposed to participate in vacuolar detoxification. Its surprising specificity for kanamycin and not for gentamycin or other antibiotics suggested that *At*WBC19 might be a helpful tool in biotechnology. Indeed, the neomycin phosphotransferase II (*nptII*) gene used in classical kanamycin resistance is derived from a bacterial source and confers resistance to many related antibiotics. *At*WBC19 might be used as a selectable marker for kanamycin resistance, avoiding the danger of horizontal gene transfer of *nptII* (Rea, 2005). Two other WBCs have been partially characterized; the first in cotton (*Gossypium hirsutum*), *Gh*WBC1, a putative plasma membrane transporter of lipids necessary for cotton fibre maturation (Zhu et al., 2003); the second in tobacco (*Nt*WBC1), which is also suspected to be responsible for lipid trafficking in reproductive tissues, such as stigmata and styles (Otsu et al., 2004). To date, most of the WBCs described are involved in sterol or lipid translocation, and none of them is plastid localized. However, in this study, I describe the first two WBCs (*At*WBC23 and 28) which are plastid localized and may be responsible for FCC export out of the chloroplast (see section 6).

Soluble proteins from the NAP family (*laf6*) have been thought to be involved in PPIX trafficking but were eventually shown to be involved in other unrelated processes (Xu et al., 2005). Elucidation of porphyrin trafficking in plants is still at its beginning and the involvement of different sets of transporters, also those not belonging to the ABC family, is likely. The detoxification of chl derivatives is most probably a selective advantage for the plant, but the complex issue of redundancy will make further studies difficult to achieve.

5. Aim of the thesis

During my PhD, I tried to advance our knowledge on several aspects of the chl degradation pathway during senescence of higher plants by:

- identifying a likely transporter for export of pFCC from the chloroplast to the cytoplasm
- describing the regulatory function of the staygreen factor
- characterizing several other novel aspects of the pathway, such as the sensitivity of the PAO/RCCR reaction towards ROS

These analyses of the pathway provide a substantial improvement of our understanding how plants are degrading chl but at the same time raise new issues for further work to be done.

6. Chlorophyll breakdown : An ABC transporter involved in chlorophyll catabolite export from the chloroplast in *A. thaliana*

This chapter is gathering data in the form of an independent paper to be submitted for publication to the Journal of Biological Chemistry.

6.1 Introduction

Chlorophyll (chl) degradation occurs during senescence of higher plants and is a well described detoxification process (Matile et al., 1999; Hörtensteiner, 2006). From the removal from its apoprotein to the final storage as colourless catabolites in the vacuole, chl is taken through a well defined degradation pathway. First, it involves the formation of pheophorbide (pheide) by removal of phytol and magnesium by chlorophyllase and a metal chelating substance (MCS), respectively. The porphyrin macrocycle is then opened by a monooxygenase (PAO) and a reductase (RCCR), to yield fluorescent chl catabolite (FCC). Pheide oxygenation results in an intermediate, red chl catabolite (RCC), which is directly reduced to primary fluorescent catabolite (pFCC). After export from the chloroplasts, pFCC is modified or conjugated in the cytosol, and finally accumulates as non fluorescent catabolites (NCCs) inside the vacuole (Matile et al., 1988; Hinder et al., 1996). A primary active transport system for *Bn*-NCC-1 has been described in barley vacuoles with a Km of 15 μM. The transporter exhibited a surprisingly high affinity for an FCC (Hinder et al., 1996) and it could be shown that FCCs are non-enzymatically tautomerized to NCCs inside the acidic vacuole (Oberhuber et al., 2003). FCC, RCC and NCC as linear tetrapyrroles have a spatial configuration which is almost flat indicating that *in vitro* all three could be accepted as substrate for transport. Although two ABC transporters *At*MRP2 and *At*MRP3 have been shown to transport NCCs in yeast, the exact molecular identity of the *in vivo* vacuolar transporters is still missing (Lu et al., 1998; Tommasini et al., 1998). The *Arabidopsis* genome contains 15 MRPs, several of which, like MRP4, localize to the tonoplast (Klein et al., 2004) and they might have a redundant function. A first transport step for chl catabolites is needed to export FCCs from the chloroplast. Export of pFCC and a modified FCC out of isolated barley gerontoplasts is also

associated with a primary active process, which has been shown to require MgATP hydrolysis (Matile et al., 1992). The nature of the chloroplast exporter is not yet known. A knock-out mouse devoid of an ABC transporter of the G family, ABCG2 (BCRP1), (Krishnamurthy and Schuetz, 2006) has been shown to produce a porphyria-like phenotype (Jonker et al., 2002). ABCG2 is one of the most studied ABCG transporters and is known to be involved in extrusion out of the cells of a diverse set of structurally unrelated xenobiotics and drugs (mitoxanthrone, topotecan, camptothecin), as well as sterols and porphyrins (Abbott, 2003; Hardwick et al., 2007). It is involved in porphyrin homeostasis in erythroid cells and is able to transport heme, protoporphyrin IX (PPIX), pheide and other tetrapyrroles, but not monopyrroles (Krishnamurthy and Schuetz, 2005, 2006). The mammalian ABCG family is comprised of 5 members: ABCG1 and ABCG4 are responsible for cholesterol and desmosterol efflux from high density liposomes in the brain (Wang et al., 2007), and ABCG5/8 are also involved in sterol homeostasis. These two transporters are working as dimers and a defect causes β-systerolemia (Schmitz et al., 2001; Mannucci et al., 2007). $ABCG2^{-/-}$ mice fed with pheide have been shown to develop photosensitive lesions located at the ears, the most light-exposed part of the animal. The lesions result from accumulation of pheide-derived products in the blood as well as in the bile (Jonker et al., 2002). Moreover, $ABCG2^{-/-}$ mice erythrocytes accumulated PPIX, suggesting an additional role of ABCG2 in porphyrin homeostasis in erythroid cells.

As ABCG2 is able to extrude chl-derived porphyrins back into the intestine (Krishnamurthy et al., 2007), plant homologs of this transporter namely members of the WBC family of transporters are likely candidates for FCC export from the plastid. These transporters belong to the superfamily of primary active ABC (ATP Binding Cassette) transporters, with 120 ORFs predicted in *Arabidopsis* (Rea, 2007). They are characterized by the association of ATP hydrolysis with a substrate-specific transport. An active translocator consists of two transmembrane domains (TMD), each domain including 4 to 6 transmembrane helices and two nucleotide-binding folds (NBF), each containing Walker A, B and C boxes (Sanchez-Fernandez et al., 2001). Some of the ABC transporters gather all the domains in one single peptide, but others, like WBCs work as homo- or heterodimers. From the Aramemnon server (http://crombec.botanik.uni-koeln.de/) only 13 ABC transporters in *Arabidopsis* are

predicted to be chloroplastic but no chloroplast-associated ABC transporter has functionally been characterized yet.

WBC is the abbreviation of White Brown Complex initially described in *Drosophila* eyes. White and brown dimers transport drosopterine while white and scarlet transport 3-hydroxykynurenine (Mackenzie et al., 2000). The WBC sub-family is one of the largest in *Arabidopsis* with 28 members (Rea, 2007), but only a few of them have been functionally characterized. *At*WBC19 was shown to be involved in kanamycin resistance by detoxifying the antibiotic to the vacuole (Mentewab and Stewart, 2005; Rommens, 2006). An other member, *At*WBC12 (*eceriferum 5*, CER5), located in the plasma membrane of epidermal cells, is responsible for the export of wax components to the cuticule. Mutants impaired in WBC12 accumulate cytoplasmic laminates of long chain fatty acids. Wax components are not able to be secreted and the major wax components (alkanes, ketones and alcohols) are missing (Pighin et al., 2004). Recently, a close homolog, *At*WBC11 has been shown to transport lipids as well and participate in wax and cutin secretion (Panikashvili et al., 2007). Cytoplasmic lipid accumulation is similar to the phenotype observed in brain and adrenal tissue cells of humans suffering adenoleukodystrophy due to a mutation in ABCD1 (Kemp and Wanders, 2007). The cotton transporter *Gh*WBC1 (*At*WBC11 homolog) has been shown to be involved in the elongation of the cotton fibre, is plasma membrane located and showed a similar expression as lipid metabolism related genes (Zhu et al., 2003). The tobacco *Nt*WBC1 (homolog to *At*WBC16) is exclusively expressed in reproductive organs and contains a putative steroidogenic acute regulatory protein signature (START) domain, involved in sterol-dependent transduction pathways (Otsu et al., 2004). None of the WBC transporters described so far are localized to the chloroplast, and *in vivo* substrates have not been elucidated, even if an involvement in lipid transport has been suggested. Like most of the ABC transporters, members of the WBC family might allow translocation of a wide range of substrates (Pighin et al., 2004).

In this study, we describe the identification and characterization of a putative half-size ABC transporter, namely *At*WBC23 involved in chl catabolite export from plastids. We base our analysis on the finding that the homologous ABCG2 transporter is responsible for chl catabolite detoxification in mouse. *At*WBC23 is shown to localize to the chloroplast and is expressed in a senescence related manner. When heterologously expressed in C2C12 cells, it confers transport of pheide. Finally *wbc23*

knockout lines are delayed in chl breakdown during senescence. We conclude that *At*WBC23 participates in chl catabolite export from the chloroplast, but most likely other transporters are involved in addition.

6.2 Materials and methods

6.2.1 Mouse bile extract analysis

Bile from ABCG2$^{-/-}$ mice fed with synthetic food containing pheide was obtained from H. Jonker and A. Schinkel (Amsterdam, The Netherlands). Bile was collected according to published methods (Jonker et al., 2002). Bile extracts were diluted in 2 vol of methanol and centrifuged at 16000 g for 2 min. The supernatant was analyzed by reversed-phase HPLC according to published procedures (Pružinská et al., 2007).

6.2.2 Plant material and senescence induction

The Columbia (Col-0) ecotype of *Arabidopsis thaliana* was used as the wild type. Seeds of *wbc23* (At5g06530) T-DNA insertion mutants SALK_076250, SALK_113844, SALK_024391 named *wbc23-1, -2, -3,* respectively, were obtained from the European *Arabidopsis* Stock Centre (Nottingham, UK). A T-DNA line of *wbc28* (At3g52310), GABI_833F02 was obtained from GABI-KAT (Bielefeld, Germany) and named *wbc28-1*. Homozygous lines from segregating populations of all lines (Fig. 14A, B) were identified by PCR using following primers :

- LBa 5'-ATGGTTCACGTAGTGGGCCATC-3'
- 23RP-1 5'-TAAGGTCACCTCACGGCTCC-3'
- 23LP-1 5'-ACCATCCGTACGTAGAAACTG-3'
- 23RP2- 5'-ATGTCAATGGAGAAGCCACC-3'
- LB_{GABI} 5'-ATTTGGACGTGAATGTAGACAC-3'
- 28RP 5'-GCCTCTAGTGCTTCTCTTGGACTA-3'
- 28LP 5'-GTCACCTTGTATGTGATATCTATG-3'

wbc23-1 and *wbc28-1* knockout lines were used as reference lines for further investigations, and the insertion sites were cloned and sequenced (Fig. 14A and B). RCCR was silenced in *wbc23-1* using pGreen0179 vector containing silencing construct for RCCR, according to a published method (Pružinská et al., 2007).

Plants were grown on soil in long-day (16 h/8 h) or short-day (8 h/16 h) under fluorescent light of 60 to 120 µmol photons m^{-2} s^{-1} at 22°C. For senescence induction, leaves from 3 to 4 week-old (long-day) or 7 week-old (short-day) plants (Fig. 14C)

were excised and incubated in permanent darkness (dDD) on wet filter paper for up to 7 d at ambient temperature.

6.2.3 RNA isolation and real-time PCR

RNA was prepared using the Plant RNeasy kit (Qiagen). After DNA digestion with RQ1 RNase-free DNase (Promega), 1 µg of RNA was reverse-transcribed using the RETROscript kit (Ambion). Quantitative PCR was performed in a LightCycler (Roche Diagnostics) using the QuantiTect SYBR Green PCR kit (Qiagen). Ten- to 100-fold dilutions of first-strand cDNA reaction mixes (corresponding to 0.3–3 ng of RNA) were employed in 20 µl reactions and were used to calculate the real-time PCR efficiency of each sample. The relative expression ratios of the target gene (*WBC23*) were calculated in comparison to a reference gene (*S16*). The following specific primers were used:

S16f 5'-GGCGACTCAACCAGCTACTGA-3'

S16r 5'-CGGTAACTCTTCTGGTAACGA-3'

WBC23f 5'-GTGCCACTCGATGAAG-3'

WBC23r 5'-CTAATGTCCGACTGCCA-3'

6.2.4 Chlorophyll measurement

Chl was isolated from dark-incubated *Arabidopsis* by homogenization of leaf tissue in liquid nitrogen and subsequent 3-fold extraction into 80% acetone (v/v). After centrifugation (2 min, 16000 g) supernatants were combined (Pružinská et al., 2005) and chl concentrations were determined spectrophotometrically (Strain et al., 1971).

6.2.5 Colourless Catabolites

Colourless catabolites were extracted from senescent leaf tissues from *Arabidopsis*. 8 leaf discs (1 cm diameter) were extracted with 300 µl of 0.1 M Tris-HCl, pH 7/methanol (1:4), filtered through Miracloth paper and centrifuged for 2 min at 16000 g. The supernatant was transferred in a new tube, mixed with 150 µl of 50 mM potassium phosphate buffer pH 7 and separated by reversed phase HPLC. It consisted of a C18 Hypersil PDS column (250x 4.6 mm; 5 µm; MZ-Analysentechnik, Mainz, Germany), which was developed with a gradient (flow rate 0.5 ml min^{-1}) of solvent B

(20% (v/v) 50 mM potassium phosphate buffer, pH 7 and 80% methanol) in solvent A (50 mM potassium phosphate, pH 7) as follows: 25% to 75% gradient over 60 min, 75% to 100% over 5 min and 100% solvent B for 5 min. Peak detection was monitored with a System Gold 168 photodiode array detector (200-600 nm; Beckman Coulter, CA, USA) and a RF-10AXL fluorescence detector (excitation 320 nm; emission at 450 nm; Shimazu Corporation, Kyoto, Japan). Analysis of peaks was performed with a 32 Karat workstation (Beckman Coulter). Chl catabolites were identified by their absorption and fluorescence properties (Hörtensteiner, 2006).

6.2.6 GFP-fusion protein analysis

A cDNA for *AtWBC23* (pda04786) was obtained from the RIKEN resource. Genomic full length DNA of *WBC28* was obtained by PCR. Genes were PCR-amplified in two steps using Pfu polymerase (Promega) thereby adding Gateway adaptors and removing the stop codons. A first 15 PCR cycles were performed with the gene-specific primers consisting of gene sequences and half of the attB recombination sites, then the PCR product was re-amplified with an excess of attB1 and 2 primers to amplify the full BP recombination sites.

Following primers were used :

attB1-WBC23 5'-AAAAAGCAGATGTCAATGGAGAAGCCACC-3'

attB2-WBC23 5'-AGAAAGCTGGGTTGTTACGATCTTCATTTGCC-3'

attB1-WBC28 5'-AAAAAGCAGGCTATGGGAACCTCATCATCATC-3'

attB2-WBC28 5'-AGAAAGCTGGGTAGTTGAAGAGTGGAGCTTC-3'

attB1 5'-GGGGACAAGTTTGTACAAAAAAGCAGGCT-3'

attB2 5'-GGGGACCACTTTGTACAAGAAAGCTGGGT-3'

BP-recombination (Invitrogen) of both genes in pDONR207 was performed following the manufacturer's instruction. After verification by sequencing, LR-recombinations (Invitrogen) were done with pMDC84 (Curtis and Grossniklaus, 2003), allowing in frame fusion of GFP to the C-termini of WBC23 and WBC28. TIC-110-GFP expressed from pCL60-TIC110-GFP was used as a control for chloroplast envelope localization (F. Kessler, personal communication).

Arabidopsis protoplasts were isolated from 3-week old Col-0 plants according to Pruzinska et al. (2007) with some modifications. After careful injury of the abaxial leaf surface using sandpaper, cell walls were digested for 2 h in 0.5 M sorbitol, 10

mM MES-KOH, pH 5.8, 1 mM $CaCl_2$, 0.5% macerozyme and 1% cellulase. Protoplasts were liberated and purified on a Percoll density gradient (Hinder et al., 1996). Cell numbers were quantified with a Neubauer chamber and adjusted to a density of 2.10^7 cells ml^{-1}. Protoplasts were transformed by 20% polyethylene glycol (PEG) transformation with 20 µg plasmid according to published procedures (Schenk et al., 2007). After removing the PEG by washing two times with W5 buffer (150mM NaCl, 125 mM $CaCl_2$, 5 mM KCl, 5 mM glucose, 0.03% MES-KOH (w/v), pH 5.8), cells were incubated in W5, for 48 h before laser scanning confocal microscopic analysis (Meyer et al., 2006).

6.2.7 Cloning in mammalian expression vector and transport analysis

*WBC*23 cDNA (pda04786) was PCR amplified using Pfu polymerase (Promega) with following primers:

ansecF1 5'-GGAATTCTTCAATGGAGAAGCC-3'

ansecR2 5'-ATAGTTTAGCGGCCGCTGTTACGATCTTCATTTGCCTTAG-3'

Thereby the N-terminal predicted transit peptide (77 amino acids) was removed and a c-myc tag added to the C-term. After restriction digest, the fragment was cloned into *EcoR*I/*Not*I digested pSecTag2B (Invitrogen) and the sequence was verified. The obtained construct was named p23myc. pSecTag2B allows expression of proteins fused at the N-terminus to the murine Ig κ-chain leader sequence for protein secretion. C2C12 myoblasts were seeded in 10 cm dishes allowed to be 80% confluent. 24 h later cells were transfected with p23myc using Fugene HD (Roche Diagnostics, Rotkreuz, Switzerland) according to the manufacturer's protocol. 24 h post-transfection cells were typsinized and seeded in 12 well plates at a density of 150000 cells per well. 48 h post transfection the medium was changed to serum-free charcotreated DMEM containing either 20 µM pheide or 20 µM RCC, and incubated for 1 h at 37°C. Cells were then washed three times with ice cold PBS and stored at -80°C. Cells were resuspended in 60 µl methanol and centrifuged 2 min at 16000 g. Supernatant was analyzed on reversed-phase HPLC according to published procedures (Pružinská et al., 2007).

6.3 Results

6.3.1 Identification of RCC-like chl degradation products in mouse

ABCG2$^{-/-}$ mice were shown to accumulate red compounds in the blood as well as in the bile when fed with synthetic food containing pheide (Jonker et al., 2002). Analysis of bile extracts by reversed-phase HPLC demonstrated accumulation of one major and two minor compounds (Fig. 8A) which exhibited spectra similar to a standard RCC from *Chlorella prototheco*ides with absorption maxima at 320 and 485 nm (Fig. 8B). No accumulation of these compounds was observed in ABCG2$^{-/-}$ mice fed without pheide, suggesting the RCC-like products being derived from pheide. However retention times of these *Mm*RCC-like compounds (0*, 1* and 2*) did not correspond to any known RCC (Fig. 8A) (Pružinská et al., 2007). The *Mm*RCC-like pigments may traffic from the gut to the liver, and then be exported to the gall bladder. Side chain modifications such as demethylation or conjugations likely occur in a different way in the mouse than in plants. Unfortunately, the structures of the *Mm*RCC-like pigments have not been resolved yet by MS, but preliminary MS analysis indicate a relation to plant-type RCCs (T. Müller and B. Kräutler, personal communication). Further characterization of the structure and analysis of the way these RCC-like compounds are formed in ABCG2$^{-/-}$ mice, is on the way.

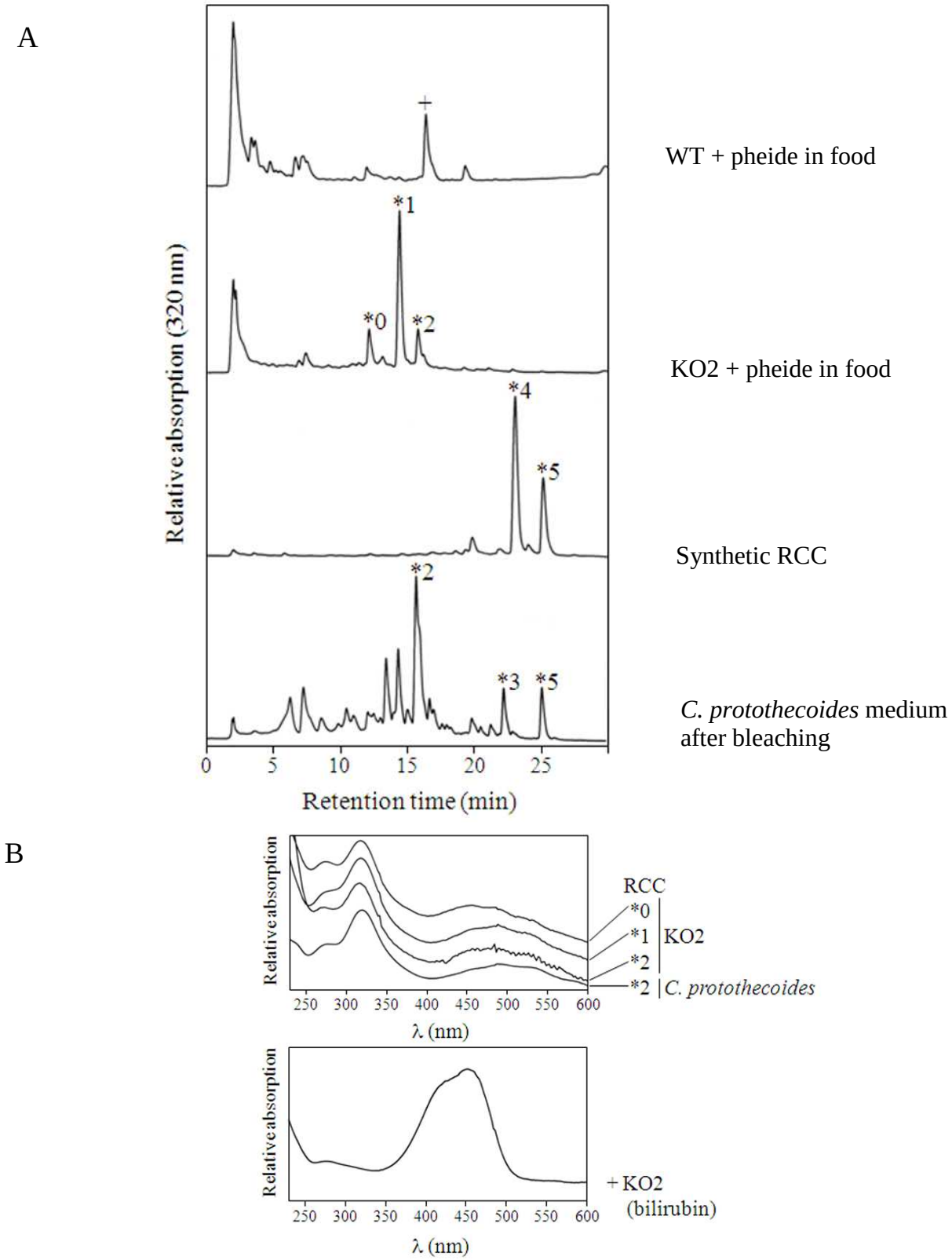

Figure 8. ABCG2$^{-/-}$ mice accumulate RCC-like compounds. A. HPLC traces of bile extracts from wild type mouse fed with pheide containing food (line 1). ABCG2$^{-/-}$ mice fed with a synthetic diet containing pheide (line 2). The bile extract of ABCG2$^{-/-}$ mouse fed with a pheide-free synthetic diet was similar to the WT (data not shown). Synthetic RCC (Kräutler et al., 1997) (line 3) and collected medium of *C. prototheco*ides after bleaching (Hörtensteiner et al., 2000) (line 4) were analyzed as standards. **B.** Spectrum of peaks *0, *1 and *2 were similar to standard RCCs. The spectrum of peak + corresponds to bilirubin.

A.

Number	Gene	Blast Score	Chlp	Mito	Sec path
At5g06530	WBC23	4e-76	4.8	0	0
At3g52310	WBC28	5e-73	15.1	0	0
At1g31770	WBC14	2e-72	0	0	0
At1g17840	WBC11	6e-69	1	0	0
At1g51500	WBC12	1e-67	0.6	0.9	0
At4g27420	WBC9	9e-67	0	0	0
At1g51460	WBC13	9e-67	0	0	1.3
At3g21090	WBC15	1e-66	0.6	1.5	0
At2g13610	WBC5	2e-64	0	0	0
At3g13220	WBC27	4e-64	0	0	0
At1g71960	WBC26	1e-63	3.8	0	0.3
At3g55130	WBC19	2e-62	0	6.6	0
At3g53110	WBC18	2e-60	1.7	0	0.1
At3g53510	WBC20	4e-60	4.6	0.6	2.4
At2g01320	WBC7	4e-59	0.3	0	9.4
At2g37360	WBC2	2e-57	1.6	1.5	0
At5g13580	WBC6	3e-57	2.5	0	0

B.

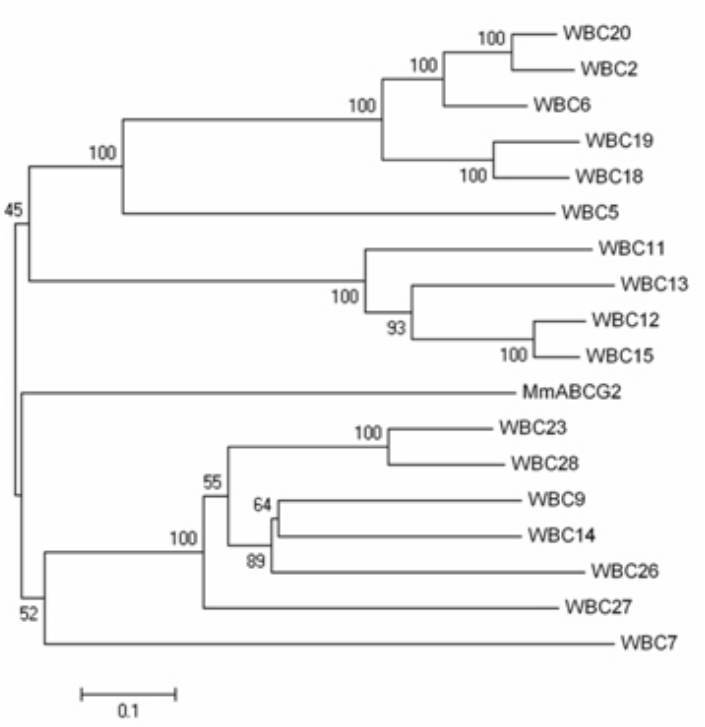

Figure 9. Identification of ABCG2 homologs in *Arabidopsis* A. Blast scores and the intracellular localization of ABCG2 homologs in the *Arabidopsis* proteome. Consensus scores of prediction from the Aramemnon database show localization prediction for chloroplast (Chlp), mitochondria (Mito) and proteins processed through the secretory pathway (Sec path). Aramemnon (http://crombec.botanik.uni-koeln.de/) is gathering 17 subcellular localization programs. **B.** Phylogenetic tree of 17 most similar to *Mm*ABCG2. Sequences were aligned using ClustaIW and the phylogenetic tree estimated with DIALIGN (http://bibiserv.techfak.uni-bielefeld.de/dialign/) using the maximum likehood method. Bootstrap values using 500 replicates are shown at branchpoints with a cut-off of 30.

6.3.2 Homologs of ABCG2 in *Arabidopsis*

ABCG2 has been shown in animals to be able to transport tetrapyrroles, such as pheide and PPIX. Plant homologs of ABCG2 may thus be able to transport porphyrins as well. We blasted ABCG2 against the *Arabidopsis* protein database and looked for the closest homologs of ABCG2. The first 17 hits all belonged to the ABCG/WBC family (Fig. 9).

In this selected transporter set, we looked for chloroplastic predicted homologs in order to identify possible candidates for FCC exporters from the chloroplast. The two closest proteins to ABCG2, WBC23 and 28, were both predicted to be localized in the chloroplast, with a high consensus score for WBC28 (Fig. 9A). More transporters, such as WBC26, 18 and 6 were also predicted to exclusively localize to the chloroplast, some others were predicted to localize to both mitochondria and chloroplast (WBC12, 15 and 2). The consensus scores shown in Fig. 9A gather prediction results from 17 programs (http://crombec.botanik.uni-koeln.de). We performed a phylogenetic analysis of the highest blast scored *At*WBCs and ABCG2 protein sequences using the maximum likehood method (Fig. 9B). Seven different WBC were clustering together with ABCG2, including WBC23 and 28, which are very close related to each other (67% similarity). Protein sequences of these seven WBC were aligned using DIALIGN (http://bibiserv.techfak.uni-bielefeld.de/dialign/) and Genedoc software (Fig. 10). Besides the significant similarity of all these transporters, a major difference separated WBC23 and 28 from the others: the presence of a N-terminal extension, which, at least for WBC23, covers the predicted chloroplast transit peptide (Fig. 10).

Concerning the gene structure, two splicing versions have been predicted for *WBC23 in silico*, giving rise to two proteins with alternative lengths of either 751 or 691 amino acids. However the short version is supported by only a single EST sequence (EST AI1992988) and might be an artefact. All further experiments and cloning was done using a cDNA corresponding to the 751 amino acid version of WBC23.

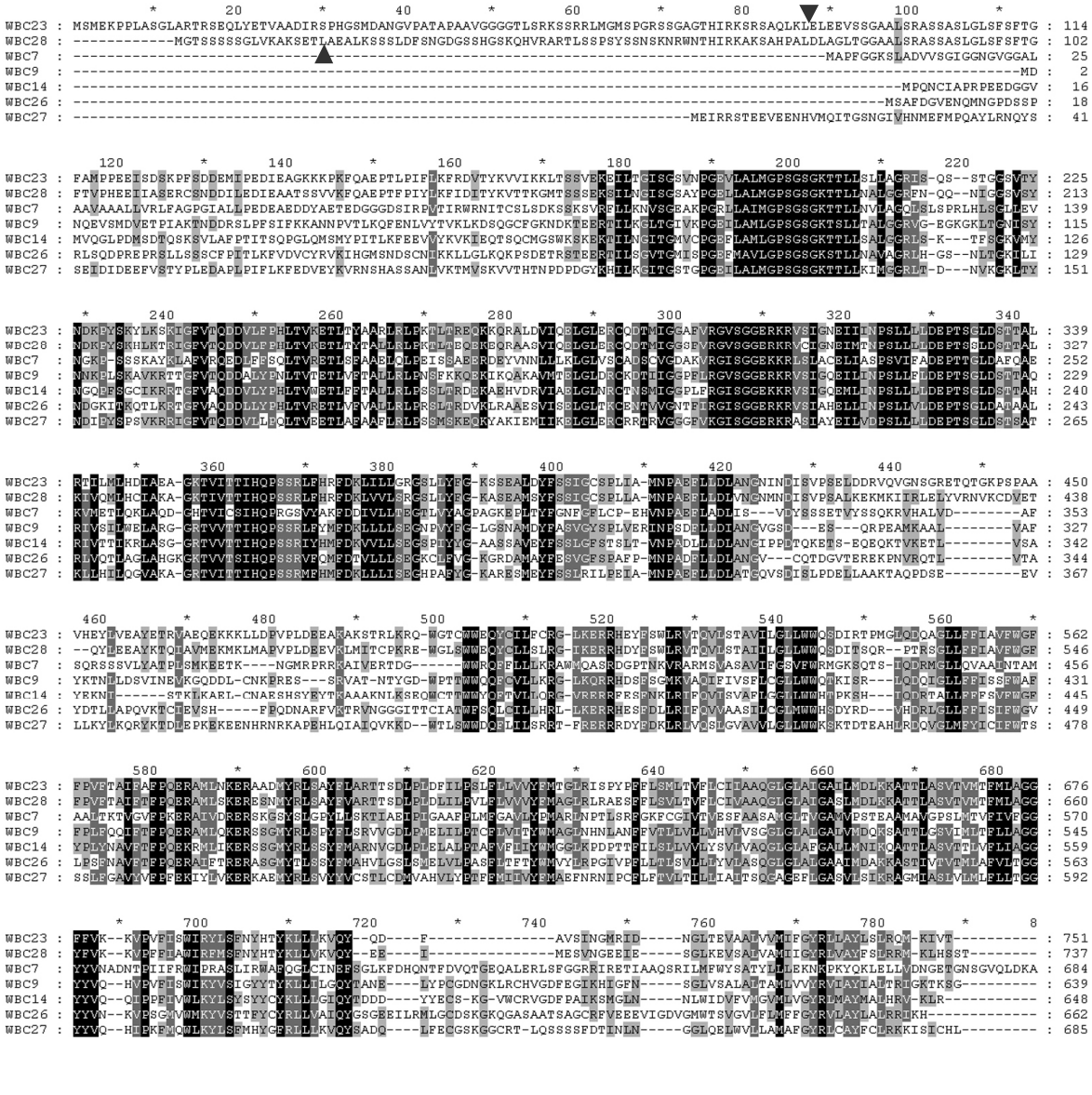

Figure 10. Sequence alignment from *At*WBCs clustering with *Mm*ABCG2. The sequences were aligned using the DIALIGN software. Black shading with white letters, grey shading with white letters and grey shading with black letters reflect 80, 60 and 40% sequence conservation, respectively, with Blosum62 similarity groups enabled. Protein sequences were obtained from TAIR (www.arabidopsis.org). Black triangles indicate predicted cleavage sites for chloroplast transit peptides in WBC23 and 28 (http://www.cbs.dtu.dk/services/ChloroP).

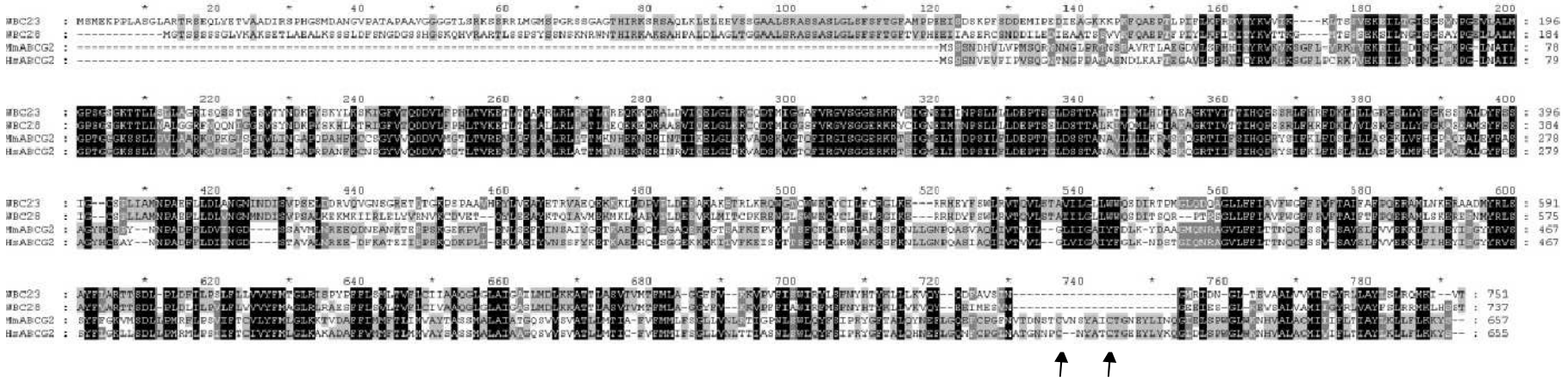

Figure 11. Sequence alignment of *At*WBC23 and 28 with human *Hs*ABCG2 and mouse *Mm*ABCG2. The sequences were aligned using the DIALIGN software. Black shading with white letters, grey shading with white letters and grey shading with black letters reflect 80, 60 and 40% sequence conservation, respectively, with Blosum62 similarity groups enabled. Arrows indicate cystein residues responsible for protein stabilization in the mammalian transporters (Wakabayashi et al., 2007). Accession numbers : *Mm*ABCG2, NP001032555; *Hs*ABCG2, AY017168.

With good similarity scores to ABCG2 and chloroplastic prediction, WBC23 and 28 were the best candidates for chl catabolite exporters in the chloroplast. Aligning WBC23 and 28 to *Mm*ABCG2 and *Hs*ABCG2 showed a significant homology, especially within the ABC signatures. N-terminal extensions are likely containing the chloroplast targeting sequences, despite the questionable prediction from ChloroP with respectively 88 and 18 amino acids, against an observed extension of 116 and 105 amino acids in length in WBC23 and 28 compared to ABCG2 (Fig. 11). WBC26 is predicted to the chloroplast as well, but is lacking a N-terminal extension, with a ChloroP predicted transit peptide of 8 amino acids (data not shown).

6.3.3 WBC23 and 28 localize in the chloroplast

To determine the subcellular localization of WBC23 and 28, we cloned WBC23 cDNA and a WBC28 genomic sequence into pMDC84 (Curtis and Grossniklaus, 2003), and thereby fused GFP to the C-termini of both proteins. The constructs were transformed into living *Arabidopsis* protoplasts and analyzed with confocal laser scanning microscopy. Both WBC23 and WBC28 showed a clear chloroplastic localization confirmed by comparison with the localization of a subunit of the translocon of the inner envelope of chloroplasts (TIC110) fused to GFP (Fig. 12). However, precise localization of both proteins within the chloroplast was not possible. The GFP signals in Fig. 12 indicate a localization of WBC23 and WBC28 in the envelope, but the picture is less clear than for TIC110. Marked differences in plastid shape are due to different growth conditions. Repetition of this experiment is on the way to get more homogenous pictures. Western blotting of transiently transformed protoplasts using anti-GFP antibodies (Sigma) confirmed the presence of the expressed fusion proteins (data not shown). Together with the predictions and alignments, the GFP data clearly indicate that *At*WBC23 and 28 are both located in the chloroplast.

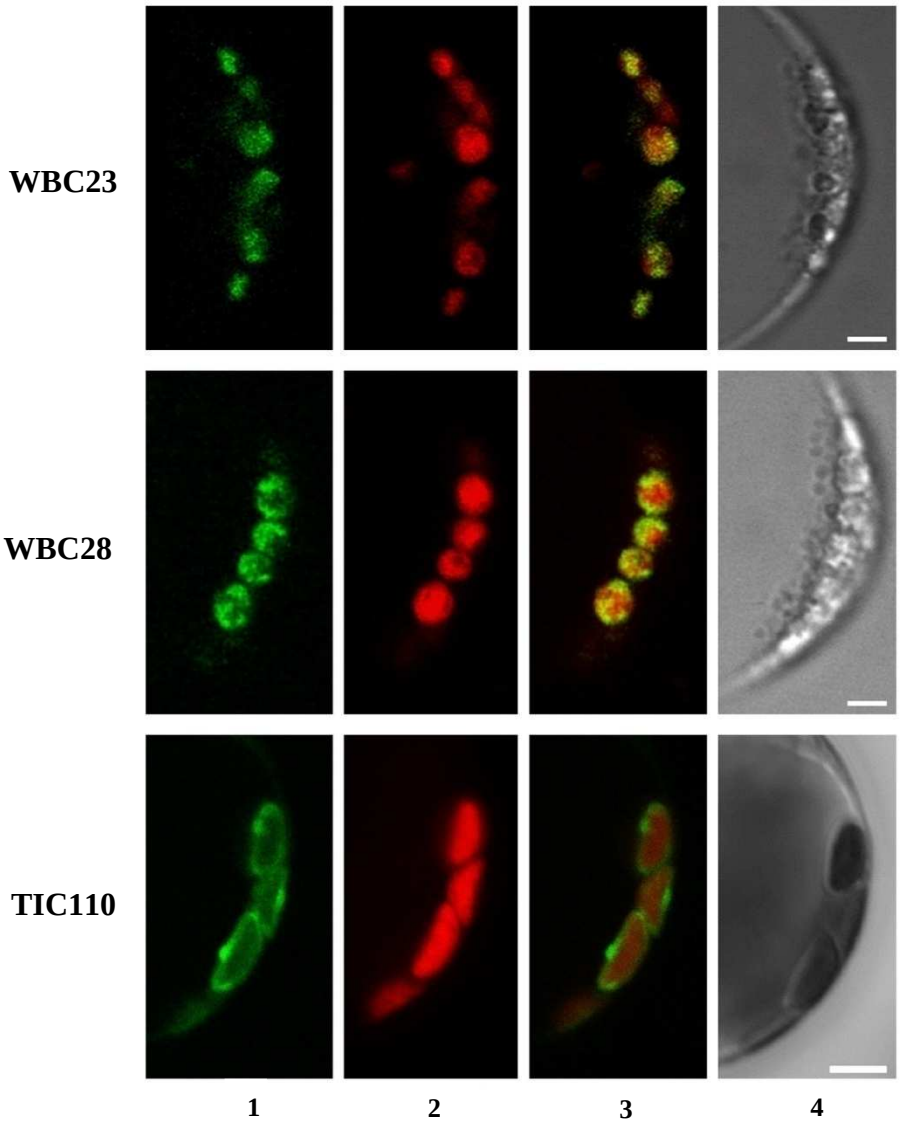

Figure 12. *At*WBC23:GFP and *At*WBC28:GFP are targeted to chloroplasts. Transient expression in *Arabidopsis* protoplasts of GFP fused in frame to the C-term of full-length *At*WBC23 or *At*WBC28. TIC110-GFP was used as control for targeting to the envelope of the chloroplast. GFP (green, lane 1) and chl autofluorescence (red, lane 2) were examined by laser scanning confocal microscopy. Merge of GFP and autofluorescence (lane 3) and bright field images (line 4). Bar length, 10 μm.

6.3.4 *WBC23* is senescence-specifically expressed

Microarray data available from the Genevestigator database (Zimmermann et al., 2004) showed increased expression of both *WBC23* and *28* in senescent leaves, cauline leaves and sepals compared to other tissues, as well as an overall upregulation of these two genes during senescence. Real-time PCR analysis on dark incubated detached leaves confirmed an approximately 5 fold increase in *WBC23* expression, compared to the housekeeping gene *S16* between 0 and 9 d in the dark. Similar results were found in senescing attached leaves, where the senescence state had been evaluated on the basis of chl content of the leaves (Fig. 13A). When analyzing the Genevestigator data, *PAO* showed similar expression to *WBC23* during the whole life span and both genes were expressed mainly in senescent and cauline leaves as well as in the sepals (Fig. 13C, D). Expression of *WBC23* in different tissues was assessed by real-time PCR. It was mainly expressed in green tissues with highest expression in the stem. Compared with *WBC23*, *WBC28* was expressed in much lower amounts and no clear data could be obtained in real-time PCR experiments. Genevestigator data confirmed our observation showing an extremely low expression (2000x less) of *WBC28* in comparison to *WBC23* (Fig. 13C, D). Altogether, the expression analysis shows that *WBC23* is a senescence activated gene, which is specifically expressed in organs where chl degradation occur, indicating a putative function in this processes. Furthermore, it shows a good correlation to *PAO* expression.

A.

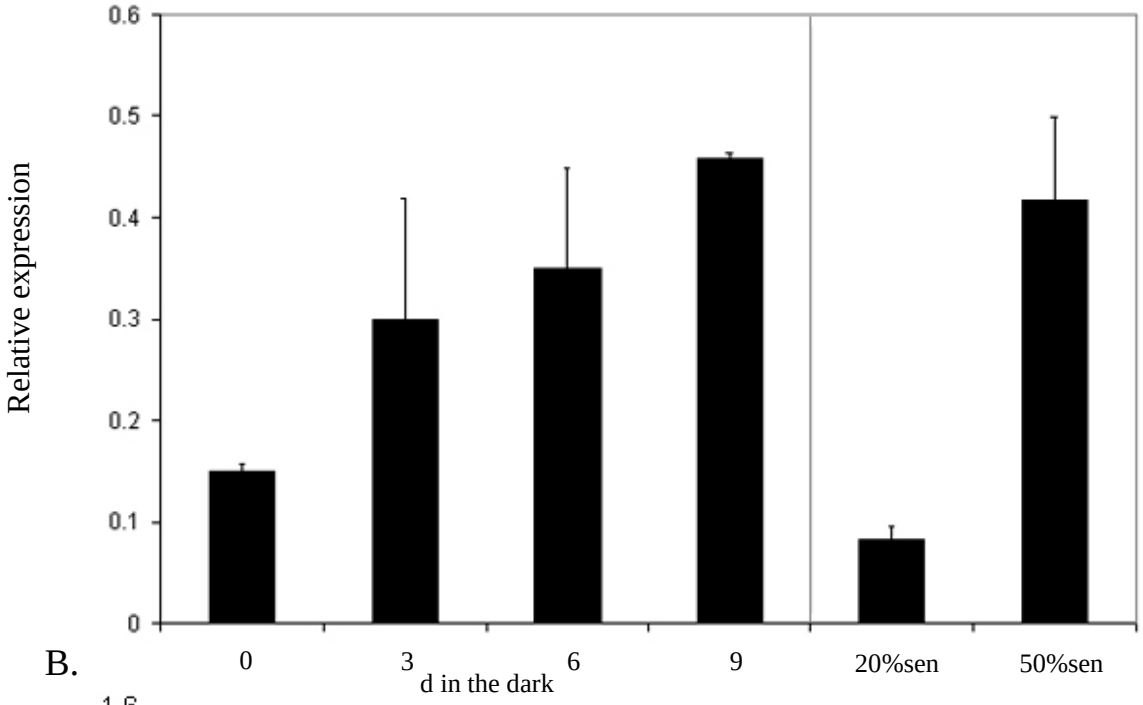
Relative expression
0.6
0.5
0.4
0.3
0.2
0.1
0
0
3
6
9
20%sen
50%sen
d in the dark

B.

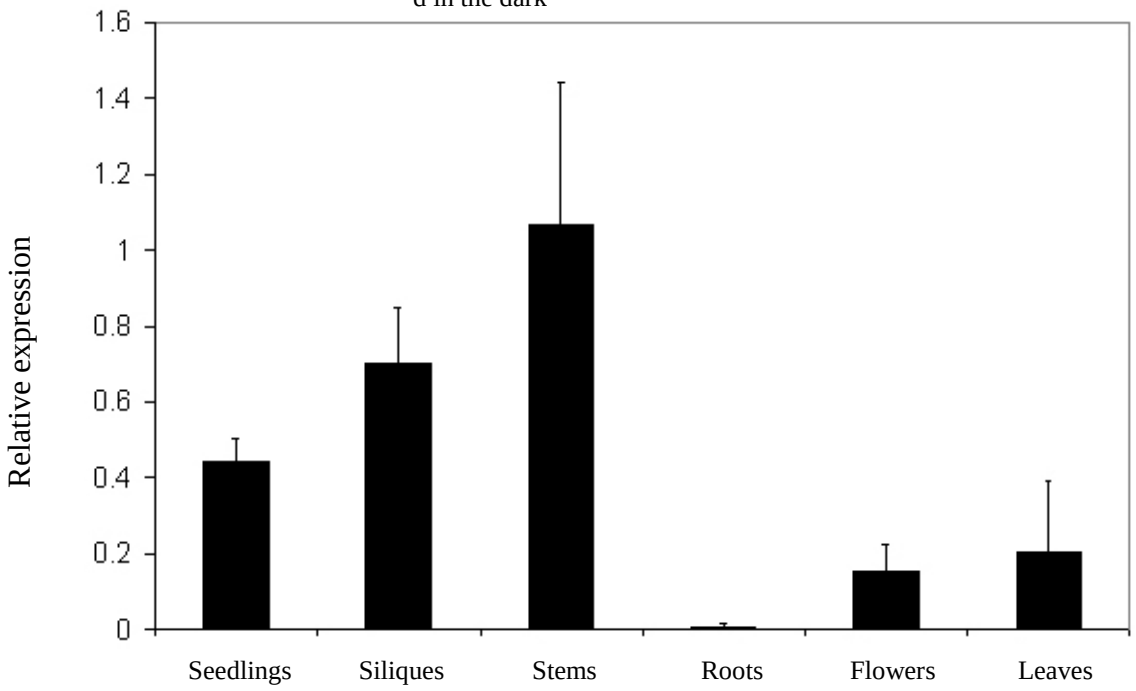
Relative expression
1.6
1.4
1.2
1
0.8
0.6
0.4
0.2
0
Seedlings
Siliques
Stems
Roots
Flowers
Leaves

C.

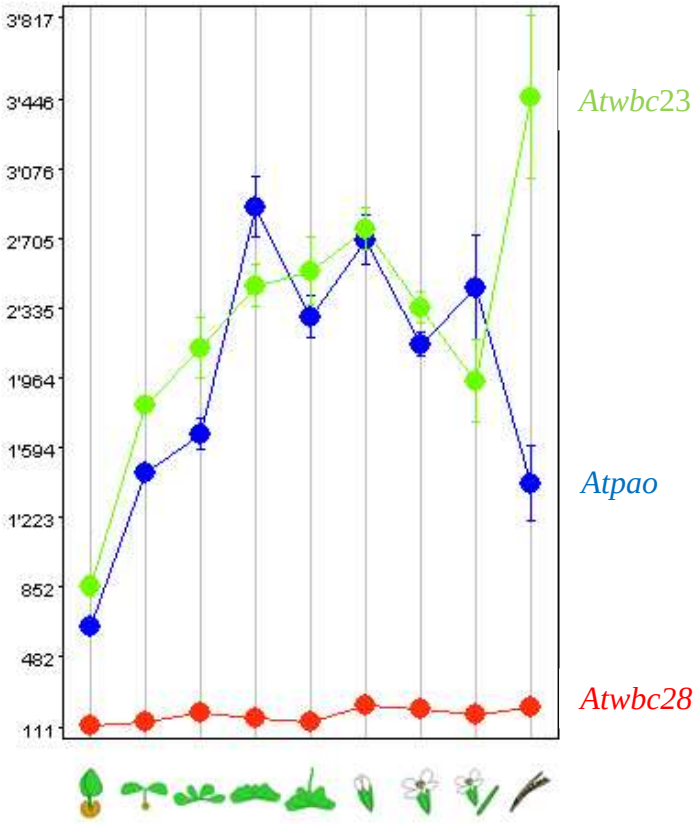

D.

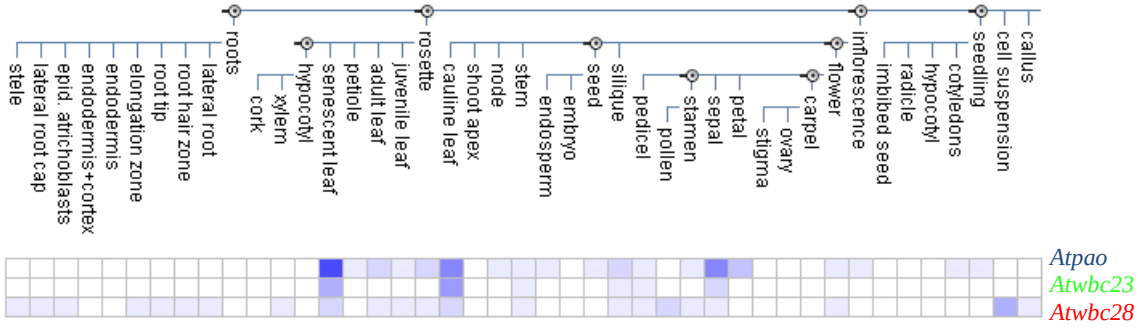

Figure 13. *WBC23* is upregulated during senescence and expressed in green tissues. A. Real-time PCR analysis of cDNA from detached leaves incubated in the dark for 0, 3, 6 and 9 days. Alternatively, senescing attached leaves were used and senescence quantified in relation to the chl content. All data are normalized to *S16* expression. Data are mean of a single representative experiment with six replicates. Error bars indicate SD. **B.** Different tissues were analyzed the same way. Leaf material used corresponded to the 0 dDD sample of panel A. **C.** Expression profiles of *WBC23*, *WBC28* and *PAO* during the life span of *Arabidopsis*. **D.** Expression profile of *WBC23*, *WBC28* and *PAO* in different organs. Data from Genevestigator (Zimmermann et al., 2004).

6.3.5 *wbc23* mutants are delayed in chl degradation

Insertion mutants for *WBC23* and *WBC28* were obtained from different sources (Fig. 14C), and the insertions of *wbc23-1* and *wbc28-1* confirmed by sequencing. The T-DNA in *wbc23-1* is inserted in the first intron, just after the first exon (Fig. 14A). *wbc23-2* and *-3* insertions were not sequenced, but are predicted to be, respectively, at the same site as in the *wbc23-1* and in the middle of the first exon. The *wbc28-1* insertion was sequenced and is located at the beginning of the second intron (Fig. 14B).

As many ABC transporter mutants, *WBC23* and *WBC28* T-DNA insertion lines had no obvious phenotype under normal growth condition (Rea, 2007). Surprisingly leaves of *wbc23-1*, *-2* and *-3* mutant lines incubated in the dark showed a partial retention of chl. This phenotype was identical in all three *wbc23* alleles and *wbc23-1* was exclusively used for further studies. This delay in chl degradation was transient and retention of chl was almost not observable after 7 dDD (Fig. 14C). In contrast to *wbc23* lines, there was no delay of chl breakdown in *wbc28-1* (Fig. 16A). To confirm absence of respective transcripts in the mutants, expression of *WBC23* and *WBC28* was assessed by semiquantitative RT-PCR in *wbc23-1* and *wbc28-1* after 5 d of dark induced senescence (Fig. 15). *ACT2* expression was used as a control.

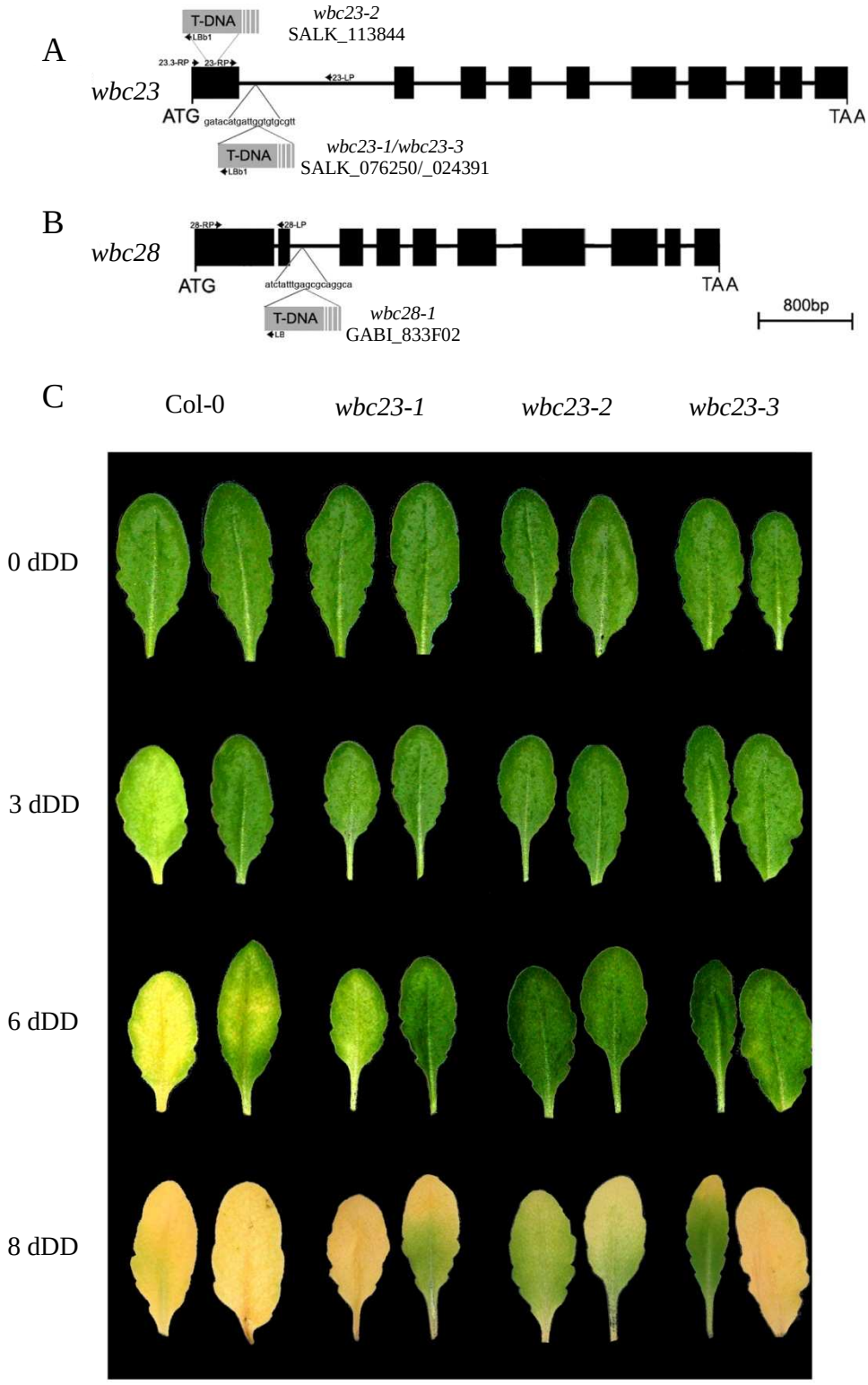

Figure 14. *At*WBC23 mutants are delayed in chl degradation. **A.** Gene structure of *Atwbc*23 (At5g06530) showing the T-DNA insertion sites of the three lines studied and primers used for isolation of homozygous lines. **B.** Gene structure of *Atwbc28* (At3g52310) showing the insertion site of *wbc28-1* and primers used for homozygous isolation. **C.** Leaves of dark incubated *wbc23* lines showing a transient retention of chl during senescence. Plants were grown under short day condition (8/16 h, under fluorescent light 100 µmol photon m^{-2} s^{-1}) during 7 weeks.

WBC23 and WBC28 showed 67% similarity, and were both localized to the chloroplast. Due to the possibility of redundant functions, we crossed *wbc23-1* with *wbc28-1* to obtain the double mutant *wbc23-1 28-1*. Expression of *wbc23* and *wbc28* was analyzed by RT-PCR to confirm absence of both genes (Fig. 15). Unfortunately, the double mutant did not show a more significant chl retention than the single mutant *wbc23-1*. Thus, WBC28 might contribute to the retention of chl but its activity seems negligible.

Degradation of chl was monitored and quantified during senescence (Fig. 16B). Chl retention was observable in *wbc23-1* at 3 dDD and 5 dDD with around 15 μg chl/leaf disc compared to a degradation in Col-0 down to 5 μg chl/leaf disc. The same chl degradation pattern as for *wbc23-1* is observed in the double mutant, with no particular effect of WBC28 absence. In fact, *wbc28-1* degraded chl in the same rate as Col-0. After 7 dDD, however, *wbc23-1* and the double mutant line showed an almost complete chl degradation with less than 3 μg chl/leaf disc which was indistinguishable from Col-0 (Fig. 16B). This transient chl accumulation suggested the presence of an alternative transport process of perhaps lower affinity, which might overcome WBC23 absence and detoxify FCCs as well. Accumulation of NCCs correlated to the degradation of chl, with a slower accumulation in *wbc23-1* at 5 dDD, with 0.9 nmol NCCs/leaf disc compared to 1.8 nmol NCCs in the wild type (Fig. 16C). Taken together all this data showed an important function of WBC23 in chl catabolite breakdown, most likely as an exporter of chl catabolites from the chloroplasts. A minor role might be played probably by its close relative, WBC28. In rice, no ortholog of WBC28 seems to exists, and a rather late gene duplication might explain the close homology of these two proteins in *Arabidopsis*.

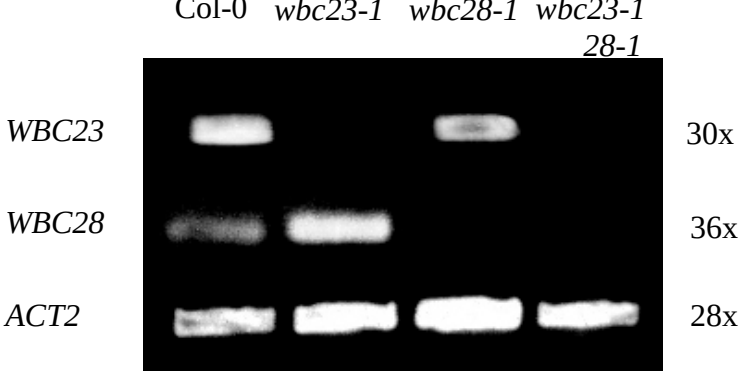

Figure 15. Semiquantitative analysis of expression of *WBC23* and *WBC28*. Confirmation of absence of expression in leaves of insertion incubated 5 dDD was performed by RT-PCR with a non saturating number of cycles as shown at the right. *ACT2* expression was used as a control.

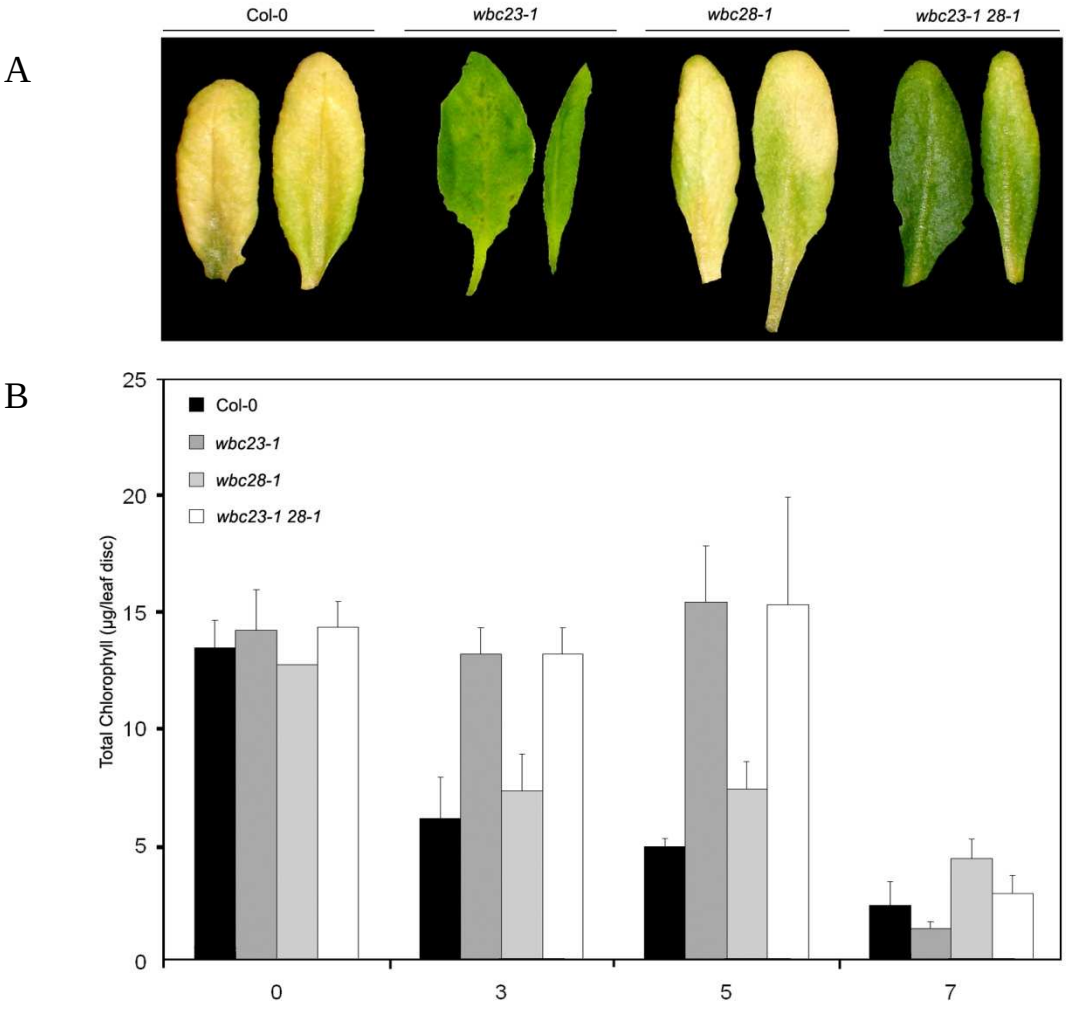

C

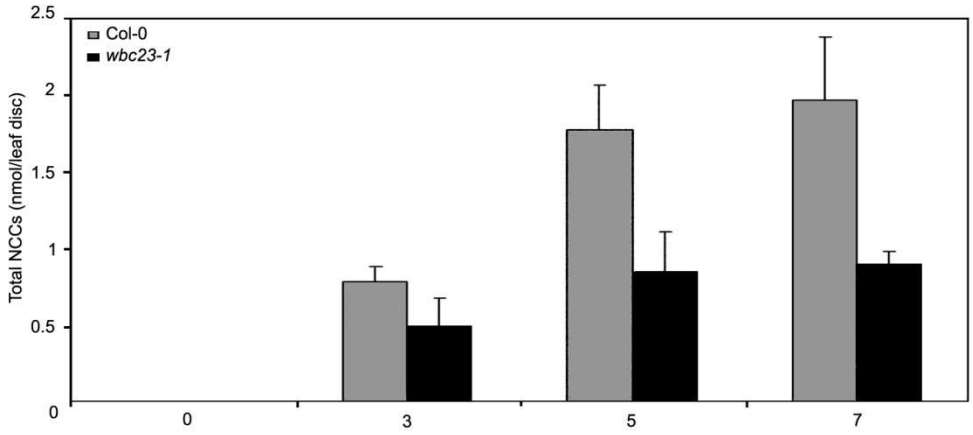

Figure 16. *At*WBC23 contributes to chl degradation. A. Phenotype of leaves of *WBC23* and *WBC28* single and double knockout lines after 5 d of dark induced senescence. **B.** Degradation of chl in Col-0 (dark), *wbc23-1* (dark grey), *wbc28-1* (light grey) and *wbc23-1 28-1* (white) during the course of detached leaf senescence. Data are means of a single representative experiment with three replicates. Error bars indicate SD. **C**. Accumulation of NCCs during detached leaf senescence in Col-0 and in *wbc23-1*. Results of a single representative experiment are shown. Data are means of three replicates. Error bars indicate SD.

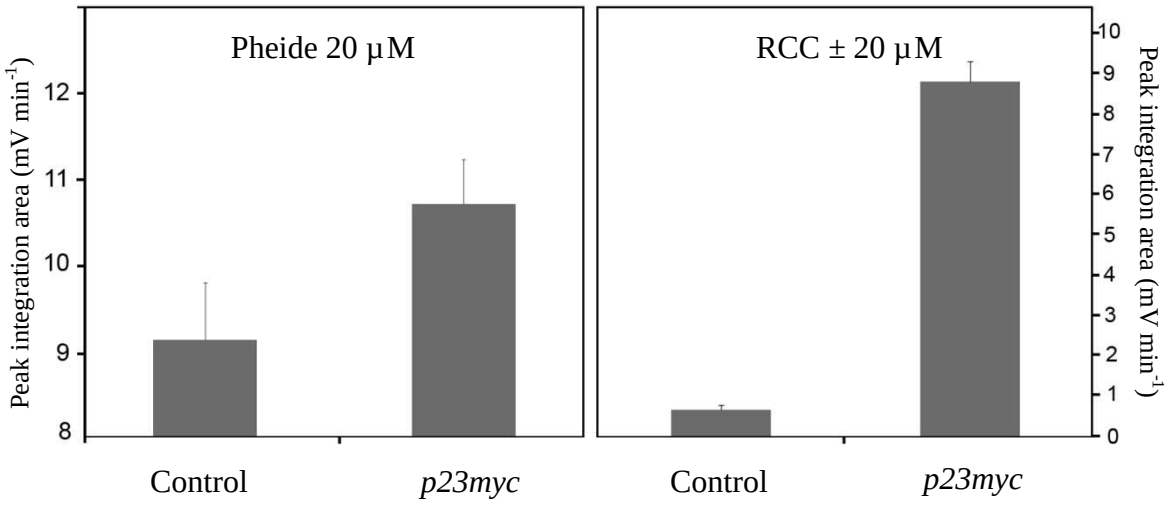

Figure 17. AtWBC23 imports RCC and pheide when expressed in C2C12 muscle cells. RCC and pheide cell contents were measured by HPLC. Empty vector was used as a control. Pheide data are means of five replicates. RCC data are means of duplicate. Error bars indicate SD.

6.3.6 *At*WBC23 is a tetrapyrrole transporter

WBC transporters reported so far transport either long chain fatty acids (LCFA) and sterols (WBC11 and 12), or xenobiotics, like kanamycin (WBC19) (Pighin et al., 2004; Mentewab and Stewart, 2005). For this reason we analyzed lipid contents in the *wbc23-1* mutant. No changes were detected in fatty acid, tocopherol or phylloquinone contents compared to the wild-type (data not shown). If WBC23 is involved in lipid metabolism, its absence does not change the overall lipid content of the plant.

*At*WBC23 was heterologously expressed in C2C12 muscle cells using pSecTag2B allowing targeting of WBC23 to the plasma membrane. Surprisingly, an overaccumulation of pheide and RCC was observed after incubation with 20 µM of substrate. This would suggest that C2C12 cells expressing WBC23 import tetrapyrroles, in contrast to the already observed export activity of ABCG2 overexpressing cells (Jonker et al., 2002). The vector used to target WBC23 to the plasma membrane is targeting the transporter via the endoplasmic reticulum, and such synthesis process might change the topology of the transporter. It is known that incorrectly expressed ABC transporters might in some case act as flipase-like transporters rather than as active transporter (K. Locher, personal communication). Inhibiting the observed transport activity using specific inhibitors for ABC transporters, such as vanadate, could help to better characterize the observed translocation. Work is in progress to confirm this WBC23 mediated transport activity.

Moreover, to complete this approach, we are producing WBC23 mutants silencing *RCCR*. *RCCR* silencing lines are known to accumulate RCC in large amounts (Pružinská et al., 2007) in the chloroplast, but also in the cytoplasm. If WBC23 is responsible for RCC export from the plastid in this case, one would expect to find less RCC outside the chloroplast in a *wbc23* background. Further work on these lines will confirm the *in vivo* participation of WBC23 as an active tetrapyrrole transporter for chl breakdown.

6.4 Discussion

6.4.1 Accumulation of RCC-like chlorophyll catabolites in mouse

Mice depleted in an ABC transporter, ABCG2 (BCRP1) have been shown to accumulate in their blood and bile large amounts of pheide when fed with chl containing diet. This accumulation leads to a “porphyria” like phenotype, with phototoxic lesions of most light-exposed organs, like the ears (Jonker et al., 2002). Surprisingly, no porphyria in human has been reported to date corresponding to an ABCG2 defect (Krishnamurthy and Schuetz, 2006). Fed with pheide, mice were no longer able to detoxify the porphyrin back into the gut and accumulated chl derivatives in their body. The mechanisms by which pheide is incorporated as well as its conversion to a linear RCC is still unknown. However ABCG2 has been shown, among a diverse set of substrates to also transport pheide (Robey et al., 2004; Krishnamurthy and Schuetz, 2005). Investigations of ABCG2$^{-/-}$ mice revealed accumulation of pheide both under treatment with synthetic food containing pheide and when fed with natural food, containing chl. The mechanism of conversion of chl to pheide is not known, but unspecific oxidative reactions might be involved. Pig liver esterase has been shown to hydrolyze C_{17} esters of porphyrins (RCC) (Kräutler et al., 1997) and dechelation of Mg most likely occurs during the digestion process in the acidic stomach. Thus, pheide should be one of the natural substrates of ABCG2 in the gut, allowing its detoxification from the body. Incorporation of chl or chl catabolites in mouse gut might be compared to incorporation of heme (Fig. 17). A large part of iron uptake in mouse occurs in the duodenum via direct heme incorporation by a facilitator (HCP1) (Shayeghi et al., 2005; Latunde-Dada et al., 2007). Incorporated heme is further translocated to the blood or converted to free iron and biliverdin (BV) by heme oxygenase. Free iron is transported to the blood by ferroportin (FPN1), but data are missing concerning the fate of BV.

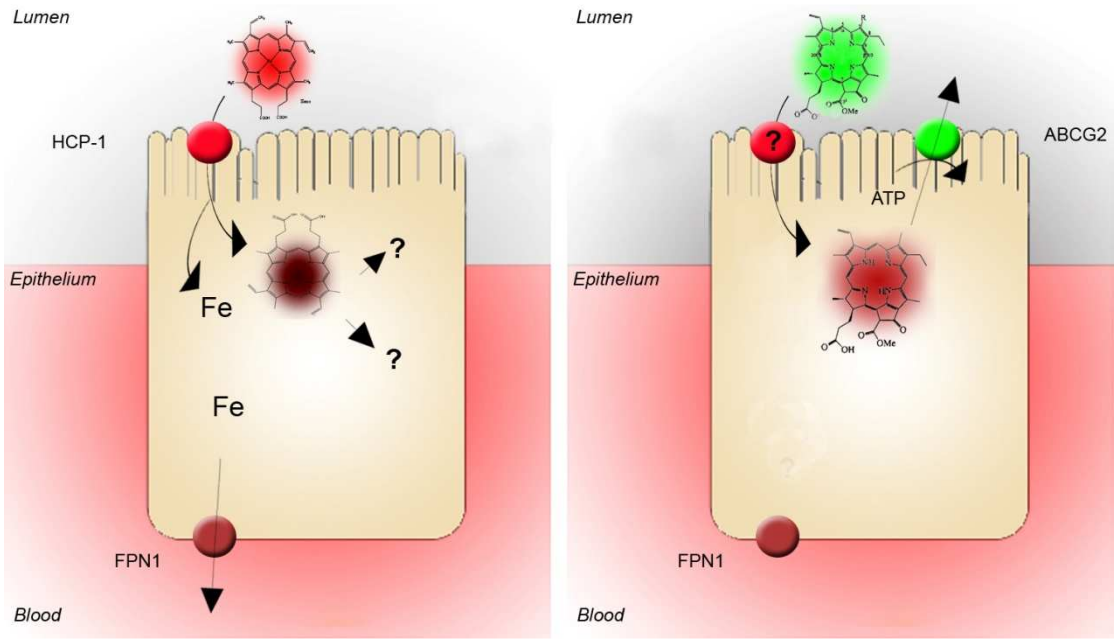

Figure 18. Schematic representation of heme and chlorophyll uptake in mammal intestine. Heme is taking up by HCP1 and cleaved into biliverdin by heme oxygenase. The iron is then imported into the blood by ferroportin (FPN1). Further degradation of biliverdin is not reported. Chl derivatives are imported by the gut cells by an unknown mechanism. Pheide is exported to the lumen via an active ABC transporter ABCG2. Modified from Latunde-Dada et al, 2006.

Absence of ABCG2 in the mouse gut led to accumulation of pheide in abnormally high concentration indicating that ABCG2 is responsible for the extrusion of pheide from the body. Pheide non-extrusion causes its accumulation in the blood, probably in the liver, as well as in the gall bladder. Thereby the bile colour changes dramatically from yellow in wild type to red in ABCG2$^{-/-}$ mice. Here we show that this colour is due to an accumulation of RCC-like compounds, most probably derived from pheide (Jonker et al., 2002). Pheide might be degraded by porphyrin ring opening in the liver through unspecific oxygenases but this hypothesis has so far no experimental basis. It is rather unlikely that this degradation reaction is due to a physiologically relevant mechanism, as pheide should not accumulate in significant amounts when ABCG2 is normally expressed. It might be possible that pheide is metabolized by chelation of iron, and subsequent opening of the porphyrin ring by heme oxygenase, *i.e.* similar to the conversion of heme to BV. Experiments in this direction might reveal a possible unknown function of the heme oxygenase in a pheide detoxification process. In analogy to the heme-BV conversion, one could expect opening of the porphyrin ring at the α-methine bridge. In contrast to PAO-catalyzed pheide ring opening, this might

lead to the loss of the C_6 methine carbon, giving rise to a RCC with slightly different polarity than all known plant RCCs (Fig. 8). Further resolution of the *Mm*RCC-like structures by MS and NMR are required for confirming this hypothesis.

In plants, RCC-related compounds are naturally not occurring, but are further reduced by RCCR to pFCC (Pružinská et al., 2007). Further degradation of *Mm*RCC-like compounds to fluorescent catabolites or even non fluorescent catabolites was not observed in ABCG2$^{-/-}$ mice. This is not surprising, as animals do not need such a process if the ABCG2 primary detoxification is working normal. However, in *Chlorella prothotecoides*, RCC is not further degraded but simply excreted, suggesting that degradation beyond RCC is not a mandatory step in chl degradation (Hörtensteiner et al., 2000). *Mm*RCCs accumulating in the bile most probably have photosensitive properties, and depending where they accumulate, they might contribute to the porphyria-like phenotype. Accumulation of RCC-like compounds in the bile of ABCG2$^{-/-}$ mice might suggest that RCC would also be a possible substrate of ABCG2 in the gall bladder.

In a clinical context, consequences of a porphyria linked to ABCG2 variants, or consequences of the absence of this major xenobiotic detoxifier are not fully understood (Krishnamurthy et al., 2007; Tamura et al., 2007).

6.4.2 Chl breakdown needs a pFCC exporter at the chloroplast envelope

Degradation of chl studies have shown accumulation of final catabolites, NCCs, in the vacuole. Vacuolar disposal is a known mechanism in detoxification processes but also highlight the requirement for two transport processes at the envelope of the chloroplast and at the tonoplast. Members of the WBC family in *Arabidopsis* are the closest relatives to ABCG from mouse and phylogenetic comparison of ABCG2 sequences showed a clustering of ABCG2 with WBC23 and 28 (Fig. 9B). As ABCG2 is able to transport chl derived pigments, WBC23 and 28 might have a similar activity. Moreover, WBC23 and 28 exhibited some similarity to a bacterial hexameric ABC transporter BtuCD which also transports a porphyrin, vitamin B12 (Hvorup et al., 2007).

WBC23 KO mutants were delayed in the degradation of chl during senescence. NCCs accumulated more slowly in *wbc23* than in wild type, suggesting a partial impairment of a transport process of chl catabolites. Since WBC23 was localized to the

chloroplast, likely at the envelope membrane, it is involved in catabolite export out of the chloroplasts. Unfortunately, in *wbc23-1* the overall chl degradation pathway was only temporarily impaired and at later stage of senescence (7 dDD) no differences in chl contents were visible anymore. WBC23 is likely an important chl catabolite transporter at the envelope but surely not the only one. The closest related member of the family, WBC28 does not seem to be involved in this process, even if localized in the chloroplast as well. Also in a *wbc23 28* double mutant WBC28 does not have an additive effect to the transient chl retention seen in the *wbc23* single mutant. Notably, the low expression of *WBC28* in leaves, may explain absence of any detectable function for this transporter. However, WBC28 would have been a good candidate for heterodimerisation with WBC23. Other WBCs such as WBC26 predicted to be chloroplast localized (Aramemnon database) and senescence induced (Zimmermann et al., 2004) might be also involved in pFCC export. Unfortunately a *wbc26-1* (SALK_128873) homozygous insertion mutant did not show any phenotype related to senescence (data not shown). Other primary active transporters might be involved in catabolite export as well. Of the 120 ABC transporters found in *Arabidopsis*, several, such as WBC6, 18 26, TAP1, PDR8, ATH8, 12, 13 and GCN1, 2 5 (ChloroP prediction) are predicted to localize to the chloroplast. Since redundancy of activity has been shown in many cases, it is likely to assume that transporters more distinct from WBCs might take over chl catabolite export function in the absence of WBC23.

6.4.3 WBC23 transport activity and potential other orthologous transporters

Attempts to express *At*WBC23 in an heterologous system have been an extremely difficult task. No expression could be obtained either in embryonic hamster kidney (HEK) cells or in yeast. Several versions with or without the N-terminal extension of WBC23, and tagged versions of the protein have been tested in both systems without any success (data not shown). This difficulty of expression is a feature already described for the WBC-related full length PDR family. Indeed, yeast PDR5p has been shown to be a relatively short-lived protein subjected to ubiquitination and vacuolar proteolysis (Egner and Kuchler, 1996). The only case where enough expression was obtained to perform transport experiments was in C2C12 muscle cells transfected with c-myc tagged WBC23 targeted to the plasma membrane of the cells through the ER. We have shown this way that WBC23 is a possible translocator able to transport

pheide and RCC, but not *Cj*-NCC-1. This is the first indication of a WBC function *in vitro*. Despite, important control experiments are yet required to confirms the transport activity as primary active transport. Here we have shown that WBC23 *in vitro* is able to transport synthetic RCC and pheide, but the predicted substrate for chloroplast export is FCC (Matile et al., 1992). This raises the question of the specificity of transport. In the *pao1* mutant, where large amounts of pheide are found, no pheide is detected outside the chloroplast during senescence (S. Aubry and S. Hörtensteiner, unpublished results) suggesting a rather defined specificity of the transporter. On the other hand, *acd2-2* depleted in RCCR and thus accumulating RCC, RCCs as well as further catabolites, such as NCCs are found outside the chloroplast (Pružinská et al., 2007) indicating that RCC is exported in this case. This might be explained by the similar planar conformation of RCCs and FCCs. In a similar situation in *Chlorella*, only RCC-like catabolites with an opened porphyrin ring are exported out of the chloroplast and the cell (Hörtensteiner et al., 2000) but not pheide (S. Hörtensteiner, personal communication). Thus, in plants efficient transport of chl catabolites seems to require an opened porphyrin ring. Pheide transport shown *in vitro* questions the relevance of such experiments. However, when expressed in C2C12 cells WBC23 seems not to be able to transport NCC, suggesting some limitation in the substrate spectrum.

During plant development, FCCs are not the only porphyrins for which export out of the chloroplast is required. In green tissues, topology and localization of chl and heme metabolic enzymes suggest the presence of different exporters (Tanaka and Tanaka, 2006). Indeed, early steps of biosynthesis of heme and chl are common, and a heme precursor, probably CPIII, is translocated to the mitochondria. Plastid to nucleus signalling might also involve a PPIX export (Tanaka and Tanaka, 2006; Ankele et al., 2007). The exact nature of the export process(es) are still missing, and identification of transporters for chl derivatives was one of the main objectives of this work. A linear tetrapyrrole transporter is moreover needed for the export from the chloroplast of phytochromobilin as the co-factor needed for phytochrome biosynthesis (Terry et al., 2002). WBC23 might be involved in one or several of these transport activities, however *WBC23* expression is low before senescence (Fig. 13A). Systematic characterization of all primary active chloroplastic transporters might be a way to obtain a more complete picture of chl and heme metabolite trafficking.

In summary, it can be concluded that WBC23 is a major exporter of chl catabolites out of the chloroplast during senescence. For the moment we cannot rule out an involvement of WBC23 in the export of other porphyrin or tetrapyrrole metabolites, or of other degradation products occurring during chloroplast dismantling, such as nitrogen containing molecules resulting from protein degradation.

7. Staygreen factor characterization in Mendel's *I* pea

7.1 From crop to model to crop: identifying the genetic basis of the staygreen mutation in the Lolium/Festuca forage and amenity grasses

Ian Armstead, Iain Donnison, Sylvain Aubry, John Harper, Stefan Hörtensteiner, Caron James, Jan Mani, Matt Moffet, Helen Ougham, Luned Roberts, Ann Thomas, Norman Weeden, Howard Thomas, Ian King.

Reprinted from: *New Phytologist* (2006) 172: 592-597

Genetic identification of the *SGR* (*Y*) gene was published in two papers, one concerning the identification in *Festuca/Lolium* and a second describing the mapping of *SGR* in *Pisum* (see following section).

The *Festuca* Bf993 mutation responsible for the staygreen phenotype had been introgressed into *Lolium*. Due to high synteny of the rice and the *Lolium* genomes and exploiting Genevestigator microarray data, one possible candidate gene, responsible for the staygreen phenotype could be identified. In staygreen lines of *Festuca* and *Lolium*, this gene had a frameshift mutation, disturbing the amino acid sequence in highly conserved regions of SGR protein from different species. This paper sets a major step for understanding the Y/SGR mechanism and biochemistry in relation to chl breakdown.

New Phytologist

Letters

From crop to model to crop: identifying the genetic basis of the staygreen mutation in the *Lolium/Festuca* forage and amenity grasses

Lolium/Festuca staygreen in context

The practical application of model systems to crop species is a topic of much current debate in the plant science community, and in this Letter we describe the progress made in determining the genetic control of staygreen in the *Lolium/Festuca* grasses, using a combination of experimental genetic analysis and publicly available genomic and transcriptomic resources. The analysis of *Lolium/Festuca* staygreen can be considered to be a useful model in this regard, as staygreen is an economically significant (and genetically recessive) trait for which molecular markers are required for efficient breeding purposes, and the gene determining staygreen plays a fundamental but, as yet, unspecified role in chlorophyll degradation. Additionally, as *Lolium/Festuca* grasses have been well characterized in terms of synteny with rice (*Oryza sativa*) (Armstead *et al.*, 2002; Jones *et al.*, 2002; Alm *et al.*, 2003; Sim *et al.*, 2005), the system is sufficiently developed to allow advantage to be taken of the available comparative genomics resources. In this Letter we will refer to the wild-type (normal yellowing) and mutant (staygreen) loci as *Y* and *y*, respectively.

Mutation of a gene regulating the pathway of chlorophyll degradation has been shown to result in the indefinite retention of greenness in senescing leaves of the temperate grass *Festuca pratensis* (Thomas & Stoddart, 1975; Thomas, 1987; Vicentini *et al.*, 1995), a phenotype that has been incorporated into *Lolium/Festuca* amenity grasses in order to enhance their year-round utility (e.g. AberNile; Department for Environment, Food and Rural Affairs, 2006, p. 6). Staygreen in *Lolium/Festuca* and other species is an example of one of a number of distinct genetic variants that interfere with the normal expression of senescence (Thomas & Smart, 1993; Thomas & Howarth, 2000) and advanced varieties of some of the world's major crops, for example maize (*Zea mays*) and *Sorghum* (Thomas & Howarth, 2000; Morgan *et al.*, 2002; Valentinuz & Tollenaar, 2004) owe their productivity and stress tolerance, at least in part, to the staygreen trait. The detailed biochemistry, cell biology, physiology, genetics and introgressive gene transfer of the staygreen phenotype from *F. pratensis* have been extensively described (Hauck *et al.*, 1997; Kingston-Smith *et al.*, 1997; Thomas *et al.*, 2002; Moore *et al.*, 2005).

Crops and models: the experimental approach

The development of the initial *Lolium/Festuca* mapping population ($n = 100$) segregating for *F. pratensis*-derived *y* was reported previously (Moore *et al.*, 2005) and this population was used to assign *y* to *Lolium/Festuca* chromosome (C) 5 using anchored comparative mapping markers (Table 1a). Earlier studies (Armstead *et al.*, 2002; Jones *et al.*, 2002; Alm *et al.*, 2003; Sim *et al.*, 2005) had indicated that this region of *Lolium/Festuca* C5 shows a degree of synteny with rice C9, a rice chromosome known to contain a quantitative trait locus (QTL) for staygreen (Cha *et al.*, 2002). Using rice sequences taken from the The Institute for Genome Research (TIGR) rice C9 pseudomolecule (http://www.tigr.org/tdb/e2k1/osa1/), which flanked the position of this QTL as templates for primer design, it was possible to develop comparative mapping markers which demonstrated that *F. pratensis*-derived and rice staygreen phenotypes were determined from syntenically equivalent genomic regions. From an extended mapping family of 1627 individuals, 60 genotypes were identified which showed recombination in a 10-cM interval around *y*. Further implementation of the comparative mapping strategy based on these 60 recombinant genotypes allowed refinement of the relationship between *Lolium/Festuca* C5 and rice C9 to the extent that *F. pratensis*-derived staygreen could be localized to an equivalent region of rice C9 consisting of *c.* 200 kb, which contained 30 rice gene models (Table 1a,b). The annotations of these gene models in the TIGR database indicated that one of these, LOC_Os09g36200, was predicted to be a senescence-inducible chloroplast stay-green protein (Table 1c), although no direct evidence for this function was available in the published literature. To provide further validation for LOC_Os09g36200 as a candidate for *y*, the 30 implicated rice gene models were analysed for the presence of putative chloroplast transit peptides, using ChloroP 1.1 (http://genome.cbs.dtu.dk/services/ChloroP/; Emanuelsson *et al.*, 1999). Additionally, the temporal and organ-specific expression patterns of their most similar Arabidopsis gene models (Table 1d) were obtained through microarray data available in the Genevestigator® Meta-Analyzer database (https://www.genevestigator.ethz.ch/; Zimmerman *et al.*, 2004). Along with seven other gene models from this region, LOC_Os09g36200 was predicted to contain a chloroplast

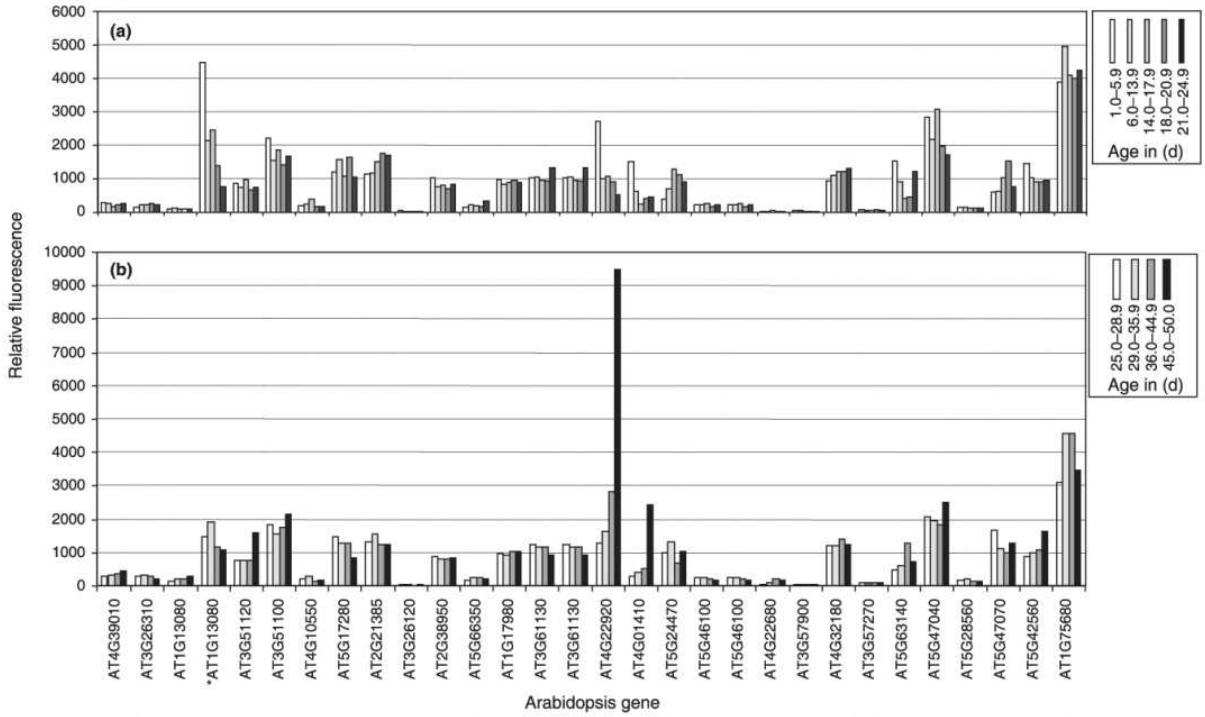

Fig. 1 Relative fluorescence values from microarray analysis of selected Arabidopsis genes; each Arabidopsis gene is an orthologue of a TIGR rice (*Oryza sativa*) gene model predicted to be nonrecombinant with *Festuca pratensis*-derived *y* on the basis of synteny (Table 1). Results are expressed according to Arabidopsis whole-plant growth stage: (a) 1–24.9 d and (b) 25–50 d (see https://www.genevestigator.ethz.ch/ for growth stage definitions). Values were obtained from the Genevestigator® Meta-Analyzer database. *Data from two different probe sets.

transit peptide (Table 1c). In terms of the expression profiles, the relative fluorescence of At4g22920 (the most similar Arabidopsis protein to LOC_Os09g36200) was clearly up-regulated in days 45–50, coinciding with maximal senescence in the Arabidopsis life-cycle (Fig. 1b). At4g01410 (the most similar Arabidopsis protein to LOC_Os09g36210) also showed a similar expression pattern, although of smaller relative magnitude (Fig. 1a). None of the remainder of the candidate genes indicated obvious specific induction in days 45–50. Examination of the tissue-specific pattern of expression of At4g01410 and At4g22920 indicated that the former was most strongly expressed in the seed and showed no specific association with the senescent leaf (Fig. 2a). The latter was also strongly expressed in the seed as well as in the petals and sepals. Notably, however, it was associated most strongly with the senescent leaf (Fig. 2b). Subsequent northern analysis of this gene in *Lolium temulentum* and staygreen *F. pratensis* confirmed senescence-associated expression in *Lolium*/*Festuca* leaves. Therefore, on the basis of genetic association, comparative genomics, putative gene function and expression profile, a recessive mutation in the *F. pratensis*-derived homologue of LOC_Os09g36200 was considered to be a strong candidate for *y*.

In order to develop an allele-specific molecular marker for staygreen, the genomic sequence of the *L. perenne* homologue of LOC_Os09g36200 was obtained by polymerase chain reaction (PCR) screening of an *L. perenne* bacterial artificial chromosome (BAC) library (Farrar *et al.*, 2006) and this was used to develop primers for the amplification of regions of *y*. Allele-specific primers are often most efficiently developed by amplifying intronic sequences; however, in this case a 4-bp ATAT insertion was identified in the second predicted exon of the candidate gene (Fig. 3). This allowed the development of both a size-specific molecular marker suitable for high-throughput screening and a cleaved amplified polymorphic sequence (CAPS) marker (the ATAT insertion removed an existing *Bst*F5I restriction enzyme site present in the wild-type sequence) suitable for analysis on agarose gels (Fig. 3a). To date, assays of these markers on experimental mapping populations and application in existing breeding lines have identified no recombination between *y* and the molecular markers.

Beyond the development of a molecular marker, the presence of a 4-bp insertion in an exon represents a translational frameshift, and comparison of the rice and *Lolium* candidate genes with homologous sequences from other species indicates that this 4-bp insertion is peculiar to staygreen lines containing the *F. pratensis*-derived *y* locus

Table 1 Syntenic relationship between *Lolium/Festuca* C5 and rice C9. (a) Genetic markers mapped in rice (*Oryza sativa*) and *Lolium/Festuca* and their equivalent positions on the TIGR rice 9 pseudomolecule. (b) Diagrammatic representation of the physical position of mapped markers and genes on the TIGR rice 9 pseudomolecule. (c) TIGR gene models and predicted functions for candidate sequences for the *Festuca pratensis* staygreen gene. (d) Most similar Arabidopsis sequence

(a)	Genetic distance of markers on *L. perenne* C5 and rice C9			Genetic distance from* or no. recombinants with† *y* on rice C9 or *Lm/Fp* C5			(b)	(c)		(d) AGI proteins (TAIR)[b]	
Marker	*Lp* C5	riceA C9	riceB C9	riceC *y**	*Lm/Fp* *y*A**	*Lm/Fp* *y*B†**	TIGR C9 gene model	TIGR gene model	TIGR putative annotation	Arabidopsis gene model	*P*
E51174S	3.1	–	–	–	49.7	–	–	Os09g36060	Endoglucanase 1 precursor	AT4G39010	2.4e-161
C1176.2	8.2	–	35.2	–	–	–	Os09g17830	Os09g36070	Cytochrome P450	AT3G26310	4.4e-70
BCD1087	8.2	–	38.5	–	–	–	Os09g17730	Os09g36080	Cytochrome P450	AT1G13080	1.0e-72
RZ206	9.2	–	38.5	–	–	–	Os09g19730	Os09g36090	Plus-3 domain	AT3G51120	3.8e-148
R1751	15.2	49.3	–	–	–	–	Os09g24200	Os09g36100[c]	Expressed protein	AT3G51100	1.2e-24
PSR574	12	62.4	–	–	–	–	Os09g27870	Os09g36110	Subtilisin N-terminal region	AT4G10550	6.1e-170
CDO412	19	–	61.9	–	10.7	–	Os09g28019	Os09g36120[c]	Expressed protein	AT5G17280	4.8e-12
RM160	–	–	–	9.7	–	–	–	Os09g36130[c]	Expressed protein	AT2G21385	2.5e-102
RG570	–		80.3	7.2	–	–	Os09g33780	Os09g36140	RNA recognition motif 2 family protein	AT3G26120	2.5e-24
S2655	–	77.7	–	–	3.4	–	Os09g33810	Os09g36150	Retrotransposon protein	AT2G38950	0.060
C1263	–	78.5	–	4.2	–	–	Os09g34960	Os09g36160	Expressed protein	AT5G66350	2.1e-40
RG662	–	–	–	1.8	–	–	–	Os09g36170	Hypothetical protein	AT1G17980	0.26
R3330	–	79.1	–	–	–	4	Os09g35710	Os09g36180[c]	Glycosyl transferase family 8 protein	AT3G61130	1.1e-221
9g35920	–	–	–	–	–	2	Os09g35920	Os09g36190[c]	Glycosyltransferase QUASIMODO1	AT3G61130	8.9e-249
9g36030	–	–	–	–	–	4	Os09g36030	Os09g36200[c]	Senescence-inducible chloroplast stay-green protein	AT4G22920	1.5e-73
9g36060	–	–	–	–	–	1	Os09g36060	Os09g36210	Harpin-induced protein 1	AT4G01410	6.6e-15
9g36200	–	–	–	–	–	0	Os09g36200	Os09g36220	Two-component response regulator-like PRR95	AT5G24470	2.9e-79
9g36270	–	–	–	–	–	0	Os09g36270	Os09g36230[c]	Hypothetical protein	AT5G46100	5.0e-33
9g36320	–	–	–	–	–	0	Os09g36320	Os09g36240	Deoxyribodipyrimidine photolyase	AT5G46100	2.7e-104
9g36350	–	–	–	–	–	2	Os09g36350	Os09g36250	ODORANT1 protein	AT4G22680	3.1e-65
C985[a]	–	82.1	–	2.1	–	–	Os09g36420	Os09g36260	Hypothetical protein	AT3G57900	0.16
R2710	65	–	–	–	3.4	–	Os09g38030	Os09g36270	Pantothenate kinase 2	AT4G32180	6.8e-297
T4	–	90.1	–	10.8	–	–	–	Os09g36280	Glycosyl hydrolases family 17	AT3G57270	3.4e-50
RM189	–	–	–	16.3	–	–	Os09g38370	Os09g36290	Serine/threonine protein phosphatase	AT5G63140	5.7e-119
RZ404	78	94.2	–	–	–	–	Os09g38580	Os09g36300	Lon protease homologue 1	AT5G47040	0.
								Os09g36310	Hypothetical protein	AT5G28560	0.21
								Os09g36320[c]	Serine/threonine-protein kinase NAK	AT5G47070	4.5e-103
								Os09g36330	Hypothetical protein	**NONE**	–
								Os09g36340	HVA22-like protein i	AT5G42560	1.5e-38
								Os09g36350	Glycosyl hydrolase family 9	AT1G75680	5.0e-168

riceA, RGP 2003 high-density rice genetic map; riceB, Cornell RFLP 2001 rice genetic map (data obtained from Gramene database; http://www.gramene.org/); riceC, Cha *et al.* (2002) *sgr* (*y*) population.
Lm/Fp *y*A, original *Lolium/Festuca* introgression *y* screening population (n = 100); *Lm/Fp* *y*B, recombinant genotypes (n = 60) identified in expanded *Lolium/Festuca* introgression *y* screening population (n = 1627).
[a]Alternative position to that in Gramene database consistent with relative genetic map position. Identified by BLAST search of GenBank accession number D22707 against rice pseudomolecules database at http://www.tigr.org/tdb/e2kl/osa1/.
[b]Most significant alignment present in Genevestigator® chipset database as determined by WU-BLAST2 searches at The Arabidopsis Information Resource (TAIR; https://www.arabidopsis.org/wublast/index2.jsp). AGI, Arabidopsis Genome Initiative.
[c]Chloroplast transit peptide predicted by ChloroP 1.1.

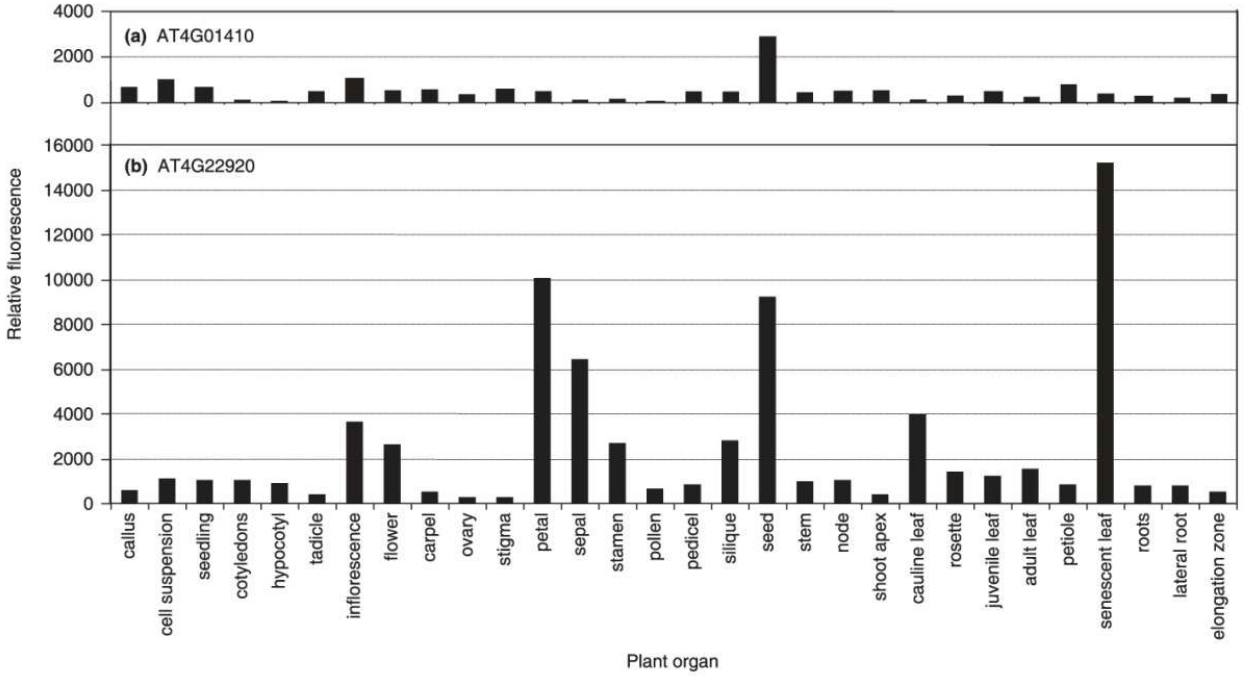

Fig. 2 Relative fluorescence values from microarray analysis of Arabidopsis genes (a) AT4g01040 and (b) AT4G22920, orthologues of TIGR rice (*Oryza sativa*) gene models LOC_Os09g36210 and LOC_Os09g36200, respectively. Results are expressed according to plant organ specificity. Values were obtained from the Genevestigator® Meta-Analyzer database.

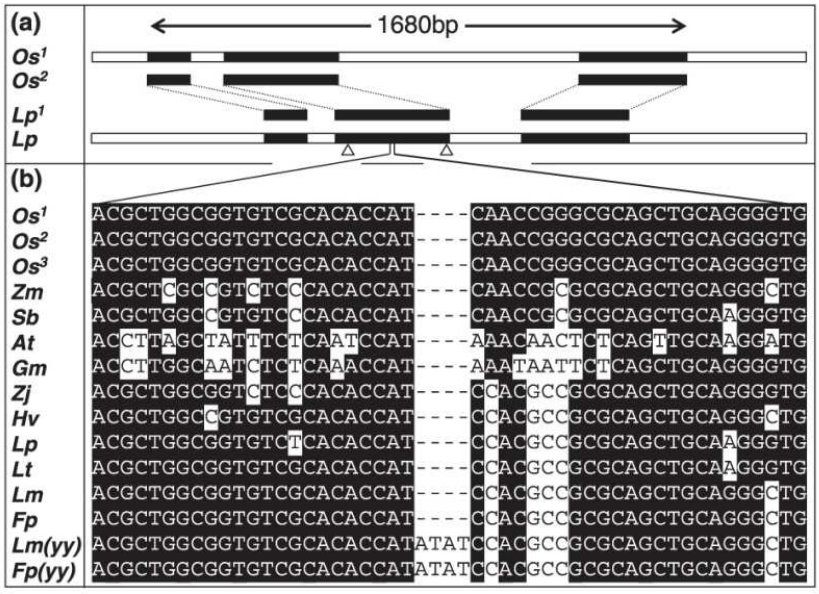

Fig. 3 (a) Diagrammatic representation of the physical distribution of exons in rice (*Oryza sativa*) LOC_Os09g36200 and its homologue from *Lolium perenne*: black horizontal bars, exons; white horizontal bars, noncoding genomic sequence; open triangles, priming sites for marker used in the detection of the ATAT insertion. Dotted lines connect equivalent exons. (b) Partial sequence alignment of exon 2 from LOC_Os09g36200 and its homologues from a number of plant species, illustrating the ATAT insertion in *Lolium/Festuca yy* genotypes. *Os*[1], LOC_Os09g36200 gene sequence; *Os*[2], LOC_Os09g36200 CDS; *Os*[3], *O. sativa* (AY850134); *Lp*, *L. perenne* bacterial artificial chromosome (BAC) sequence; *Lp*[1], *L. perenne* BAC sequence predicted coding sequences (CDS); *Hv*, *Hordeum vulgare* (AY850135); *Zj*, *Zoysia japonica* (AY850154); *Zm*, *Zea mays* (AY850138); *Sb*, *Sorghum bicolor* (AY850140); *Gm*, *Glycine max* (AY850141); *At*, *Arabidopsis thaliana* (AY850161); *Lt*, *Lm* and *Fp*, *Lolium temulentum*, Lolium multiflorum and *Festuca pratensis* genomic polymerase chain reaction (PCR) products covering the second predicted exon; (*yy*), mutant genotype expressing staygreen. GenBank accession numbers are indicated in parentheses.

(Fig. 3b). The mechanism by which this mutation was produced is unknown, but short insertion sequences of this type have been shown to arise as footprints following mobilization of a transposable element (Pooma *et al.*, 2002), although active transposition has not been characterized directly in *Lolium*/*Festuca*. Approximately 1250 bp of the *F. pratensis y* genomic sequence has been isolated so far, spanning the complete first and second exons and, up to the ATAT insertion, the peptide predicted from this is identical to the wild-type *L. perenne* protein. Use of the complete *L. perenne* gene, with and without the ATAT insertion, as a model for the comparison of mutant and wild-type proteins shows that the insertion radically changes the amino acid sequence of the mutant protein from position 100 and gives a final protein consisting of 232 residues, as compared to 279 in the wild type. The region of the protein derived from the second exon is highly conserved across a number of different species (Fig. 3b), indicating that one or more active sites may be affected by the frameshift mutation; this could give rise to a functional knockout mutation, as seen for *y*. Work is under way, using immunochemical approaches, to understand and localize the effect of mutation in *Y* on protein expression in both crop and model species

Staygreen and chlorophyll catabolism

It is established that *Y* is a key gene involved in chlorophyll catabolism, and it is interesting to speculate upon its function. The biochemical lesion represented by *y* in staygreen *F. pratensis* has been shown to be located in the pathway of chlorophyll catabolism at the step where the chlorin macrocycle is opened by oxygenolytic cleavage (Vicentini *et al.*, 1995). Measured *in vitro*, activity of the enzyme responsible (phaeophorbide a oxygenase, PaO) is abnormally low in staygreen lines. There is, however, good genetic and biochemical evidence to show that PaO is expressed, although inactive, in staygreen *Festuca* and *Lolium* (Vicentini *et al.*, 1995; Roca *et al.*, 2004): it is therefore likely that the product of the *Y* gene modulates the activity of PaO. Chlorophyll degradation is organizationally complicated, as the pigment substrates for the catabolic enzymes are complexed with thylakoid membrane proteolipids (Thomas, 1987). Disassembly of these complexes must take place in a regulated fashion if the photodynamic tendencies of chlorophyll catabolites are to be kept in check (Thomas, 1987; Eckhardt *et al.*, 2004; Hörtensteiner, 2004). Recently, a protease (FtsH6) has been described that specifically breaks down chlorophyll-binding proteins in senescence (Zelisko *et al.*, 2005). We propose that disassembly and degradation of the pigment-proteolipids of thylakoids is mediated by a complex of enzymes, including PaO (which in turn interacts with a second enzyme, red chlorophyll catabolite reductase (RCCR) reductase (Hörtensteiner *et al.*, 2000; Eckhardt *et al.*, 2004)), *Y* (Hörtensteiner, 2006) and FtsH6 (Zelisko *et al.*, 2005) – and possibly other activities too, such as acyl hydrolase (He & Gan, 2002). A search for a multienzyme complex that functions as a machine for dismantling chloroplast membranes is justifiable. Identification of *Y* and other recently reported genes as the putative components of such a machine is a significant step towards an understanding of the mechanism and control of this central event in senescence.

Conclusion

This report has described how classical genetics and detailed biochemical analysis paved the way for the identification of a strong candidate for a key gene in the chlorophyll catabolic pathway using the tools of modern comparative genomics and transcriptomics. It has also shown how, by identifying this candidate and determining its protein product, it has now become possible to formulate and test new hypotheses concerning the biochemical regulation of chlorophyll catabolism. The practical application of this work has also been significant, as it has led to the development of an allele-specific marker which, to date, has shown no recombination with *y* and which is currently being employed in breeding programmes to transfer this recessive phenotype.

Acknowledgements

This work was supported by the BBSRC (UK), the Swiss National Science Foundation (3100A0-105389) and USDA/CSREES for Hatch Project MONB00235.

Ian Armstead[1]*, Iain Donnison[1], Sylvain Aubry[2], John Harper[1], Stefan Hörtensteiner[2], Caron James[1], Jan Mani[2], Matt Moffet[3], Helen Ougham[1], Luned Roberts[1], Ann Thomas[1], Norman Weeden[3], Howard Thomas[1] and Ian King[1]

[1]Institute of Grassland and Environmental Research, Aberystwyth SY23 3EB, UK; [2]Institute of Plant Sciences, University of Bern, Altenbergrain 21, CH-3013 Bern, Switzerland; [3]Department of Plant Sciences and Plant Pathology, Montana State University, Bozeman, MT 59717, USA.
(*Author for correspondence:
tel +1970 823108; fax +1970 823242;
email ian.armstead@bbsrc.ac.uk)

References

Alm V, Fang C, Busso CS, Devos KM, Vollan K, Grieg Z, Rognli OA. 2003. A linkage map of meadow fescue (*Festuca pratensis* Huds) and comparative mapping with other Poaceae species. *Theoretical and Applied Genetics* **108**: 5–40.

Armstead IP, Turner LB, King IP, Cairns AJ, Humphreys MO. 2002. Comparison and integration of genetic maps generated from F2 and BC1-type mapping populations in perennial ryegrass. *Plant Breeding* **121**: 501–507.

Cha KW, Lee YJ, Koh HJ, Lee BM, Nam YW, Paek NC. 2002. Isolation, characterization, and mapping of the stay green mutant in rice. *Theoretical and Applied Genetics* **104**: 526–532.

Department for Environment, Food and Rural Affairs. 2006. *Plant varieties and seeds gazette.* Special edition number 501. Cambridge, UK: The Plant Variety Rights Office.

Eckhardt U, Grimm B, Hörtensteiner S. 2004. Recent advances in chlorophyll biosynthesis and breakdown in higher plants. *Plant Molecular Biology* **56**: 1–14.

Emanuelsson O, Nielsen H, von Heijne G. 1999. ChloroP, a neural network-based method for predicting chloroplast transit peptides and their cleavage sites. *Protein Science* **8**: 978–984.

Farrar K, Asp T, Lubberstedt T, Xu M, Thomas A, Christiansen C, Humphreys MW, Donnison IS. 2006. Construction of two *Lolium perenne* BAC libraries and identification of BACs containing candidate genes for disease resistance and forage quality. *Molecular Breeding.* (In press.)

Hauck B, Gay AP, Macduff J, Griffiths CM, Thomas H. 1997. Leaf senescence in a non-yellowing mutant of *Festuca pratensis*, implications of the stay-green mutation for photosynthesis, growth and nitrogen nutrition. *Plant, Cell & Environment* **20**: 1007–1018.

He Y, Gan S. 2002. A gene encoding an acyl hydrolase is involved in leaf senescence in *Arabidopsis. Plant Cell* **14**: 805–815.

Hörtensteiner S. 2004. The loss of green color during chlorophyll degradation – a prerequisite to prevent cell death? *Planta* **219**: 191–194.

Hörtensteiner S. 2006. Chlorophyll degradation during senescence. *Annual Review of Plant Biology* **57**: 55–77.

Hörtensteiner S, Rodoni S, Schellenberg M, Vicentini F, Nandi OI, Qui YL, Matile P. 2000. Evolution of chlorophyll degradation, the significance of RCC reductase. *Plant Biology* **2**: 63–67.

Jones ES, Mahoney NL, Hayward MD, Armstead IP, Jones JG, Humphreys MO, King IP, Kishida T, Yamada T, Balfourier F, Charmet G, Forster JW. 2002. An enhanced molecular marker-based map of perennial ryegrass (*Lolium perenne* L.) reveals comparative relationships with other Poaceae species. *Genome* **45**: 282–295.

Kingston-Smith AH, Thomas H, Foyer CH. 1997. Chlorophyll a fluorescence, enzyme and antioxidant analysis provide evidence for the operation of an alternative electron sink during leaf senescence in a stay-green mutant of *Festuca pratensis. Plant, Cell & Environment* **20**: 1323–1337.

Moore BJ, Donnison IS, Harper JA, Armstead IP, King J, Thomas H, Jones RN, Jones TH, Thomas HM, Morgan WG, Thomas A, Ougham HJ, Huang L, Fentem T, Roberts LA, King IP. 2005. Molecular tagging of a senescence gene by introgression mapping of a mutant stay-green locus from *Festuca pratensis. New Phytologist* **165**: 801–806.

Morgan PW, Finlayson SA, Childs KL, Mullet JE, Rooney WL. 2002. Opportunities to improve adaptability and yield in grasses, lessons from sorghum. *Crop Science* **42**: 1791–1799.

Pooma W, Gersos C, Grotewold E. 2002. Transposon insertions in the promoter of the *Zea mays* a1 gene differentially affect transcription by the myb factors P and C1. *Genetics* **161**: 793–801.

Roca M, James C, Pruzinska A, Hortensteiner S, Thomas H, Ougham H. 2004. Analysis of the chlorophyll catabolism pathway in leaves of an introgression senescence mutant of *Lolium temulentum. Phytochemistry* **65**: 1231–1238.

Sim S, Chang T, Curley J, Warnke SE, Barker RE, Jung G. 2005. Chromosomal rearrangements differentiating the ryegrass genome from the Triticeae, oat, and rice genomes using common heterologous RFLP probes. *Theoretical and Applied Genetics* **110**: 1011–1019.

Thomas H. 1987. Sid, a Mendelian locus controlling thylakoid membrane disassembly in senescing leaves of *Festuca pratensis. Theoretical and Applied Genetics* **73**: 551–555.

Thomas H, Howarth CJ. 2000. Five ways to stay green. *Journal of Experimental Botany* **51**: 329–337.

Thomas H, Ougham H, Canter P, Donnison I. 2002. What stay-green mutants tell us about nitrogen remobilisation in leaf senescence. *Journal of Experimental Botany* **53**: 801–808.

Thomas H, Smart CM. 1993. Crops that stay green. *Annals of Applied Biology* **123**: 193–219.

Thomas H, Stoddart JL. 1975. Separation of chlorophyll degradation from other senescence processes in leaves of a mutant genotype of meadow fescue (*Festuca pratensis*). *Plant Physiology* **56**: 438–441.

Valentinuz OR, Tollenaar M. 2004. Vertical profile of leaf senescence during the grain-filling period in older and newer maize hybrids. *Crop Science* **44**: 827–834.

Vicentini F, Schellenberg M, Thomas H, Matile P. 1995. Chlorophyll breakdown in senescent leaves, identification of the biochemical lesion in a stay-green genotype of *Festuca pratensis* Huds. *New Phytologist* **129**: 247–252.

Zelisko A, Garcia-Lorenzo M, Jackowski G, Jansson S, Funk C. 2005. AtFtsH6 is involved in the degradation of the light-harvesting complex II during high-light acclimation and senescence. *Proceedings of the National Academy of Sciences, USA* **102**: 13699–13704.

Zimmermann P, Hirsch-Hoffmann M, Hennig L, Gruissem W. 2004. GENEVESTIGATOR *Arabidopsis* microarray database and analysis toolbox. *Plant Physiology* **136**: 2621–2632.

Key words: Arabidopsis, chlorophyll catabolism, comparative genomics, *Festuca*, *Lolium*, rice, senescence, staygreen.

7.2 Cross-species identification of Mendel's I locus

Ian Armstead, Iain Donnison, Sylvain Aubry, John Harper, Stefan Hörtensteiner, Caron James, Jan Mani, Matt Moffet, Helen Ougham, Luned Roberts, Ann Thomas, Norman Weeden, Howard Thomas, Ian King.

Reprinted from: *Science* (2007) 315, 73

In this *Brevia*, it is shown that the *SGR* locus identified in *Festuca pratensis* is the same as the *Pisum I* locus used by Gregor Mendel for describing the genetic laws of heredity. Confirmation of the SGR function has been achieved by silencing an SGR ortholog in *Arabidopsis thaliana*, leading to staygreeness of the leaves during senescence. This publication identified the third out of seven loci Mendel was using for his studies.

Cross-Species Identification of Mendel's *I* Locus

Ian Armstead,[1]* Iain Donnison,[1] Sylvain Aubry,[2] John Harper,[1] Stefan Hörtensteiner,[2] Caron James,[1] Jan Mani,[2] Matt Moffet,[3] Helen Ougham,[1] Luned Roberts,[1] Ann Thomas,[1] Norman Weeden,[3] Howard Thomas,[1] Ian King[1]

We identified gene homologs in *Pisum sativum* (pea), *Arabidopsis thaliana*, and *Festuca pratensis* (meadow fescue), mutations of which partially disable plant senescence. The biochemical properties and map location of this gene in pea indicate that it is the same locus that determines yellow (*I*) and green (*i*) cotyledon color, as originally described by Mendel in his seminal paper (*1*). Staygreen (the gene *sgr*), the indefinite retention of greenness in senescing leaves and cotyledons, is a genetic variant that interferes with the normal expression of senescence. Biochemical (*2*, *3*) (Fig. 1A) and genetic analyses of *sgr* from pea and *F. pratensis* (*4*) show that it segregates as a discrete phenotype with equivalents in maize, sorghum, and rice (*5*, *6*). By using the *Lolium-Festuca* gene introgression system and extrapolating from genetic synteny, we show that *F. pratensis sgr* on chromosome (C)5 maps to a position corresponding to *sgr* on rice C9 (*4*, *6*, *7*). Fine mapping in *Festuca* delimits this to a region equivalent to circa 200 kb of the rice genome containing 30 annotated gene models, including a predicted senescence-inducible chloroplast-specific stay-green protein (*4*, *7*, *8*).

We investigated the temporal and tissue-specific expression patterns of the most similar *Arabidopsis* gene model, At4g22920, through the Genevestigator Meta-Analyzer database (*9*). These patterns indicate that At4g22920 is up-regulated in days 45 to 50 during maximal senescence in the *Arabidopsis* life cycle (fig. S1A) and that the strongest expression of this gene occurs in senescent leaves, although it is also detected in seeds, petals, and sepals. RNA interference (RNAi) was also used to silence the expression of At4g22920 in *Arabidopsis*, resulting in plants with leaves exhibiting prolonged chlorophyll retention upon dark incubation (Fig. 1B), phenotypically equivalent to *sgr F. pratensis*. Thus, alleles of *F. pratensis* and rice homologs of *Arabidopsis* At4g22920 likely underlie the monocot stay-green phenotypes.

In order to explore the parallels between Mendel's pea cotyledons and the stay-green leaf phenotypes in *Arabidopsis*, *Festuca*, and rice, we genetically mapped the pea homolog of *sgr* in two different pea populations segregating for cotyledon color polymorphism (*I* and *i*). No recombination between *I* and *sgr* was observed in 104 progeny, reflecting a theoretical maximum distance between *sgr* and *I* of 0.48 cM (fig. S1B). Northern analysis in pea indicates that *sgr* has reduced expression in mutant senescing leaves when compared with that of wild type (Fig. 1C).

This report characterizes a rare example of an unbroken chain from gene sequence to trait through biochemical, cell biological, and physiological definitions of phenotype, in which genomics and functional analysis in model species have played a critical role. This study results in the identification of a gene that plays a fundamental role in chlorophyll catabolism during plant senescence. In addition, it suggests that the cotyledon color trait described by Mendel reflects allelic variation in a pea gene, homologs of which are responsible for the stay-green phenotype in both dicots and monocots.

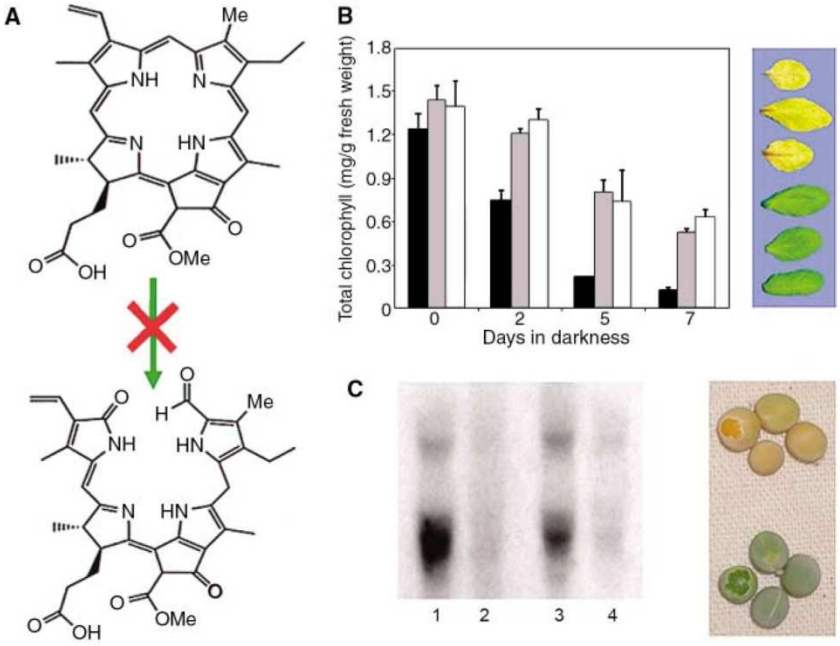

Fig. 1. (**A**) In mutant and silenced genotypes, inhibition (X) of the ring-opening step between (top) pheophorbide and (bottom) red chlorophyll catabolite in the chlorophyll breakdown pathway (*3*) leads to retention of greenness in senescing leaves. (**B**) RNAi silencing of *Arabidopsis* At4g22920 causes a stay-green phenotype. (Left) Degradation of chlorophyll in control (black) and two independently RNAi-silenced genotypes (gray and white) during dark-induced, detached leaf senescence. Error bars indicate standard deviation. (Right) Wild-type (top) and stay-green (bottom) leaf phenotypes of *Arabidopsis* after 5 days of dark-induced, detached-leaf senescence. (**C**) (Left) Northern analysis using RNA extracted from senescing leaves of wild-type (lanes 1 and 3) and stay-green (lanes 2 and 4) pea plants. (Right) Wild-type (top) and stay-green (bottom) pea cotyledons illustrating Mendel's *I* and *i* phenotypes, respectively.

References and Notes

1. G. Mendel, *Verh. Naturforsch. Ver. Brünn.* **4**, 3 (1866).
2. H. Thomas, M. Schellenberg, F. Vicentini, P. Matile, *Bot. Acta* **109**, 3 (1996).
3. S. Hörtensteiner, *Annu. Rev. Plant Biol.* **57**, 55 (2006).
4. I. P. Armstead *et al.*, *New Phytol.*, **172**, 592 (2006).
5. H. Thomas, C. M. Smart, *Ann. Appl. Biol.* **123**, 193 (1993).
6. K. W. Cha *et al.*, *Theor. Appl. Genet.* **104**, 526 (2002).
7. Materials and methods are available as supporting material on *Science* Online.
8. Institute for Genomic Research (TIGR), gene model LOC_Os09g36200, www.tigr.org.
9. Eidgenössische Technische Hochschule Zurich, www.genevestigator.ethz.ch/.
10. This work was supported by the Biotechnology and Biological Sciences Research Council (UK), the Swiss National Science Foundation (3100A0-105389), and Cooperative State Research, Education, and Extension Service, U.S. Department of Agriculture, for Hatch Project MONB00235.

Supporting Online Material

www.sciencemag.org/cgi/content/full/315/5808/73/DC1
Materials and Methods
Fig. S1
Table S1
References

24 July 2006; accepted 16 October 2006
10.1126/science.1132912

[1]Institute of Grassland and Environmental Research, Aberystwyth SY23 3EB, UK. [2]Institute of Plant Sciences, University of Bern, Altenbergrain 21, CH-3013 Bern, Switzerland. [3]Department of Plant Sciences and Plant Pathology, Montana State University, Bozeman, MT 59717, USA.

*To whom correspondence should be addressed. E-mail: ian.armstead@bbsrc.ac.uk

7.3 Stay-green protein, defective in Mendel's green cotyledon mutant, acts independent and upstream of pheophorbide a oxygenase pathway in the chlorophyll catabolic pathway

Sylvain Aubry, Jan Mani, Stefan Hörtensteiner

Reprinted from *Plant Molecular Biology*, published on-line February 2008

In this study, we characterized the SGR mutation in *Pisum* and obtained more information on the biochemical function of SGR factor in relation to degradation of chl. Characterizing the staygreen *Pisum* line JI2775, as well as different sets of transgenic *Arabidopsis*, we tried to understand the molecular basis of the staygreen phenotype of those lines. In contrast to most of the literature published to date on SGR, we confirm that SGR does not act as a PAO regulating factor, but rather as an upstream element regulating of degradation of the photosystems.

Plant Mol Biol
DOI 10.1007/s11103-008-9314-8

Stay-green protein, defective in Mendel's green cotyledon mutant, acts independent and upstream of pheophorbide *a* oxygenase in the chlorophyll catabolic pathway

Sylvain Aubry · Jan Mani · Stefan Hörtensteiner

Received: 18 October 2007 / Accepted: 12 February 2008

Abstract Type C stay-green mutants are defined as being defective in the pathway of chlorophyll breakdown, which involves pheophorbide *a* oxygenase (PAO), required for loss of green color. By analyzing senescence parameters, such as protein degradation, expression of senescence-associated genes and loss of photosynthetic capacity, we demonstrate that JI2775, the green cotyledon (*i*) pea line used by Gregor Mendel to establish the law of genetics, is a true type C stay-green mutant. *STAY-GREEN* (*SGR*) had earlier been shown to map to the *I* locus. The defect in JI2775 is due to both reduced expression of *SGR* and loss of SGR protein function. Regulation of PAO through SGR had been proposed. By determining PAO protein abundance and activity, we show that PAO is unaffected in JI2775. Furthermore we show that pheophorbide *a* accumulation in the mutant is independent of PAO. When silencing *SGR* expression in *Arabidopsis pao1* mutant, both pheophorbide *a* accumulation and cell death phenotype, typical features of *pao1*, are lost. These results confirm that SGR function within the chlorophyll catabolic pathway is independent and upstream of PAO.

Keywords Chlorophyll breakdown · Gregor Mendel · Pea *I* locus · Pheophorbide *a* oxygenase · Stay-green mutant · Senescence

Abbreviations

chl	Chlorophyll
chlide	Chlorophyllide
EST	Expressed sequence tags
LHCII	Light harvesting complex of photosystem II
NCCs	Nonfluorescent chlorophyll catabolites
pheide	Pheophorbide
PAO	Pheophorbide *a* oxygenase
pFCC	Primary fluorescent chlorophyll catabolite
PS	Photosystem
RCCR	Red chlorophyll catabolite reductase
Sgr	Stay-green

Introduction

Chlorophyll (chl) breakdown is widely used as a tool for monitoring physiological senescence in plants. Thereby green chl is converted in a multistep pathway to linear colorless and nonfluorescent tetrapyrroles, NCCs. The pathway starts with the consecutive removal from chl of phytol and the Mg atom by chlorophyllase and a metal-chelating substance, respectively. Loss of the green color occurs during the subsequent opening of the porphyrin macrocycle of pheophorbide (pheide) *a* by the coupled action of pheide *a* oxygenase (PAO) and red chl catabolite reductase (RCCR). This yields a primary fluorescent

Electronic supplementary material The online version of this article (doi:10.1007/s11103-008-9314-8) contains supplementary material, which is available to authorized users.

S. Aubry · S. Hörtensteiner (✉)
Institute of Plant Biology, University of Zurich, Zollikerstrasse 107, 8008 Zurich, Switzerland
e-mail: shorten@botinst.uzh.ch

J. Mani · S. Hörtensteiner
Institute of Plant Sciences, University of Bern, Altenbergrain 21, 3013 Bern, Switzerland

Present Address:
J. Mani
Institute of Cell Biology, University of Bern, Baltzerstr. 4, 3012 Bern, Switzerland

catabolite (pFCC), which is exported from the plastid by a primary active transporter. Further steps in the pathway are reminiscent of detoxification processes widely occurring in plants (Kreuz et al. 1996). Thus, pFCCs are activated by hydroxylation and after further modification they are imported into the vacuole by another primary active transport system. Due to the acidic vacuolar pH, FCCs eventually tautomerize non-enzymatically to NCCs (Oberhuber et al. 2003; Hörtensteiner 2006).

All but one of the NCCs isolated so far from higher plants have been shown to derive from chl *a* (Hörtensteiner 2006; Müller et al. 2006). One reason for this is the substrate-specificity of PAO for pheide *a*, with pheide *b* being a competitive inhibitor (Hörtensteiner et al. 1995). Furthermore, reduction of chl *b* to chl *a* within the chl-protein complexes of the photosystems (PS), has been suggested a prerequisite for chl degradation, leading to the destabilization of these chl-protein complexes (Hörtensteiner 2006). The recent cloning of NYC1 from rice (Kusaba et al. 2007) corroborated this assumption. *nyc1* mutants show a stay-green phenotype and besides the retention of both chl *a* and *b*, *nyc1* specifically retains light harvesting complex of photosystem II (LHCII) subunits known to bind large proportions of chl *b*. In this respect NYC1 represent an early (primary) element of metabolic regulation of chl breakdown.

Another step of regulation is at the level of PAO. Like *NYC1*, *PAO* expression is senescence-specific and absence of PAO in a respective mutant, *pao1*, leads to a stay-green phenotype in the dark. Due to the accumulation of phototoxic pheide *a*, *pao1* plants show a light-dependent lesion mimic phenotype (Pružinská et al. 2005).

Recently, a third type of stay-green mutants has become a major focus in plant senescence research. These mutants are defective in a gene identified in the Bf993 mutant of *Festuca pratensis* (Thomas 1987). The gene was termed *SID* (*senescence-induced degradation*), but orthologous genes from rice, pea and *Arabidopsis* have now been designated *SGR* (*STAY-GREEN*) (Jiang et al. 2007; Park et al. 2007; Sato et al. 2007), *SGN* (Park et al. 2007) or *NYE1* (*nonyellowing*) (Ren et al. 2007). Introgression of the *sid* locus into different *Lolium* species allowed the molecular tagging of the gene (Thomas 1997). By exploiting the high micro synteny between *Lolium-Festuca* and rice, it was possible to identify the candidate locus in a *Lolium* stay-green mapping population that corresponded to a stay-green locus (*SGR*) in rice (Armstead et al. 2006). Silencing of the orthologous gene, *AtSGR1* (At4 g22920) of *Arabidopsis*, caused the same stay-greenness as in *Festuca* or *Lolium* (Armstead et al. 2007).

Furthermore, it has been shown that *SGR* maps to the *I* locus of Mendel's green cotyledon mutant (Armstead et al. 2007). Thus, the *I* locus is only the third identified locus of the seven traits Gregor Mendel used for establishing his laws of genetic inheritance (Mendel 1866). The first locus that has been molecularly identified is the so-called *r* (*rugosus*) locus. The mutation, which is due to a 0.8 kb insertion, resides in a gene encoding a starch branching enzyme and causes the formation of wrinkled seeds (Bhattacharyya et al. 1990). The second identified gene (*Le* locus), encodes gibberellin 3β-hydroxylase. The loss of function missense mutation near the active site abolishes gibberellin biosynthesis and, thus, affects stem length (Lester et al. 1997). Recently, the mutation of Mendel's *I* locus was elucidated molecularly (Sato et al. 2007). In contrast to an earlier finding of reduced *SGR* gene expression in the mutant (Armstead et al. 2007), gene expression was found to be normal. By complementing a rice *sgr* mutant with rice *SGR* gene exhibiting a 6-bp-insertion, it was concluded that the analogous mutation present in Mendel's green pea *SGR* gene abolished SGR function (Sato et al. 2007).

The *Festuca sid* mutant is a classical representative of the so-called 'cosmetic' type C stay-green mutants (Thomas and Howarth 2000). In these non-functional stay-greens, retention of chl is uncoupled from other senescence events, such as loss of photosynthetic capacity, which proceed normally (Hilditch et al. 1986, 1989). Hence, the gene mutations of type C mutants were considered to affect the pathway of chl breakdown directly. This has been confirmed and is obvious for *pao1* and *nyc1*, which are affected in catabolic steps of the pathway (Pružinská et al. 2003, 2005; Kusaba et al. 2007). The situation is different for *sgr/sid* mutants, since so far the function of SGR/SID could not unequivocally be demonstrated. Several early reports deal with the biochemical lesion of *sid* and *sid*-like mutants, including Mendel's *I* mutant (Vicentini et al. 1995; Thomas et al. 1996; Roca et al. 2004). The cumulative results of these investigations indicated that SGR/SID affects PAO activity. Thus, the mutants consistently accumulated chlorophyllide (chlide) and pheide *a* during senescence and they exhibited reduced PAO activities. It was argued that pheide *a* accumulation would feed back inhibit chl breakdown, in order to prevent further chl intermediate accumulation, thereby minimizing the phototoxic potential of these pigments (Thomas 1997; Matile et al. 1999; Hörtensteiner 2006). Along with the retention of chl, chl-binding proteins were shown to be retained in the mutants (Hilditch et al. 1989; Jiang et al. 2007; Park et al. 2007; Sato et al. 2007). Recently, it was demonstrated that rice SGR is able to specifically interact with LHCII subunits (Park et al. 2007). This together with the retention of these proteins in the mutants, suggested that SGR might be involved in dismantling chl-protein complexes as a prerequisite for both chl and apoprotein degradation.

The aim of this study was to thoroughly characterize Mendel's pea mutant (JI2775) in respect to senescence and

chl breakdown. We confirm that JI2775 is a classical type C stay-green mutant by analyzing different parameters of senescence, such as chl fluorescence and degradation, expression of senescence associated genes and protein degradation. We further show that JI2775 is impaired not only in SGR protein function, but by *SGR* expression and SGR immunoblot analysis demonstrate that gene expression is affected as well in the mutant. We re-addressed the proposed linkage between SGR and PAO. Using PAO activity assays and immunoblot analysis, we show that PAO function is unaffected in JI2775. Furthermore, we show that the amount of pheide *a* accumulating in the mutant is independent of the activity of PAO. Silencing of *SGR* expression in *pao1*, results in the losses of pheide *a* accumulation and cell death phenotype, typical features of *pao1*. We conclude that the function of SGR is upstream and independent of PAO. This together with the previously demonstrated interaction of SGR with LHCII, and retention during senescence of *sgr* mutants of chl binding proteins indicates a (predominant) role of SGR in dismantling of chl-protein complexes during senescence.

Experimental procedures

Plant material and senescence induction

Pisum sativum lines JI4 (yellow cotyledons) and JI2775 (green cotyledons) were obtained from the *Pisum* germplasm collection of the John Innes Center, Norwich, UK. The Columbia (Col-0) ecotype of *Arabidopsis* (*Arabidopsis thaliana*) was used as wild type. For silencing of *AtSGR1* by RNA interference, a pHannibal-derived construct as described in Armstead et al. (2007) was used. *pao1* was transformed by a floral dip method and homozygous *pao1 atsgr1*i lines selected by kanamycin resistance. This was possible, since *pao1* is not resistant to kanamycin (Alonso et al. 2003; Pružinská et al. 2005). Production of the *AtSGR1*-silencing lines, *atsgr1*i, has been described (Armstead et al. 2007). A homozygous *AtSGR2* T-DNA insertion line of the SALK collection (Alonso et al. 2003) was obtained from the European Arabidopsis Stock Center, Nottingham, UK. T-DNA insertion was verified by sequencing a PCR product obtained with the left T-DNA border primer LBb1 (5′-GCGTGGACCGCTTGCTGCAA T-3′) and an *AtSGR2*-specific primer (5′-GCAACTGGT GAAAGCAAGAAC-3′). A *Lolium* line carrying a *sid* gene introgression has been described (Roca et al. 2004) and was obtained from H. Ougham, IGER, Aberystwyth, Wales, UK.

Plants were grown on soil in long-day condition (16 h/8 h) under fluorescent light of 60–120 µmol photons m^{-2} s^{-1} at 22°C. For senescence induction, leaves from 3- to 4-week-old plants were excised and incubated in permanent darkness on wet filter paper for up to 11 days at ambient temperature. Alternatively, attached leaves were individually covered with aluminum foil.

Cloning strategy

Genomic DNA and cDNA was isolated from both JI4 and JI2775 leaves as described (Murray and Thompson 1980; Pružinská et al. 2005). *PsSGR* was amplified with primers PsSGR-LP (5′-CG*GGATCC*ATGGATACTCTAACGAG TGCTC-3′) and PsSGR-RP (5′-TT*CTGCAG*TTACAAGTT ACCATGTTGGGTTC-3′) using the proofreading Pfu polymerase (Promega). After digestion with *Bam*HI and *Pst*I, fragments were cloned into pQE30 (Qiagen) to yield pQEJI4 and pQEJI2775, and inserts sequenced. For constructing binary plasmids, *SGR* open reading frames were amplified from both pQE plasmids with PsSGR-LP2 (5′-GT A*CCATGG*ATACTCTAACGAGTGCTCCTTTACTC-3′) and PsSGR-RP2 (5′-GC*GGATCC*TTACAAGTTACCATG TTGGGTTC-3′) and, after restriction with *Nco*I and *Bam*HI cloned into pHannibal (Wesley et al. 2001) containing the CaMV 35S-double enhancer promoter and a *nos* terminator. The gene constructs were excized by *Not*I and cloned into pGreen0029 (Hellens et al. 2000) yielding pGr-JI4-SGR and pGr-JI2775-SGR, respectively. After verifying inserts by sequencing, constructs were transformed into *Agrobacterium* together with pSOUP (Hellens et al. 2000).

Plant transformation

For transient expression in *Nicotiana benthamiana* leaves, 5 ml of *Agrobacterium* harboring the respective plasmids were grown overnight at 28°C. Cells were collected by centrifugation (3,000 g, 15 min), pellets resuspended in 1 ml of acetosyringone buffer (1 mM $MgCl_2$, 150 mM acetosyringone, 1 mM Mes-KOH pH 5.6) and grown again for 4 h (Llave et al. 2000). Using a 1 ml syringe, the abaxial side of leaves of 5-week-old *N. benthamiana* plants was infiltrated with the *Agrobacterium* cultures. For transformation of *Arabidopsis pao1* with a pHannibal-derived *AtSGR1* silencing construct (Armstead et al. 2007), the floral dip method was used (Sidler et al. 1998).

RNA isolation and real-time PCR

For RT-PCR analysis, total RNA was prepared from *Pisum* leaves and reverse transcribed as described (Pružinská et al. 2005). Quantitative PCR was performed in a LightCycler (Roche Diagnostics) using the QuantiTect SYBR Green PCR kit (Qiagen). 10- to 100-fold dilutions of first-strand cDNA reaction mixes (corresponding to 0.3–3 ng of RNA) were employed in 20 µl reactions and were used to

calculate the real-time PCR efficiency of each sample. The relative expression ratios of target gene (SGR) were calculated in comparison to a reference gene, *ACT2* (Kürsteiner et al. 2003). For semiquantitative and/or quantitative PCR the following specific primers were used: *PsACT2* (forward, 5′-TGGAATCCACGAGACAACCTA-3′ and reverse, 5′-TTCTGTGAACGATTCCTGGAC-3′); *PsSGR* (forward, 5′-ACGGTGACGGCAATTTATTC-3′ and reverse, 5′-TTCAACGGTGGAAAACAACA-3′); *PsSAG12* (forward, 5′-TCTGAGCAAGAGCTTGTGGA-3′ and reverse 5′-TATCCCCCAGCATCAATAGC-3′); *AtSGR1* (forward, 5′-TGGGCAAATAGGCTATACCG-3′ and reverse, 5′-AAGTTCCCATCTCCATGCAC-3′); *AtSGR2* (forward, 5′-TCCAACATCCCGGAGTAC-3′ and reverse, 5′-AGGGTTAGGTATTTCCAAC-3′); *ACT2* (forward, 5′-TGGAATCCACGAGACAACCTA-3′ and reverse, 5′-TTCTGTGAACGATTCCTGGAC-3′).

Southern blot analysis

High molecular weight genomic DNA was isolated from both *Pisum* lines (Chakraborti et al. 2006). Each 15 μg was digested with restriction endonucleases, electrophoresed on 0.9% agarose gels and transferred to positively charged nylon membrane (Roche). The blot was hybridized overnight at 42°C with a digoxigenin-UTP-labeled 1.5 kb PCR fragment (using pQEJI4 and primers PsSGR-RP and PsSGR-LP) and washed at 65°C with 0.2× SSC, 0.1% SDS. Subsequent detection by anti-digoxigenin-AP (Roche), and bromochloroindolyl phosphate/nitroblue tetrazolium as substrate was according to the manufacturer's protocol.

Analysis of chl and chl catabolites

Chl was isolated from dark-incubated *Arabidopsis* and pea leaves, or from *N. benthamiana* according to Pružinská et al. (2005) and chl concentrations were determined spectrophotometrically (Strain et al. 1971). Chl and green pigments (chlide and pheide) were extracted and analyzed as described (Pružinská et al. 2005). For bipyridyl treatments, leaf discs were senesced in the dark by floating on water, 1% DMSO or 1 mM 2,2′-bipyridyl (containing 1% DMSO).

PAO protein extraction and activity measurement

PAO was isolated from *Pisum* chloroplast membranes by Triton X-100 solubilization according to a standard procedure (Hörtensteiner et al. 1995; Pružinská et al. 2005; Ren et al. 2007). PAO activity was monitored *in vitro* essentially as described (Pružinská et al. 2007) but using 0.06 μg μl^{-1} of His_6-AtRCCR (Pružinská et al. 2007), and 100 U of catalase (Sigma) to replace red chl catabolite-forming factor (Pružinská et al. 2005). pFCC formation was followed by reversed-phase HPLC and fluorescence detection (320/450 nm) using 36% (v/v) 50 mM potassium phosphate buffer, pH 7, in methanol as solvent (Pružinská et al. 2005).

Production of anti-AtSGR antiserum and immunoblot analysis

A polyclonal anti-AtSGR antiserum was obtained from rabbits immunized with two polypeptides directed against two AtSGR peptides (NH_2-EGVNGYSGTQTEGIAT-COOH and NH_2-SQSINNSQLQGWAN-COOH). The serum was purified by affinity purification and tested by ELISA (Eurogentec, Seraing, Belgium).

After separation by SDS-PAGE, proteins were transferred to nitrocellulose membranes according to standard procedures. Proteins were labeled with monoclonal antibodies against PAO (1:500; Gray et al. 2004) and polyclonal antibodies against the following proteins: AtSGR (1:1,000), LHCII (1:2,000; Pružinská et al. 2003), Rubisco small subunit (1:2,000; S. Gepstein, Israel), Rubisco LS (1:2,000; S. Gepstein, Israel), PsaA (1:5,000; J.D. Rochaix, Geneva, Switzerland), PsaD (1:5,000; J.D. Rochaix, Geneva, Switzerland), Lhca (1:2,000; AgriSera, Sweden), PsbA (1:1,000; H. Ougham, Aberystwyth, Wales), and Cytf (1:1,000; H. Ougham, Aberystwyth, Wales). Subsequently, the membranes were labeled with alkaline phosphatase- or peroxidase-conjugated secondary antibodies, and visualized using bromochloroindolyl phosphate/nitroblue tetrazolium (PsbA and Cytf), or with the chemiluminescent peroxidase substrate kit (Sigma). Chemiluminescence signals were quantified using an ImageQuant 400 system (GE Healthcare). Immunoblot analyses were carried out in duplicate or triplicate.

Chlorophyll fluorescence and CO_2 assimilation rate

Senescence was induced by darkening attached leaves with aluminum foil. Using a portable photosynthesis system LI-COR 6400 (Li-Cor, Lincoln, NE), maximum quantum yield of PSII (F_v/F_m) and minimal chl *a* fluorescence following dark incubation (F_0) were determined. Quantum efficiency of electron transport through PSII (ΦPSII) was measured after adaptation to day light for 20 min (Maxwell and Johnson 2000). Rates of CO_2 assimilation were determined at a flux density of 500 μmol m^{-2} s^{-1} and a CO_2 concentration of 380 μmol mol^{-1}.

SGR protein accession numbers

The GenBank accession numbers of SGRs and SGR-like proteins in plants, algae and bacteria species are as follows: *Arabidopsis thaliana* AtSGR1, AAW82962; AtSGR2, AAU05981; AtSGR3, AAM14392; *Bacillus sp.* BsSGR1,

ZP_01859452; BsSGR2, ZP_01170511; *Clostridium botulinum* CbSGR, CAL83726; *Clostridium purfigens* CpSGR, Q8XH99; *Glycine max* GmSGR1, AAW82959; GmSGR2, AAW82960; *Hordeum vulgare* HvSGR, AAW82955; *Lycopersicon esculentum* LeSGR, AAY98500; *Oryza sativa* OsSGR1, AAW82954; OsSGR2, BAF16284; OsSGR3, CAE05787; *Ostreococcus lucimarinus* OlSGR, XP_001420948; *Ostreococcus tauri* OtSGR, CAL56489; *Pisum sativum* PsSGR-JI4, CAP04954; PsSGR-JI2775, CAP04955; *Sorghum bicolor* SbSGR, AAW82958; *Vitis vinifera* VvSGR1, CAO63641; VvSGR2, CAO63642; VvSGR3, CAN81476; *Zea mays* ZmSGR1, AAW82956; ZmSGR2, AAW82957; *Zoysia japonica* ZjSGR, AAW82961. The following protein sequences were obtained from the Joint Genome Institute (http://jgi.doe.gov) (protein IDs are given) *Populus trichocarpa* PtSGR1, 548540; PtSGR2, 646534; *Chlamydomonas reinhardtii* CrSGR1, 144728; CrSGR2, 168164; *Physcomitrella patens* PpSGR1, 128024; PpSGR2, 139487; PpSGR3, 114221; PpSGR4, 27214.

Results and discussion

Mendel's *i* mutant exhibits a non-functional stay-green phenotype

Gregor Mendel's green cotyledon mutant, JI2775 (*i*/*i*), was compared with JI4 (*I*/*I*), a wild type line showing normal yellowing of seeds during maturation (Fig. 1a) (White 1916). JI4 and JI2775 are non-isogenic lines and exhibit some differences in respect to morphology, like a difference in average size of mature leaves (JI4: 12.63 ± 1.24 cm^2; JI2775: 8.33 ± 1.25 cm^2), or seed weight (JI4: 284 ± 30.5 mg; JI2775: 212.25 ± 39 mg). The stay-green phenotype of JI2775 was evident in all green parts of the plants, i.e. besides seeds and leaves (Fig. 1a) also in pods and stems (not shown).

To induce senescence, detached leaves were incubated in permanent darkness (Fig. 1a). After 8d dark incubation, 84% of chl was retained in JI2775, thus showing a stronger retention than stay-green *Lolium temulentum* (Roca et al. 2004) or *Arabidopsis nye1* (Ren et al. 2007). Increase in the chl *a* to *b* ratio is a characteristic of senescence-related chl breakdown (Pružinská et al. 2005). This is caused by chl *b* to *a* reduction, which is a prerequisite of breakdown beyond the level of pheide (Scheumann et al. 1999). Consequently, the chl *a*:*b* ratio increased during dark-incubation of JI4 leaves, but not in JI2775, indicating that both chl *a* and *b* are retained to the same extend in the mutant (Fig. 1c).

Stay-greenness during senescence does not necessarily imply a conservation of photosynthetic capacity, as seen in other instances of non-functional or so called cosmetic stay-greens (Kingston-Smith et al. 1997; Thomas and Howarth 2000). To examine the correlation between the greenness and leaf functionality, we covered attached pea leaves with aluminum foil in order to induce senescence and determined the maximal fluorescence yield (F_v/F_m) of photosystem II (PSII), reflecting the maximum quantum yield of the primary photochemistry of PSII (Fig. 2a). F_v/F_m decreased during the dark incubation in both lines, but the decrease was somewhat slower in JI2775 compared to JI4. We further analyzed F_0, an indicator of the connectivity of PSII

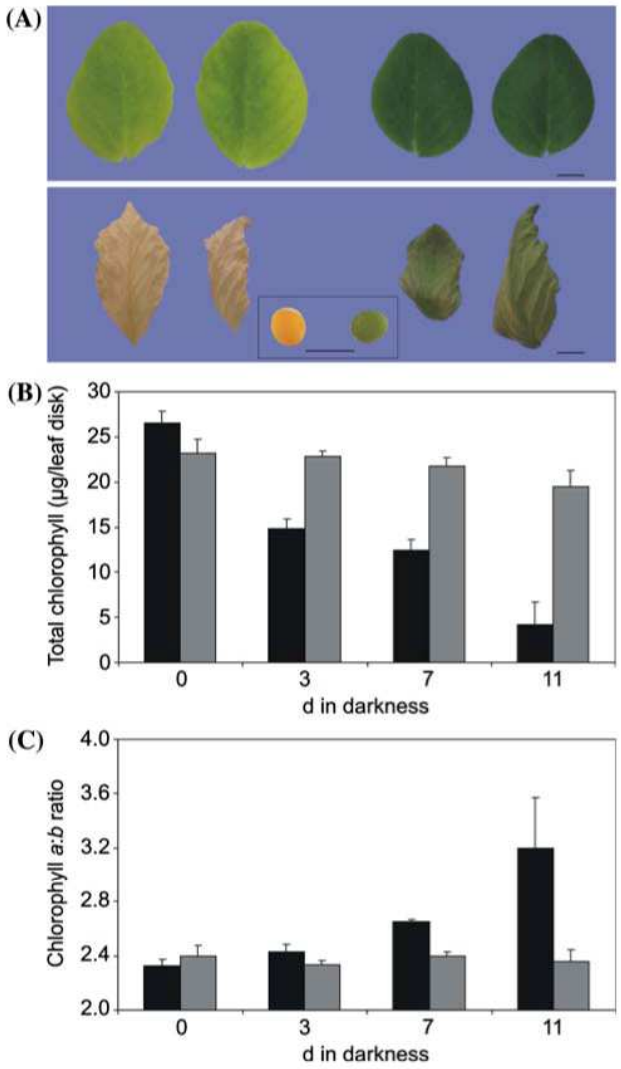

Fig. 1 Phenotype of the green cotyledon mutant JI2775 during chl breakdown. (**a**) Phenotype of individual leaves of JI4 (left) and JI2775 (right) after 11 days of dark-induced (upper panel) or natural senescence (lower panel). Inset, mature seeds from JI4 (left) and JI2775 (right) with the testa removed. Scale bars, 1 cm. (**b**) Degradation of chl in JI4 (black) and JI2775 (gray) during the course of dark-induced senescence. Data are means of a single representative experiment with three replicates. Error bars indicate SD. (**c**) Chl *a*:*b* ratio in JI4 (black) and JI2775 (gray) during the course of dark-induced senescence. Data are means of a single representative experiment with three replicates. Error bars indicate SD

antenna with the core center (Havaux 1993; Oh et al. 2000). During leaf senescence, F_0 increased more drastically in JI4 (Fig. 2b), indicating dissociation of LHCII complexes from the PSII core. In contrast, in the mutant PSII integrity seemed to be retained much longer. Finally, the quantum yield of PSII electron transport (Φ_{PSII}) decreased slower in JI2775, but after 11 days had reached similar values like JI4 (Supplemental Fig. 1). Together, these fluorescence parameters indicated that senescence-related reduction of photosynthetic activity was somewhat slower in JI2775, but eventually reached levels comparable to the wild type. Moreover, the rate of net photosynthesis as determined by measuring net CO_2 fixation, decreased similarly during the course of senescence in both lines (Fig. 2c). Hence, photosynthetic activity was uncoupled from chl metabolism in the mutant, qualifying JI2775 a type C stay-green mutant according to a recently suggested nomenclature of stay-green mutants (Thomas and Howarth 2000).

To further characterize the senescence behavior of JI2775, expression of *SAG12*, a commonly accepted marker of senescence (Quirino et al. 2000), was investigated by semiquantitative RT-PCR. In both lines, expression of *PsSAG12* increased to a similar extend during dark-induced senescence (Fig. 2d), indicating that senescence was initiated normally in the mutant.

We analyzed protein metabolism as a further marker of senescence progression. Again JI2775 behaved like JI4, i.e. overall protein degradation during dark-induced senescence was rather similar in both lines (data not shown). Nevertheless, differences were observed when individual photosynthesis-related proteins were analyzed by immunoblotting (Fig. 3a, b). LHCII was fully retained during the course of senescence in JI2775, a feature that has been described in different stay-green mutants (Hilditch et al. 1989; Bachmann et al. 1994; Pružinská et al. 2003; Park et al. 2007), but in contrast to the stay-green mutant Bf993 of *Festuca pratensis* (Thomas and Howarth 2000), proteolytic fragments of LHCII could not be detected in JI2775. In addition, core subunits of PSI (PsaD) and PSII (PsbA) were also retained to some extend in the mutant, and degradation of Rubisco subunits was somewhat slower in JI2775 compared to JI4. Together these data confirm earlier observations of high LHCII retention in stay-green mutants (Hilditch et al. 1989; Jiang et al. 2007; Park et al. 2007).

Overall, the diverse physiological data presented here confirm that JI2775 exhibits typical features of non-functional, type C stay-green mutants.

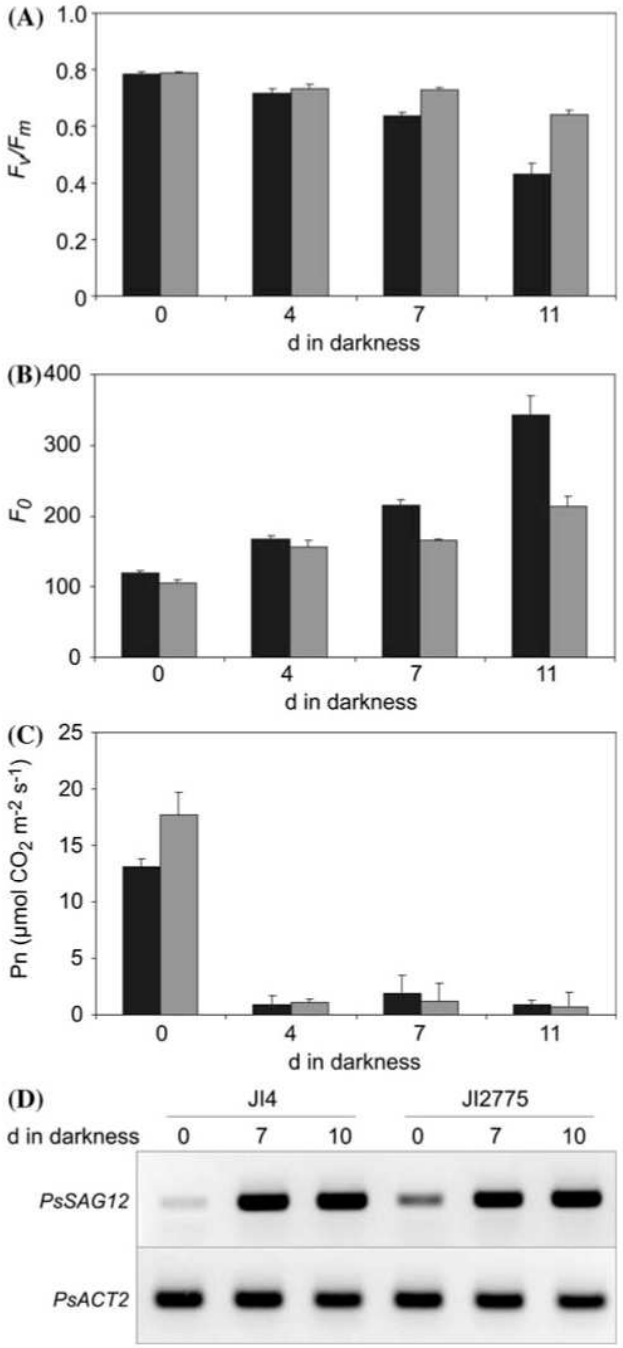

Fig. 2 Characterization of the senescence behavior of JI4 and JI2775. (**a**–**c**) Maximum quantum yield of PSII (F_v/F_m; **a**), minimum fluorescence in the dark (F_0; **b**) and net photosynthesis (Pn; **c**) during leaf senescence in JI4 (black) and JI2775 (gray). For senescence induction, attached leaves were covered with aluminum foil. Data are means of a single representative experiment with 6 replicates. Error bars indicate SE. (**d**) Semiquantitative analysis of expression of *PsSAG12* during senescence. *PsACT2* expression was used as control

Isolation and characterization of *SGR* genes and proteins

By genomic mapping, SGR has been shown to locate to the *I* locus of Gregor Mendel's green cotyledon mutant (Armstead et al. 2007). This was recently indirectly confirmed by a segregation analysis exploiting the size differences of intron three of the pea *SGR* gene (Sato et al.

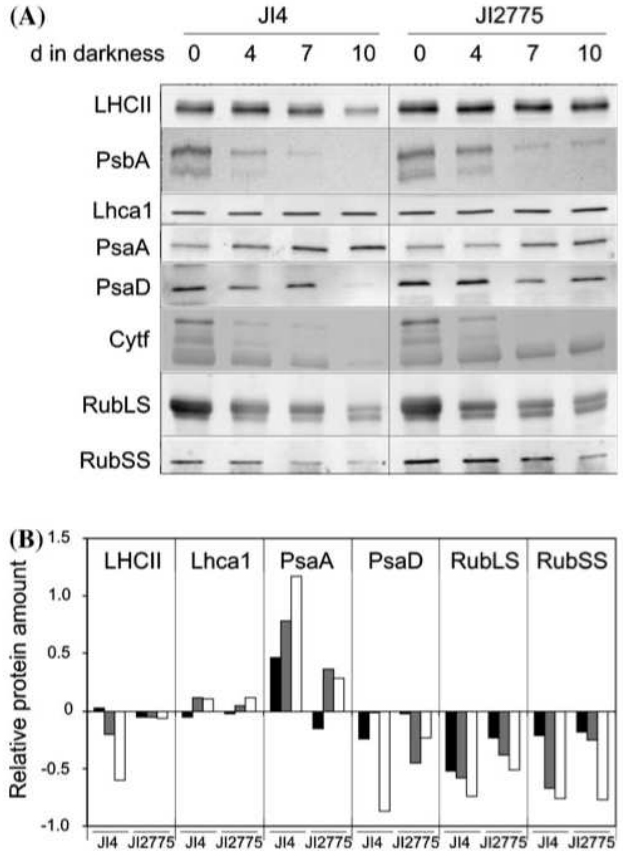

Fig. 3 Analysis of protein degradation during leaf senescence of JI4 and JI2775. (**a**) Immunoblot analysis of photosynthesis-related protein abundance in leaves of JI4 and JI2775 during dark-induced senescence. Antibodies against the following proteins were employed: LHCII and PsbA (photosystem II), LhcaI, PsaA and PsaD (photosystem I), Cytf (cytochrom b_6f complex) and Rubisco large (RubLS) and small subunit (RubSS). Gel loadings are based on equal amounts of fresh weight. (**b**) Relative changes of protein abundance as determined by quantifying the chemiluminescence signals of blots shown in (**a**). Bars represent relative changes of protein amounts after 4 days (black), 7 days (gray) and 10 days (white) of senescence as compared to 0 days samples. Thereby, negative values reflect degradation; positive values reflect increase of respective protein amounts. PsbA and Cytf blots (panel **a**) were visualized with a color substrate and, therefore, signals were not quantified

2007). We cloned the coding region of *PsSGR* from genomic DNA isolated from JI4 and JI2775. Thereby the genomic sequence was 81% and the coding sequence 99.8% identical between the two lines. Sequence differences were found at the same three positions of the coding region as described before (Sato et al. 2007), resulting in two missense mutations (Thr12Ser and Asn38Lys) and an Ile-Leu insertion after Ile189 of the deduced SGR protein of JI2775 as compared to JI4. Surprisingly, within the introns, sequence differences were limited to the third intron with an increase in size from 802 bases (JI4 SGR gene) to 923 bases in JI2775. Sequence identity of the third intron was 64%.

The completed *Arabidopsis* and rice genomes as well as additional available genomic sequences of SGRs were used to compare the exon/intron structure of SGR genes (Fig. 4a). The exact positions of introns were deduced by alignment of the genomic regions with expressed sequence tag (EST) sequences from respective species. The gene structure was conserved within the monocots and dicots, but differed from each other by the presence in the dicot genes of an additional intron splitting exon 2 of the monocot SGR genes (Fig. 3a). In all cases, introns were present at exactly the same positions within the coding regions indicating that SGR genes had existed prior to monocot and dicot divergence about 200 million years ago and that divergence is characterized by the occurrence of the additional intron. Consequently SGR-like genes are also found in lower plants, such as Gymnosperms (Ren et al. 2007), *Physcomitrella patens*, and eukaryotic algae, but also in some bacteria. The derived proteins cluster into several subclades, whereby monocot (clade I) and dicot SGR members (clade II) cluster together and are separated from lower species (Supplemental Fig. 2). Interestingly, a phylogenetically distant subclade of SGR homologues (clade III) contained further proteins from different higher plants, such as *Arabidopsis* and rice. In most cases of higher plant SGRs, expression of respective genes is supported by the presence of ESTs (not shown), but it remains to be demonstrated whether lower plant SGRs are functional orthologs of the higher plant proteins. An interesting feature of the monocot and dicot sequences in clade I and II, and of two *P. patens* sequences was the presence of a novel conserved motif near the C-terminal ends (Fig. 4b). The motif can be defined as Cys-X_3-Cys-X-Cys-Cys-Phe-Pro-X_7-Pro and is separated from the highly homologous core region of SGRs by a variable region of 12–38 amino acids in length. This motif was absent from the SGR-like proteins of clade III, and from lower plant and bacterial homologues. The presence of 4 conserved Cys residues implies possible functions in inter- or intramolecular crosslinking, or in redox regulation, but this has not yet been experimentally tested.

Interestingly, different isoforms are found in the (nearly) finished sequenced genomes of several species, such as *Arabidopsis thaliana*, *Vitis vinifera*, *Populus trichocarpa*, maize and rice. In *Arabidopsis* three *SGR* genes have been annotated, but a fourth gene, *AtSGR4*, is present as a tandem repeat of *AtSGR2* (At4g11910). This most likely represents a non-functional pseudogene, since ESTs cannot be identified in the available databases (data not shown). In order to identify the *SGR* gene number in pea, Southern blot analysis was performed with restricted genomic DNA of JI4 and JI2775 (Fig. 4c). The pattern of bands hybridizing with a *PsSGR* cDNA probe, indicate the presence in both pea lines of two *SGR* genes. This is confirmed by the

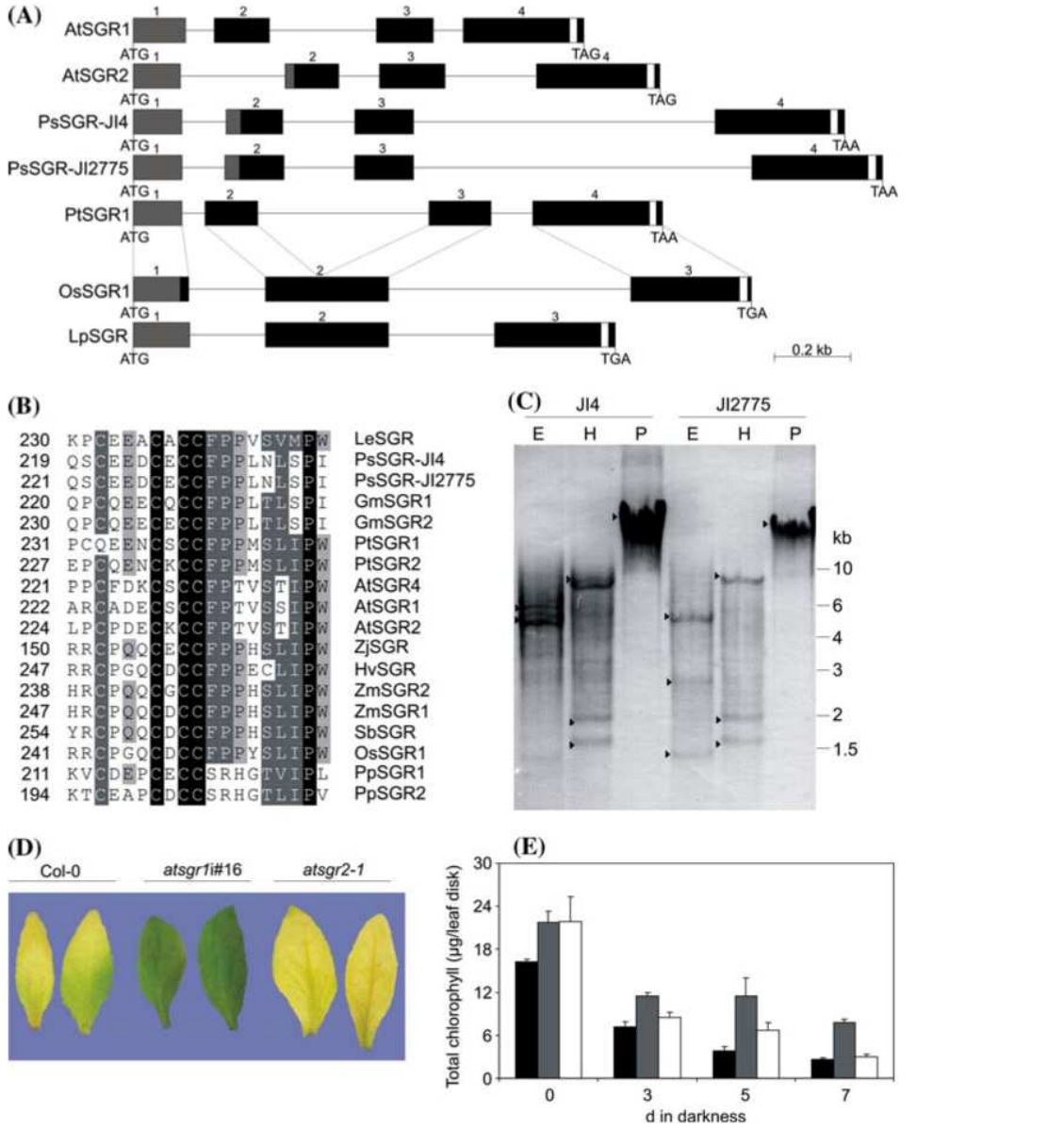

Fig. 4 SGR gene analyses, and analysis of *Arabidopsis SGR*-deficient lines. (**a**) Gene structure of dicotyledons and monocotyledons SGR genes with numbered exons (blocks) and introns (lines). Start and stop codons are shown. Predicted transit peptides (gray) and a conserved cystein-rich motif of unknown function (white; see also panel **b**) are shown. Intron/exon structures were determined by pair wise comparison of genomic and coding sequences. The accession numbers of sequences used in this analysis are as follows. Genomic sequences: *A. thaliana*, AtSGR1, NC_003075; AtSGR2, NC_003075; rice OsSGR, AP008215; pea PsSGR-JI4, AM884277; PsSGR-JI2775, AM884278; cDNA sequences: *A. thaliana*, AtSGR1, AY850161; AtSGR2, AY699948; OsSGR, AY850134; PsSGR-JI4, AB303331; PsSGR-JI2775, AB303332. *Populus trichocarpa* (PtSGR) sequences were obtained from the Joint Genome Institute (http://genome.jgi-psf.org/Poptr1_1/Poptr1_1.home.html; eugene3.00010981) *Lolium perenne* LpSGR sequences were provided by I.S. Donnison (personal communication). (**b**) Alignment of partial sequences from different plant SGRs identifies a novel conserved motif, which can be defined as C-X_3-C-X-C_2FP-X_7-P. Amino acid sequences were aligned using Dialign (http://bibiserv.techfak.uni-bielefeld.de/dialign). Black shading with white letters, gray shading with white letters, and gray shading with black letters reflect 100, 80, and 60% sequence conservation, respectively, with Blosum62 similarity groups enabled. For accession numbers of protein sequences, see Experimental procedures. (**c**) DNA gel blot analysis of *PsSGR*. 15 µg of genomic DNA from both JI4 and JI2775 were digested by *Eco*RI (E), *Hin*dIII (H) or *Pst*I (P) and probed with a digoxygenin-labeled *PsSGR* fragment from JI4. Arrowheads indicate cross-reacting bands. Sizes of DNA marker bands are indicated on the right. (**d**) Phenotype of leaves of Col-0, a *SGR1* silencing line (Armstead et al. 2007; *atsgr1*i#16) and a T-DNA insertion line of *AtSGR2* (*atsgr2-1*) after 5 days of dark-induced senescence. (**e**) Degradation of chl in Col-0 (black), *atsgr1*i#16 (gray) and *atsgr2-1* (white) during the course of detached leaf senescence. Data are means of a single representative experiment with 3 replicates. Error bars indicate SD.

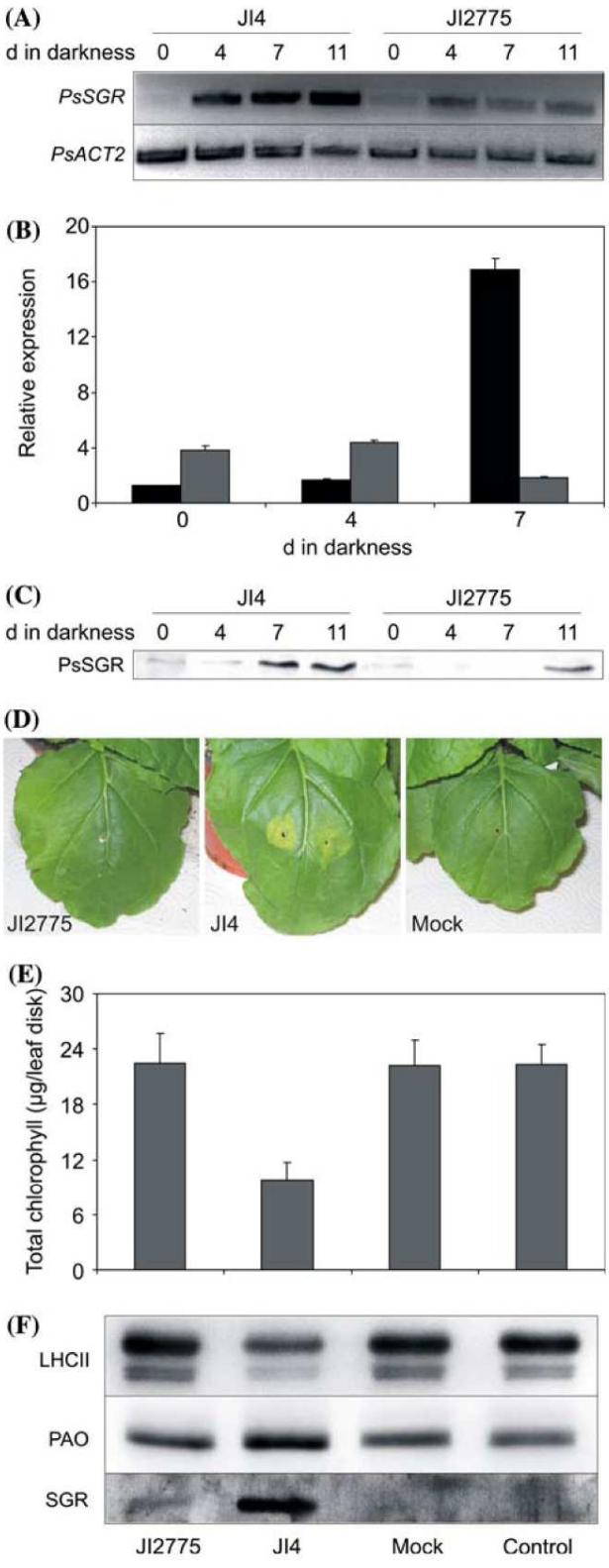

Fig. 5 PsSGR mRNA and protein abundance, and PsSGR protein functionality test. (**a**) Semiquantitative analysis of *PsSGR* expression during leaf senescence in JI4 and JI2775. RNA abundance of *PsACT2* was used as control (**b**) Real-time RT-PCR quantification of *PsSGR* expression during senescence. Levels of expression were normalized to levels of *PsACT2* mRNA. Values are means of three replicates. (**c**) Immunoblot analysis of PsSGR protein levels during the course of detached leaf senescence. Gel loadings are based on equal amounts of fresh weight. (**d**) Transient expression of *PsSGR* in 3-week-old *N. benthamiana* plants. Leaves were infiltrated with *Agrobacterium tumefaciens* cultures containing plasmids for expression of PsSGR-JI2775 (JI2775), PsSGR-JI4 (JI4), or empty vector (Mock). Pictures show plants after 6 days of infiltration. (**e**, **f**) Analysis of leaf tissue after infiltration as in (**d**). (**e**) Total chl levels; (**f**) Immunoblot analysis of LHCII, PAO and SGR levels in the treatments. Gel loadings are based on equal sizes of leaf material. Control, non-infiltrated leaf tissue

presence in the databases of a pea EST (GenBank accession number AM162161), which is highly homologous, but not identical to *PsSGR*.

Two functional SGR genes have been identified in *Arabidopsis*, but so far only for the senescence-regulated *AtSGR1* (At4g22920) has an important function in chl breakdown been demonstrated (Armstead et al. 2007; Ren et al. 2007). In order to analyze whether *AtSGR2*, whose expression is also up-regulated during senescence (Park et al. 2007), is involved in chl catabolism as well, a homozygous T-DNA insertion line (SALK_003830C) was obtained from the SALK resource (Alonso et al. 2003). The line was termed *atsgr2-1* and position of the T-DNA within the first intron was confirmed by sequencing (Supplemental Fig. 3A). Expression of *AtSGR2* was absent (Supplemental Fig. 3B) indicating that *atsgr2-1* represents a null allele. During dark-induced senescence, chl was degraded at similar rates like in Col-0, in contrast to an *AtSGR* RNA silencing line (*atsgr1i#16*) (Armstead et al. 2007), which retained a large proportion of chl after 7 days of senescence (Fig. 4d, e). Although in *atsgr1i#16*, expression of *AtSGR2* was also slightly reduced (Supplemental Fig. 3B), silencing of *AtSGR1* expression in the knockout line *atsgr2-1* did not enhance the stay-green phenotype observed in *atsgr1i* (data not shown). This indicated that AtSGR2 does not significantly contribute to chl degradation in *Arabidopsis*. Likewise, the presence of two or more SGR gene copies in different species indicates either redundancy of SGR function in chl breakdown or implies that SGR might have additional role(s) in plant development that so far have escaped detection. Furthermore, the unclear role of the structurally similar SGR isoproteins of higher plants, such as AtSGR2, even more questions a function in chl breakdown of the less homologous SGR-like proteins from higher (clade III proteins) and lower plants (Supplemental Fig. 2). This has to be functionally tested, e.g. through complementation of the *nye1* mutant of *Arabidopsis*.

JI2775 is a loss-of-function mutant

In order to determine the molecular or biochemical defect of the pea mutant JI2775, we analyzed *PsSGR* gene

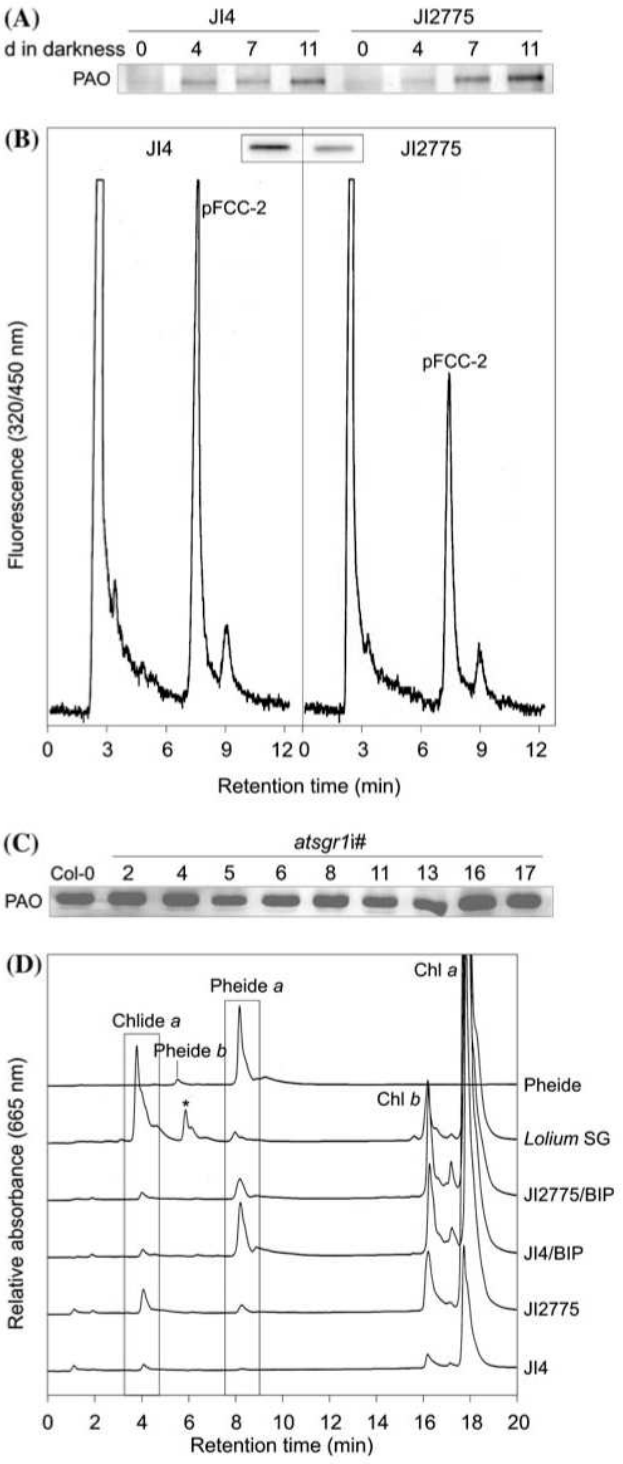

Fig. 6 Absence of SGR does not affect PAO abundance and activity. (**a**) Immunoblot analysis of PAO levels during the course of detached leaf senescence in JI4 and JI2775. Gel loadings are based on equal amounts of fresh weight. (**b**) Formation of pFCC-2 in PAO/RCCR assays with PAO extracted from leaves of JI4 or JI2775 after 8 days of dark-induced senescence. Activities are based on equal amounts of fresh weight. HPLC traces (fluorescence at 320/450 nm) are shown. Inset, Immunoblot analysis of PAO abundance in the extracts used for PAO/RCCR assays. Gel loadings are based on equal amounts of fresh weight. (**c**) Immunoblot analysis of PAO levels of individual *AtSGR1*-silencing lines (*atsgr1*i; Armstead et al. 2007) after 5 days of dark-induced senescence. Gel loadings are based on equal amounts of fresh weight. (**d**) HPLC traces of leaf extracts from pea JI4 and JI2775, and of a *Lolium* stay-green line (*Lolium* SG; Roca et al. 2004) after 8 and 5 days of dark-induced senescence, respectively, in the absence or presence of 1 mM 2,2′ bipyridyl (BIP). Absorption of green-colored chl catabolites was monitored at 665 nm. Analyzed extracts correspond to equal amounts of fresh weight. Pigments were identified by their absorption spectra and by comparison to authentic standards. Pheide, standard containing both, pheide *a* and pheide *b*. The asterisk marks a non-identified peak exhibiting a chl *a* spectrum

expression during leaf senescence by semiquantitative (Fig. 5a) and real time RT-PCR (Fig. 5b). As shown earlier for rice and *Arabidopsis SGRs* (Jiang et al. 2007; Park et al. 2007; Ren et al. 2007), *PsSGR* expression was strongly induced upon senescence induction of JI4. In contrast, mRNA levels of JI2775 were kept on a lower level during the course of senescence. This result was obtained repeatedly in independent samples and confirmed the low signals obtained in Northern blots from senescent JI2775 leaves (Armstead et al. 2007). Sato et al. (2007) reported that *PsSGR* gene expression was unaltered in JI2775. To further analyze this discrepancy, SGR protein levels were analyzed by immunoblotting using an antiserum directed against conserved motifs of SGR. In line with our expression analysis, the senescence-related increase in SGR protein observed in JI4 was significantly reduced in the mutant (Fig. 5c). Together these data indicate that the defect in JI2775 likely results from reduced expression of *PsSGR*.

Nevertheless, the deduced protein sequence of SGR from JI2775 exhibited changes compared to JI4-SGR, in particular a two-amino acid insertion within a highly conserved region that could affect SGR function. Therefore, binary constructs were produced for both gene versions in order to transform JI2775. Unfortunately, it was not possible to regenerate genetically transformed immature embryos from JI2775 (A. Nadolska-Orczyk, personal communication). Instead, we addressed this question by heterologous transient expression in *Nicotiana benthamiana* leaves of *SGR* cDNA from either JI4 or JI2775. Five days after infiltration, loss of chl was observed in the leaf areas of plants that had been challenged with JI4-derived SGR (Fig. 5d, e). In contrast, expression of SGR from JI2775 did not induce chl breakdown in *N. benthamiana* (Fig. 5d, e). Induction of senescence in the case of JI4-SGR expression was confirmed by immunoblot analyses of total protein extracts, which showed increased levels of PAO as well as degradation of LHCII proteins (Fig. 5f). Although *SGR* expression was comparable in both cases (data not shown), much less protein accumulated in the case of JI2775-SGR, compared to JI-SGR (Fig. 5f). This directly

demonstrated a loss of function of the mutated SGR, most likely caused by a loss of protein stability and, thus, confirms the indirect functional test performed by Sato et al. (2007). In conclusion, JI2775 is a loss-of-function mutant, which results from both reduced *SGR* gene expression and loss of SGR protein function.

SGR absence in JI2775 does not influence the PAO pathway

It had been proposed that the stay-green phenotype of the SGR/SID-deficient mutants Bf993 of *Festuca pratensis, nye1* of *Arabidopsis* and Mendel's green cotyledon mutant was caused by the (partial) loss of PAO function, which was in line with the observed accumulation during senescence of pheide *a* (Vicentini et al. 1995; Thomas et al. 1996; Roca et al. 2004; Ren et al. 2007). We re-addressed this assumption using JI4 and JI2775 and determining PAO abundance and activity. During 11 days of dark-induced senescence, PAO contents increased to comparable levels in both lines as judged by immunodetection (Fig. 6a). On the other hand, after extraction from senescent chloroplast membranes according to an established protocol (Hörtensteiner et al. 1995; Pružinská et al. 2005), PAO activity was 40% lower in extracts of JI2775 compared to the wild type (Fig. 6b). At first glance, this result indicated a posttranslational regulation of PAO, as has been proposed in canola seed development (Chung et al. 2006). In contrast, data on expression, protein abundance and activity suggest that PAO is transcriptionally regulated during *Arabidopsis* leaf senescence (Pružinská et al. 2005). When determining by immunoblotting the PAO content within the pea membrane extracts used for PAO assays, proportionally less PAO was found in the PAO extracts from the mutant (Fig. 6b, inset). This could be explained by the presence in senescent JI2775 leaves of large quantities of chloroplast membranes, which made a quantitative extraction of PAO impossible. We conclude that PAO abundance (and activity) are unchanged in the mutant compared to JI4. Likewise, PAO levels of senescent leaves were unaltered in different SGR-silencing lines of *Arabidopsis* (Fig. 6c). The same was true for a *Lolium* introgression line carrying the stay-green allele of *Festuca pratensis* Bf993 (H. Ougham, S. Hörtensteiner, I. Armstead, I. Donnison, I. King, H. Thomas and L. Mur, unpublished), although there lower PAO activities had been observed as well (Roca et al. 2004). Finally, Ren et al. (2007) also identified lower PAO activity in *nye1*, but unfortunately PAO protein abundance was not determined in this study. Altogether, the observed lower PAO activities in *sgr/sid* mutants (Fig. 6b; Vicentini et al. 1995; Roca et al. 2004; Ren et al. 2007) are due to misinterpretation of results and no indication remains of a posttranslational regulation of PAO through SGR as suggested (Sato et al. 2007).

We also re-investigated the observation of pheide *a* accumulation in *sgr/sid* mutants. Pheide *a* did not accumulate in senescent JI4 leaves, but small quantities (5–10 nmol pheide *a* g^{-1} fresh weight) were found in JI2775 (Fig. 6d). If the occurrence in JI4 of pheide *a* would solely be the result of partial inhibition of PAO in an otherwise normally active chl breakdown pathway, it could be expected that entire inhibition of PAO would increase the amount of pheide *a*. To analyze this, leaves were senesced in the presence of 2,2′-bipyridyl, an iron chelator, which among other reactions has been shown to inhibit PAO (Hörtensteiner et al. 1995; Hörtensteiner et al. 2000). In wild type, bipyridyl-treatment largely enhanced the accumulation of pheide *a* (80 nmol g^{-1} fresh weight), but this increase was much smaller in JI2775 (35 nmol g^{-1} fresh weight). These data indicate that occurrence of pheide *a* is independent of PAO. Instead, pheide *a* formation could result from non-physiological conversion from chlide *a*. This might be due to tissue acidification as a consequence of tonoplast rupture upon cell damage or death occurring at later stages of leaf senescence. Chlide *a* repeatedly accumulated to higher concentrations in senescent leaves of the mutant compared to JI4 (Fig. 6d), an observation that had been made also in other instances of *sgr/sid* mutants (Vicentini et al. 1995; Roca et al. 2004). Particularly in Bf993 and the stay-green introgression lines of *Lolium*, large quantities accumulated in senescent leaves. This intriguing observation correlates to the fact that, compared to rice and pea *sgr* mutants, the *Festuca/Lolium sid* lines are null mutants, caused by a frame shift mutation within the second exon of the gene (Armstead et al. 2006). In this respect it is possible to argue that SGR/SID might affect Mg-dechelation. This step in chl breakdown was shown to be catalyzed nonenzymatically by a heat-stable, low molecular weight compound, termed metal chelating substance. Metal-chelating substances of different species have different molecular weights, but their structures have so far not been elucidated (Costa et al. 2002; Suzuki et al. 2005). Alternatively, metal-chelating substance might represent the metal-chelating cofactor of a Mg-dechelatase enzyme (Hörtensteiner 2006) and it remains to be investigated whether SGR could have this function.

Altogether the data presented here refute the suggestion of several groups of impairment of PAO function in SGR mutants, hence, most likely the biochemical steps of the PAO pathway of chl breakdown are not regulated by SGR.

SGR acts upstream of PAO

If SGR does not regulate the biochemical enzymes of chl breakdown, at which level does it then interfere with chl

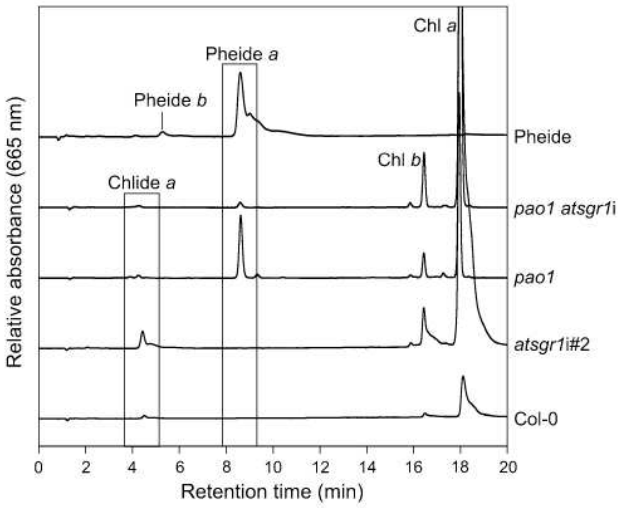

Fig. 7 HPLC analysis of green chl catabolites in *SGR1*- and *PAO*-deficient *Arabidopsis*. Equal amounts of leaf extracts from Col-0, *atsgr1*i#2 (Armstead et al. 2007), *pao1* (Pružinská et al. 2005) and a representative line silencing *AtSGR1* in *pao1* background (*pao1 atsgr1*i) were separated by reversed-phase HPLC, and A_{665} was monitored. Pigments were identified by their absorption spectra and by comparison to authentic standards. Pheide, standard containing both, pheide *a* and pheide *b*

metabolism? In order to address this question, we silenced expression of *AtSGR1* in the *pao1* background (Pružinská et al. 2005). Two independent homozygous lines, *pao1 atsgr1*i#1 and *pao1 atsgr1*i#2, were isolated and further analyzed. During senescence, the lines exhibited a stay-green phenotype, but a cell death phenotype, typical for *pao1*, did not establish in the *pao1 atsgr1*i lines (data not shown). Furthermore, in contrast to *pao1*, pheide *a* accumulation was largely reduced in the *pao1 atsgr1*i lines (Fig. 7). This result indicated that abolishment of SGR function prevents pheide *a* formation, hence confirms that the SGR target is located upstream of PAO.

Conclusion

The identification and analysis of the role of SGR/SID proteins during plant senescence has recently become a major focus in plant senescence research. This is demonstrated by the high number of reports about identification of *sgr/sid* mutants and the recent cloning of *SGR/SID* genes from *Arabidopsis*, *Festuca/Lolium*, pea and rice (Armstead et al. 2006, 2007; Jiang et al. 2007; Park et al. 2007; Ren et al. 2007; Sato et al. 2007). It is likely that additional stay-green mutants, such as tomato *green flesh* (*gf*; Akhtar et al. 1999) and pepper *chlorophyll retainer* (*cl*; Efrati et al. 2005) are defective in *SGR* as well. Only some of these mutants have been attributed to the class of type C non-functional stay-greens. Here we show that Gregor Mendel's *I* mutant also belongs to this class.

Analysis of the different *sgr/sid* mutants available so far, indicate that overall reduction of SGR gene expression (Armstead et al. 2007) or loss of function due to mutations within the open reading frames of SGR genes (Jiang et al. 2007; Park et al. 2007; Ren et al. 2007) can cause the stay-green phenotype. In this respect, Mendel's *I* mutant is exceptional, since we here show that both gene expression and protein function are affected. An explanation for the reduced mRNA level most probably is an altered SGR promoter activity in the mutants, but this remains to be confirmed.

SGR/SID proteins constitute a new class of senescence proteins, which are widely distributed in plants. The absence of known domains makes it impossible to deduce a function from the primary sequence of SGR proteins. Conflicting reports in the literature indicated an activity of SGR in relation to either PAO function and/or chl-apoprotein dismantling (Vicentini et al. 1995; Thomas et al. 1996; Roca et al. 2004; Park et al. 2007; Ren et al. 2007). With the results presented here, we unambiguously demonstrate that SGR does not regulate PAO. We furthermore show that SGR functions upstream of PAO, but the exact site of action remains to be elucidated. Park et al. (2007) showed physical interaction between SGR and LHCII subunits and suggested that SGR might be required for dismantling of chl-apoprotein complexes. In this case SGR would *senso stricto* not be part of the catabolic machinery of chl breakdown directly, but its action would be a prerequisite for allowing the catabolic enzymes to get access to their substrate. An interesting observation is that in *pao1 SGR* gene expression is not up-regulated during senescence (Park et al. 2007). It is likely that this regulation is achieved through pheide *a*, although, in contrast to the suggested retrograde signaling by porphyrin intermediates of chl biosynthesis (Nott et al. 2006), pheide *a* most probably is not a retrograde signal itself. Nevertheless, the proposed function in the dismantling of chl-protein complexes (Park et al. 2007) provides an ideal point of control of chl breakdown. In addition, the retention of chl-binding proteins suggests that proteases known to degrade LHC proteins during senescence, such as FtsH6 (Zelisko et al. 2005), are either directly regulated through SGR or complex-dismantling is also a prerequisite for the respective proteases to get access to their substrate proteins. In this respect, the analysis of the rice *nyc1* mutant provides an interesting alternative (Kusaba et al. 2007); chl *b* is known to be required in a certain stoichiometry to chl *a* in order to stabilize chl-protein complexes (Horn and Paulsen 2004), thus, prevention of chl *b* to chl *a* conversion in *nyc1* would stabilize the complexes. It will be interesting to analyze the regulation of SGR in *nyc1* and to

see whether NYC1 or SGR or both regulate chl-protein complex stability.

Acknowledgements We thank B. Burla, University of Zurich, for his help with phylogenetic analyses. We thank S. Schelbert, University of Zurich, for critical reading of the manuscript and I. Anders, University of Bern, for technical support. This work was supported by the Swiss National Science Foundation (3100A0-105389) and the National Center of Competence in Research Plant Survival, research program of the Swiss National Science Foundation.

References

Akhtar MS, Goldschmidt EE, John I, Rodoni S, Matile P, Grierson D (1999) Altered patterns of senescence and ripening in *gf*, a stay-green mutant of tomato (*Lycopersicon esculentum* Mill.). J Exp Bot 50:1115–1122

Alonso JM, Stepanova AN, Leisse TJ, Kim CJ, Chen H, Shinn P, Stevenson DK, Zimmermann J, Barajas P, Cheuk R, Gadrinab C, Heller C, Jeske A, Koesema E, Meyers CC, Parker H, Prednis L, Ansari Y, Chory N, Deen H, Geralt M, Hazari N, Hom E, Karnes M, Mulholland C, Ndubaku R, Schmidt I, Guzman P, Aguilar-Henonin L, Schmid M, Weigel D, Carter DE, Marchand T, Risseeuw E, Brogden D, Zeko A, Crosby WL, Berry CC, Ecker JR (2003) Genome-wide insertional mutagenesis of *Arabidopsis thaliana*. Science 301:653–657

Armstead I, Donnison I, Aubry S, Harper J, Hörtensteiner S, James C, Mani J, Moffet M, Ougham H, Roberts L, Thomas A, Weeden N, Thomas H, King I (2006) From crop to model to crop: identifying the genetic basis of the staygreen mutation in the *Lolium/Festuca* forage and amenity grasses. New Phytol 172:592–597

Armstead I, Donnison I, Aubry S, Harper J, Hörtensteiner S, James C, Mani J, Moffet M, Ougham H, Roberts L, Thomas A, Weeden N, Thomas H, King I (2007) Cross-species identification of Mendel's *I* locus. Science 315:73

Bachmann A, Fernández-López J, Ginsburg S, Thomas H, Bouwcamp JC, Solomos T, Matile P (1994) *Stay-green* genotypes of *Phaseolus vulgaris* L.: chloroplast proteins and chlorophyll catabolites during foliar senescence. New Phytol 126:593–600

Bhattacharyya MK, Smith AM, Ellis THN, Hedley C, Martin C (1990) The wrinkled-seed character of pea described by Mendel is caused by a transposon-like insertion in a gene encoding starch-branching enzyme. Cell 60:115–122

Chakraborti D, Sarkar A, Gupta S, Das S (2006) Small and large scale genomic DNA isolation protocol for chickpea (*Cicer arietinum* L.), suitable for molecular marker and transgenic analyses. Afr J Biotechnol 5:585–589

Chung DW, Pružinská A, Hörtensteiner S, Ort DR (2006) The role of pheophorbide *a* oxygenase expression and activity in the canola green seed problem. Plant Physiol 142:88–97

Costa ML, Civello PM, Chaves AR, Martinez GA (2002) Characterization of Mg-dechelatase activity obtained from *Fragaria* × *ananassa* fruit. Plant Physiol Biochem 40:111–118

Efrati A, Eyal Y, Paran I (2005) Molecular mapping of the *chlorophyll retainer* (*cl*) mutation in pepper (*Capsicum* spp.) and screening for candidate genes using tomato ESTs homologous to structural genes of the chlorophyll catabolism pathway. Genome 48:347–351

Gray J, Wardzala E, Yang M, Reinbothe S, Haller S, Pauli F (2004) A small family of LLS1-related non-heme oxygenases in plants with an origin amongst oxygenic photosynthesizers. Plant Mol Biol 54:39–54

Havaux M (1993) Characterization of thermal damage to the photosynthetic electron transport system in potato leaves. Plant Sci 94:19–33

Hellens R, Edwards EA, Leyland NR, Bean S, Mullineaux PM (2000) pGreen: a versatile and flexible binary Ti vector for *Agrobacterium*-mediated plant transformation. Plant Mol Biol 42:819–832

Hilditch P, Thomas H, Rogers L (1986) Leaf senescence in a non-yellowing mutant of *Festuca pratensis*: Photosynthesis and photosynthetic electron transport. Planta 167:146–151

Hilditch PI, Thomas H, Thomas BJ, Rogers LJ (1989) Leaf senescence in a non-yellowing mutant of *Festuca pratensis*: proteins of photosystem II. Planta 177:265–272

Horn R, Paulsen H (2004) Early steps in the assembly of light-harvesting chlorophyll *a/b* complex - Time-resolved fluorescence measurements. J Biol Chem 279:44400–44406

Hörtensteiner S (2006) Chlorophyll degradation during senescence. Annu Rev Plant Biol 57:55–77

Hörtensteiner S, Vicentini F, Matile P (1995) Chlorophyll breakdown in senescent cotyledons of rape, *Brassica napus* L.: enzymatic cleavage of phaeophorbide *a in vitro*. New Phytol 129:237–246

Hörtensteiner S, Chinner J, Matile P, Thomas H, Donnison IS (2000) Chlorophyll breakdown in *Chlorella protothecoides*: characterization of degreening and cloning of degreening-related genes. Plant Mol Biol 42:439–450

Jiang H, Li M, Liang N, Yan H, Wei Y, Xu X, Liu J, Xu Z, Chen F, Wu G (2007) Molecular cloning and function analysis of the *stay green* gene in rice. Plant J 52:197–209

Kingston-Smith AH, Thomas H, Foyer CH (1997) Chlorophyll *a* fluorescence, enzyme and antioxidant analyses provide evidence for the operation of alternative electron sinks during leaf senescence in a *stay-green* mutant of *Festuca pratensis*. Plant Cell Environ 20:1323–1337

Kreuz K, Tommasini R, Martinoia E (1996) Old enzymes for a new job. Herbicide detoxification in plants. Plant Physiol 111:349–353

Kürsteiner O, Dupuis I, Kuhlemeier C (2003) The *pyruvate decarboxylase1* gene of Arabidopsis is required during anoxia but not other environmental stresses. Plant Physiol 132:968–978

Kusaba M, Ito H, Morita R, Iida S, Sato Y, Fujimoto M, Kawasaki S, Tanaka R, Hirochika H, Nishimura M, Tanaka A (2007) Rice NON-YELLOW COLORING1 is involved in light-harvesting complex II and grana degradation during leaf senescence. Plant Cell 19:1362–1375

Lester DR, Ross JJ, Davies PJ, Reid JB (1997) Mendel's stem length gene (*Le*) encodes a gibberellin 3β-hydroxylase. Plant Cell 9:1435–1443

Llave C, Kasschau KD, Carrington JC (2000) Virus-encoded suppressor of posttranscriptional gene silencing targets a maintenance step in the silencing pathway. Proc Natl Acad Sci USA 97:13401–13406

Matile P, Hörtensteiner S, Thomas H (1999) Chlorophyll degradation. Annu Rev Plant Physiol Plant Mol Biol 50:67–95

Maxwell K, Johnson GN (2000) Chlorophyll fluorescence—a practical guide. J Exp Bot 51:659–668

Mendel G (1866) Versuche über Pflanzenhybriden. Verh Naturforsch Ver Brünn 4:3–47

Müller T, Moser S, Ongania K-H, Pružinská A, Hörtensteiner S, Kräutler B (2006) A divergent path of chlorophyll breakdown in the model plant *Arabidopsis thaliana*. ChemBioChem 7:40–42

Murray MG, Thompson WF (1980) Rapid isolation of high molecular-weight plant DNA. Nucl Acids Res 8:4321–4325

Nott A, Jung HS, Koussevitzky S, Chory J (2006) Plastid-to-nucleus retrograde signaling. Annu Rev Plant Biol 57:739–759

Oberhuber M, Berghold J, Breuker K, Hörtensteiner S, Kräutler B (2003) Breakdown of chlorophyll: a nonenzymatic reaction accounts for the formation of the colorless "nonfluorescent" chlorophyll catabolites. Proc Natl Acad Sci USA 100:6910–6915

Oh MH, Kim YJ, Lee CH (2000) Leaf senescence in a stay-green mutant of *Arabidopsis thaliana*: disassembly process of photosystem I and II during dark-incubation. J Biochem Mol Biol 33:256–262

Park S-Y, Yu J-W, Park J-S, Li J, Yoo S-C, Lee N-Y, Lee S-K, Jeong S-W, Seo HS, Koh H-J, Jeon J-S, Park Y-I, Paek N-C (2007) The senescence-induced staygreen protein regulates chlorophyll degradation. Plant Cell 19:1649–1664

Pružinská A, Anders I, Tanner G, Roca M, Hörtensteiner S (2003) Chlorophyll breakdown: pheophorbide *a* oxygenase is a Rieske-type iron-sulfur protein, encoded by the *accelerated cell death 1* gene. Proc Natl Acad Sci USA 100:15259–15264

Pružinská A, Tanner G, Aubry S, Anders I, Moser S, Müller T, Ongania K-H, Kräutler B, Youn J-Y, Liljegren SJ, Hörtensteiner S (2005) Chlorophyll breakdown in senescent Arabidopsis leaves: characterization of chlorophyll catabolites and of chlorophyll catabolic enzymes involved in the degreening reaction. Plant Physiol 139:52–63

Pružinská A, Anders I, Aubry S, Schenk N, Tapernoux-Lüthi E, Müller T, Kräutler B, Hörtensteiner S (2007) In vivo participation of red chlorophyll catabolite reductase in chlorophyll breakdown. Plant Cell 19:369–387

Quirino BF, Noh YS, Himelblau E, Amasino RM (2000) Molecular aspects of leaf senescence. Trends Plant Sci 5:278–282

Ren G, An K, Liao Y, Zhou X, Cao Y, Zhao H, Ge X, Kuai B (2007) Identification of a novel chloroplast protein AtNYE1 regulating chlorophyll degradation during leaf senescence in Arabidopsis. Plant Physiol 144:1429–1441

Roca M, James J, Pružinská A, Hörtensteiner S, Thomas H, Ougham H (2004) Analysis of the chlorophyll catabolism pathway in leaves of an introgression senescence mutant of *Lolium temulentum*. Phytochemistry 65:1231–1238

Sato Y, Morita R, Nishimura M, Yamaguchi H, Kusaba M (2007) Mendel's green cotyledon gene encodes a positive regulator of the chlorophyll-degrading pathway. Proc Natl Acad Sci USA 104:14169–14174

Scheumann V, Schoch S, Rüdiger W (1999) Chlorophyll *b* reduction during senescence of barley seedlings. Planta 209:364–370

Sidler M, Hassa P, Hasan S, Ringli C, Dudler R (1998) Involvement of an ABC transporter in a developmental pathway regulating hypocotyl cell elongation in the light. Plant Cell 10:1623–1636

Strain HH, Cope BT, Svec WA (1971) Analytical procedures for the isolation, identification, estimation and investigation of the chlorophylls. Methods Enzymol 23:452–476

Suzuki T, Kunieda T, Murai F, Morioka S, Shioi Y (2005) Mg-dechelation activity in radish cotyledons with artificial and native substrates, Mg-chlorophyllin *a* and chlorophyllide *a*. Plant Physiol Biochem 43:459–464

Thomas H (1987) *Sid*: a Mendelian locus controlling thylakoid membrane disassembly in senescing leaves of *Festuca pratensis*. Theor Appl Genet 73:551–555

Thomas H (1997) Chlorophyll: a symptom and a regulator of plastid development. New Phytol 136:163–181

Thomas H, Howarth CJ (2000) Five ways to stay green. J Exp Bot 51:329–337

Thomas H, Schellenberg M, Vicentini F, Matile P (1996) Gregor Mendel's green and yellow pea seeds. Bot Acta 109:3–4

Vicentini F, Hörtensteiner S, Schellenberg M, Thomas H, Matile P (1995) Chlorophyll breakdown in senescent leaves: identification of the biochemical lesion in a *stay-green* genotype of *Festuca pratensis* Huds. New Phytol 129:247–252

Wesley SV, Helliwell CA, Smith NA, Wang M, Rouse DT, Liu Q, Gooding PS, Singh SP, Abbot D, Stoutjesdijk PA, Robinson SP, Gleave AP, Green AG, Waterhouse PM (2001) Construct design for efficient, effective and high-throuput gene silencing in plants. Plant J 27:581–590

White OE (1916) Inheritance studies in *Pisum* I Inheritance of cotyledon color. Am Nat 50:530–547

Zelisko A, Garcia-Lorenzo M, Jackowski G, Jansson S, Funk C (2005) AtFtsH6 is involved in the degradation of the light-harvesting complex II during high-light acclimation and senescence. Proc Natl Acad Sci USA 102:13699–13704

7.4 Additional non published experiments on SGR

Despite our and other researchers efforts to characterize pea, rice and *Arabidopsis* lines, SGR function remains unclear. Since SGR was shown to bind LHC subunits (Park et al., 2007), it was suggested that SGR is involved in dismantling chl apoprotein complexes. In this chapter I describe an experiment performed to also identify hypothetical partners of SGR *in vivo* via tandem affinity purification (TAP). Briefly, SGR was cloned and stably transformed in *Arabidopsis* with several tags allowing a multistep purification of *in vivo* interacting partners. Unfortunately, only preliminary results are shown here and further efforts will be needed to identify SGR interacting partners.

7.4.1 TAPa construct generation

Prior to cloning into the pC-TAPa and pN-TAPa plasmids (Rubio et al., 2005), *At*SGR cDNA (Aubry et al., 2008) was PCR-amplified using partial attB sequence containing primers and cloned into the pDONR 207 plasmid using the gateway BP reaction (Invitrogen). Full length SGR was amplified and cloned into pC-TAPa (Fig. 19B), and cDNA depleted in the predicted chloroplast transit peptide was cloned into pN-TAPa containing the RubisCO small subunit (RBCS) transit peptide N-terminal of the tags (Fig. 19A). The pN-TAPa cloning site is not in-frame with the two lysine codons (AAA–AAA) in the upstream attR1 sequence; it is misplaced by 2 bp (CAA–AAA–AGC). Therefore, to keep the frame, two pENTRY vectors (Invitrogen) had to be designed, the insets of which were sequenced for confirmation. The transfer of genes from the ENTRY vectors to the corresponding TAPa vectors was performed using the LR reaction (Invitrogen). A plasmid containing RBCS-GFP as a control (Fig. 19C) was kindly provided by U. Eckhard (Humbold University, Berlin). Following primers were used:

attB1-NTAP 5’-AAAAAAGCAGGCTAATGTGTAGTTTGTCGGCGATTATG-3’
attB2-NTAP 5’-AGAAAGCTGGGTAGAGTTTCTCCGGATTTGG-3’
attB1-CTAP 5’-AAAAAAGCAGGCTAGCAAGGTTGTTTGGACCGGCG-3’
attB2-CTAP 5’-AGAAAGCTGGGTACTAGAGTTTCTCCGGATTTGG-3’

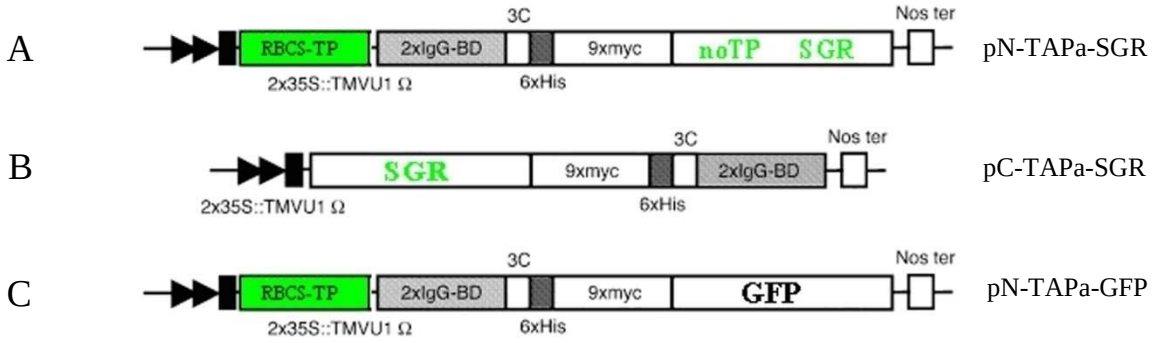

Figure 19. Constructs used for TAPa analysis. A. SGR without its predicted transit peptide was cloned to the pN-TAPa vector, adding the RBCS chloroplast targeting signal and three tags, IgG-BD, 6xHis and 9xmyc, N-terminal to SGR. **B.** SGR full length cDNA was cloned into pC-TAPa with the tag cassette C-terminal to the protein. **C.** As a control GFP cloned into pN-TAPa was used. All constructs were under the control of the 35S promoter (2x35S::TMVU1 Ω) and contained a 3C protease cleavage site (3C).

7.4.2 TAPa purification procedure

Purification was performed according to Rubio et al. (2005) with some modifications,. C-TAPa-SGR lines (15 g fresh weight) were ground in liquid nitrogen, thawed in 2 volumes of extraction buffer (50 mM Tris–HCl pH 7.5, 150 mM NaCl, 10% glycerol, 0.1% Nonidet P-40, 1 mM PMSF, and 1x complete protease inhibitor cocktail, Roche), filtered through four layers of cheesecloth, and centrifuged at 12000 g for 10 min at 4°C. The protein concentration in the supernatant was determined by Bradford assay (Bio-Rad). Extracts containing similar amounts of total protein were incubated with 500 µl IgG beads (Amersham Biosciences) for 2 h at 4°C with gentle rotation. After centrifugation at 150 g for 3 min at 4°C, the IgG beads were recovered and washed three times with 10 ml of washing buffer (50 mM Tris–HCl pH 7.5, 150 mM NaCl, 10% glycerol, 0.1% Nonidet P-40) and once with 10 ml of cleavage buffer (50 mM Tris–HCl pH 7.5, 150 mM NaCl, 10% glycerol, 0.1% Nonidet P-40, 1 mM DTT). Elution from the IgG beads was performed by incubation with 50 µl (100 units) of 3C protease (Prescission protease; GE Healthcare) in 5 ml of cleavage buffer at 4°C with gentle rotation. Supernatants were recovered after centrifugation at 150 g for 3 min at 4°C and stored. The IgG beads were washed with 5 ml of washing buffer and centrifuged again. Supernatants were recovered and the eluates pooled. Pooled eluates were loaded onto a 1 ml Hi-trap column (GE Healthcare) equilibrated with washing buffer (50 mM Tris–HCl pH 7.5, 150 mM NaCl, 10% glycerol, 0.1% Nonidet P-40). The flow through was again loaded onto the column. After washing the column with

30 ml of washing buffer, elution was performed using each 5 ml of imidazole-containing buffer (50 mM Tris–HCl pH 7.5, 150 mM NaCl, 10% glycerol, 0.1% Nonidet P-40 and 10, 50 or 150 mM imidazole). All purification steps were carried out at 4°C. Proteins in each fraction (except total plant extracts) were concentrated using STRATARESIN (Stratagene) and separated on a 12% SDS-PAGE gel. Protein bands were visualized, independently, by immunoblotting using c-myc antibodies and by silver staining according to published procedures (Mortz et al., 2001). Silver-stained gels were cut into pieces and trypsinised using (1:50) potein:trypsin (Sigma) (Mortz et al., 2001). MS-MS analysis was performed in collaboration with S. Baginski (ETH Zürich).

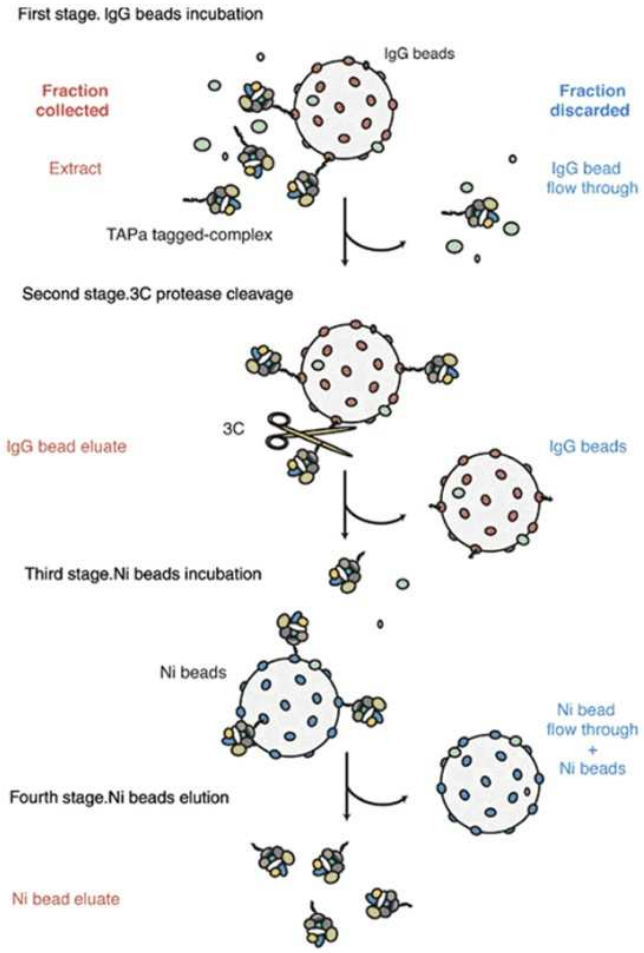

Figure 20. Description of the TAPa system applied for SGR partner identification. Incubation of a protein extract with IgG beads allows the tagged protein to bind with potential partners. Subsequent digest of the first tag (IgG binding domain) by a specific 3C protease allows enrichment of bait-pray complexes in the eluate. A second purification step is performed using the hexa-histidine tag thereby binding a nickel column, and eluting with imidazole. The final eluate is collected and further analyzed by MS-MS. From Rubio et al., 2004.

7.4.3 Results

Stable transgenic *Arabidopsis* lines were produced overexpressing the three different constructs under the control of the 35S promoter (Fig. 19). By immunoblotting, all lines were confirmed to expressed the tagged proteins. Fig. 21 shows data only for a line containing construct pC-TAPa-SGR and further characterization has only performed with this line.

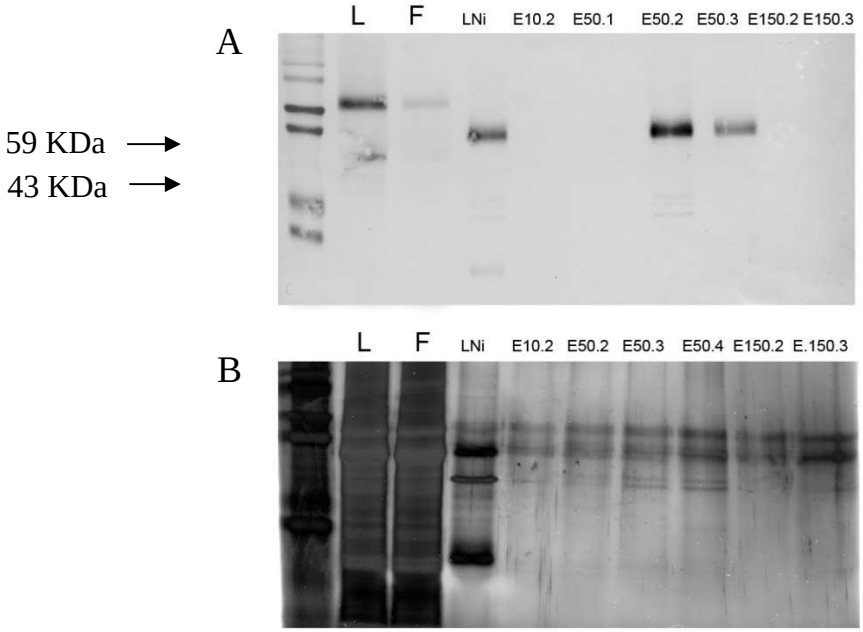

Figure 21. Tandem affinity purification profile of a pC-TAP-SGR line. A. Western blot using anti-c-myc antibodies show tagged SGR proteins. L, load on IgG beads; F, flow through; LNi, load on Ni column; E10.2, elution at 10 mM imidazole; E50.1-4, elution at 50 mM imidazole, E150.2-3, elution at 150 mM imidazole. **B.** Corresponding fractions on SDS-PAGE stained by Blum silver staining.

Partial purification of SGR protein partners was performed by tandem affinity purification (TAP) using IgG-sepharose beads and a Ni column. Western blots using a monoclonal anti-myc antibody revealed the overexpressed protein in the plant extract used for loading on the beads at 59 kDa, corresponding to the size predicted without transit peptide. After incubation with 3C protease, the size was reduced to 43 kDa, indicating the loss of the IgG binding site. Enrichment of tagged SGR along the Ni purification process showed maximum elution of the protein at 50 mM imidazole (Fig. 21). It was assumed that SGR partners would be co-purified and isolated with these fractions. Thus, fractions E50.1-3 were subsequently concentrated and loaded on SDS-PAGE for size separation. The gel was stained by silver staining, and slices cut

and trypsinised. After elution, peptide mixes were analyzed by MS-MS for protein identification (Table 1). Unfortunately the bait itself was not identified in the MS analysis, even though Western data clearly showed presence of the tagged protein in the analyzed mixture. If potential SGR partners bound to SGR in an equimolar ratio, they will probably have escaped detection as well. Running of the GFP control through the same purification process and repetition of the purification with improved conditions are required for a correct analysis of SGR partners. We might speculate about an interaction of SGR with PSBb and PSBc found in the TAP experiment. Both proteins are known to bind chl, but true interaction will have to be confirmed by alternative methods, such as co-immunoprecipitation.

Table 1. Proteins identified by MS-MS after TAP processing. 13 different proteins were found in the purified eluate that could include SGR partners. Tagged SGR itself was not identified. Repetition and improvement of the purification may allow clearer results in the future.

Proteins identified by MS	**AGI number**	**Peptides**
47 kDa psbB	Atcg00680	1
44 kDa psbC	Atcg00280	4
RCActivase	At2g39730	1
ATPase F1	Atcg00480	1
RubisCO large subunit	Atcg00490	6
Myrosinase binding prot	At3g16470	4
Tu transcription elongation factor	At4g20360	3
ATP synthase beta	Atcg00480	3
probable mito peptidase	At3g02090	1
endoglucanase	At4g02290	1
aldehyde deshydrogenase	At1g44170	1
syntaxin	At1g32270	1
UTP-glc P uridyl transferase	At3g03250	1

7.4.4 SGR overexpressing lines show sensitivity to biotic and abiotic stress

The transgenic lines overexpressing the full-length SGR tagged at the C-term (pCTAPa-SGR), showed an interesting phenotype. When leaves got older or were exposed to pathogens, they locally developed necrotic lesions phenotypically similar to the hypersensitive response (HR) (Fig. 22A; L. Mur and H. Ougham, personal communication). This interesting finding correlated with higher expression of *SGR* under biotic stress, specifically with pathogens which induce HR in a light-dependent manner (Fig. 21B, Genevestigator data). SGR might have a function in triggering HR and further characterization of this line is in progress (H. Ougham and L. Mur, Aberystwyth. UK).

A

B

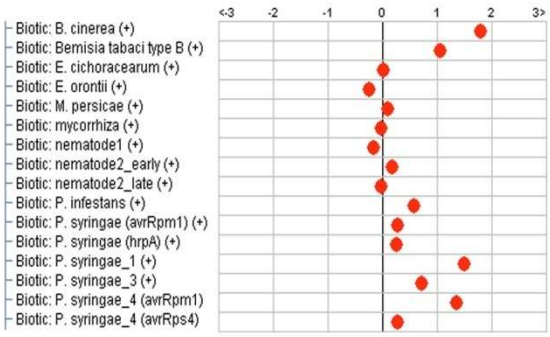

Figure 22. A. Constitutive overexpression of SGR provokes light-induced lesions. **B**. SGR expression is increased by pathogen treatments (Genevestigator data).

7.4.5 Conclusion

Within chl breakdown research, studying SGR factor is an amazingly dynamic niche with six publications since November 2006 (Armstead et al., 2006, 2007; Jiang et al., 2007; Park et al., 2007; Ren et al., 2007; Sato et al., 2007), but unfortunately without unequivocally having unravelled its physiological function yet. A first claimed function of SGR being involved in PAO regulation (Armstead et al., 2006, 2007; Ren et al., 2007; Sato et al., 2007) was recently withdrawn by better characterization of SGR in rice, but also in peas and in *Arabidopsis.* This led to a second hypothesis, suggesting a role of SGR upstream PAO, at the level of photosystem degradation (Park et al., 2007; Aubry et al., 2008). Further studies using different molecular and biochemical strategies might give more clues about the function of this intriguing factor.

8. Biochemical identification of the RFF activity

8.1 Introduction

The key step of chl degradation is the irreversible opening of the porphyrin ring at the α-methine group of pheide. This reaction is catalyzed by the coupled action of an iron-sulphur Rieske type monooxygenase, PAO, and red chl catabolite reductase (RCCR). *In vivo*, depletion of PAO leads to the accumulation of its substrate pheide, without occurrence of further downstream catabolites (RCCs, FCCs and NCCs) (Pružinská et al., 2003; Pružinská et al., 2005). In contrast, RCCR depletion causes the accumulation of RCC, but also of further catabolites (Pružinská et al., 2007). This metabolic "leakage" might suggest that an enzyme different from RCCR might reduce RCC to pFCC. Recently, *in vivo* proof of involvement of RCCR in RCC reduction has been gained by exploiting formation of different stereospecific pFCCs depending on the RCCR source (Pružinská et al., 2007). Even though some proof of interaction between PAO and RCCR had been obtained using a double-hybrid strategy (Pružinská et al., 2007), further proofing of interaction was unsuccessful so far, despite intensive efforts in this direction, including cross-linking and co-immunoprecipitation (S. Aubry and S. Hörtensteiner, unpublished). As a matter of fact, the mechanism of the PAO and RCCR reaction and the way, pheide/pFCC conversion is channelled without release of RCC (Hörtensteiner, 2006) is unclear. Here I report new advances in understanding what are the requirements for a proper PAO/RCCR reaction to take place *in vitro*.

Based on cloning of both enzymes, *in vitro* studies have been performed for investigating the PAO/RCCR reaction (Pružinská et al., 2003). PAO proved difficult to be isolated in an active form from heterologous expression systems, but has been partially purified from *Brassica napus* or *Capsicum annuum* membranes (Hörtensteiner et al., 1995; Moser and Matile, 1997). RCCR has been cloned with an hexa-histidine tag and has been successfully expressed in *E.* coli (Pružinská et al., 2007). A standard *in vitro* assay has been developed which includes Fd and a Fd-reducing system (Hörtensteiner et al., 1995; Wüthrich et al., 2000). The assay combines the two steps of PAO/RCCR, thereby in a first step PAO introduces one molecule of dioxygen at the α-methine bridge on ring B of pheide to form an RCC.

Then a second molecule of oxygen is added on ring A, probably derived from water (Hörtensteiner et al., 1998). The second step is catalyzed by RCCR by reducing the C_{20}/C_1 bond of RCC to give pFCC. Assaying the two enzymes independently is rather inefficient, indicating metabolic channelling of RCC (Rodoni et al., 1997), but still amounts of products are formed, allowing the individual analysis of PAO and RCCR. Comparing individual and coupled reactions, it turned out that PAO required another factor to produce RCC *in vitro* (Fig. 23). Soluble protein extracts of *E. coli* have been used to restore PAO activity and this activity was tentatively called RFF (RCC forming factor) (A. Pruzinska and S. Hörtensteiner, unpublished results) (Pružinská et al., 2005), RFF was thought to be an additional factor involved in the reaction, like a second reductase. In this project I identified RFF required to get proper PAO activity *in vitro*, and which might be required as well in the PAO/RCCR reaction *in vivo*. To this end, I isolated RFF from soluble proteins of dark incubated *Brassica napus* cotyledons and purified the activity by multistep chromatography. RFF activity was purified up to 250 times during this process and allowed the identification of RFF as a peroxidase using mass spectrometry.

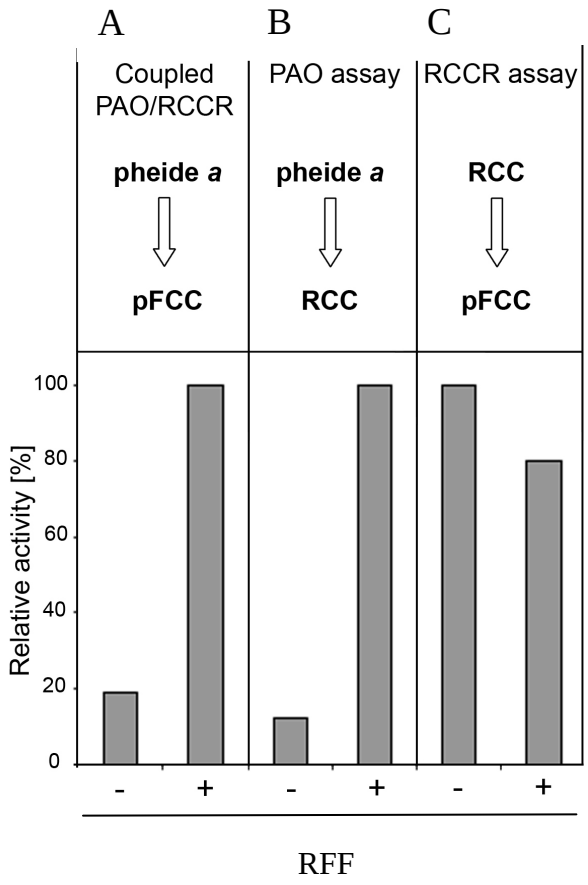

Fig 23. RFF is needed for PAO activity *in vitro*. A. Full assay containing both PAO and RCCR is only efficient when RFF is supplied. **B**. 1st half assay. Conversion of pheide to RCC is also dependent on RFF activity. **C.** 2nd half assay. Conversion of RCC to pFCC is independent of RFF activity. RFF was supplied to standard assays as 5 µl *E. coli* soluble protein extract in 50 µl assay reaction. Adapted from A. Pruzinska and S. Hörtensteiner (unpublished).

8.2 Material and methods

8.2.1 *Brassica napus* membrane isolation

Brassica napus (canola) seeds were sown on soil and grown at 120 µmol m^{-2} s^{-1} at 16 h light/8 h dark). For purification of RFF, 10 d old seedlings were cut and put in the dark for senescence induction during three days. 20 g cotyledons were homogenized in buffer 1 (0.4 M sorbitol, 25 mM Tricine-KOH pH 8, 2 mM EDTA, 1 mM $MgCl_2$), filtrated through a nylon mesh and centrifuged for 4 min at 8000 g. Pelleted membranes were resuspended in 0.4 M sorbitol and 25 mM Tricine-KOH pH 8. After centrifugation (4 min, 8000 g), the pellet was resuspended in Tricine-KOH pH 8 with a paint brush and centrifuged for 5 min at 16000 g. The supernatant was filtered though 0.2 µm filter and used in subsequent purification steps as stromal soluble protein source (S1). Three subsequent chromatographic steps were performed to purify and identify RFF.

8.2.2 Purification process : AEX, HIC, HPT

All chromatographic steps were performed on an ECONO chromatography system (BioRad) and performed at 4°C with a flow of 1 ml/min (0.8 ml/min for step III). Each fraction was monitored by an *in vitro* assay containing 5 µl of desalted fraction (see section 8.2.4 for assay description). Desalting of fractions was performed according to Helmerhorst and Stokes using Sephadex G50 (GE Healthcare) (Helmerhorst and Stokes, 1980).

Step I: Anion exchange chromatography (AEX)

S1 fraction was equilibrated in 2x buffer A to a final concentration of 100 mM NaCl. A HiTrap-Q-HP column (GE Healthcare) was washed with buffer A (Tris/Mes pH 8, 10% glycerol, 100 mM NaCl). After loading of the sample (around 40 ml), the column was washed with buffer A for 30 min and elution carried out using buffer B (Tris/Mes pH 8, 10% glycerol, 1 M NaCl). 1 ml fractions were collected individually for monitoring RFF activity. 1 M NaCl fractions were desalted.

Step II: Hydrophobic interaction chromatography (HIC)

A Hi-Trap Octyl-FF column (GE Healthcare) was equilibrated with buffer C containing 40 mM KPi pH 7 and 1 M ammonium sulphate. AEX fractions containing RFF activity were pooled and equilibrated 1:1 in 2x C then applied to the column. After 10 min washing in C, a linear gradient from C to D (40 mM KPi pH 7) over 20 min was applied to the column and 1 ml fractions collected.

Step III: Hydroxyapatite chromatography (HPT)

The HIC fractions containing highest RFF activity were pooled and desalted in buffer E (10 mM KPi pH 7). This solution was applied to an Econo-Pac CHT-II column (BioRad) that had been equilibrated in buffer D. A KPi step gradient was performed at 0.8 ml/min with 40, 200 and 400 mM KPi pH 7.

8.2.3 SDS-PAGE and MS-MS analysis

The collected active HPT fractions were pooled and concentrated on an Amicon Ultra-15 column (Millipore). The sample was mixed with SDS loading buffer and boiled for 5 min, to be then load on a 12.5% polyacrylamide gel. Protein bands were visualized according to Blum's silver staining protocol (Mortz et al., 2001). Gel slices were cut and trypsinised overnight according to published procedures (Shevchenko et al., 1996). Peptides were then eluted from the gel and identified by MS-MS (S. Baginsky, ETH Zürich).

8.2.4 Isolation of PAO from pepper

Pepper membranes were extracted according to published procedures (Moser and Matile, 1997) using slightly modified conditions. Homogenization buffer was used at 1 ml/g fresh weight and the membrane pellet not frozen during the process. Pelleted membranes were resuspended in T/M pH 8 and centrifuged for 5 min at 13000 rpm. The obtained pellet was resuspended in T/M pH 8 and solubilised with 1% Triton X-100. After centrifugation the supernatant was collected and used as crude PAO source (cPAO).

Subsequently, an EAH purification was performed with cPAO according to published procedures (Hörtensteiner et al., 1998), the column was washed with 0.05 M KCl in Tris/Mes containing 0.1% Triton X-100 (buffer F) for 30 min and then PAO was

eluted with buffer F containing 0.2 M KCl. After desalting into KCl free buffer F, fractions were used as EAH purified PAO source (pPAO) without any RCCR activity left.

8.2.5 *In vitro* assay for characterization of RFF activity

PAO/RCCR/RFF activities were assessed according to published procedures (Hörtensteiner et al., 1995; Pružinská et al., 2005). 50 µl assays contained pPAO (equivalent to 0.5 g tissue) and purified His_6-*At*-RCCR (2.9 µg). 5 µl of every single desalted fraction was tested as source of RFF. The assays were supplemented with 0.5 mM pheide *a* (Hörtensteiner et al., 1995), 10 µg of Fd, and a Fd-reducing system consisting of 2 mM glucose-6-phosphate, 1 mM NADPH, 50 milliunits of glucose-6-phosphate dehydrogenase, and 5 milliunits of ferredoxin NADPH oxidoreductase. After 1 h of incubation at 25°C, reactions were terminated by the addition of 80 µl of methanol. Formation of pFCC was followed by reversed-phase HPLC with 36% (v/v) 50 mM potassium phosphate buffer, pH 7.0, in methanol as solvent. Activities were determined as integrated fluorescence units (IU; 320/450 nm) of pFCC-1.

8.2.6 Leaf disc incubation

Arabidopsis leaf discs (1 cm diameter) from mature leaves were floated on water containing 0, 0.1, 0.5 and 1% freshly prepared H_2O_2 and dark incubated for 3 d. Proteins were extracted and PAO Western blots performed according to published protocols (Pružinská et al., 2007).

8.2.7 Staining for catalase activity and H_2O_2 with NBT

10% native polyacrylamide gels were incubated in 0.003% hydrogen peroxide for 10 min. The gels were then stained with 1% ferric chloride and 1% potassium ferricyanide for 30 min (Wood et al., 2006). Finally, the gel was washed extensively with water. Achromatic white areas revealed catalase activity. H_2O_2 staining was performed using 1 µl NBT (50 µg/µl) in a 50 µl assay. Dark brown colour appears when H_2O_2 is produced.

8.2.8 Protein determination

Protein amounts of fractions were determined using Bradford assay (Bio-Rad) according to the manufacturer's protocol.

8.3 Results

8.3.1 Purification of "RFF" activity

Three successive steps were necessary to obtain a protein fraction that was pure enough to identify RFF. In the first step, I used a weak anion exchange column for a crude purification of the S1 extract. 100 mM NaCl was used to load the sample, and all the activity eluted without binding to the column (Fig. 24A), while most of the proteins were binding, as shown in the OD_{280} trace, and only eluted with 1 M NaCl. This step allowed to remove two third of the proteins and enriched the specific activity by 10 fold (Fig. 25A). All active fractions were directly used for the second step without desalting. In the second step I used a middle range hydrophobic medium (octyl-FF) and after loading the pooled active fraction of the first step, a linear decreasing gradient of ammonium sulphate, from 1 M to 0 M in 10 min was applied. RFF eluted at around 350 mM NH_4SO_4 (Fig. 24B). Active fractions were pooled and desalted on Sephadex G-25. This step allowed only a 2x increase of specific activity, probably because of the broad elution profile. In a third step, the active HIC fractions were applied to an affinity chromatography using a hydroxyapatite resin. The column was performed with a step gradient of phosphate buffer increasing from 0 to 300 mM (Fig. 24C). Most of the activity eluted at around 100 and 200 mM. The third step was the most successful purification step with an increase of specific activity at around 13x of RFF. Thus, overall purification was around 250 fold with a yield of less than 2% of RFF activity (Fig. 25A). Fractions were pooled and desalted before concentration on AmiconUltra column and analysis by SDS-PAGE. A decreasing complexity of the different fractions along the purification process could be evaluated after silver staining (Fig. 25B).

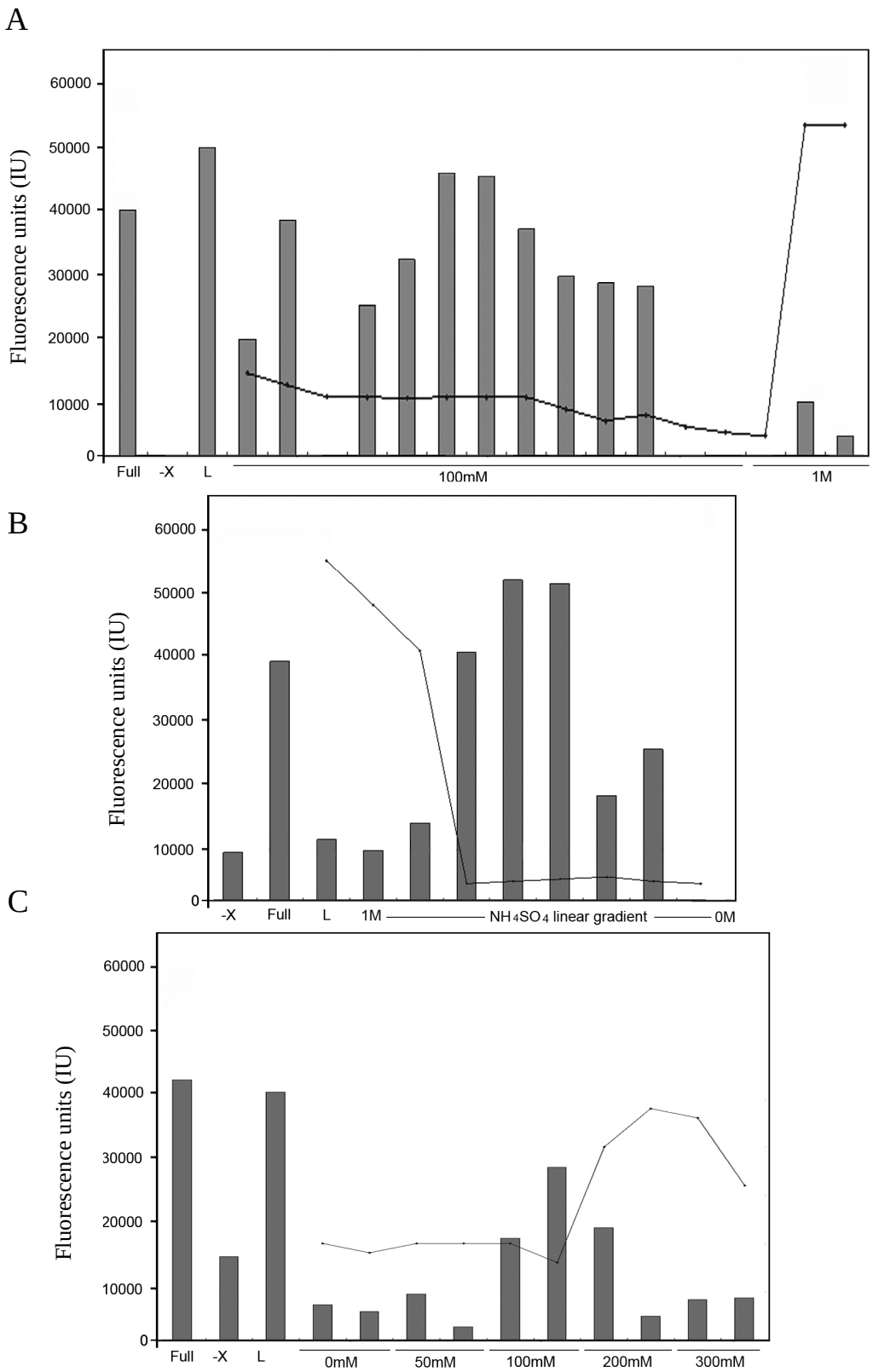

Figure 24. Purification of RFF. **A**. Anion exchange chromatography. The column was processed with 100 mM and 1 M NaCl. **B**. Hydrophobic interaction chromatography. **C**. Hydroxyapatite chromatography performed with a step gradient of 0-300mM KPi. Assays (gray columns) were performed with 5 µl of individual fractions as shown. Full, positive control with RFF from *E. coli*; –X, assay minus RFF; L, load on the column. Lines represent relative OD280, indicating protein content of the fractions. Fractions containing more than 30000 IU were collected, pooled and loaded on the next step.

A

Sample	Volume (µl)	Concentration (µg/µl)	Total protein (µg)	Activity 5 µl	Activity 1 µl	Total Activity (IU)	Specific activity (IU)	Yield (%)	Purif (fold)
L	17000	1.427	24259	77786	15557	264472400	0.64	100	1
AEX	14000	0.057	799.42	26545	5309	74326000	6.64	28.1	10.3
HIC	5000	0.066	328.98	20309	4061.8	20309000	12.34	7.68	19.2
HPT	1000	0.026	25.79	20987	4197.4	4197400	162.74	1.59	253.7

B

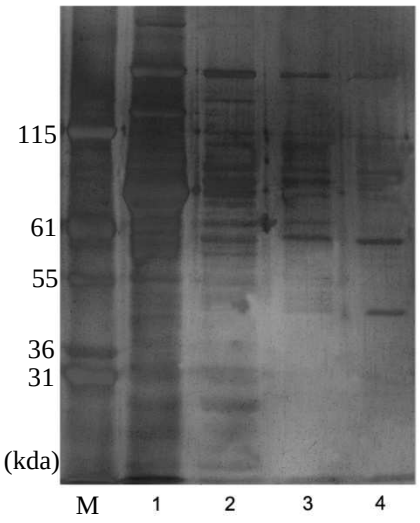

Figure 25. RFF purification summary. **A.** Table of the protein purification. L, loading (S1 from canola). AEX, anion exchange chromatography. HIC, hydrophobic interaction chromatography. HPT, hydroxyapatite chromatography. Total RFF enrichment of 250 fold was achieved after the total process. **B.** Silver stained gel of the fractions from the purification process. 1. S1 diluted 10x. 2. Pooled fractions loaded on HIC. 3. Pooled fractions loaded on HPT. 4. Pooled fractions obtained after HPT which were used for MS analysis.

Gel slices were cut, trypsinised and analyzed by MS-MS. All peptides identified were from *B. napus*. When sequences were compared with the *in silico* trypsinised *Arabidopsis* proteome, it was possible to identify 5 major proteins present in final the highly enriched final RFF extract, although based on the silver-stained gel (Fig. 25B), it is clear that not all proteins present in the fraction were identified. Identified proteins were the following :

Accession	**Name**
Q42547	Catalase 3
O81248	Alanine glyoxylate aminotransferase
Q43743	Glyoxisomal malate dehydrogenase
Q8VYW9	Aminotransferase 1
O49124	Putative serine-glyoxylate aminotransferase

Surprisingly, most of the identified proteins are localized in glyoxisomes and peroxisomes which most probably had been co-purified with the stromal proteins. In cotyledons of *B. napus* it is known that peroxisomes and glyoxisomes are extremely abundant, due to strong remobilization of lipids (Hayashi et al., 2001). Facing these results, I investigated the only reasonable candidate for RFF out of the five proteins identified and added catalase (Sigma) to the PAO/RCCR assay. Indeed, addition of 10 units of catalase restored PAO activity and pFCC production (Fig. 26B) and this could replace the addition to the assay of bacterial extract. Catalases are converting H_2O_2 into water and oxygen (Asada, 2006) and it was likely to assume that the function of RFF was to remove reactive oxygen species formed as a result of PAO activity. To test this, I added H_2O_2 to the *in vitro* assay and strongly inhibited pFCC formation in a concentration dependent manner (Fig. 26B). Thus, I concluded that H_2O_2 directly inhibited PAO. This inhibition was partially reversed by the addition of excess catalase (Fig. 26C).

8.3.2 Role of ROS in the PAO/RCCR reaction and potential *in vivo* relevance

-H_2O_2 effect *in vitro*

An intriguing fact was the incapacity of superoxide dismutase (catalyzing the conversion of superoxide to hydrogen peroxide) to act as a protective ROS scavenging agent like catalase (Fig. 26C). As a monooxygenase, PAO mechanism is using an iron-peroxo intermediate during activation of oxygen (Solomon et al., 2000). It seems possible that SOD traps this intermediate and thus inhibits the reaction. Catalases are known to be localized to peroxisomes. If a H_2O_2-detoxifying activity is required for PAO activity, one has to assume that *in vivo* the activity would be due to chloroplast-localized peroxidases, like ascorbate peroxidase rather than catalase itself.

-*In vitro* production of ROS by PAO and NADPH

Production of ROS *in vitro* was assessed by staining with nitroblue tetrazolium (NBT) (Fryer et al., 2002). ROS production was associated with pPAO or RCCR only if incubated with NADPH (Fig. 27A), but RCCR activity was not sensitive to ROS production (data not shown).

-Pepper chromoplast membranes contains catalase activity

Pepper fruit chromoplast membranes are known to have a strong PAO activity (Moser and Matile, 1997). Knowing RFF to be identical to catalase/peroxidase, I wanted to know whether these particularly strong activity was due to any protective peroxidase activity present in either membrane pepper extracts (cPAO) or EAH purified PAO (pPAO). A native gel was stained for catalase activity and indeed some hydrogen peroxide degrading activity could be detected in cPAO fractions, however no activity could be observed in the pPAO fraction of lower activity (Fig. 27B). Destruction of PAO activity in the absence of an efficient peroxidase protection was evaluated to be less than 10 min (data not shown).

-PAO levels are reduced by hydrogen peroxide *in vivo*

Incubation of leaf discs in hydrogen peroxide solution showed a retention of greenness and a decrease in PAO content with increasing H_2O_2 concentrations. Thus PAO seemed to be sensitive to oxidative stress *in vivo* (Fig. 28). However it remains

to be shown that ROS effect is linked to the loss of PAO or to a broader senescence process. To investigate the *in vivo* requirements of peroxidases for PAO activity, we analyzed PAO levels in mutants overexpressing the stromal APX (Murgia et al., 2004), or knockout lines for the stromal and thylakoid APX (K. Van Wijk, personal communication). Unfortunately, no differences of PAO protein levels, analyzed by Western blot could be observed in those lines (data not shown).

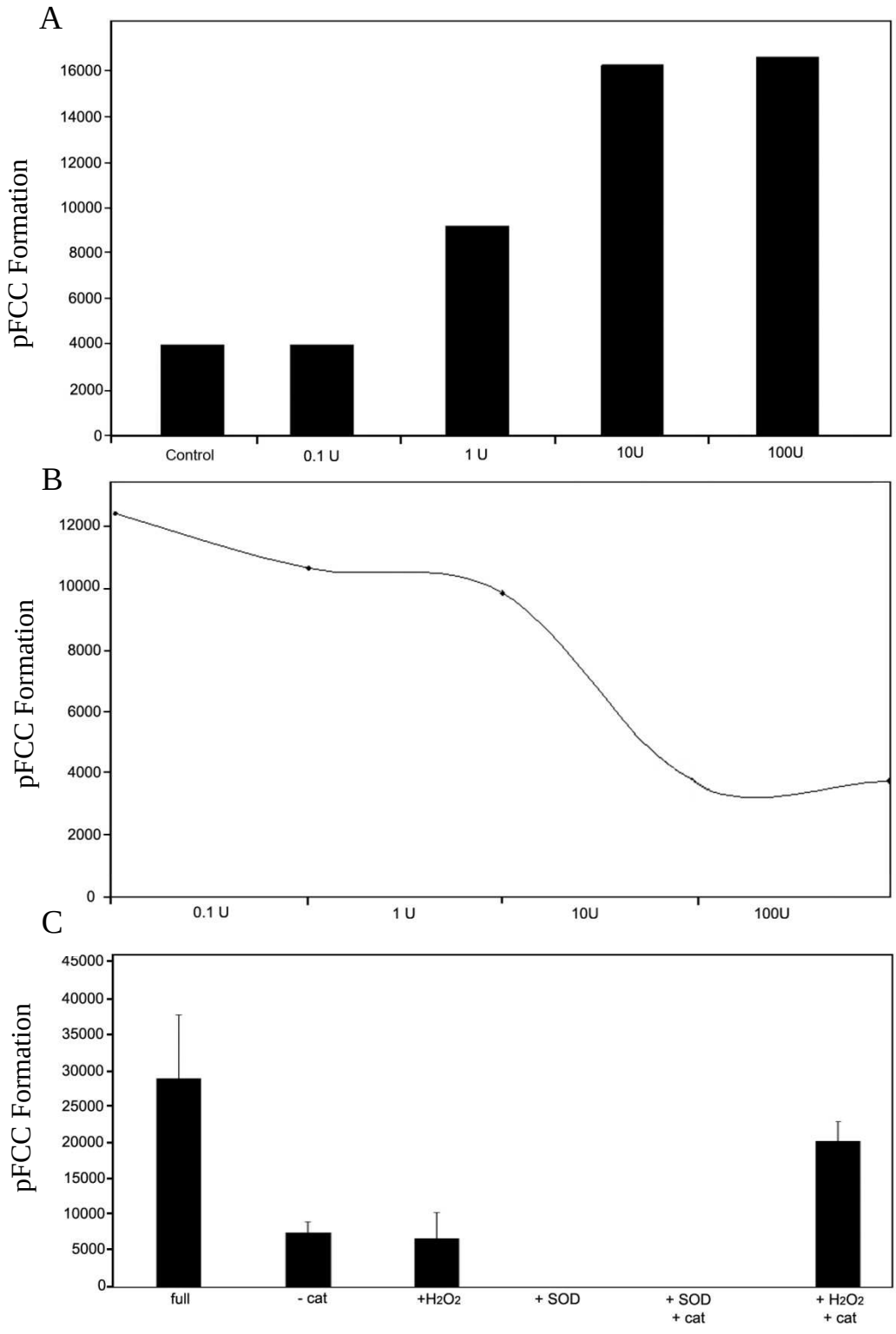

Figure 26. The PAO/RCCR assay needs a ROS detoxifying activity. A. Catalase mimics RFF activity by protecting PAO. Control without catalase. **B**. Addition of H_2O_2 in a full assay leads to the decrease of pFCC formation. **C**. Superoxide dismutase (SOD) inhibits the reaction completely.

A

1 2 3 4

B

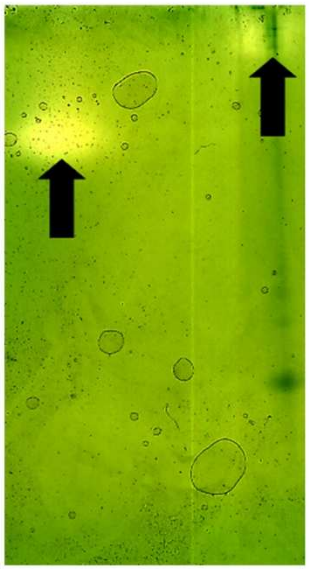

n.d. ± 25000 ± 150000 PAO activity (IU)

1 **2** **3**

Figure 27. A. H_2O_2 staining with NBT in full assays. Line 1. NADPH + purified PAO (pPAO). Line 2. pPAO alone. Line 3. pPAO + RCCR. Line 4. RCCR + NADPH. **B**. Demonstration of peroxidase activity via potassium ferricyanide staining of a native polyacrylamide gel. Line 1. Pure catalase. Line 2. Purified pepper PAO. Line 3. membrane of high PAO activity (cPAO), see section 8.2.4.

8.4 Discussion

RFF study and its purification led to a surprising result of requirement of a peroxidase in the PAO reaction and to a better understanding of the PAO/RCCR reaction. In contrast to our basic hypothesis there is *a priori* no additional factor needed in this reaction. It seems that *in vitro*, detoxifying reactive oxygen species is a prerequisite to obtain significant PAO activity. Production of pFCC required RFF/catalase activity as well as the presence of the substrate pheide, O_2 and reduced Fd.

In the coupled *in vitro* assay, Fd-NADPH oxidoreductase (FNR), which reduces Fd, is most probably responsible for a large part of the ROS production. Staining of H_2O_2 using NBT showed ROS production only if PAO or RCCR were incubated with NADPH (Fig. 27A). But under oxygenic conditions, some ROS production is linked to PAO activity. cPAO fractions showed around 2 to 5 times higher PAO activity compared to pPAO. Checking for catalase activity in these extracts showed major amounts of catalase in cPAO (Fig. 27B), which may explain this unusual high PAO activity compared to canola, barley or *Arabidopsis* membrane extracts.

Assessing PAO activity and stability *in vitro* and demonstration of catalase /peroxidase activity requirement still questioned its *in vivo* relevance. During senescence, ROS content in the plastid largely increases (Mach, 2004), it might be necessary to protect PAO in order to retain sufficient chl degradation. Usually, the Rieske type monooxygenase mechanism involves an activated oxygen intermediate bound to the mononuclear iron which might have an inhibitory effect on the enzyme itself (Fig. 29). Naphthalene dioxygenase (NDO) has been shown under certain conditions to form a superoxide anion as well as hydrogen peroxide via an uncoupled electron transfer. O_2 binds to the ferrous mononuclear iron at the active site and produces hydroxyl radicals $^{\cdot}OH$ (Lee, 1999). It is surprising to observe that PAO as an enzyme which is specifically involved in a high oxidative environment (dismantling chloroplasts) is sensitive to ROS. Pheide degradation due to direct oxidative effects of H_2O_2 could be ruled out by pre-incubating the enzyme with H_2O_2, and loosing its activity as well. Such ROS activity on porphyrins have been however suggested by Bollivar and Beale during purification of PPIX monomethyl ester cyclase (Bollivar and Beale, 1996).

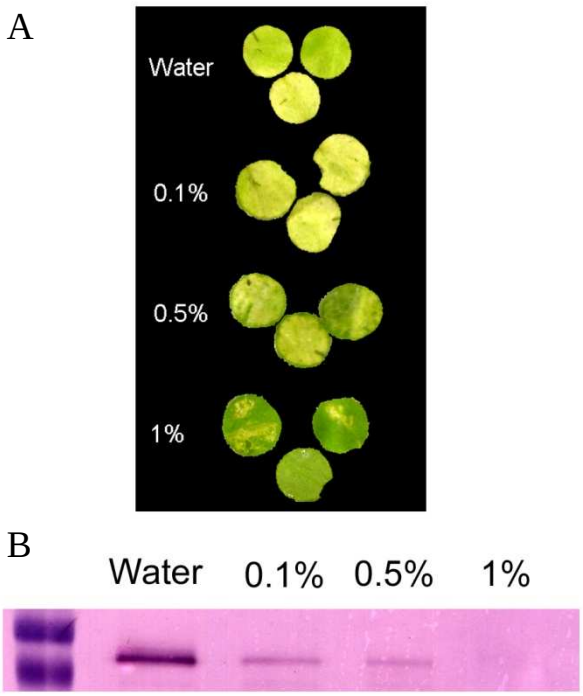

Figure 28. H_2O_2 effect on leaf disc senescence and PAO levels. A. Leaf discs from Col-0 were floated for 5 days in the dark on 0.1 to 1% hydrogen peroxide. **B**. PAO Western blot of leaf discs from panel A.

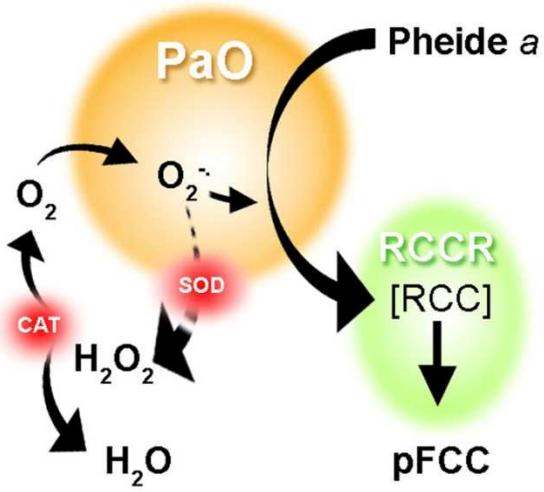

Figure 29. Hypothetical model of action of catalase/peroxidase and ROS on PAO activity. PAO activates dioxygen and might produce some ROS via oxygen intermediate or via FNR *in vitro*. Catalase activity allows protection of PAO by detoxifying H_2O_2 to water and oxygen. SOD might act on the intermediate and shut down the reaction by converting activated oxygen to H_2O_2, thereby removing the cosubstrate required for incorporation into pheide *a*.

Previous to the present identification of RFF activity, it has been shown that RFF activity is not senescence-specific and not restricted to leaves in the *Arabidopsis acd2* mutant (A. Pruzinska and S. Hörtensteiner, unpublished), suggesting a general process not necessarily involved directly in PAO activity.

Even if catalase activity is most probably the strongest activity allowing to protect PAO function *in vitro* it is not the enzyme responsible for this function *in vivo*. All three cloned catalases in *Arabidopsis*, and most probably also in oilseed rape are located to the peroxisome. However a catalase activity has been associated, but not molecularly identified with photosystem II (Sheptovitsky and Brudvig, 1996).

Protection of PAO by other chloroplastic peroxidizing enzymes like ascorbate peroxidase, superoxide dismutase, or peroxiredoxine (Apel and Hirt, 2004) is most likely. Yet, investigating PAO levels in lines overexpressing or knocking out stromal and/or thylakoid ascorbate peroxidase did not show any instability (data not shown). The complexity of the ROS detoxifying enzyme network in the chloroplast will make further studies *in vivo* on PAO instability rather difficult. It is of interest to remark that even if PAO expression is increasing until the end of the senescence period, PAO protein levels are decreasing at later stages (Pružinská et al., 2005). Such observation might suggest a need for an *in vivo* ROS-free environment for PAO in order to degrade chl.

9. Chlorophyll breakdown in *Arabidopsis*: Characterization of chlorophyll catabolites and of chlorophyll catabolic enzymes involved in the degreening reaction

Adriana Pruzinska, Gaby Tanner, Sylvain Aubry, Iwona Anders, Simone Moser, Thomas Müller, Jarl-Hans Ongania, Bernhard Kräutler, Ji-Young Youn, Sarah J. Liljegren, and Stefan Hörtensteiner

Plant Physiology
AMERICAN SOCIETY OF PLANT BIOLOGISTS

Reprinted from *Plant Physiology* (2005) 139; 52-63

In this publication, we describe the PAO degradation pathway of chl in *Arabidopsis*. It is a fundamental paper gathering data concerning mutants impaired in the *PAO* gene. We furthermore describe the complexity of *Arabidopsis* chl catabolites and discuss about the function and regulation of PAO, as the key step of the degradation of chl.

Chlorophyll Breakdown in Senescent Arabidopsis Leaves. Characterization of Chlorophyll Catabolites and of Chlorophyll Catabolic Enzymes Involved in the Degreening Reaction[1]

Adriana Pružinská, Gaby Tanner[2], Sylvain Aubry, Iwona Anders, Simone Moser, Thomas Müller, Karl-Hans Ongania, Bernhard Kräutler, Ji-Young Youn, Sarah J. Liljegren, and Stefan Hörtensteiner*

Institute of Plant Sciences, University of Bern, CH–3013 Bern, Switzerland (A.P., G.T., S.A., I.A., S.H.); Institute of Organic Chemistry and Center of Molecular Biosciences, University of Innsbruck, A–6020 Innsbruck, Austria (S.M., T.M., K.-H.O., B.K.); and Department of Biology, University of North Carolina, Chapel Hill, North Carolina 27599 (J.-Y.Y., S.J.L.)

During senescence, chlorophyll (chl) is metabolized to colorless nonfluorescent chl catabolites (NCCs). A central reaction of the breakdown pathway is the ring cleavage of pheophorbide (pheide) *a* to a primary fluorescent chl catabolite. Two enzymes catalyze this reaction, pheide *a* oxygenase (PAO) and red chl catabolite reductase. Five NCCs and three fluorescent chl catabolites (FCCs) accumulated during dark-induced chl breakdown in Arabidopsis (*Arabidopsis thaliana*). Three of these NCCs and one FCC (primary fluorescent chl catabolite-1) were identical to known catabolites from canola (*Brassica napus*). The presence in Arabidopsis of two modified FCCs supports the hypothesis that modifications, as present in NCCs, occur at the level of FCC. Chl degradation in Arabidopsis correlated with the accumulation of FCCs and NCCs, as well as with an increase in PAO activity. This increase was due to an up-regulation of *Pao* gene expression. In contrast, red chl catabolite reductase is not regulated during leaf development and senescence. A *pao1* knockout mutant was identified and analyzed. The mutant showed an age- and light-dependent cell death phenotype on leaves and in flowers caused by the accumulation of photoreactive pheide *a*. In the dark, *pao1* exhibited a stay-green phenotype. The key role of PAO in chl breakdown is discussed.

Chlorophyll (chl) degradation is an integral part of leaf senescence and fruit ripening. The fate of chl during senescence has been well established in recent years (for review, see Matile et al., 1999; Hörtensteiner, 1999; Hörtensteiner and Kräutler, 2000; Kräutler, 2003; Eckhardt et al., 2004). Thereby, chl is converted to colorless nonfluorescent chl catabolites (NCCs; Fig. 1) in a pathway that is probably active in all higher plants (Pružinská et al., 2003; Gray et al., 2004).

Structure elucidation of NCCs from different species has unraveled a common tetrapyrrolic skeleton with an oxygenolytically opened porphyrin macrocycle (Kräutler, 2003). Peripheral modifications at several side chains within different NCCs (Fig. 1, R_1–R_3) are species specific (Berghold et al., 2002, 2004), and hence have been proposed to occur rather late in the pathway (Hörtensteiner, 1999). Indeed, a primary chl breakdown product (primary fluorescent chl catabolite-1 [pFCC-1]), which exhibits a blue fluorescence, could be identified as a common product of porphyrin ring cleavage (Fig. 1; Mühlecker et al., 1997). Thus, the sequence of reactions is the removal of phytol and magnesium (Mg) by chlorophyllase and Mg-dechelatase, respectively, followed by the conversion of pheophorbide (pheide) *a* to pFCC-1, which requires the activity of two enzymes, pheide *a* oxygenase (PAO) and red chl catabolite (RCC) reductase (RCCR; Rodoni et al., 1997; Hörtensteiner, 1999).

PAO is a chloroplast envelope-bound Rieske-type iron-sulfur oxygenase, which is identical to lethal leaf spot 1 (LLS1) from maize (*Zea mays*) and accelerated cell death 1 (ACD1) from Arabidopsis (*Arabidopsis thaliana*; Pružinská et al., 2003; Yang et al., 2004). PAO has an intriguing specificity for pheide *a*, with pheide *b* inhibiting in a competitive manner (Hörtensteiner et al., 1995; Pružinská et al., 2003). Consequently, all NCCs identified so far from higher plants are derived from chl *a* (Fig. 1) and chl *b* is proposed to be reduced to chl *a* before entering the catabolic pathway through PAO (Hörtensteiner, 1999). In contrast to PAO, RCCR is a soluble protein identical to Arabidopsis ACD2, which mainly localizes to chloroplasts, but in young seedlings has been associated with mitochondria as well (Wüthrich et al., 2000; Mach et al., 2001).

[1] This work was supported by the Swiss National Science Foundation (grant nos. 3100–063628 and 3100A0–105389), by the National Centre of Competence in Research (NCCR), Plant Survival, research program of the Swiss National Science Foundation, and the Austrian National Science Foundation (FWF; P–16097).

[2] Present address: Institute of Medical Molecular Genetics, University of Zurich, Schorenstrasse 16, CH–8603, Schwerzenbach, Switzerland.

* Corresponding author; e-mail shorten@ips.unibe.ch; fax 41–31–631–49–42.

Article, publication date, and citation information can be found at www.plantphysiol.org/cgi/doi/10.1104/pp.105.065870.

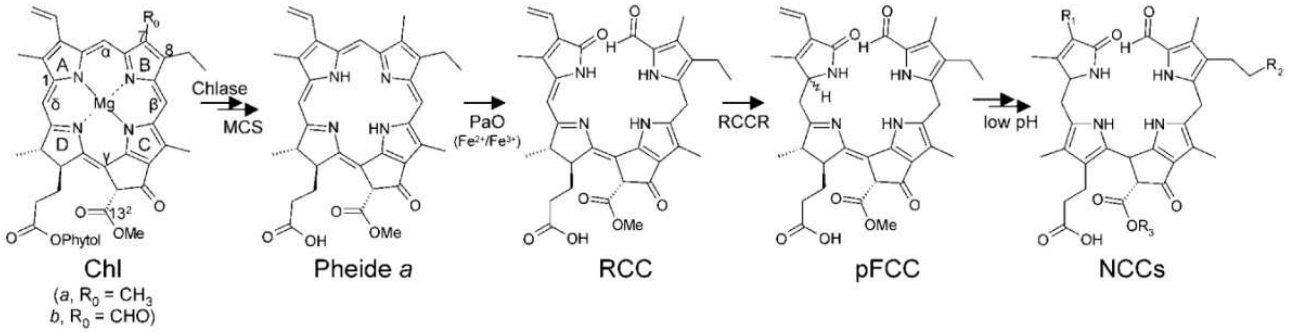

Figure 1. The pathway of chl breakdown in higher plants. The chemical constitutions of chl and of chl catabolites are shown. Pyrrole rings (A–D), methine bridges (α–δ), and relevant carbon atoms are labeled. Sites of peripheral modifications as present in different NCCs are indicated (R_1–R_3). Abbreviations are as indicated in the text. Chlase, chlorophyllase; MCS, Mg-dechelating substance.

Chl breakdown is a multistep pathway that, in addition to the catabolic enzymes described above, requires transport processes for the export of catabolites to their final destination, the vacuole (Matile et al., 1988). Vacuolar uptake of catabolites has been shown to be mediated by a primary active transport system (Hinder et al., 1996; Tommasini et al., 1998). The complexity of the pathway demands a fine-tuned regulation in order to prevent the accumulation of photodynamic breakdown intermediates, such as pheide *a* and RCC. Indeed, mutations in or antisense expression of either *Pao* or *Rccr* genes have been shown to cause the occurrence of lesion-mimic phenotypes (Greenberg and Ausubel, 1993; Greenberg et al., 1994; Gray et al., 1997; Spassieva and Hille, 2002; Pružinská et al., 2003; Tanaka et al., 2003; Yao et al., 2004), but so far a correlation between the phenotype and an accumulation of the respective intermediates has not been proven unequivocally (Pružinská et al., 2003). Activity of PAO has been demonstrated to be restricted to senescence (Ginsburg et al., 1994), although in a recent investigation limited PAO activity was found in presenescent tissues (Pružinská et al., 2003). In contrast, other chl catabolic enzymes, including RCCR, seem to be constitutively active (Matile et al., 1999). Together, these data indicate an important regulatory role for PAO. *Pao/Lls1/Acd1* is considerably expressed before the onset of senescence and also in non-green tissues, but is up-regulated during senescence and upon wounding (Gray et al., 2002; Pružinská et al., 2003; Yang et al., 2004).

The investigation of leaf senescence and of chl breakdown requires a system where senescence can be induced in a controlled manner. In this respect, Arabidopsis is not ideal for several reasons. First, in Arabidopsis, natural senescence coincides with a switch from vegetative to reproductive growth. In addition, rosette leaf senescence is sequential, starting in the older leaves first (Hensel et al., 1993; Miao et al., 2004). Furthermore, the small size of Arabidopsis makes it impossible to use cotyledons for the analysis of chl catabolic enzyme activities or for the identification of chl catabolites, as has been successfully done in canola (*Brassica napus*; Ginsburg and Matile, 1993; Ginsburg et al., 1994). Nonetheless, we used Arabidopsis as a system to analyze senescence-related chl breakdown. In this article, we identified several Arabidopsis chl catabolites and compared their formation during senescence of detached dark-incubated leaves and individually darkened attached leaves. In particular, we identified two novel modified fluorescent chl catabolites (FCCs), which supports the idea that side chain modifications of chl catabolites occur at the level of FCC. Employing a T-DNA-tagged *pao1* mutant, we substantiate the key role of PAO for chl breakdown during senescence. In addition, by a detailed analysis of expression, protein, and activity levels, we show that a major regulation of PAO is at the transcriptional level.

RESULTS

Identification and Characterization of Chl Catabolites

To induce senescence in Arabidopsis, detached leaves of short-day-grown ecotype Columbia (Col-0) plants were incubated in permanent darkness. After extraction, chl catabolites were separated by HPLC (Fig. 2). A total of five different NCCs (Fig. 2A) tentatively numbered *At*-NCC-1 through *At*-NCC-5 (for a nomenclature of NCCs, see Ginsburg and Matile, 1993) were identified by their typical UV/Vis spectrum (Kräutler et al., 1991). By comparison, using mass spectroscopy (MS) and HPLC with known NCCs from senescent canola cotyledons (Fig. 2B; Mühlecker and Kräutler, 1996; S. Moser, J. Berghold, T. Müller, S. Hörtensteiner, and B. Kräutler, unpublished data), compounds *At*-NCC-1, *At*-NCC-2, and *At*-NCC-5 were suggested to be identical to canola *Bn*-NCC-2, *Bn*-NCC-3, and *Bn*-NCC-4, respectively. MS analysis (see "Materials and Methods" for MS data) suggested the structures of the remaining NCCs, as summarized in Table I. Thus, three of the NCCs in Arabidopsis are identical to known chl catabolites from canola and are different from each other with

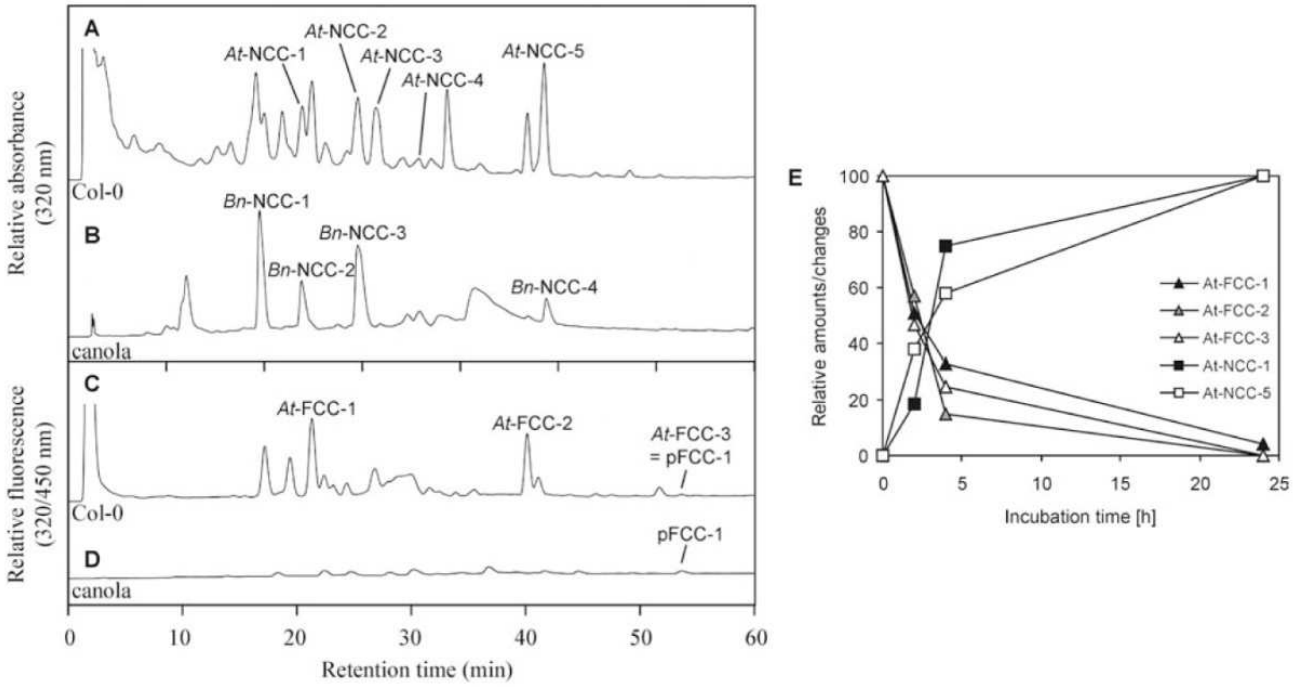

Figure 2. HPLC analysis of chl catabolites in Arabidopsis and canola. Chl catabolites of senescent Arabidopsis (A and C) and canola (B and D) leaves were separated by HPLC as described in "Materials and Methods." A_{320} (A and B) and fluorescence (C and D) were recorded. For the identification and characterization of FCCs and NCCs, see Table I. E, Conversion of FCCs to NCCs during incubation of Arabidopsis leaf extracts at pH 5. Formation of NCCs (squares: black, *At*-NCC-1; white, *At*-NCC-5) is expressed as difference in peak area at 320 nm relative to the peak area at 0 h (24-h sample set to 100). Decrease in FCCs (triangles: black, *At*-FCC-1; gray, *At*-FCC-2; white, *At*-FCC-3) is expressed as relative difference in fluorescence (320/450 nm; 0-h sample set to 100).

respect to modifications at the $C8^2$ position. Hence, the ethyl side chain, as present in *At*-NCC-5, carries a hydroxyl group in *At*-NCC-2, which is further modified with a Glc moiety in *At*-NCC-1. In contrast, the major catabolite of canola, *Bn*-NCC-1, which is malonylated at $C8^2$, is absent in Arabidopsis. The remaining NCCs, *At*-NCC-3 and *At*-NCC-4, are shown to differ from known NCCs and the elucidation of their chemical structures is underway (S. Moser, T. Müller, S. Hörtensteiner, and B. Kräutler, unpublished data).

In addition to NCCs, rather large quantities of three different FCCs were identified in Arabidopsis by their typical absorption and fluorescence properties (Fig. 2C; Mühlecker et al., 1997). In contrast, in canola, FCCs occur only in trace amounts (Fig. 2D). MS analysis

Table I. *Identification of FCCs and NCCs occurring during chl breakdown in Arabidopsis*

Name	R_2[a]	R_3[a]	Identification[b]	Identity with	Reference
At-NCC-1	*O*-glucosyl	H	s, c, m	*Bn*-NCC-2	Mühlecker et al. (1996); this work
At-NCC-2	OH	H	s, c, m	*Bn*-NCC-3	Mühlecker et al. (1996); this work
At-NCC-3	OH[c]	H	s, m	–	This work
At-NCC-4	*O*-glucosyl[c]	CH_3	s, m	–	This work
At-NCC-5	H	H	s, c, m	*Bn*-NCC-4[d]	This work
At-FCC-1	OH[c]	H	s, m	–	This work
At-FCC-2	H	H	s, m	–	This work
At-FCC-3	H	CH_3	s, c, m	pFCC-1	Mühlecker et al. (1997); this work

[a]R_2 and R_3 indicate residues at $C8^2$ and $C13^2$ side positions, respectively, of FCCs or NCCs as shown in Figure 1. R_1 is ethyl in all determined cases. [b]s, Peak identification by UV/Vis spectra (Hörtensteiner, 1999); c, cochromatography with respective standards; m, MS. [c]In *At*-NCC-3, the site of hydroxylation is indicated to be $C7^1$ (rather than $C8^2$); in *At*-NCC-4 and *At*-FCC-1, the sites of attachment of the Glc moiety and the OH group, respectively, are not yet defined (S. Moser, T. Müller, S. Hörtensteiner, and B. Kräutler, unpublished data). [d]S. Moser, J. Berghold, T. Müller, S. Hörtensteiner, and B. Kräutler (unpublished data).

indicates *At*-FCC-2 to be the fluorescent isomer of *At*-NCC-5 (= *Bn*-NCC-4; Table I), while *At*-FCC-3 is identical to pFCC-1 (Mühlecker et al., 1997). The structure of *At*-FCC-1 remains to be established; however, its molecular formula (for MS data, see "Materials and Methods") indicates that it is an isomer of *At*-NCC-2 (i.e. of *Bn*-NCC-3).

It has been shown that in vitro stereoselective nonenzymatic conversion of an FCC to the respective NCC readily occurs at acidic pH (Oberhuber et al., 2003) and it was concluded that in vivo the acidic pH of the vacuole, the final site of chl catabolite accumulation (Matile et al., 1988; Hinder et al., 1996), is responsible for the observed rapid conversion (Oberhuber et al., 2003). To investigate whether the differences in FCC content between Arabidopsis and canola could be due to differences in vacuolar pH, i.e. to a slower FCC-to-NCC conversion after import of FCCs into the vacuoles in Arabidopsis, the pH values of cell saps as representing the vacuolar pH (Barthe and Vaillant, 1993) were determined in leaves. Surprisingly, the pH values of canola (pH 5.82 $\pm$ 0.06) and Arabidopsis (5.60 $\pm$ 0.13) did not differ significantly. Furthermore, subcellular fractionation studies of senescent Arabidopsis mesophyll cells demonstrated the exclusive localization of FCCs outside the vacuole (A. Pružinská and S. Hörtensteiner, unpublished data). Despite this, incubation of Arabidopsis extracts from senescent leaves at a pH of 5.0 resulted in a fast disappearance of FCC peaks, which was concomitant with an increase in the amount of NCCs (Fig. 2E).

Accumulation of Chl Catabolites Correlates with Progression of Leaf Senescence

Two different methods were used to induce senescence and to investigate the dynamics of the formation of chl catabolites in Arabidopsis: (1) detached leaves incubated in permanent darkness and (2) attached leaves that were covered with aluminum foil (Weaver and Amasino, 2001). Progression of senescence was followed by measuring different senescence parameters, such as loss of chl and protein, and by an increase in the chl *a*/*b* ratio (Fig. 3, A and B). Colorless chl catabolites were absent before senescence induction, but the content of the five different *At*-NCCs increased steadily (Fig. 3C). FCCs and NCCs accumulated simultaneously, since their relative amounts remained constant during the incubation period (Fig. 3D). Similar results as shown for the detached leaf incubations (Fig. 3) were obtained when attached leaves were covered with aluminum foil (data not shown).

Analysis of PAO and RCCR during Leaf Senescence in Arabidopsis

As shown previously (Rodoni et al., 1997), the formation of pFCC-1 from pheide *a* requires the joint action of membrane-bound PAO and soluble RCCR. Ongoing biochemical analysis aiming at a detailed investigation of this reaction has led to the identification of a new factor that is indispensable for PAO/RCCR activity in vitro (data not shown). This factor most probably is a protein and is required for the formation of RCC; thus, we tentatively name it RCC-forming factor (RFF). RFF is present both in *Escherichia coli* and in plants, indicating a rather general role. The catalytic properties of RFF will be described in detail elsewhere. Furthermore, work is in progress to identify the molecular nature of RFF.

Hence, the formation of pFCC-1 from pheide *a* requires the activity of three enzymes, PAO, RFF, and RCCR. To assess the activities of PAO and RCCR during leaf senescence in Arabidopsis, respective proteins were isolated from detached dark-incubated leaves (Hörtensteiner et al., 1995) and employed in two assays differing in the sources of the respective enzymes used. Thus, for measuring PAO activity, *E. coli*-expressed His_6-AtRCCR was employed together with PAO isolated from the tissues of interest. Conversely, RCCR activity was determined with soluble proteins of the tissues of interest (containing RCCR) incubated together with a partially purified standard PAO preparation (Hörtensteiner et al., 1998). Both assays were supplemented with extracts of *E. coli* JM109 as a source of RFF and cofactors as described in "Materials and Methods."

In different independent experiments, PAO activity transiently increased during dark incubation of detached leaves (Fig. 4A). Although the extent of activity induction was variable between experiments, consistently maximal activities were obtained at around day 5. A senescence-related (transient) increase in PAO activity had been observed previously in different species, such as canola and *Festuca pratensis* (Hörtensteiner et al., 1995; Vicentini et al., 1995), but to date it is not clear whether this is due to an up-regulation of *Pao* gene expression and/or to a posttranscriptional activation of PAO (Pružinská et al., 2003). To investigate this in more detail, PAO activities were compared with levels of PAO protein as well as with *Pao* expression. Figure 4, B and C, show the data of a representative experiment, which indicate that PAO protein amounts correlate with *Pao* gene expression throughout the dark-incubation treatment. Expression and protein abundance are also comparable to PAO activities during early senescence, but in contrast to protein levels, measurable PAO activity dropped toward the end of the senescence period (Fig. 4, A and B). This is explained by the instability of solubilized PAO (Hörtensteiner et al., 1995, 1998), which may become particularly evident when PAO is extracted from tissue at later stages of senescence. Nonetheless, these data indicate that, in Arabidopsis, senescence-related induction of PAO activity is regulated (mainly) at the transcriptional level. For comparison, PAO regulation was analyzed in canola cotyledons. Employing semiquantitative reverse transcription (RT)-PCR and immunoblot analysis, we could again show that, during

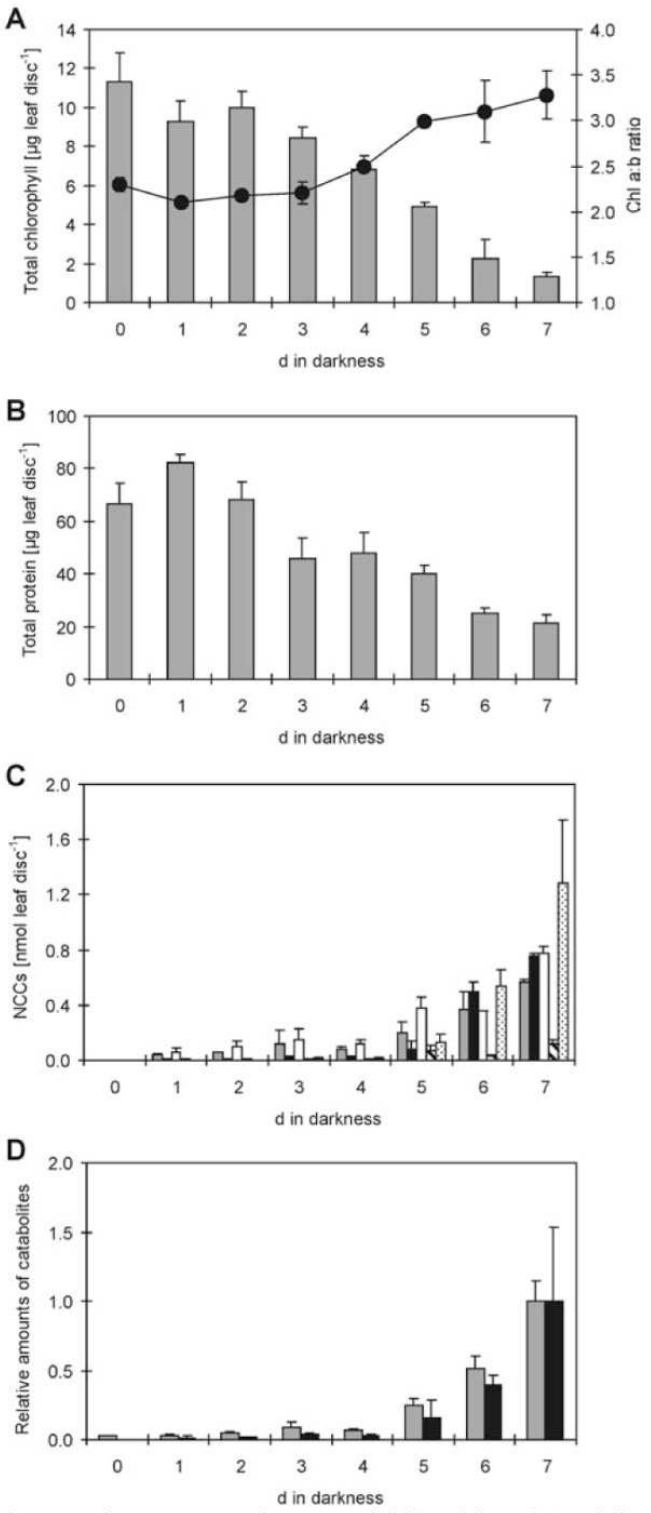

Figure 3. Characterization of protein and chl breakdown during dark-induced senescence of detached Arabidopsis Col-0 leaves. A, Degradation of chl (columns) and changes in the chl *a*/*b* ratio (line). B, Degradation of total proteins. C, Accumulation during senescence of five different NCCs (gray, *At*-NCC-1; black, *At*-NCC-2; white, *At*-NCC-3; hatched, *At*-NCC-4; dotted, *At*-NCC-5). D, Relative amounts of NCCs (gray) and FCCs (black) remain constant throughout the incubation time. Results of a single representative senescence experiment are shown. Data are means of three replicates. Error bars indicate SD.

induction of senescence, an increase of PAO activity (Hörtensteiner et al., 1995) correlates with increased PAO protein levels and *Pao* gene expression (data not shown).

In contrast to PAO, RCCR activities were almost constant during the course of detached leaf senescence (Fig. 4A) and correlated with RCCR levels and *Rccr* gene expression (Fig. 4, B and C). This indicates that RCCR is not regulated during leaf senescence.

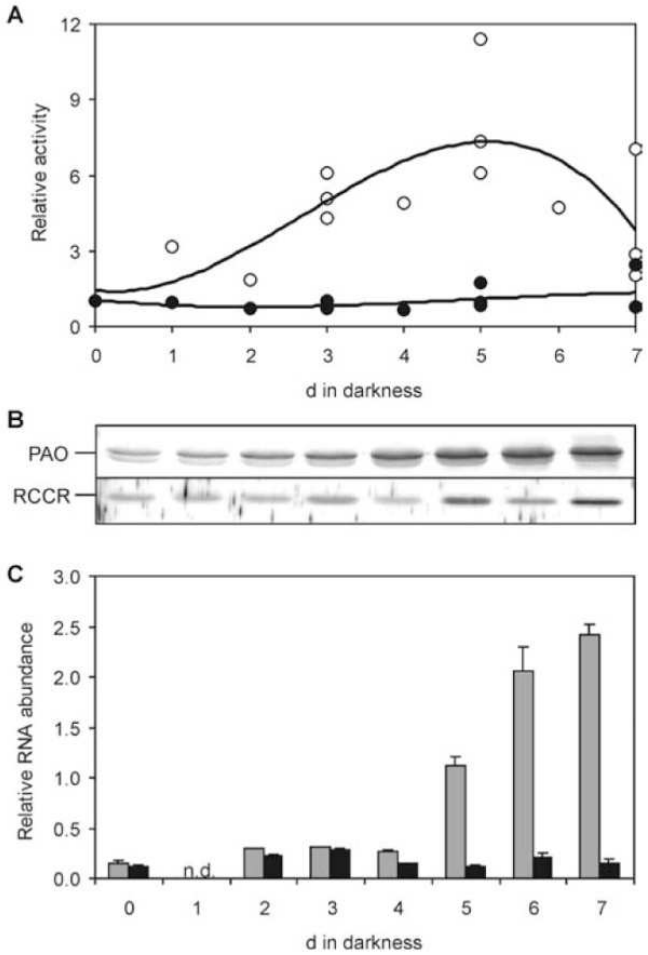

Figure 4. Analysis of PAO and RCCR activities (A), protein abundance (B), and gene expression (C) during dark-induced senescence of Arabidopsis leaves. A, For the determination of their activities, PAO and RCCR, respectively, were isolated from the tissues of interest and assessed in RFF-containing assays that were supplemented with purified His_6-AtRCCR (determination of PAO activity, white circles) and a standard preparation of PAO (determination of RCCR, black circles), respectively. Values are data from several independent experiments showing the great variability of PAO activity. B, Representative immunoblots of PAO and RCCR extracts used for measuring enzyme activities as shown in A. Gel loadings are based on equal amounts of fresh weight. Blots were labeled and developed as described in "Materials and Methods" using polyclonal antibodies against PAO and RCCR, respectively. C, RNA abundance of *Pao* (gray) and *Rccr* (black) was quantified by real-time RT-PCR and normalized to levels of mRNA encoding the actin 2 protein. Values are means of three replicates. Error bars indicate SD. n.d., Not determined.

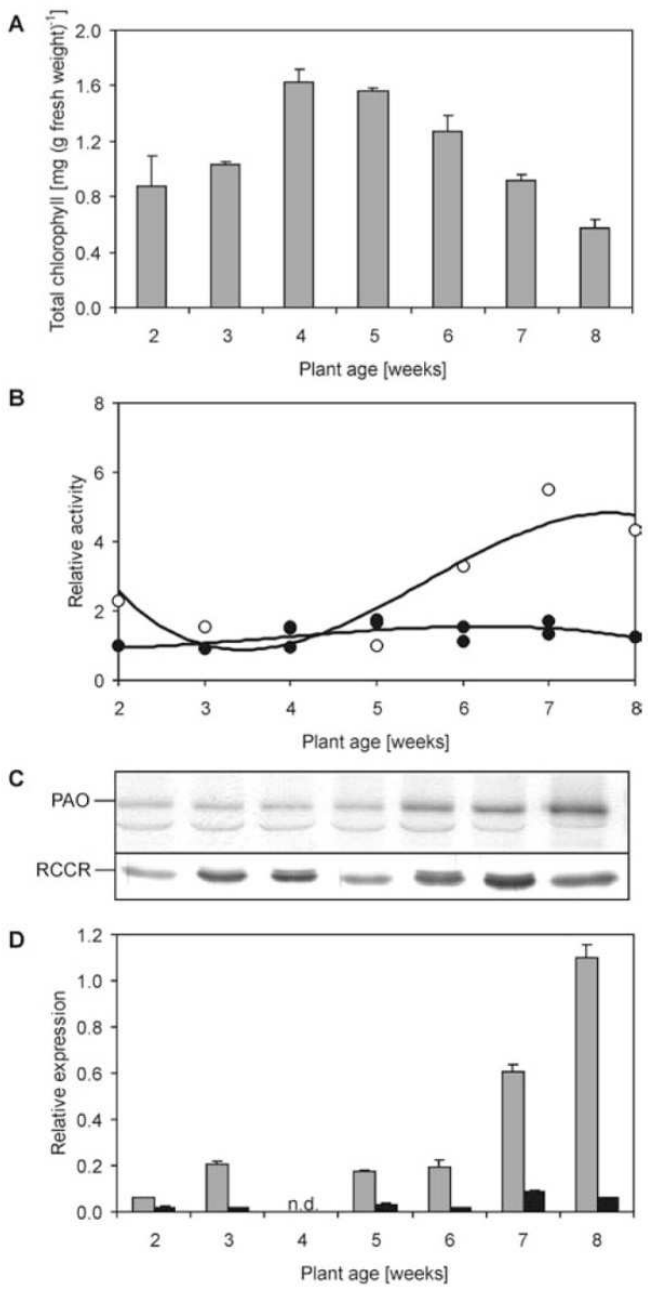

Figure 5. Analysis of chl content and characterization of PAO and RCCR during rosette development in Arabidopsis. Entire rosettes of plants grown under long-day conditions were harvested at the indicated times and analyzed for chl content (A), PAO and RCCR activities (B), protein abundance (C), and gene expression (D). A, Values are means of at least three independent samples. Error bars indicate SD. B, For the determination of their activities, PAO and RCCR, respectively, were isolated from the tissues of interest and assessed in RFF-containing assays that were supplemented with purified His_6-AtRCCR (determination of PAO activity, white circles) and a standard preparation of PAO (determination of RCCR, black circles), respectively. C, Representative immunoblots of PAO and RCCR extracts used for measuring enzyme activities as shown in B. Gel loadings are based on equal amounts of fresh weight. Blots were labeled and developed as described in "Materials and Methods" using polyclonal antibodies against PAO and RCCR, respectively. D, RNA abundance of *Pao* (gray) and *Rccr* (black) was quantified by real-time RT-PCR and normalized to levels of mRNA encoding the actin 2 protein. Values are means of three replicates. Error bars indicate SD. n.d., Not determined.

PAO and RCCR Are Present throughout Arabidopsis Leaf Development

The observation that PAO and RCCR are expressed and active in nonsenescent tissues (see above) allowed us to investigate their activities and expression levels during Arabidopsis rosette leaf development. For this, the entire rosettes of 2- to 8-week-old plants grown under long-day conditions were used. Chl concentrations were at maximum after 4 weeks and then declined (Fig. 5A). The age-dependent decrease in chl was accompanied by the occurrence of colorless chl catabolites starting from week 6, which coincided with yellowing of the oldest rosette leaves (data not shown). PAO activity was present already in young seedlings but started to increase after 5 weeks. Again, PAO activities, PAO protein levels, and *Pao* expression changed to comparable levels (Fig. 5, B–D). In contrast, expression and activity of RCCR was only weakly regulated.

Isolation and Characterization of a *Pao* T-DNA Insertional Mutant

PAO has been described as a key component of chl breakdown in barley (*Hordeum vulgare*), canola, and maize (Schellenberg et al., 1993; Hörtensteiner et al., 1995; Pružinská et al., 2003). To confirm this role in Arabidopsis, the T-DNA insertion mutant 111333, in which At3g44880 (*Pao*/*Acd1* gene) is tagged, was obtained from the Salk resource (Alonso et al., 2003). T-DNA insertion near the 3′ border of intron 5 of At3g44880 was confirmed by PCR and cloning of the left T-DNA border (Fig. 6A). After identification of homozygote lines, absence of PAO was confirmed by immunoblot analysis (Fig. 6B) and activity measurements (data not shown). This mutant was designated *pao1*. *pao1* developed a lesion-mimic phenotype on the leaves (Fig. 6D), which was similar to the phenotype described for several *acd1* mutants (Greenberg and Ausubel, 1993; Yang et al., 2004). The lesions of *pao1* occurred in a development-related, light-dependent fashion, coinciding with the initiation of leaf senescence in the wild type (Fig. 6, C and D). Premature cell death was also observed in *pao1* flowers (Fig. 6, E–H). In the mutant, petals and sepals started to disintegrate earlier than in the wild type, resulting in flowers that never fully opened. In addition, about 40% of seeds aborted at an early stage of development in *pao1* (Fig. 6J; Table II). These data, together with the finding that expression of *Pao* is rather high in flowers and siliques (Fig. 6K), indicate that, in addition to chl breakdown during senescence, PAO has an important function in flower and/or seed development in Arabidopsis. The data obtained for *pao1* were confirmed by constitutive silencing of *Pao* in Col-0 using an RNA interference strategy (data not shown).

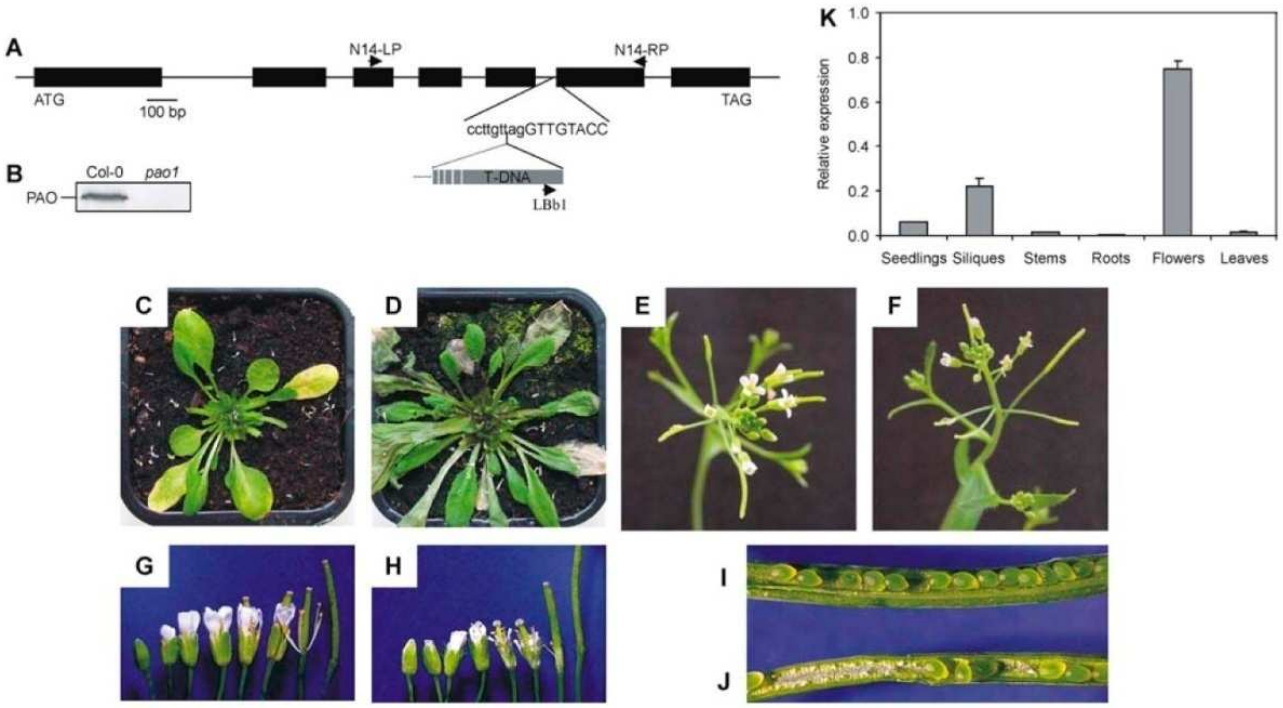

Figure 6. Characterization of the *pao1* mutant and tissue specificity of *Pao* expression. A, Gene structure of *Pao* (At3g44880) showing the insertion site of the T-DNA in the *pao1* mutant and the location of primers used to identify homozygous knockout lines. B, Immunoblot of protein extracts from senescent Col-0 and *pao1* leaves, labeled with anti-PAO monoclonal antibodies. C to J, Phenotype of *pao1* (D, F, H, and J) compared to Col-0 (C, E, G, and I). Plants were grown for 4 weeks under long-day conditions. C and D, *pao1* (D) exhibits a cell death phenotype, which correlates to senescence in Col-0 (C). Before taking pictures, inflorescences were removed. E and F, In contrast to Col-0 (E), flowers of *pao1* (F) do not fully open. G and H, Series of flowers at different stages of development. Sepals and petals senesce earlier in *pao1* (H) compared to Col-0 (G). I and J, Early seed abortion occurs in *pao1* (J) at a high ratio, but not in the wild type (I). For quantification, see Table II. K, RNA abundance of *Pao* in different tissues was quantified by real-time RT-PCR and normalized to levels of mRNA encoding the actin 2 protein. Values are means of three replicates. Error bars indicate SD.

Pheide *a* Is Responsible for the Cell Death Phenotype of *pao1*

To induce senescence without an interference of light, detached leaves were incubated in permanent darkness. Under these conditions, chl was largely retained in *pao1*, resulting in a stay-green phenotype (Fig. 7, A and B). The absence of PAO resulted in the accumulation of pheide *a* in a time-dependent manner (Fig. 7C). Pheide *a* content positively correlated with the light-dependent death reaction. Thus, cell death, as measured by ion leakage of leaf discs, was faster after longer dark incubation, i.e. at higher pheide *a* content (Fig. 7D). In contrast, leaf discs stayed intact in the wild type, where pheide *a* did not accumulate (Fig. 7, C and E). This indicates that pheide *a* is responsible for the cell death reaction observed in *pao1*.

DISCUSSION

The Pathway of Chl Breakdown in Arabidopsis

Chl catabolism is an integral process of leaf senescence and fruit ripening. The biochemistry of chl breakdown has been analyzed intensively during recent years, mainly in plant species other than Arabidopsis (Hörtensteiner et al., 1995; Wüthrich et al., 2000; Pružinská et al., 2003). One reason may be that, in Arabidopsis, leaf senescence is induced sequentially in individual leaves within the rosette rather than in the whole plant (Hensel et al., 1993). Thus, developmental senescence is difficult to control and incubation of entire plants in the dark has been shown to inhibit induction of senescence (Weaver and Amasino, 2001). Hence, much senescence-related work in Arabidopsis has been performed with either dark-incubated detached leaves or individually darkened attached leaves. These two systems were employed in this article in order to address chl breakdown in Arabidopsis.

Table II. *Seed development in Col-0 and pao1*

	Embryos per Silique	Aborted Embryos
		%
Col-0	31.40 ± 4.90	2.29 ± 3.52
pao1	28.94 ± 3.78	42.25 ± 28.14

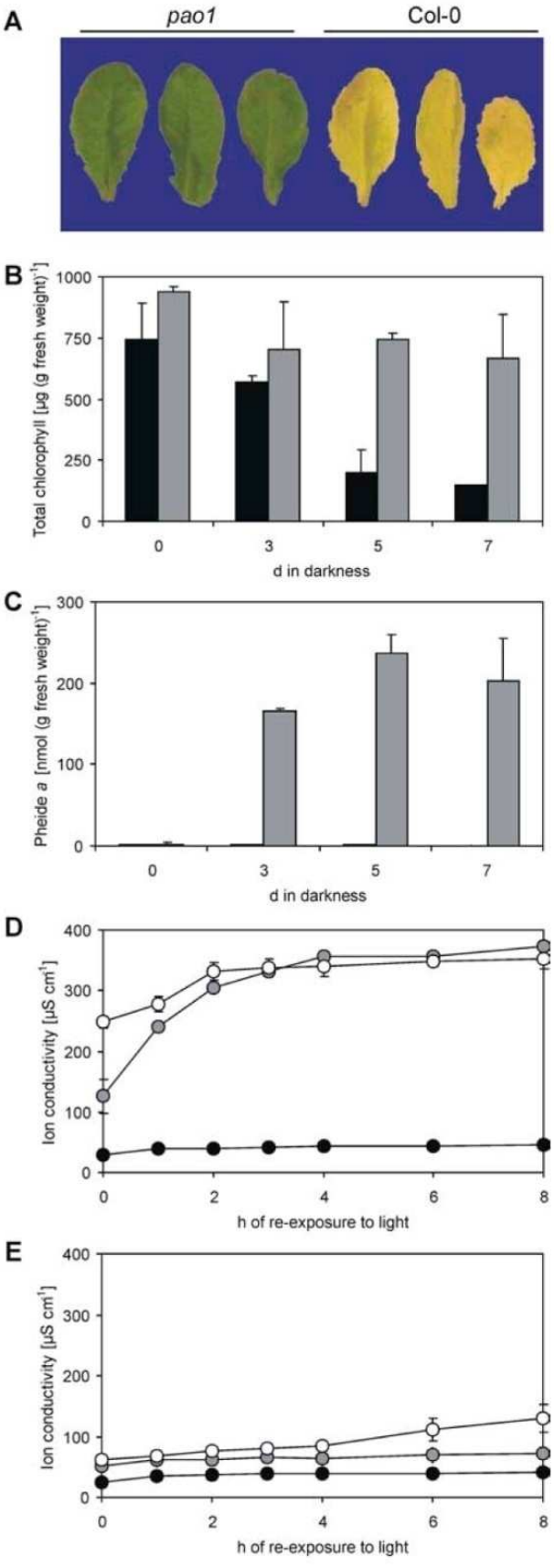

Independent of the type of senescence induction, chl was degraded to an identical set of colorless chl catabolites, indicating that there is one common pathway active in breaking down chl during senescence in Arabidopsis. In addition, the amounts of accumulating colorless catabolites roughly matched the amounts of degraded chl, indicating that, in Arabidopsis, as has been shown for canola (Ginsburg and Matile, 1993), degradation of chl exclusively occurs through the formation of FCCs (and subsequently NCCs) catalyzed by PAO/RCCR. A comparison of the structures of NCCs from canola and Arabidopsis uncovered similarities, but also major differences. Thus, structures of three of the five *At*-NCCs are identical to canola NCCs, but a malonylated NCC, the major catabolite in canola, is absent from Arabidopsis. Furthermore, two additional (new) NCCs are found in Arabidopsis, but are absent from canola. These findings indicate that the two closely related species contain different sets of chl catabolic enzymes that are responsible for the species-specific modifications of side chains present in NCCs.

In other plant species analyzed so far, NCCs, but not FCCs, have been identified as final chl catabolites (Curty and Engel, 1996; Mühlecker and Kräutler, 1996; Kräutler, 2003; Berghold et al., 2004). Thus, it was surprising to find rather large quantities of FCCs during chl breakdown in Arabidopsis. The conversion of FCCs to NCCs occurs after import into the vacuole due to the acidic vacuolar milieu (Oberhuber et al., 2003). A high FCC-to-NCC ratio (Fig. 3D) may be explained by a rather high vacuolar pH in Arabidopsis. Our data show that vacuolar pH values are similar in canola and Arabidopsis, thus excluding this possibility. Alternatively, catabolite transport at the tonoplast could be slower in Arabidopsis than in other species. Such transport has been shown to be a primary active process in barley (Hinder et al., 1996) and most probably involves members of the multidrug resistance-associated protein subfamily of ATP-binding cassette transporters (Lu et al., 1998; Tommasini et al., 1998). Vacuolar uptake experiments were performed with NCCs, but inhibition studies, together with data of FCC-to-NCC conversion at low pH, suggest that the true substrates for vacuolar import are FCCs (Hörtensteiner, 1999). Consequently, modifications that are present at different side groups of the tetrapyrrolic skeleton in Arabidopsis NCCs (Table I) most likely occur at the level of FCCs outside the vacuole. This hypothesis is supported by the identification in this study of two modified FCCs, *At*-FCC-1 and *At*-FCC-2

Figure 7. Characterization of chl breakdown in *pao1*. A, Detached *pao1* and Col-0 leaves after 5-d senescence in the dark. B, Degradation of chl in Col-0 (black) and *pao1* (gray). C, Accumulation of pheide *a* in response to dark incubation of Col-0 (black) and *pao1* (gray) leaves. D and E, Determination of ion leakage as a measure for cell death in *pao1* (D) and Col-0 (E) leaves. Before re-exposure to the light for up to 8 h, leaves were incubated in the dark for 0 (black circles), 3 (gray circles), or 5 (white circles) d. Results of a single representative experiment are shown. Data are means of three replicates. Error bars indicate SD.

(Fig. 2; Table I). Hence, Arabidopsis proves to be a suitable system to study the biochemical processes that are involved in the late steps of chl catabolism and are responsible for peripheral modifications of FCCs.

PAO Has a Key Role in Chl Breakdown

In contrast to chlorophyllase, where two genes have been identified in Arabidopsis (Tsuchiya et al., 1999), PAO and RCCR are single-copy genes. We have analyzed properties of these two proteins and their respective genes during leaf senescence. Our data indicate an important regulatory role for PAO, but not for RCCR. Thus, PAO activity, protein abundance, and *Pao* gene expression positively correlate with rates of chl breakdown (Figs. 4 and 5). In contrast, RCCR protein and RNA levels do not change significantly during development and senescence (Figs. 4 and 5; Mach et al., 2001). Regulation of PAO at the post-transcriptional level had been suggested from phosphatase treatments that inhibited PAO activity (M. Roca and S. Hörtensteiner, unpublished data; Pružinská et al., 2003). The results presented here show that such regulation would not necessarily be required to explain the observed senescence-related increase in PAO activity. In addition, we were unable to repeat the original phosphatase experiments in this work (data not shown). Thus, we conclude that regulation of PAO occurs at the transcriptional level.

The analysis of *pao1*, a knockout mutant in the *Pao* gene, further substantiates a key role for PAO during chl catabolism. In contrast to mutants in RCCR, which are still able to produce FCCs and NCCs (A. Pružinská and S. Hörtensteiner, unpublished data), absence of PAO completely inhibits chl breakdown at the level of pheide *a*. Hence, like in the stay-green mutant Bf 993 of *F. pratensis* and in an introgression mutant of *Lolium temulentum* (Roca et al., 2004), most pigment is retained as chl during dark-induced senescence in *pao1* (Fig. 7). In maize *lls1*, which is affected in the ortholog of Arabidopsis PAO, chl retention is accompanied by the retention of chl-binding proteins. This phenomenon has been observed in several instances of stay-green mutants that are affected in PAO activity (Hilditch et al., 1989; Bachmann et al., 1994; Pružinská et al., 2003). Together, these data indicate the existence of a feedback mechanism, which limits metabolism of chl in mutants that are unable to degrade chl beyond pheide *a*. Whether such a proposed mechanism would act on chlorophyllase, the first enzyme of chl breakdown, or on so-far unknown proteases that would be involved in the degradation of chl-binding proteins, remains to be shown. The strategy of plants to avoid extensive chl breakdown if the degradation pathway is blocked has its explanation in the phenotype observed in the *pao1* mutant. *pao1* shows a cell death phenotype in leaves and flowers, which is age and light dependent (Figs. 6 and 7). A lesion-mimic phenotype has also been described for other PAO mutants, such as *acd1* and *lls1* (Greenberg and Ausubel, 1993; Gray et al., 1997). Analysis of maize double mutants of *lls1* with *oil-yellow* or *iojap*, which have drastically reduced chl content, indicated that a chl-derived compound mediates cell death (Gray et al., 2002). Here we show that the cell death-promoting substance in *pao1* is pheide *a* (Fig. 7), which has been demonstrated to be a potent phototoxin (Jonker et al., 2002). Light absorption by pheide *a* is believed to cause the production of singlet oxygen, which in turn induces cell death. Such a singlet oxygen-triggered cell death reaction has been described in the *flu* mutant, where the disruption of feedback inhibition of chl biosynthesis causes the accumulation of photodynamic protochlorophyllide in the dark (Meskauskiene et al., 2001). In this system, the EXECUTER protein has been shown to be a (early) component of a cell death-signaling pathway (Wagner et al., 2004). In order to analyze whether cell death in *pao1* proceeds by the same pathway, we started to produce and analyze *pao1/ex1* double mutants.

MATERIALS AND METHODS

Plant Material and Senescence Induction

The Columbia (Col-0) ecotype of Arabidopsis (*Arabidopsis thaliana*) was used as the wild type. Seeds of the T-DNA insertion mutant SALK_111333 were obtained from the Nottingham Arabidopsis Stock Centre (Nottingham, UK). Presence of the T-DNA insertion within the *Pao* gene (At3g44880) in SALK_111333 was confirmed by sequencing the PCR product generated from genomic DNA with the gene-specific primer N14-RP (5′-GGCTCACCT-GACGCTTGGTTA-3′) and the T-DNA left border primer, LBb1 (5′-GCG-TGGACCGCTTGCTGCAAT-3′). Homozygous lines from the segregating population of SALK_111333 seeds were identified by PCR using primers LBb1, N14-RP, and N14-LP (5′-CGACGGTGACAATTCAAAGGG-3′). One of the homozygous lines was renamed *pao1* and used for further analysis.

Plants were grown on soil either in short-day (8/16 h) or long-day (16/8 h) growth rooms under fluorescent light of 60 to 120 μmol photons m^{-2} s^{-1} at 22°C. For senescence induction, leaves from 3- to 4-week-old (long-day) or 8-week-old (short-day) plants were excised and incubated in permanent darkness on wet filter paper for up to 7 d at ambient temperature. Alternatively, individual attached leaves were wrapped with aluminum foil.

Canola (*Brassica napus*) was grown on soil and senescence of cotyledons was induced by dark incubation of 10-d-old seedlings in the dark (Hörtensteiner et al., 1995).

Pao RNA Interference Plants

A full-length cDNA clone of *Pao* (pda07874) was obtained from the RIKEN Tsukuba Institute BioResourceCenter (Seki et al., 2002). Primer combinations R4XN (5′-GACCTCGAGCCATGGAATGTGCCAACCCCGTTC-3′)/R4K (5′-CCGGTACCTTGTGATGAGCAAAATC-3′) and R4B (5′-GATTTGGA-TCCGAATGTGCC-3′)/R4C (5′-CCATCGATGAGCAAAATCTATATGG-3′) were used to amplify by PCR two 480-bp fragments of *Pao*. Appropriate restriction sites linked to the primers enabled a two-step cloning of the PCR products in opposite directions into pHannibal (Wesley et al., 2001). After digestion with *Not*I, the RNA interference construct was introduced into *Not*I-restricted pGreen0029 (Hellens et al., 2000) to produce pGpao-c. Arabidopsis (Col-0) plants were transformed by the floral-dip method (Sidler et al., 1998). From the original 10 kanamycin-resistant T_1 plants that were analyzed for the accumulation of pheide *a* after senescence induction, two lines (IIIa and IIIb) were selected for further analysis.

Analysis of Chl and Chl Catabolites

Chl and Green Catabolites

Chl was isolated from leaf tissue by homogenization in liquid nitrogen and subsequent 3-fold extraction into 80% (v/v) acetone containing 1 μM KOH.

After centrifugation (2 min, 16,000*g*), supernatants were combined and chl concentrations were determined spectrophotometrically (Strain et al., 1971).

For extraction of green polar chl catabolites (pheide and chlorophyllide), leaf material (four to eight 1-cm leaf discs) was homogenized in liquid nitrogen and resuspended in 100 μL 0.5 M Tris-HCl, pH 8.0. After the addition of 400 μL acetone and centrifugation (2 min, 16,000*g*), the supernatant was analyzed by HPLC essentially as described (Langmeier et al., 1993). Pigments were identified by their absorption spectra and quantified using authentic standards (Ginsburg and Matile, 1993; Hörtensteiner et al., 1995).

Colorless Chl Catabolites

Colorless chl catabolites were extracted as described (Pružinská et al., 2003) and either directly or after concentration on a C18-SepPak cartridge (Waters; Mühlecker et al., 1997) analyzed by HPLC. The reversed-phase system consisted of a C18 Hypersil ODS column (250 × 4.6 mm; 5 μm; MZ-Analysentechnik), which was developed with a gradient (flow rate 0.5 mL min^{-1}) of solvent B (20% [v/v] 25 mM potassium phosphate buffer, pH 7.0, and 80% methanol) in solvent A (50 mM potassium phosphate, pH 7.0) as follows: 25% to 75% over 60 min, 75% to 100% over 5 min, and 100% solvent B for 5 min. Peak detection was with sequential monitoring using a System Gold 168 photodiode array detector (200–600 nm; Beckman Coulter) and a RF-10AXL fluorescence detector (excitation at 320 nm, emission at 450 nm; Shimadzu Corporation). Analysis of peaks was performed with a 32K workstation (Beckman Coulter). Chl catabolites were identified by their absorption (FCCs and NCCs; Hörtensteiner, 1999) and fluorescence (FCCs) properties. Peak areas of NCCs were quantified with a standard *Cj*-NCC-1 (Oberhuber et al., 2001) at defined concentrations (log $\varepsilon_{315\ nm}$ = 4.2; Kräutler et al., 1991).

MS

A Finnigan MAT 95-S mass spectrometer (Thermo Electron Corporation) in the positive-ion mode was employed. Settings for electrospray ionization (ESI)-MS are as follows: flow rate, 600 μL min^{-1}; spray voltage, 3.2 kV; solvent, methanol:water 1:1 (v/v); values are *m/z* (% relative intensity). For high-resolution fast atom bombardment (HR FAB)-MS, a cesium ion gun at 20 keV was employed; matrix, glycerin; values are *m/z* (measured versus calculated values).

At-NCC-1: ESI-MS, 815.3 (100, $[M + Na + H]^+$), 831.4 (90, $[M + K + H]^+$); HR FAB-MS, 793.328 ($[M + H]^+$; calc. 793.3291). *At*-NCC-2: ESI-MS, 669.2 (95, $[M + K + H]^+$), 707.2 (100, $[M + 2K + H]^+$). *At*-NCC-3: ESI-MS, 669.2 (100, $[M + K + H]^+$), 707.2 (30, $[M + 2K + H]^+$); HR FAB-MS, 631.280 ($[M + H]^+$; calc. 631.2762). *At*-NCC-4: ESI-MS, 845.4 (100, $[M + K + H]^+$), 883.1 (15, $[M + 2K + H]^+$). *At*-NCC-5: ESI-MS, 615.2 (20, $[M + H]^+$), 653.2 (100, $[M + K + H]^+$); HR FAB-MS, 615.283 ($[M + H]^+$; calc. 615.2813). *At*-FCC-1: ESI-MS, 625.2 (20, $[M + K + H\text{-}CO_2]^+$), 663.2 (100, $[M + 2K + H\text{-}CO_2]^+$). *At*-FCC-2: ESI-MS, 609.2 (100, $[M + K + H\text{-}CO_2]^+$), 615.3 (25, $[M + H]^+$), 653.3 (25, $[M + K + H]^+$). *At*-FCC-3: ESI-MS, 629.3 (50, $[M + H]^+$), 667.3 (100, $[M + K + H]^+$).

FCC-to-NCC Conversion

A sample of colorless chl catabolites extracted from senescent Col-0 leaves and concentrated on a C18-SepPak cartridge (see above) was acidified to pH 5.0 by the addition of 0.25 volumes of 0.2 M citrate buffer. After degassing, the mixture was incubated at ambient temperature in the dark. Samples were withdrawn and analyzed by HPLC as indicated in Figure 2E.

pH Determination

To measure the pH values of leaf extracts, leaves were homogenized in liquid nitrogen and defrosted. After filtration through miracloth (Calbiochem), extracts were diluted 4-fold and 10-fold, respectively, with MilliQ-water (Millipore) and the pH values were determined using a Knick pH meter (Escolab) equipped with an Orion 8102 Ross electrode (Cambridge Scientific Products).

cDNA Cloning of His_6-AtRCCR

Primers AtFOR1 (5′-GGGATCCATGGAAGACCACGACG-3′) and AtRCCR5 (5′-TTCTGCAGAGAACACCGAAAGCT-3′), with pGEM-AtRCCR as template (Wüthrich et al., 2000), were used to amplify a truncated fragment of Arabidopsis *Rccr* covering codons from Ser-40, the predicted cleavage site of the chloroplast transit peptide of AtRCCR, to the end of the protein. *Bam*HI and *Pst*I sites located within the primers were employed for in-frame ligation of this fragment to the His_6-tag of pQE30 (pQE-1.1). After confirming the fidelity of pQE-1.1 by sequencing, His_6-AtRCCR was expressed in *Escherichia coli* JM109 (Wüthrich et al., 2000).

RNA Isolation and Real-Time PCR

RNA was prepared using the Plant RNeasy kit (Qiagen). After DNA digestion with RQ1 RNase-free DNase (Promega), 1 μg of RNA was reverse transcribed using the RETROscript kit (Ambion). Quantitative PCR was performed in a LightCycler (Roche Diagnostics) using the QuantiTect SYBR Green PCR kit (Qiagen). Ten- to 100-fold dilutions of first-strand cDNA reaction mixes (corresponding to 0.3–3 ng of RNA) were employed in 20-μL reactions and were used to calculate the real-time PCR efficiency of each sample. The relative expression ratios of target genes (*Pao*, *Rccr*) were calculated in comparison to a reference gene (*Act2*; Kürsteiner et al., 2003). The following specific primers were used: *Act2* (forward, 5′-TGGAATCCACGAGACAACCTA-3′ and reverse, 5′-TTCTGTGAACGATTCCTGGAC-3′); *Pao* (*Acd1*; forward, 5′-ACGGCATGGTAAGAGTCAGC-3′ and reverse, 5′-AAACCAGCAAGAACCAGTCG-3′); and *Rccr* (*Acd2*; forward, 5′-ATCGCCTCCAATCACAACTC-3′ and reverse, 5′-TTAGCACAAGCGACTTGGAA-3′).

Protein Extraction and Immunoblot Analysis

His_6-AtRCCR and Total E. coli Proteins

For the isolation of proteins from *E. coli*, JM109 or JM109 expressing His_6-AtRCCR from pQE-1.1 were used. Soluble proteins were extracted and His_6-AtRCCR purified on a HiTrap chelating column (General Electric Healthcare) according to published procedures (Wüthrich et al., 2000).

Extraction of Soluble Plant Proteins

Proteins were extracted from Arabidopsis leaves and precipitated with ammonium sulfate according to published procedures (Rodoni et al., 1997; Wüthrich et al., 2000; Pružinská et al., 2003).

Extraction of PAO

PAO was isolated from canola or Arabidopsis chloroplast membranes by Triton X-100 solubilization according to a standard procedure (Hörtensteiner et al., 1995). Canola PAO was partially purified on EAH Sepharose 4B (General Electric Healthcare; Hörtensteiner et al., 1998). In contrast to canola, where typically at least 50 g of leaf tissue were used, extraction of PAO from Arabidopsis required downscaling of the above method and a minimum of 2 g of leaves was used for each extraction.

Immunoblot Analysis

After separation by SDS-PAGE, proteins were transferred to nitrocellulose membranes according to standard procedures. Proteins were labeled with antibodies against Arabidopsis RCCR (1:1,000; Wüthrich et al., 2000) or PAO (monoclonal, 1:500; polyclonal, 1:2,000; Gray et al., 2004), and thereafter with alkaline phosphatase-conjugated second antibodies, and visualized using bromochloroindolyl phosphate/nitroblue tetrazolium as substrate.

Protein Quantification

Protein content was measured according to Bradford (1976) using bovine serum albumin as standard.

Enzyme Assays

PAO and RCCR activities were assessed in different assays according to published procedures (Hörtensteiner et al., 1995; Wüthrich et al., 2000). Briefly,

assays (total volume of 50 μL) contained different combinations of PAO (equivalent to 0.5 g of tissue), *E. coli* (50 μg) protein extracts as a source of RFF, and purified His_6-AtRCCR (2.9 μg) or ammonium sulfate-precipitated proteins extracted from Col-0 (equivalent to 13.3 mg of leaf tissue) as a source of RCCR. The assays were supplemented with 0.5 mM pheide *a* (Hörtensteiner et al., 1995), 10 μg ferredoxin (Fd), and a Fd-reducing system consisting of 2 mM Glc-6-P, 1 mM NADPH, 50 milliunits of Glc-6-P dehydrogenase, and 5 milliunits of Fd-$NADP^+$ oxidoreductase. After 1-h incubation at 25°C, reactions were terminated by the addition of 80 μL methanol. Formation of pFCC-1 was followed by reversed-phase HPLC with 36% (v/v) 50 mM potassium phosphate buffer, pH 7.0, in methanol as solvent. Activities are determined as integrated fluorescence units (320/450 nm) of pFCC-1 (FU_{pFCC}). Identity of pFCC-1 was confirmed with authentic standards (Kräutler et al., 1997; Mühlecker et al., 1997, 2000).

Ion Leakage

For ion conductivity analysis, senescence was induced in detached leaves that were incubated in the dark for up to 7 d. Eight leaf discs (1-cm diameter) were excised and transferred to 6-well cell culture plates (Sarstedt) containing 5 mL water. After reexposure to light (150 μmol photons m^{-2} s^{-1}) for up to 8 h, ion leakage from the leaf discs as a measure of cellular damage was determined by measuring the conductivity of the solution with a CDH-42 conductivity meter (Omega Engineering).

ACKNOWLEDGMENTS

We thank John Gray, University of Toledo, for the generous gift of antibodies against PAO/ACD1, and Esther Tapernoux-Lüthi, University of Zurich, for her help in sequencing.

Received May 24, 2005; revised June 16, 2005; accepted June 20, 2005; published August 19, 2005.

LITERATURE CITED

Alonso JM, Stepanova AN, Leisse TJ, Kim CJ, Chen H, Shinn P, Stevenson DK, Zimmermann J, Barajas P, Cheuk R, et al (2003) Genome-wide insertional mutagenesis of *Arabidopsis thaliana*. Science **301:** 653–657

Bachmann A, Fernández-López J, Ginsburg S, Thomas H, Bouwcamp JC, Solomos T, Matile P (1994) *Stay-green* genotypes of *Phaseolus vulgaris* L.: chloroplast proteins and chlorophyll catabolites during foliar senescence. New Phytol **126:** 593–600

Barthe P, Vaillant V (1993) Changes in the buffering capacity of cell sap in senescing rose petals. Sci Hortic **54:** 165–174

Berghold J, Breuker K, Oberhuber M, Hörtensteiner S, Kräutler B (2002) Chlorophyll breakdown in spinach: on the structure of five nonfluorescent chlorophyll catabolites. Photosynth Res **74:** 109–119

Berghold J, Eichmüller C, Hörtensteiner S, Kräutler B (2004) Chlorophyll breakdown in tobacco: on the structure of two nonfluorescent chlorophyll catabolites. Chem Biodivers **1:** 657–668

Bradford MM (1976) A rapid and sensitive method for the quantitation of microgram quantities of protein utilizing the principle of protein-dye binding. Anal Biochem **72:** 248–254

Curty C, Engel N (1996) Detection, isolation and structure elucidation of a chlorophyll *a* catabolite from autumnal senescent leaves of *Cercidiphyllum japonicum*. Phytochemistry **42:** 1531–1536

Eckhardt U, Grimm B, Hörtensteiner S (2004) Recent advances in chlorophyll biosynthesis and breakdown in higher plants. Plant Mol Biol **56:** 1–14

Ginsburg S, Matile P (1993) Identification of catabolites of chlorophyll porphyrin in senescent rape cotyledons. Plant Physiol **102:** 521–527

Ginsburg S, Schellenberg M, Matile P (1994) Cleavage of chlorophyll-porphyrin. Requirement for reduced ferredoxin and oxygen. Plant Physiol **105:** 545–554

Gray J, Close PS, Briggs SP, Johal GS (1997) A novel suppressor of cell death in plants encoded by the *Lls1* gene of maize. Cell **89:** 25–31

Gray J, Janick-Bruckner D, Bruckner B, Close PS, Johal GS (2002) Light-dependent death of maize *lls1* cells is mediated by mature chloroplasts. Plant Physiol **130:** 1894–1907

Gray J, Wardzala E, Yang M, Reinbothe S, Haller S, Pauli F (2004) A small family of LLS1-related non-heme oxygenases in plants with an origin amongst oxygenic photosynthesizers. Plant Mol Biol **54:** 39–54

Greenberg JT, Ausubel FM (1993) *Arabidopsis* mutants compromised for the control of cellular damage during pathogenesis and aging. Plant J **4:** 327–341

Greenberg JT, Guo A, Klessig DF, Ausubel FM (1994) Programmed cell death in plants: a pathogen-triggered response activated coordinately with multiple defense functions. Cell **77:** 551–563

Hellens R, Edwards EA, Leyland NR, Bean S, Mullineaux PM (2000) pGreen: a versatile and flexible binary Ti vector for *Agrobacterium*-mediated plant transformation. Plant Mol Biol **42:** 819–832

Hensel LL, Grbic V, Baumgarten DA, Bleecker AB (1993) Developmental and age-related processes that influence the longevity and senescence of photosynthetic tissues in Arabidopsis. Plant Cell **5:** 553–564

Hilditch PI, Thomas H, Thomas BJ, Rogers LJ (1989) Leaf senescence in a non-yellowing mutant of *Festuca pratensis*: proteins of photosystem II. Planta **177:** 265–272

Hinder B, Schellenberg M, Rodoni S, Ginsburg S, Vogt E, Martinoia E, Matile P, Hörtensteiner S (1996) How plants dispose of chlorophyll catabolites. Directly energized uptake of tetrapyrrolic breakdown products into isolated vacuoles. J Biol Chem **271:** 27233–27236

Hörtensteiner S (1999) Chlorophyll breakdown in higher plants and algae. Cell Mol Life Sci **56:** 330–347

Hörtensteiner S, Kräutler B (2000) Chlorophyll breakdown in oilseed rape. Photosynth Res **64:** 137–146

Hörtensteiner S, Vicentini F, Matile P (1995) Chlorophyll breakdown in senescent cotyledons of rape, *Brassica napus* L.: enzymatic cleavage of phaeophorbide *a in vitro*. New Phytol **129:** 237–246

Hörtensteiner S, Wüthrich KL, Matile P, Ongania K-H, Kräutler B (1998) The key step in chlorophyll breakdown in higher plants. Cleavage of pheophorbide *a* macrocycle by a monooxygenase. J Biol Chem **273:** 15335–15339

Jonker JW, Buitelaar M, Wagenaar E, van der Valk MA, Scheffer GL, Scheper RJ, Plösch T, Kuipers F, Oude Elferink RPJ, Rosing H, et al (2002) The breast cancer resistance protein protects against a major chlorophyll-derived dietary phototoxin and protoporphyria. Proc Natl Acad Sci USA **99:** 15649–15654

Kräutler B (2003) Chlorophyll breakdown and chlorophyll catabolites. *In* KM Kadish, KM Smith, R Guilard, eds, The Porphyrin Handbook, Vol 13. Elsevier Science Publishing, New York, pp 183–209

Kräutler B, Jaun B, Bortlik K-H, Schellenberg M, Matile P (1991) On the enigma of chlorophyll degradation: the constitution of a secoporphinoid catabolite. Angew Chem Int Ed Engl **30:** 1315–1318

Kräutler B, Mühlecker W, Anderl M, Gerlach B (1997) Breakdown of chlorophyll: partial synthesis of a putative intermediary catabolite. Helv Chim Acta **80:** 1355–1362

Kürsteiner O, Dupuis I, Kuhlemeier C (2003) The *pyruvate decarboxylase1* gene of Arabidopsis is required during anoxia but not other environmental stresses. Plant Physiol **132:** 968–978

Langmeier M, Ginsburg S, Matile P (1993) Chlorophyll breakdown in senescent leaves: demonstration of Mg-dechelatase activity. Physiol Plant **89:** 347–353

Lu Y-P, Li Z-S, Drozdowicz Y-M, Hörtensteiner S, Martinoia E, Rea PA (1998) AtMRP2, an Arabidopsis ATP binding cassette transporter able to transport glutathione *S*-conjugates and chlorophyll catabolites: functional comparisons with AtMRP1. Plant Cell **10:** 267–282

Mach JM, Castillo AR, Hoogstraten R, Greenberg JT (2001) The Arabidopsis-accelerated cell death gene ACD2 encodes red chlorophyll catabolite reductase and suppresses the spread of disease symptoms. Proc Natl Acad Sci USA **98:** 771–776

Matile P, Ginsburg S, Schellenberg M, Thomas H (1988) Catabolites of chlorophyll in senescing barley leaves are localized in the vacuoles of mesophyll cells. Proc Natl Acad Sci USA **85:** 9529–9532

Matile P, Hörtensteiner S, Thomas H (1999) Chlorophyll degradation. Annu Rev Plant Physiol Plant Mol Biol **50:** 67–95

Meskauskiene R, Nater M, Goslings D, Kessler F, op den Camp R, Apel K (2001) FLU: a negative regulator of chlorophyll biosynthesis in *Arabidopsis thaliana*. Proc Natl Acad Sci USA **98:** 12826–12831

Miao Y, Laun T, Zimmermann P, Zentgraf U (2004) Targets of the WRKY53 transcription factor and its role during leaf senescence in Arabidopsis. Plant Mol Biol **55:** 853–867

Mühlecker W, Kräutler B (1996) Breakdown of chlorophyll: constitution of nonfluorescing chlorophyll-catabolites from senescent cotyledons of the dicot rape. Plant Physiol Biochem **34:** 61–75

Mühlecker W, Kräutler B, Moser D, Matile P, Hörtensteiner S (2000) Breakdown of chlorophyll: a fluorescent chlorophyll catabolite from sweet pepper (*Capsicum annuum*). Helv Chim Acta **83:** 278–286

Mühlecker W, Ongania K-H, Kräutler B, Matile P, Hörtensteiner S (1997) Tracking down chlorophyll breakdown in plants: elucidation of the constitution of a ''fluorescent'' chlorophyll catabolite. Angew Chem Int Ed Engl **36:** 401–404

Oberhuber M, Berghold J, Breuker K, Hörtensteiner S, Kräutler B (2003) Breakdown of chlorophyll: a nonenzymatic reaction accounts for the formation of the colorless ''nonfluorescent'' chlorophyll catabolites. Proc Natl Acad Sci USA **100:** 6910–6915

Oberhuber M, Berghold J, Mühlecker W, Hörtensteiner S, Kräutler B (2001) Chlorophyll breakdown - on a nonfluorescent chlorophyll catabolite from spinach. Helv Chim Acta **84:** 2615–2627

Pružinská A, Anders I, Tanner G, Roca M, Hörtensteiner S (2003) Chlorophyll breakdown: pheophorbide *a* oxygenase is a Rieske-type iron-sulfur protein, encoded by the *accelerated cell death 1* gene. Proc Natl Acad Sci USA **100:** 15259–15264

Roca M, James J, Pružinská A, Hörtensteiner S, Thomas H, Ougham H (2004) Analysis of the chlorophyll catabolism pathway in leaves of an introgression senescence mutant of *Lolium temulentum*. Phytochemistry **65:** 1231–1238

Rodoni S, Mühlecker W, Anderl M, Kräutler B, Moser D, Thomas H, Matile P, Hörtensteiner S (1997) Chlorophyll breakdown in senescent chloroplasts. Cleavage of pheophorbide *a* in two enzymic steps. Plant Physiol **115:** 669–676

Schellenberg M, Matile P, Thomas H (1993) Production of a presumptive chlorophyll catabolite *in vitro*: requirement for reduced ferredoxin. Planta **191:** 417–420

Seki M, Narusaka M, Kamiya A, Ishida J, Satou M, Sakurai T, Nakajima M, Enju A, Akiyama K, Oono Y, et al (2002) Functional annotation of a full-length Arabidopsis cDNA collection. Science **296:** 141–145

Sidler M, Hassa P, Hasan S, Ringli C, Dudler R (1998) Involvement of an ABC transporter in a developmental pathway regulating hypocotyl cell elongation in the light. Plant Cell **10:** 1623–1636

Spassieva S, Hille J (2002) A lesion mimic phenotype in tomato obtained by isolating and silencing an *Lls1* homologue. Plant Sci **162:** 543–549

Strain HH, Cope BT, Svec WA (1971) Analytical procedures for the isolation, identification, estimation and investigation of the chlorophylls. Methods Enzymol **23:** 452–476

Tanaka R, Hirashima M, Satoh S, Tanaka A (2003) The *Arabidopsis-accelerated cell death* gene *ACD1* is involved in oxygenation of pheophorbide *a*: inhibition of pheophorbide *a* oxygenase activity does not lead to the ''stay-green'' phenotype in *Arabidopsis*. Plant Cell Physiol **44:** 1266–1274

Tommasini R, Vogt E, Fromenteau M, Hörtensteiner S, Matile P, Amrhein N, Martinoia E (1998) An ABC transporter of *Arabidopsis thaliana* has both glutathione-conjugate and chlorophyll catabolite transport activity. Plant J **13:** 773–780

Tsuchiya T, Ohta H, Okawa K, Iwamatsu A, Shimada H, Masuda T, Takamiya K (1999) Cloning of chlorophyllase, the key enzyme in chlorophyll degradation: finding of a lipase motif and the induction by methyl jasmonate. Proc Natl Acad Sci USA **96:** 15362–15367

Vicentini F, Hörtensteiner S, Schellenberg M, Thomas H, Matile P (1995) Chlorophyll breakdown in senescent leaves: identification of the biochemical lesion in a *stay-green* genotype of *Festuca pratensis* Huds. New Phytol **129:** 247–252

Wagner D, Przybyla D, op den Camp R, Kim C, Landgraf F, Lee KP, Würsch M, Laloi C, Nater M, Hideg E, et al (2004) The genetic basis of singlet oxygen-induced stress responses of *Arabidopsis thaliana*. Science **306:** 1183–1185

Weaver LM, Amasino RM (2001) Senescence is induced in individually darkened Arabidopsis leaves, but inhibited in whole darkened plants. Plant Physiol **127:** 876–886

Wesley SV, Helliwell CA, Smith NA, Wang M, Rouse DT, Liu Q, Gooding PS, Singh SP, Abbot D, Stoutjesdijk PA, et al (2001) Construct design for efficient, effective and high-throughput gene silencing in plants. Plant J **27:** 581–590

Wüthrich KL, Bovet L, Hunziker PE, Donnison IS, Hörtensteiner S (2000) Molecular cloning, functional expression and characterisation of RCC reductase involved in chlorophyll catabolism. Plant J **21:** 189–198

Yang M, Wardzala E, Johal GS, Gray J (2004) The wound-inducible *Lls1* gene from maize is an orthologue of the *Arabidopsis Acd1* gene, and the LLS1 protein is present in non-photosynthstic tissues. Plant Mol Biol **54:** 175–191

Yao N, Eisfelder BJ, Marvin J, Greenberg JT (2004) The mitochondrion—an organelle commonly involved in programmed cell death in *Arabidopsis thaliana*. Plant J **40:** 596–610

10. *In vivo* participation of red chlorophyll catabolite reductase in chlorophyll breakdown

Adriana Pruzinska, Iwona Anders, Sylvain Aubry, Nicole Schenk, Esther Tapernoux-Lüthi, Thomas Müller, Bernhard Kräutler, and Stefan Hörtensteiner

Reprinted from: *The Plant Cell* (2007) 19, 369-387

This paper appeared in the context of discussion about the biochemical involvement of RCCR in the degradation of chl. We show that RCCR is unequivocally involved in the reduction of RCC to pFCC, and provide some more data characterizing RCCR mutant phenotype and a hypothetical PAO/RCCR interaction. This study provides *in vivo* confirmation of the involvement of RCCR in the chl degradation pathway.

This article is published in *The Plant Cell* Online, *The Plant Cell* Preview Section, which publishes manuscripts accepted for publication after they have been edited and the authors have corrected proofs, but before the final, complete issue is published online. Early posting of articles reduces normal time to publication by several weeks.

In Vivo Participation of Red Chlorophyll Catabolite Reductase in Chlorophyll Breakdown [W]

Adriana Pružinská,[a,1,2] Iwona Anders,[a,1] Sylvain Aubry,[a] Nicole Schenk,[a] Esther Tapernoux-Lüthi,[b] Thomas Müller,[c] Bernhard Kräutler,[c] and Stefan Hörtensteiner[a,3]

[a] Institute of Plant Sciences, University of Bern, CH-3013 Bern, Switzerland
[b] Institute of Plant Biology, University of Zürich, CH-8008 Zürich, Switzerland
[c] Institute of Organic Chemistry and Center of Molecular Biosciences, Leopold-Franzens-University Innsbruck, A-6020 Innsbruck, Austria

A central reaction of chlorophyll breakdown, porphyrin ring opening of pheophorbide *a* to the primary fluorescent chlorophyll catabolite (pFCC), requires pheophorbide *a* oxygenase (PAO) and red chlorophyll catabolite reductase (RCCR), with red chlorophyll catabolite (RCC) as a presumably PAO-bound intermediate. In subsequent steps, pFCC is converted to different fluorescent chlorophyll catabolites (FCCs) and nonfluorescent chlorophyll catabolites (NCCs). Here, we show that RCCR-deficient *Arabidopsis thaliana* accumulates RCC and three RCC-like pigments during senescence, as well as FCCs and NCCs. We also show that the stereospecificity of *Arabidopsis* RCCR is defined by a small protein domain and can be reversed by a single Phe-to-Val exchange. Exploiting this feature, we prove the in vivo participation of RCCR in chlorophyll breakdown. After complementation of RCCR mutants with RCCRs exhibiting alternative specificities, patterns of chlorophyll catabolites followed the specificity of complementing RCCRs. Light-dependent leaf cell death observed in different RCCR-deficient lines strictly correlated with the accumulation of RCCs and the release of singlet oxygen, and PAO induction preceded lesion formation. These findings suggest that RCCR absence causes leaf cell death as a result of the accumulation of photodynamic RCC. We conclude that RCCR (together with PAO) is required for the detoxification of chlorophyll catabolites and discuss the biochemical role(s) for this enzyme.

INTRODUCTION

Senescence is the final stage of leaf development, which, except for some cases in which the regreening of yellow, senescent leaves has been reported (Thomas et al., 2003), is followed by the death of the whole leaf. Among different biochemical and physiological processes, chlorophyll degradation is integrally associated with leaf senescence and, as the most obvious sign of senescence, is widely used for senescence quantification. Chlorophyll is degraded in a pathway that is probably active in all higher plant species (Kräutler and Matile, 1999; Pružinská et al., 2003; Gray et al., 2004) and that leads to the formation of linear tetrapyrrolic breakdown products (nonfluorescent chlorophyll catabolites [NCCs]) that are deposited in the vacuoles of senescing cells.

The chlorophyll breakdown pathway has well been established in recent years (for reviews, see Kräutler, 2002; Eckhardt et al., 2004; Hörtensteiner, 2006; Kräutler and Hörtensteiner, 2006). It starts with the successive removal of phytol and magnesium by chlorophyllase (Takamiya et al., 2000) and magnesium-chelating substance (Suzuki and Shioi, 2002), respectively, followed by the conversion of pheophorbide (pheide) *a* to primary fluorescent chlorophyll catabolite (pFCC) (Mühlecker et al., 1997). The latter conversion has been attributed to the action of two enzymes, pheophorbide *a* oxygenase (PAO) and red chlorophyll catabolite reductase (RCCR) (Hörtensteiner et al., 1995; Rodoni et al., 1997), with red chlorophyll catabolite (RCC) occurring as an intermediate, but recent data suggest the involvement of an additional protein RCC forming factor (RFF), which together with PAO is required for RCC formation (Pružinská et al., 2005). pFCC is modified at several peripheral side positions by common or species-specific reactions, thus producing a species-specific set of modified FCCs. Finally, a primary active transport system (Hinder et al., 1996) at the tonoplast imports these FCCs into the vacuole, where they spontaneously convert to the respective NCCs, catalyzed by the acidic vacuolar pH (Oberhuber et al., 2003). In contrast with many other species, in which FCC conversion is fast and, hence, FCCs are barely detectable in senescence, *Arabidopsis thaliana* accumulates substantial amounts of both NCCs and FCCs in senescent leaves (Pružinská et al., 2005).

RCCR exhibits an intriguing specificity toward reduction of the C20/C1 double bond of RCC (see Figure 5C below). Thus, depending on the plant species used as a source of RCCR in an in vitro assay, together with PAO and pheide *a* as substrate, one of two possible C1 epimers of pFCC, pFCC-1 (Mühlecker et al., 1997) or pFCC-2 (= 1-*epi*-pFCC) (Mühlecker et al., 2000), is

[1] These authors contributed equally to this work.
[2] Current address: Department of Biochemistry, Umeå University, S-901 87 Umeå, Sweden.
[3] To whom correspondence should be addressed. E-mail shorten@ips.unibe.ch; fax 41-31-631-49-42.
The author responsible for distribution of materials integral to the findings presented in this article in accordance with the policy described in the Instructions for Authors (www.plantcell.org) is: Stefan Hörtensteiner (shorten@ips.unibe.ch).
[W] Online version contains Web-only data.
www.plantcell.org/cgi/doi/10.1105/tpc.106.044404

formed (Hörtensteiner et al., 2000b). RCCR is a soluble protein identical to *Arabidopsis* Accelerated Cell Death2 (ACD2). RCCR/ACD2 localizes to chloroplasts, as judged by chloroplast import experiments (Wüthrich et al., 2000), but in young seedlings and in response to stress it partially locates to mitochondria as well (Mach et al., 2001; Yao et al., 2004; Yao and Greenberg, 2006). *RCCR/ACD2* is a single-copy gene in *Arabidopsis* (At4g37000) that is constitutively expressed; accordingly, RCCR activity is rather constant during all phases of leaf development (Pružinská et al., 2005). By contrast, PAO gene expression, protein abundance, and activity are highly upregulated during senescence (Pružinská et al., 2005). Furthermore, PAO has been shown to be located at the plastid inner envelope membrane (Pružinská et al., 2003; Kleffmann et al., 2004). Despite these differences in localization and patterns of activity, biochemical evidence suggests a close interaction between PAO and RCCR during catalysis. Thus, the intermediate RCC formed by the activity of PAO (and RFF) does not accumulate in vivo, and in vitro, RCC occurs only in trace amounts in respective assays (Rodoni et al., 1997). RCC seems to be efficiently reduced to pFCC by RCCR without release from PAO, which has been interpreted as a kind of metabolic channeling (Hörtensteiner, 1999). Further evidence for the PAO–RCCR interaction has been derived from the finding that in vitro the stereospecificity of RCCR is lost in the absence of PAO (Rodoni et al., 1997; Wüthrich et al., 2000).

Formation of pFCC from pheide *a* is the critical transformation in chlorophyll breakdown because it is responsible for the loss of green pigment, thus rendering potentially phototoxic chlorophyll into a colorless catabolite. The importance of this conversion is demonstrated by the analysis of PAO mutants, such as *lls1* of maize (*Zea mays*) and *acd1* and *pao1* of *Arabidopsis* (Greenberg and Ausubel, 1993; Gray et al., 1997; Pružinská et al., 2003, 2005). They belong to the class of propagation lesion-mimic mutants (Lorrain et al., 2003) and exhibit a light- and age-dependent cell death phenotype in leaves and flowers. ACD1, which is identical to PAO, has been suggested to be active in a signaling pathway that prevents programmed cell death (PCD) (Greenberg and Ausubel, 1993). On the other hand, the close correlation between cell death and the accumulation of pheide *a* in *lls1* and *pao1* (Pružinská et al., 2003, 2005), together with the identification of lesion-mimic mutants that are defective in different steps of chlorophyll biosynthesis (Hu et al., 1998; Ishikawa et al., 2001; Meskauskiene et al., 2001), suggest that in certain cases phenotypically observed cell death is not programmed but is the result of a nonnatural accumulation of photoreactive chlorophyll metabolites (Pružinská et al., 2003). Mutants in RCCR/ACD2, such as *acd2-2* (Greenberg et al., 1994), have not been analyzed to date with respect to chlorophyll breakdown, although RCC accumulation has been assumed to trigger cell death in the mutant (Mach et al., 2001). Recently, a role for ACD2 in the reduction of PCD triggered by *Pseudomonas syringae* and protoporphyrin IX treatment was suggested (Yao et al., 2004; Yao and Greenberg, 2006). Using an *Arabidopsis* protoplast system, stress-related targeting of portions of the cellular ACD2 pool to mitochondria and involvement of the early mitochondrial oxidative burst in PCD were demonstrated. It was discussed that ACD2 might play a role in the detoxification of porphyrin-related molecules, such as protoporphyrin IX. Furthermore, ACD2 prevented cell death in root protoplasts, indicating that chlorophyll degradation is not obligatory for the anti-PCD function of ACD2 (Yao and Greenberg, 2006). Together, these data questioned a prevailing role of RCCR/ACD2 in the degradation of chlorophyll in vivo.

The intentions of this work were to elucidate whether RCCR participates in chlorophyll breakdown in vivo and to analyze whether the accumulation of RCC triggers cell death in RCCR mutants. To this end, we characterized different RCCR-deficient lines in relation to chlorophyll breakdown. We show that during dark-induced leaf senescence, RCC and RCC-like compounds accumulate in these mutants. Leaf cell death only occurred in lines that also accumulate RCCs and correlated to the light-dependent release of singlet oxygen. Surprisingly, FCCs and NCCs (i.e., downstream products of the site of RCCR action) were found in the mutants as well, further questioning the role of RCCR in chlorophyll breakdown. By molecular engineering of RCCRs, we show that a single amino acid exchange alters the C1 stereospecificity of At-RCCR from pFCC-1 to the formation of pFCC-2 (1-*epi*-pFCC). Exploiting this feature, *acd2-2* was functionally complemented with *Arabidopsis* RCCRs exhibiting alternative C1 stereospecificities. Thereby, the pattern of FCCs and NCCs accumulating during senescence followed the specificity of the complementing RCCR, thus demonstrating the in vivo participation of RCCR in chlorophyll breakdown. Finally, we further substantiate earlier evidence of a biochemical interaction between RCCR and PAO. We conclude that RCCR is truly involved in chlorophyll breakdown, although its proposed catalytic role in the RCC-to-pFCC reduction remains to be confirmed. Furthermore, we propose that RCC accumulation is a major inducer of cell death observed in RCCR-depleted leaves.

RESULTS

Isolation of *Arabidopsis* T-DNA Insertional Mutants and Transgenic Lines Deficient in RCCR

In this study, *Arabidopsis* lines of different accessions that are defective in RCCR activity (Figure 1C; see Supplemental Figure 1B online) were used. *acd2-2*, obtained by ethyl methanesulfonate mutagenesis of ecotype Columbia (Col-0), contains a G-to-A mutation at the 3′ splice site of the single intron of At4g37000 (*RCCR/ACD2* gene) (Figure 1A) (Mach et al., 2001). Attempts to overexpress RCCR in the C24 background produced several lines, including line 68-13-1, in which constitutive expression of At-RCCR from pSC4 (Figure 1B) caused silencing of the endogenous *RCCR* gene of *Arabidopsis*. Silencing of *RCCR* in 68-13-1 was confirmed by RCCR activity measurements (Figure 1C) and immunoblot analysis (Figure 1D) and was stable for several generations. In contrast with *acd2-2*, in which neither RCCR protein nor activity could be detected, traces of RCCR proteins were present in 68-13-1, and 2.1% of the respective wild type activity was detected.

acd2-2 and 68-13-1 exhibited a lesion-mimic phenotype in a development-related manner, which was first visible in the older leaves of the rosette (Figure 1E) (Mach et al., 2001). In contrast with the PAO mutant, *pao1*, in which lesion formation coincided with the initiation of leaf senescence (Pružinská et al., 2005),

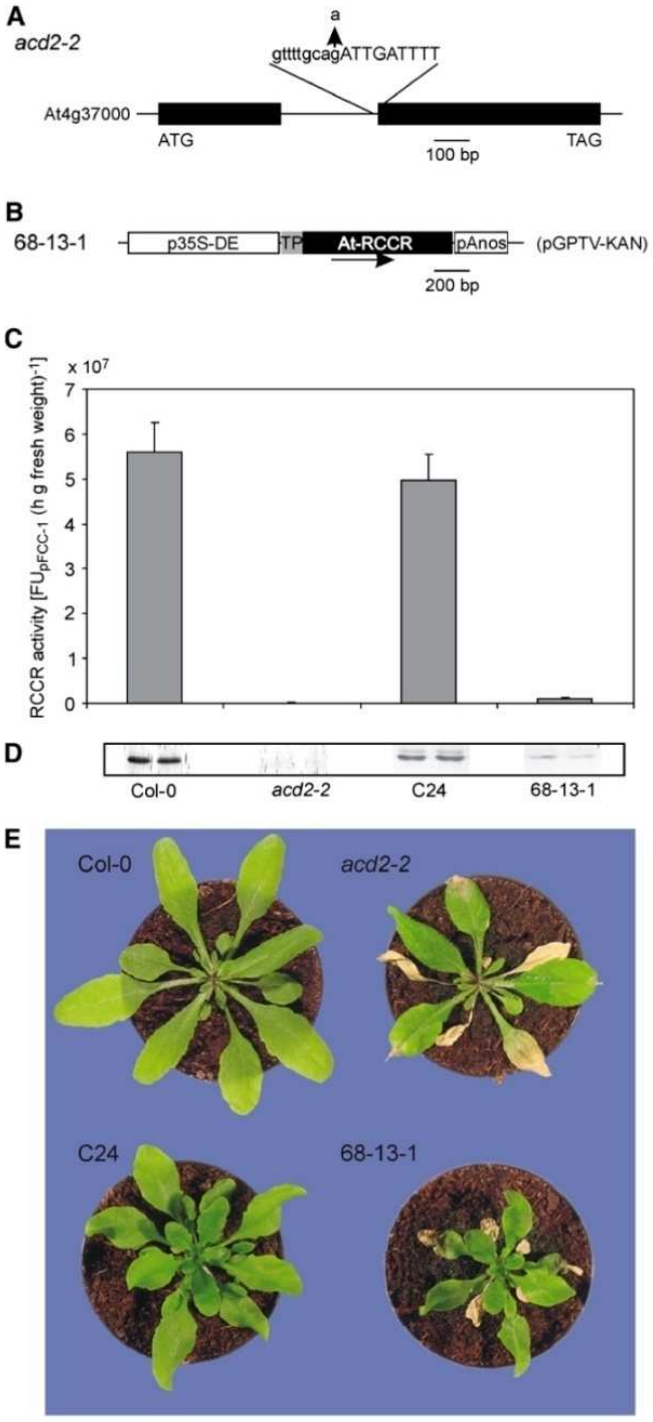

Figure 1. Characterization of RCCR-Deficient Lines in *Arabidopsis*.

(A) Gene structure of *RCCR* (At4g37000) showing the point mutation of the 3′ splice site of the intron present in *acd2-2*.

(B) At-RCCR gene construct used for the production of the cosuppressing line 68-13-1. TP, chloroplast transit peptide of *Arabidopsis* RCCR.

(C) RCCR activity in RCCR-deficient lines and respective wild types. RCCR was extracted from mature green leaves, and activities were determined in coupled PAO/RFF/RCCR assays. Values are means of three independent determinations. Error bars indicate SD.

(D) Immunoblot of RCCR extracts used to measure enzyme activities as shown in **(C)**. For each line, two independent extracts were analyzed. Gel loadings are based on equal amounts of fresh weight.

(E) Cell-death phenotype of RCCR-deficient lines. Plants were grown under long-day conditions (100 $\mu mol \cdot m^{-2} \cdot s^{-1}$) for 3 weeks.

lesions in *acd2-2* and 68-13-1 already occurred at presenescent stages. Premature flower senescence and early seed abortion had been observed in *pao1* (Pružinská et al., 2005). However, flower and seed development were not affected in the RCCR mutants (data not shown).

In addition to these lines, a T-DNA insertion line, *acd2-9*, was isolated by screening the Arabidopsis Knockout Facility (Wassilewskija [Ws] background) at the University of Wisconsin (Krysan et al., 1999). T-DNA insertion before the third codon of At4g37000 was confirmed by PCR and by cloning of the left T-DNA border (see Supplemental Figure 1A online). Although RCCR activity was largely lost (see Supplemental Figure 1B online), *acd2-9* did not show cell death symptoms, nor was the senescence behavior affected (see Supplemental Figures 1C and 1D online). Yet, constitutive silencing of *RCCR* expression in Ws using an RNA interference strategy resulted in RCCR-deficient lines that exhibited symptoms of cell death, but compared with the respective silencing in Col-0, lesions developed only at later stages of plant development (see Supplemental Figures 1E and 1F online). The differences between *acd2-9* and silencing lines in the development of premature cell death were confirmed both at the seedling stage and in mature leaves (see Supplemental Figures 1G and 1H online). In addition, analysis of chlorophyll catabolites (see below for details on the analyses of chlorophyll catabolites) further corroborated these differences: patterns of nongreen chlorophyll catabolites were identical in *acd2-9* and Ws but were altered significantly in the silencing lines (see Supplemental Figure 2 online). The observed differences in these lines were difficult to explain, so we decided to focus our further studies on *acd2-2* and 68-13-1.

Dark-Induced Senescence of RCCR Mutants Does Not Result in a Stay-Green Phenotype

To analyze the senescence behavior of the different RCCR mutants, detached leaves were incubated in permanent darkness. Under these conditions, lesions did not occur, confirming earlier data showing that light is required for lesion formation in *acd2* mutants (Greenberg et al., 1994; Mach et al., 2001; Yao et al., 2004). Senescence progression in the wild-type lines was evident by a progressive yellowing of leaves during dark treatment. *acd2-2* and 68-13-1 differed from their respective wild types by a faint red-orange coloration of the leaves after 5 to 7 d. Extraction into methanol, which does not extract protein-bound chlorophyll, caused a red coloration, indicating that red pigment(s) accumulated during the course of dark-induced senescence in *acd2-2* and 68-13-1 (Figure 2A, insets). Red coloration of extracts was not detectable during natural senescence, or within the lesions of *acd2-2* or 68-13-1, but red pigments accumulated when individual attached leaves were covered with aluminum foil to induce senescence (data not shown).

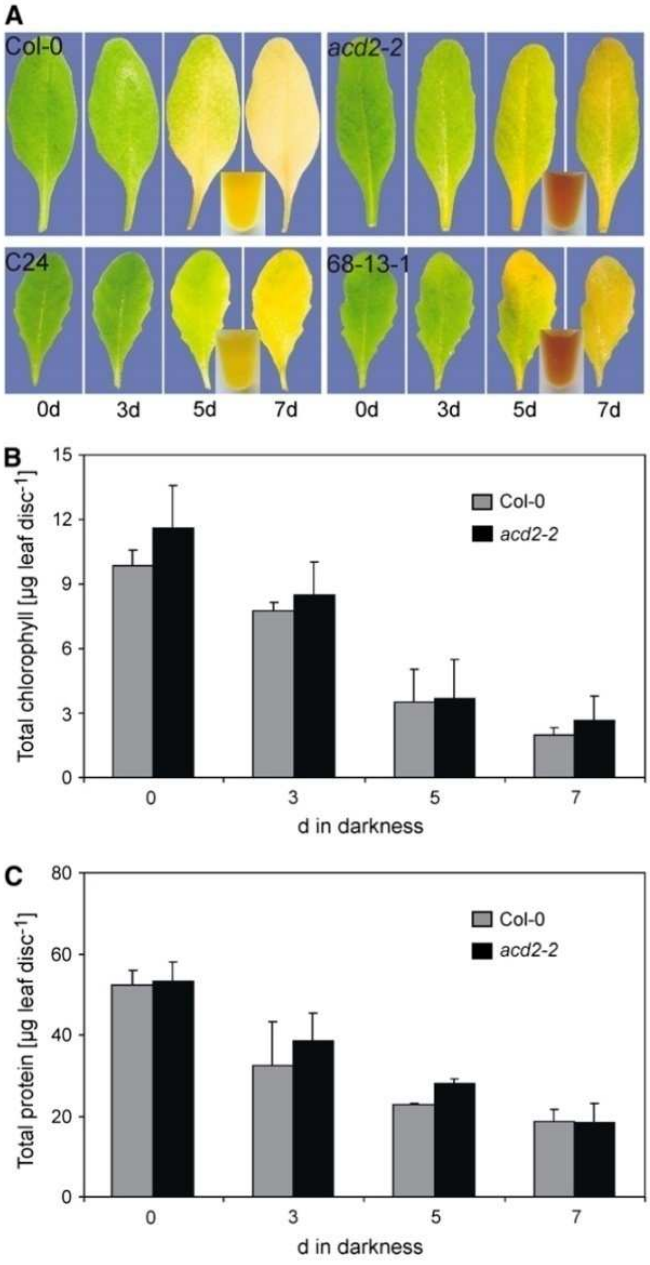

Figure 2. Senescence of Detached, Dark-Incubated Leaves of RCCR-Deficient Lines.

(A) Phenotypes of individual detached leaves of *acd2-2* and 68-13-1 and corresponding wild types after incubation in the dark for 0, 3, 5 and 7 d. Note the orange-red coloration in *acd2-2* and 68-13-1 leaves after 5 to 7 d. Insets, methanolic extracts of leaves after 7 d in the dark indicate the accumulation of red pigments in *acd2-2* and 68-13-1.

(B) Degradation of chlorophyll in Col-0 (gray bars) and *acd2-2* (black bars) during the course of detached leaf senescence. Data are means of a single representative experiment with three replicates. Error bars indicate SD.

(C) Degradation of total proteins in Col-0 (gray bars) and *acd2-2* (black bars) during the course of detached leaf senescence. Data are means of a single representative experiment with three replicates. Error bars indicate SD.

During the course of dark-induced senescence, chlorophyll and protein contents decreased to similar extents in both the mutants and their respective wild types. Figures 2B and 2C depict these data for *acd2-2* and Col-0, and similar results were obtained for the C24 and 68-13-1 plants (data not shown). Thus, absence of RCCR did not cause a stay-green phenotype in the dark, unlike *pao1*, in which chlorophyll was largely retained during dark-induced senescence (Pružinská et al., 2005).

RCCR Mutants Accumulate RCC and RCC-Like Pigments during Chlorophyll Breakdown

It seemed possible that the red color observed in senescent leaf extracts of *acd2-2* and 68-13-1 (Figure 2) was caused by the accumulation of RCC, the substrate of RCCR. To analyze this in more detail, extracts from leaves after 5 d of dark-induced senescence were analyzed by reverse-phase HPLC. An identical set of previously characterized FCCs and NCCs (Pružinská et al., 2005; Müller et al., 2006) were identified in the different wild-type lines, but surprisingly, several FCCs and NCCs were also present in the RCCR-deficient lines (see Figure 5 below). In addition to the rather polar FCCs and NCCs, a total of four less polar fractions exhibiting a typical ultraviolet/visible (UV/Vis) spectrum of RCCs (Kräutler, 2003) were detected in *acd2-2* and 68-13-1 but not in the wild-type lines (Figure 3A). Following an established nomenclature for colorless chlorophyll catabolites (Ginsburg and Matile, 1993), these four peaks were tentatively named At-RCC-1 through At-RCC-4 (see Figure 5 below and Table 1 for tentative structures of RCCs). By comparison with authentic RCC standards (Figure 3A) (Kräutler et al., 1997) and using mass spectrometry (MS; see Methods for MS data), At-RCC-3 and At-RCC-4 were identified as the primary cleavage product of pheide *a*, RCC, and an isomer, respectively. As RCC has been shown to isomerize readily at $C13^2$ in aqueous solution (Kräutler et al., 1997), At-RCC-4 may be assumed to have the structure of the $C13^2$ epimer of At-RCC-3. At-RCC-1 comigrated with a major polar red pigment accumulating in the medium of degreened *Chlorella protothecoides* cultures (Figure 3A). Mass analysis indicated that it represents the $C13^2$-demethylated form of RCC (Table 1). By the same means, At-RCC-2 was characterized as another modified RCC, as the decarboxylation product of At-RCC-1 (Engel et al., 1991). In analogy with the accumulation of modified FCCs and NCCs during senescence (Pružinská et al., 2005; Müller et al., 2006), At-RCC-1 would be the result of a hydrolyzing enzymatic activity and At-RCC-2 would represent its chemical decarboxylation product.

In the wild type, FCCs are believed to be exported from senescing chloroplasts and modified before they are disposed of into the vacuole, where tautomerization to the respective NCCs is catalyzed by the acidic vacuolar milieu (Oberhuber et al., 2003). To analyze the subcellular localization of RCCs in RCCR mutants, protoplasts were isolated from *acd2-2* leaves after 4 d of dark-induced senescence. By ultracentrifugation, protoplasts were subfractionated into evacuolated protoplasts and vacuoplasts (Hörtensteiner et al., 1992, 1994). The purity of fractions was analyzed photographically and by immunoblot analysis using antibodies against proteins specific for different subcellular

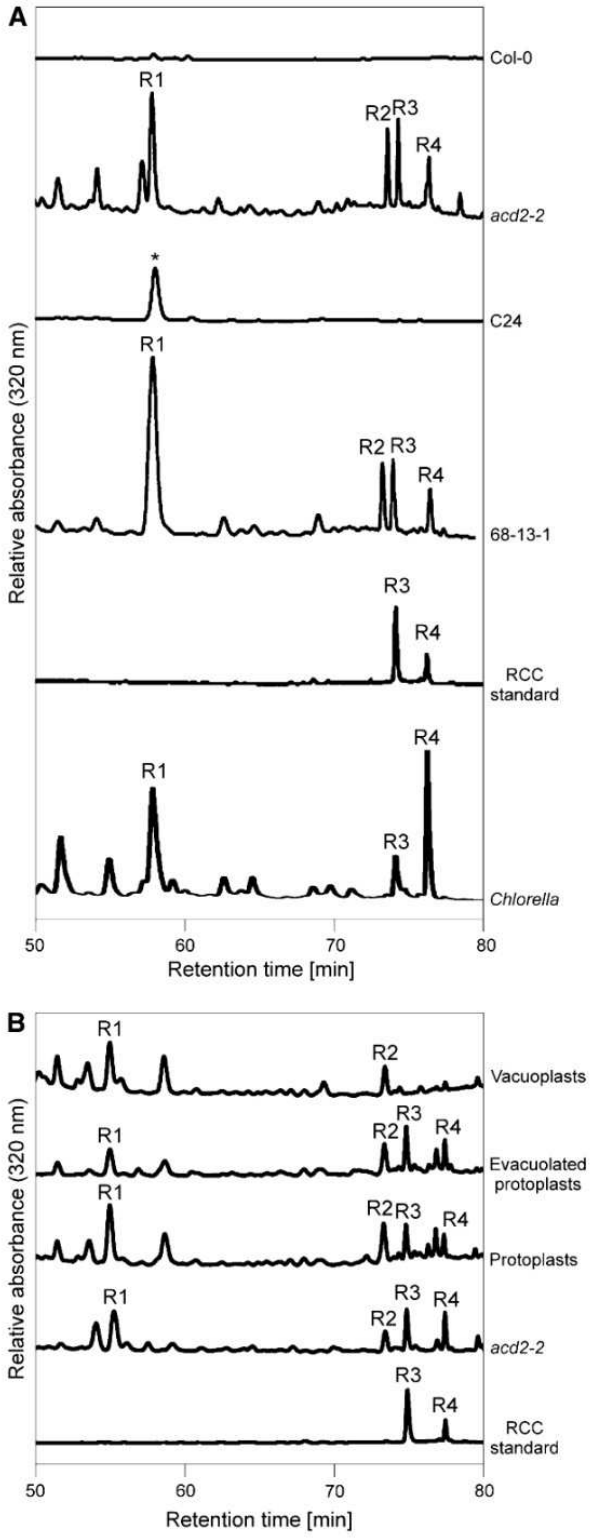

Figure 3. RCCR-Deficient Lines Accumulate RCC and RCC-Like Compounds.

(A) Partial HPLC traces (A_{320}) of senescent leaf extracts. Detached leaves of the indicated lines were dark-incubated for 5 d. RCC and RCC-like compounds (R1 to R4) were identified by their characteristic spectra (Hörtensteiner, 1999) and by comparison with a RCC standard (Kräutler et al., 1997) and RCC-containing *Chlorella protothecoides* extracts (Engel et al., 1996). For further identification and characterization of R1 to R4, see Table 1. In the C24 spectrum, the asterisk indicates an unknown peak with a retention time similar to that of R1 that does not have a RCC spectrum.

(B) Subcellular localization of RCCs in *acd2-2*. Partial HPLC traces (A_{320}) of extracts from senescent *acd2-2* leaves and from protoplasts, evacuolated protoplasts, and isolated vacuoplasts. A RCC standard was analyzed as a control.

compartments (see Supplemental Figure 3 online). Whereas large fractions of the plastids were recovered in evacuolated protoplasts, they were devoid of vacuoles. By contrast, vacuoplasts (vacuoles surrounded by plasmalemma) did not contain plastids or mitochondria. These fractions were analyzed by HPLC for the presence of RCCs (Figure 3B). In protoplasts and evacuolated protoplasts, all four RCCs, At-RCC-1 to At-RCC-4, were present in significant and similar quantities compared with an *acd2-2* leaf extract. At-RCC-3 and At-RCC-4, on the other hand, were largely absent from the vacuoplast fraction.

Cell Death in RCCR Mutant Leaves Correlates with the Accumulation of RCCs and the Induction of PAO

As shown in Figures 2A and 3, RCC and RCC-like compounds accumulated during senescence in *acd2-2* and 68-13-1. This finding indicated that the occurrence of RCCs correlated with the formation of leaf lesions in respective lines. To investigate this interconnection in more detail, either detached leaves of *acd2-2* (data not shown) or attached leaves that were individually covered with aluminum foil were incubated in the dark before ion leakage from leaf discs was determined as a measure of cell death. RCC content increased during the incubation period (Figure 4A) and positively correlated with a light-dependent cell death reaction (Figure 4C). Thus, cell death was faster after longer dark treatment (i.e., at higher concentrations of RCCs). By contrast, Col-0 exhibited only some weak tissue leakage toward the end of the senescence period (Figure 4B). Similar results were obtained for 68-13-1 (data not shown). Preliminary experiments indicate that lesion formation can also be induced by infiltration of leaf discs with RCC-containing extracts of *C. prototheocoides* cultures. Under these conditions, fast cell death occurred in *acd2-2* in a light- and concentration-dependent manner, but Col-0 leaf discs also exhibited a cell death reaction at high RCC concentrations (A. Pružinská and S. Hörtensteiner, unpublished data).

The positive correlation between the accumulation of RCCs and cell death implied that these photodynamic compounds could trigger lesion formation in leaves, probably through singlet oxygen production, as has been demonstrated in the protochlorophyllide-dependent cell death reaction of the *Arabidopsis flu* mutant (op den Camp et al., 2003). Furthermore, RCCs are chemically similar to phycobilins, which have been shown to produce singlet oxygen upon irradiation (Zhang et al., 2000). Release of singlet oxygen was tested in vivo by measuring the

Table 1. Identification of RCCs, FCCs, and NCCs Occurring during Chlorophyll Breakdown in *acd2-2* and Complemented Lines

Peak[a]	Name	R_2[b]	R_3[b]	Identification[c]	Reference
R1	At-RCC-1	H	COOH	s, c, m	This work
R2	At-RCC-2[d]	H	—	s, m	Engel et al. (1991); this work
R3	At-RCC-3	H	$COOCH_3$	s, c, m	Kräutler et al. (1997); this work
R4	At-RCC-4[e]	H	$COOCH_3$	s, c, m	This work
N1	At-NCC-1	*O*-glucosyl	COOH	s, c, m	Mühlecker and Kräutler (1996); Pružinská et al. (2005); this work
N1′	C1-*epi*-At-NCC-1[f]	*O*-glucosyl	COOH	s	This work
N2	At-NCC-2	OH	COOH	s, c, m[h]	Mühlecker and Kräutler (1996); Pružinská et al. (2005); Müller et al. (2006); this work
N2′	C1-*epi*-At-NCC-2[f]	OH	COOH	s, m[h]	This work
N3	At-NCC-3[g]	H	COOH	s, c, m[h]	Pružinská et al. (2005); this work
N3′	C1-*epi*-At-NCC-3[f,g]	H	$COOCH_3$	s, m[h]	This work
N5	At-NCC-5	H	COOH	s, c, m	Pružinská et al. (2005); Müller et al. (2006); this work
N5′	C1-*epi*-At-NCC-5[f]	H	COOH	s, m	This work
F2	At-FCC-2	H	COOH	s, c, f	Pružinská et al. (2005); this work
F2′	C1-*epi*-At-FCC-2[f]	H	COOH	s, f	This work
F3	At-FCC-3 (= pFCC-1)	H	$COOCH_3$	s, c, f	Mühlecker et al. (1997); Pružinská et al. (2005); this work
F4	At-FCC-4 (= pFCC-2)	H	$COOCH_3$	s, c, f	Mühlecker et al. (2000); this work

[a] Peak labels as depicted in Figures 3, 5, and 7.
[b] R_2 and R_3 indicate residues at the $C8^2$ and $C13^2$ side positions, respectively, of RCCs, FCCs, and NCCs, as shown in Figure 5C.
[c] Peak identification by UV/Vis spectra(s) (Hörtensteiner, 1999) and cochromatography with authentic standards (c), fluorescence (f), and mass spectrometry (m).
[d] In At-RCC-2, the $C13^2$ methoxycarbonyl residue is absent.
[e] At-RCC-4 is an isomer of At-RCC-3 (see text).
[f] Tentative stereochemical assignment.
[g] In At-NCC-3, a hydroxyl group is attached to C7 (Müller et al., 2006).
[h] The molecular masses determined do not allow an assignment to one of the four structural isomers N2, N2′, N3, and N3′ (see Methods).

fluorescence quenching of dansyl-2,2,5,5,-tetramethyl-2,5-dehydro-*1H*-pyrrole (DanePy) (Hideg et al., 1998; Kálai et al., 1998). DanePy fluorescence decreased rapidly after light exposure of dark-incubated *acd2-2* leaves but not in wild type leaves or in mutants before senescence induction (Figure 4D).

In contrast with *pao1*, in which pheide *a* accumulated in the necrotic tissue (Pružinská et al., 2005), RCCs could not be detected within *acd2-2* lesions of light-grown plants, probably because of the RCC's instability in light (data not shown). The formation of RCC requires the activity of PAO; therefore, we investigated whether the amount of PAO correlates with lesion formation in *acd2-2*. Leaves of similar age but with different severity of cell death were collected, and PAO abundance was estimated by immunoblot analysis (Figure 4E). In all samples exhibiting lesions, PAO was more abundant than in phenotypically healthy leaves. In addition, in leaves that just started to develop small lesions at the tip, a gradient of PAO could be observed. In contrast with the leaf base (i.e., the region most distant from the lesions), PAO abundance was increased within the area of lesions but also in the phenotypically still healthy middle region of the leaves (Figure 4E). Thus, the occurrence of lesions correlated with PAO abundance. Furthermore, the results suggested that before the development of visible lesions, PAO levels are increased, likely causing increased amounts of RCC in respective areas. These results are in agreement with the observation that, unlike in *pao1*, pheide *a* did not accumulate in healthy or necrotic tissues of RCCR-depleted lines (data not shown), thus excluding the possibility of pheide *a* being a trigger of cell death in the mutants.

RCCR-Deficient Lines Accumulate NCCs and FCCs

Five NCCs (At-NCC-1 to At-NCC-5) and three FCCs (At-FCC-1 to At-FCC-3) have been identified during chlorophyll breakdown in *Arabidopsis* (Pružinská et al., 2005). To our surprise, At-NCC-1, At-NCC-3, At-NCC-5, At-FCC-2, and At-FCC-3 (pFCC-1) were detected in HPLC runs of senescent leaf extracts of *acd2-2* (Figures 5A and 5B). The identity of chlorophyll catabolites was confirmed by HPLC-MS analysis (see Methods for MS data) and/or chromatography with authentic standards (Table 1). Further analysis indicated the presence in *acd2-2* of C1 stereoisomers of certain catabolites (Table 1). Thus, in addition to pFCC-1, its C1 stereoisomer, pFCC-2, was present as well (Figure 5B). Furthermore, a NCC with an identical mass but slightly different retention time accompanied At-NCC-5 (arrow in Figure 5A) and was tentatively named C1-*epi*-At-NCC-5 (N5′) (see Supplemental Figure 2C online). The same observation was also made for At-NCC-3 and At-FCC-2, in which double peaks were observed (arrows in Figures 5A and 5B), which suggested the presence of respective NCC and FCC isomers (N3′ and F2′), but to date their identity has not been unambiguously confirmed (Table 1; see Methods for MS data). Identical results were obtained with 68-13-1 (data not shown). These results suggest a reduction of RCC in the absence of RCCR. RCC-to-pFCC reduction in *acd2-2* was accompanied by a loss in stereospecificity, indicating that a stereounselective reduction by unknown mechanisms had occurred in the mutant.

During the course of dark-induced senescence, NCCs and FCCs accumulated progressively in Col-0, whereas in *acd2-2*,

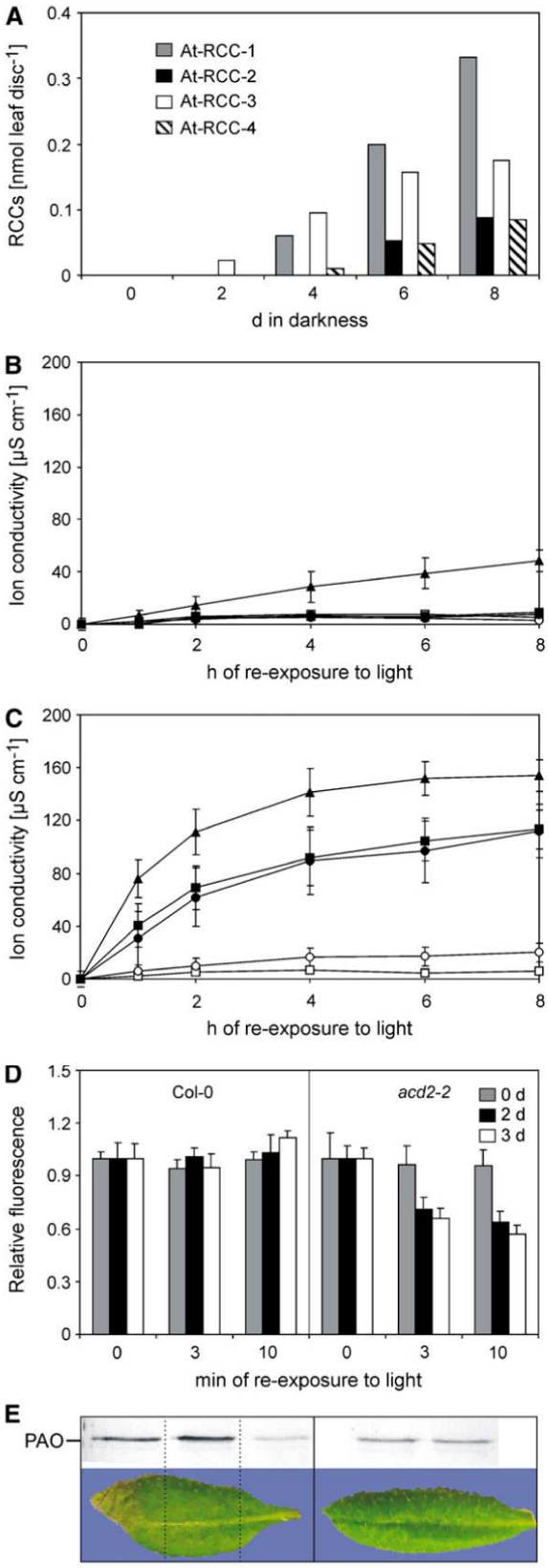

Figure 4. Cell Death of *acd2-2* and Induction of PAO Correlate with the Accumulation of RCCs.

FCCs remained almost constant (Figure 5D). RCCs accounted for nearly 50% of the catabolites found in *acd2-2* after 7 d, but the total amount of tetrapyrrolic catabolites was similar to that in the wild type (Figure 5E).

Exchange of a Single Amino Acid Changes the Stereospecificity of At-RCCR

RCCR exhibits an intriguing stereospecificity toward the reduction of the C20/C1 double bond of RCC; thus, depending on the source of the enzyme, one of two pFCC isomers, pFCC-1 or pFCC-2, is formed, indicating the presence of two types of RCCRs (type-1 and type-2 RCCR, respectively) (Hörtensteiner et al., 2000b; Wüthrich et al., 2000). Screening the GenBank/EMBL data libraries for the presence of RCCR sequences revealed deduced proteins or protein fragments from >20 species of different taxa within angiosperms, gymnosperms, and mosses (see Supplemental Figure 4A online), but RCCR-like sequences were not readily identifiable from the available genomes of photosynthetic prokaryotes and *Chlamydomonas reinhardtii* (data not shown). Figure 6A shows an alignment of At-RCCR with selected RCCRs from different species. The sequences were obtained by resequencing of ESTs. With identities between 36% (*Marchantia polymorpha*) and 84% (canola [*Brassica napus*]) the sequences were homologous with At-RCCR, and all (near) full-length proteins contained N-terminal chloroplast transit peptides as predicted by ChloroP (Emanuelsson et al., 1999). Identity as RCCRs was confirmed by heterologous expression of predicted mature forms of RCCRs from *Arabidopsis* and tomato (*Solanum lycopersicum*) (see below), canola, *Pinus taeda*, and *Citrullus lanatus* (data not shown). Furthermore, in vitro analysis of the RCCR activities in protein extracts from 21 different species confirmed the presence of RCCR in each species. With the

(A) Amounts of different RCCs (gray bars, At-RCC-1; black bars, At-RCC-2; white bars, At-RCC-3; hatched bars, At-RCC-4) accumulating during dark-induced leaf senescence in *acd2-2*. RCCs did not accumulate in Col-0 (data not shown). Results of a single representative experiment are shown. Experiments were performed three times (each single determinations) with similar results.

(B) and **(C)** Determination of ion leakage as a measure of cellular death in Col-0 **(B)** and *acd2-2* **(C)**. Before reexposure to light (150 $\mu mol \cdot m^{-2} \cdot s^{-1}$) for up to 8 h, leaves were incubated in the dark for 0 d (open squares), 2 d (open circles), 4 d (closed circles), 6 d (closed squares), or 8 d (closed triangles). Results of the experiment corresponding to **(A)** are shown. Data are means of three replicates. Error bars indicate SD. Experiments were performed three times with similar results.

(D) Release of singlet oxygen in *acd2-2* after dark incubation. Detached Col-0 and *acd2-2* leaves were incubated in the dark for 0 d (gray bars), 2 d (black bars), or 3 d (white bars) before reexposure to light for 0, 3, and 10 min. Leaf discs were infiltrated with DanePy under green safelight, and subsequently, singlet oxygen trapping was measured as relative quenching of DanePy fluorescence (Hideg et al., 1998). Results of a single representative experiment are shown. Data are means of 12 replicates. Error bars indicate SE.

(E) Representative immunoblots of PAO protein abundance in *acd2-2* leaf areas showing different degrees of cell death as indicated. Left, leaf with a lesion at the tip; right, two independent *acd2-2* leaves without visible symptoms. Gel loadings are based on equal areas of leaf tissue.

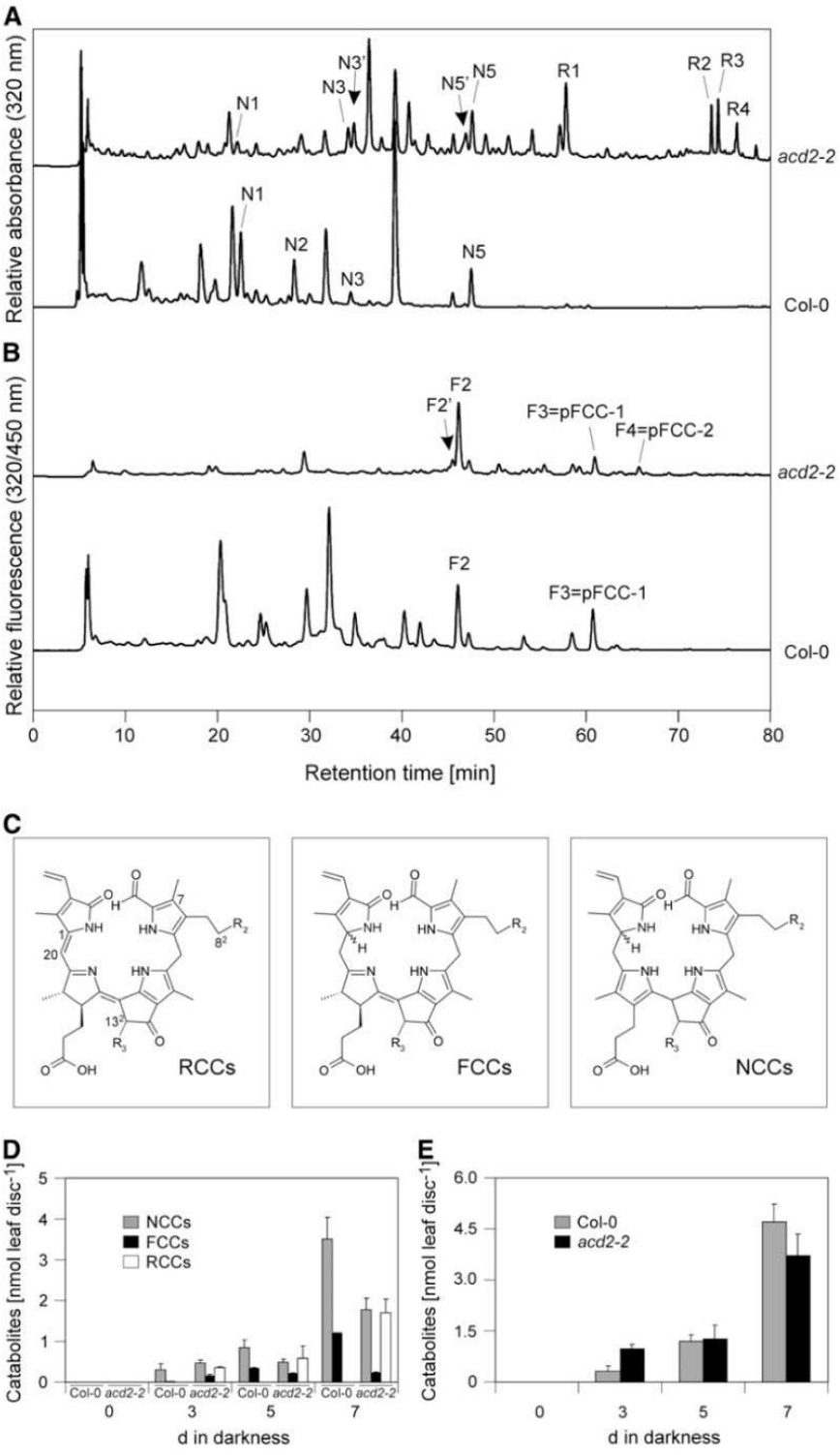

Figure 5. HPLC Analysis of Chlorophyll Catabolites in *acd2-2*.

(A) and **(B)** Chlorophyll catabolites of leaves from *acd2-2* and Col-0 after 5 d of dark-induced senescence were separated by reverse-phase HPLC. A_{320} **(A)** and fluorescence **(B)** were recorded. For the identification and characterization of RCCs (R1 to R4), FCCs (F2 to F4), and NCCs (N1 to N5), see Table 1. Arrows indicate stereoisomers of known Col-0 catabolites (N3′, N5′, and F2′) that were detected in *acd2-2*. Note that the A_{320} traces of *acd2-2* and Col-0 between 50 and 80 min are identical to the respective traces in Figure 3A.

(C) Chemical constitutions of RCCs, FCCs, and NCCs. Sites of peripheral modification present in the different chlorophyll catabolites (see Table 1) are indicated (R_2 and R_3). Relevant carbon atoms are labeled in RCCs.

(D) Accumulation of NCCs (gray bars), FCCs (black bars), and RCCs (white bars) during detached leaf senescence in Col-0 and *acd2-2*. Results of a single representative experiment are shown. Data are means of three replicates. Error bars indicate SD.

(E) Sums of chlorophyll catabolites of Col-0 (gray bars) or *acd2-2* (black bars) shown in **(D)**.

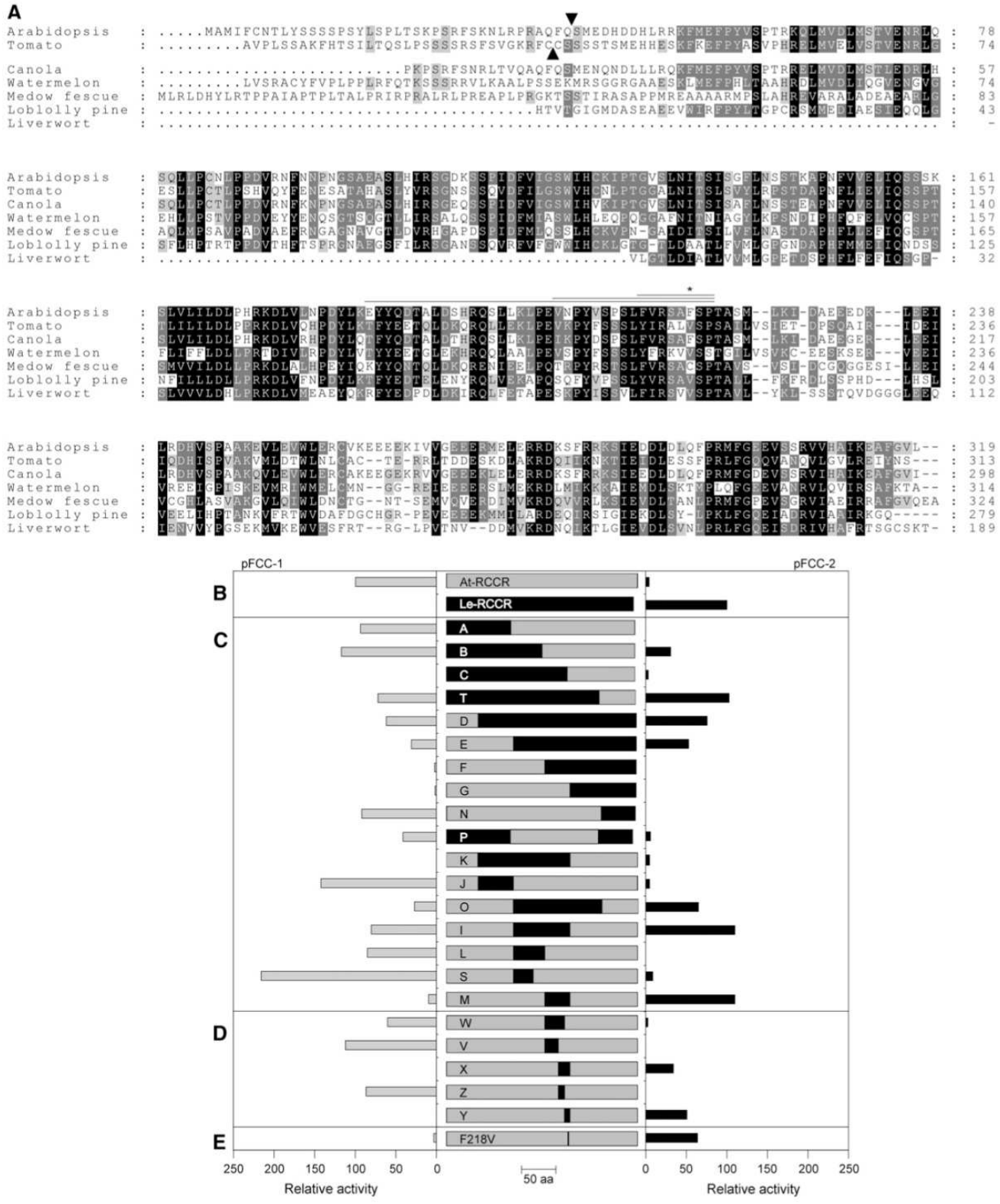

Figure 6. Engineering of the C1 Stereospecificity of RCCRs.

(A) Sequence alignment of RCCRs from different species. The sequences were aligned using the program DIALIGN. Black shading with white letters, gray shading with white letters, and gray shading with black letters reflect 80, 60, and 40% sequence conservation, respectively, with Blosum62 similarity groups enabled. GenBank/EMBL/Swissprot accession numbers are as follows: Q8LDU4 for *Arabidopsis thaliana* RCCR, CAJ80766.1

exception of the Brassicaceae and a few Gramineae species, which produced pFCC-1, pFCC-2 was formed in all other species. One exception was hexaploid wheat (*Triticum aestivum*), in which both pFCCs occurred simultaneously (see Supplemental Figure 4A online). Subsequent analysis of diploid and tetraploid *Triticum* and *Aegilops* ancestors (Isidore et al., 2005) showed that in modern wheat the B and D genomes contribute a type-2 and type-1 RCCR, respectively, whereas the A genome contributes either two enzymes with different specificities or a mixed-type RCCR (see Supplemental Figure 4B online).

After heterologous expression in *Escherichia coli*, the specificities of tomato RCCR (Le-RCCR) and At-RCCR as type-2 and type-1 RCCRs, respectively, were confirmed (Figure 6B). To identify regions within RCCR that could be responsible for the stereospecificity, chimeric RCCRs were produced in *E. coli* by replacing parts of mature At-RCCR with the respective Le-RCCR sequences. In a first round, 17 different engineered RCCRs were analyzed (Figure 6C). Loss of activity occurred in four proteins (C, F, G, and K), whereas six proteins (B, D, E, I, O, and T) retained activity but had (partially) lost stereospecificity (i.e., produced both isomers simultaneously). A reversal of specificity was found in protein M, in which a domain of 37 amino acids of At-RCCR had been replaced with the respective Le-RCCR domain (single line in Figure 6A). This region was further dissected, resulting in type-2 RCCR proteins X and Y, in which the replaced region had been reduced to 17 (double line in Figure 6A) and 8 (triple line in Figure 6A) amino acids, respectively (Figure 6D). Comparison of the available RCCR sequences from 21 different species within this region indicated that the presence of a Phe residue (Phe-218 in At-RCCR; asterisk in Figure 6A) is important in defining specificity (see Supplemental Figure 5 online). Replacing Phe-218 with the Le-RCCR–specific Val residue was indeed sufficient to switch At-RCCR stereospecificity from pFCC-1 to pFCC-2 production (Figure 6E).

Formation of FCCs and NCCs Follows the Stereospecificity of Engineered RCCRs Used for *acd2-2* Complementation

The presence in RCCR mutants of catabolites occurring downstream of RCCR (see above) raised doubts about the participation of RCCR in chlorophyll breakdown. To address this question, we complemented *acd2-2* using At-RCCR and chimeric protein X (At-RCCR-X) (Figure 6D; see above) that exhibit alternative stereospecificities. Both constructs (Figure 7A) complemented the phenotype conferred by *acd2-2* (Figure 7B). Respective transgenic lines (*acd2-2*+At-RCCR and *acd2-2*+At-RCCR-X) exhibited normal plant development and leaf senescence and were indistinguishable from the wild type (data not shown). The specificity of the complementing RCCRs was confirmed in assays using soluble protein extracts of respective lines as a source of RCCR (Figure 7C). Finally, in vivo formation of chlorophyll catabolites from senescent leaves of complemented lines was analyzed by HPLC. Thereby, the different in vitro stereospecificities of At-RCCR and At-RCCR-X were reflected by differences in retention times of FCCs (Figure 7D) and NCCs (Figure 7E) accumulating in respective lines. In particular, pFCC-1 and pFCC-2 exclusively occurred in *acd2-2*+At-RCCR and *acd2-2*+At-RCCR-X, respectively. Furthermore, patterns of pFCCs, At-FCC-2, At-NCC-3, and At-NCC-5 peaks accumulating in *acd2-2*, were identical to the fingerprint of FCC/NCC peaks after coinjection of *acd2-2*+At-RCCR and *acd2-2*+At-RCCR-X extracts. Together, these data confirm that RCCR participates in chlorophyll breakdown inside the chloroplast.

Does RCCR Form a Protein Complex with PAO?

The formation of pFCC from pheide *a* requires the activity of three protein components, PAO, RFF, and RCCR (Rodoni et al., 1997; Pružinská et al., 2005), and different lines of evidence (see Introduction) indicate that PAO and RCCR (and probably RFF) act together, thereby channeling the intermediary RCC. This suggests that PAO and RCCR may interact, possibly through the formation of a stable protein complex. To analyze this notion in more detail, PAO activity and protein abundance during leaf senescence were investigated in the RCCR-deficient lines *acd2-2* and 68-13-1. As shown previously (Pružinská et al., 2005), in the wild-type lines PAO activity transiently increased during the course of dark-induced senescence (Figure 8A; data shown for

Figure 6. (continued).

(fragment) for tomato (*Solanum lycopersicum*) RCCR, CAJ80767.1 (fragment) for canola (*Brassica napus*) RCCR, CAJ80768.1 (fragment) for watermelon (*Citrullus lanatus*) RCCR, CAJ87104.1 for meadow fescue (*Festuca pratensis*) RCCR, CAJ80770.1 (fragment) for loblolly pine (*Pinus taeda*) RCCR, and CAJ80769.1 (fragment) for liverwort (*Marchantia polymorpha*) RCCR. Dashes indicate gaps. Single, double, and triple overlined sequences indicate regions of *Arabidopsis* RCCR that were replaced with the respective tomato RCCR regions in engineered RCCR proteins M, X, and Y, respectively, as shown in **(C)** and **(D)**. The asterisk indicates Phe-218 of *Arabidopsis* RCCR, whose replacement with Val-214 of tomato RCCR (F218V in **[E]**) changes the C1 stereospecificity of *Arabidopsis* RCCR. The arrowheads indicate cleavage sites of the chloroplast transit peptides of *Arabidopsis* and tomato RCCR as predicted by ChloroP.

(B) to **(E)** The middle panels show schemes of engineered RCCR proteins consisting of parts of the predicted mature RCCRs from tomato (Le-RCCR) and *Arabidopsis* (At-RCCR). The left and right panels show RCCR-dependent production of the C1 stereoisomers, pFCC-1 and pFCC-2, respectively. aa, amino acids.

(B) Engineered RCCRs were expressed as His_6-tagged proteins in *E. coli*, and after extraction, RCCR activities were determined. Activities are based on identical volumes of RCCR-containing *E. coli* extracts and are related to the activities of the predicted mature *Arabidopsis* (At-RCCR) and tomato (Le-RCCR) enzymes. Data of single representative experiments are shown.

(C) Of 17 engineered RCCRs, protein M showed a change in stereospecificity.

(D) Dissection of the exchanged region of protein M.

(E) A single Phe-to-Val exchange in At-RCCR is sufficient to change the specificity.

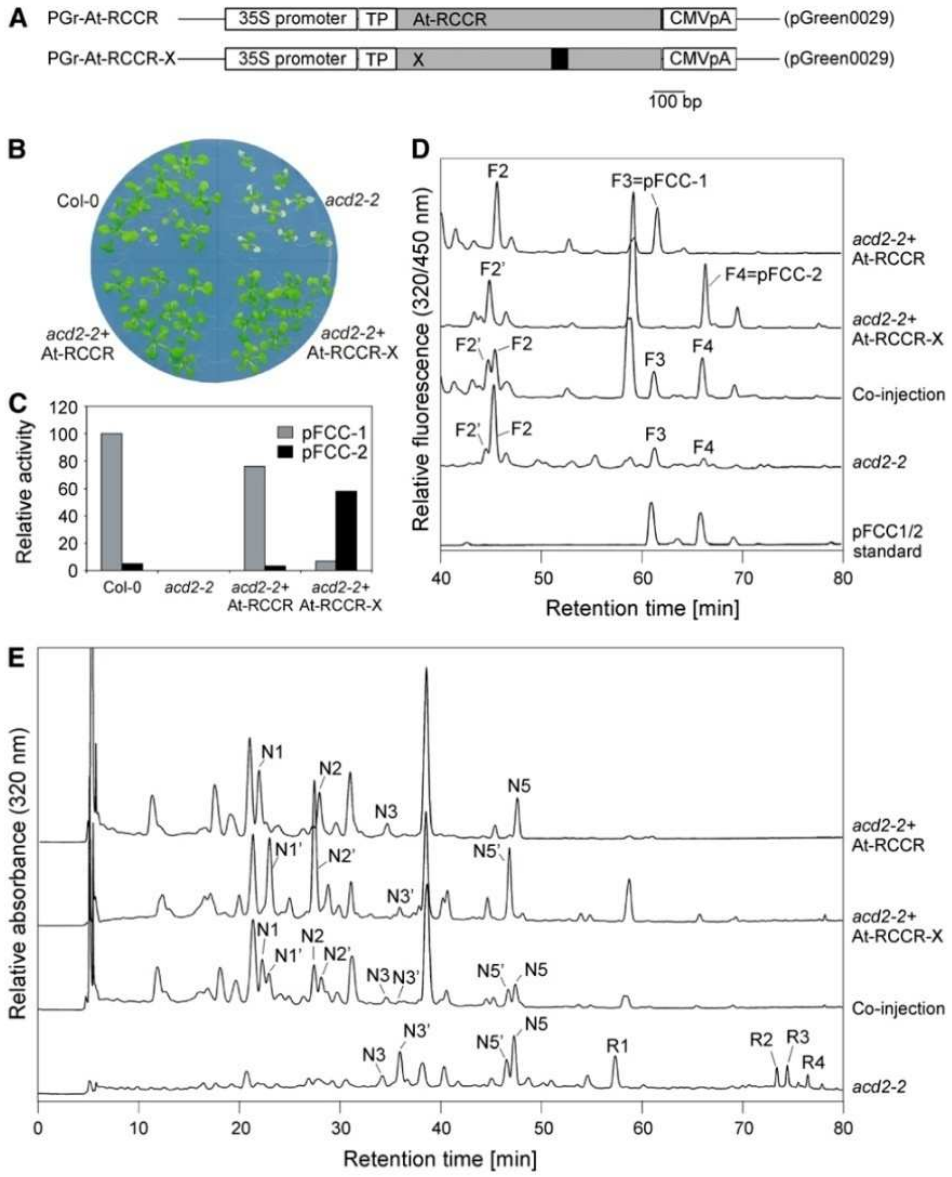

Figure 7. Complementation of *acd2-2*.

(A) Schemes of the constructs used for complementation of *acd2-2*. pGr-At-RCCR, wild type *Arabidopsis* RCCR construct. In pGr-At-RCCR-X, the region identical to the engineered region of RCCR protein X (At-RCCR-X; see Figure 6D) had been replaced with the respective tomato RCCR sequence (black region). *Arabidopsis* lines *acd2-2*+At-RCCR and *acd2-2*+At-RCCR-X, obtained after transformation of *acd2-2* with pGr-At-RCCR and pGr-At-RCCR-X, respectively, were further analyzed. TP, chloroplast transit peptide of *Arabidopsis* RCCR.

(B) Complementation of the *acd2-2* cell-death phenotype in seedlings of *acd2-2*+At-RCCR and *acd2-2*+At-RCCR-X. Col-0 was used as a control. Plants were grown on Murashige and Skoog medium for 1 week, incubated in the dark for another week, and then reexposed to light for 1 d.

(C) RCCR activity of complemented lines. RCCR was extracted from green mature leaves, and activities were determined. Data from representative single point determinations are shown. Experiments were repeated twice with similar results.

(D) and **(E)** HPLC traces of leaf extracts from complemented *acd2-2* lines. Chlorophyll catabolites of leaves after 5 d of dark-induced senescence were separated by reverse-phase HPLC, and fluorescence **(D)** and A_{320} **(E)** were monitored. For the identification and characterization of FCCs **(D)** and NCCS and RCCs **(E)**, see Table 1. For coinjection, equal quantities of extracts from *acd2-2*+At-RCCR and *acd2-2*+At-RCCR-X were mixed and analyzed by HPLC. As controls, extracts of *acd2-2* and a pFCC1/2 standard, containing both pFCC-1 (F3) and pFCC-2 (F4) (Rodoni et al., 1997), were used.

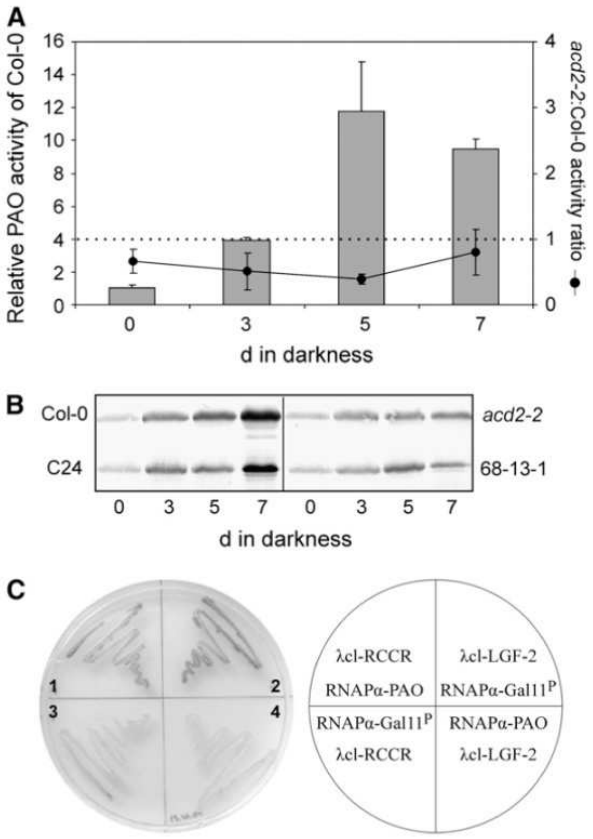

Figure 8. Analysis of PAO Activity, and Interaction of PAO and RCCR.

(A) PAO activity during dark-induced senescence of Col-0 (bars) compared with *acd2-2*, presented as the *acd2-2*:Col-0 PAO activity ratios (solid line). Note that at all measured times, the *acd2-2*:Col-0 PAO activity ratio was <1 (dotted line). Data are means of three independent measurements. Error bars indicate SD.

(B) Representative immunoblots of PAO extracts used for measuring the activities in **(A)** and in 68-13-1 and C24 (data not shown). Gel loadings are based on equal amounts of fresh weight.

(C) BacterioMatch two-hybrid screen demonstrating interaction between PAO and RCCR. Reporter strains were cotransformed with the plasmids as indicated, and interaction was analyzed by reconstitution of β-galactosidase activity. 1, interaction of PAO and RCCR; 2, positive control; 3 and 4, combinations of control plasmids with PAO or RCCR constructs.

Col-0) concomitant with an increase in PAO protein levels (Figure 8B). By contrast, PAO levels and activities remained low in the respective RCCR-deficient lines (Figures 8A and 8B; PAO activity data shown for *acd2-2*). This finding indicated that the increase of PAO level during senescence is affected by the absence of RCCR. However, it remains to be shown whether this is attributable to changes in senescence-related *PAO* expression (Pružinská et al., 2005) or to reduced PAO stability. Because typical senescence parameters such as chlorophyll and protein degradation are normal in RCCR-deficient lines (Figure 2), senescence induction and progression seem not to be affected in the mutants, and it can be assumed that most likely the absence of RCCR decreases PAO stability. To this end, a possible interaction of PAO and RCCR was investigated using a bacterial two-hybrid system. Protein interaction, as demonstrated by reconstitution of β-galactosidase activity, was indeed demonstrated in cells coexpressing PAO and RCCR, but not when either of them was coexpressed with the respective control plasmid (Figure 8D). Subsequently, different methods, such as coimmunoprecipitation, binding of PAO to RCCR-immobilized columns, and chemical cross-linking, were used to investigate whether PAO and RCCR form a protein complex. However, none of these attempts was successful (data not shown), indicating that despite a likely interaction during catalysis, PAO and RCCR do not form a stable protein complex.

DISCUSSION

RCC Accumulation Causes Cell Death in RCCR-Deficient Lines

Tetrapyrrolic compounds, such as precursors and breakdown products of both chlorophyll and heme, are potentially phototoxic; thus, metabolism of tetrapyrroles is highly compartmentalized and regulated (Eckhardt et al., 2004; Hörtensteiner, 2006). Free tetrapyrroles may act as photosensitizers that upon illumination generate reactive oxygen species, leading to severe photooxidative damage. Analysis of an *ACD1/PAO* knockout mutant, *pao1*, had demonstrated that pheide *a* accumulation triggers the premature cell death observed in the mutant (Pružinská et al., 2005). It had been speculated that photodynamic RCC might cause the phenotype conferred by *acd2* (Mach et al., 2001). Here, we provide evidence that, indeed, accumulation of RCC triggers leaf cell death. Thus, cell death positively correlated with concentrations of RCC and the occurrence of lesions strictly correlated with RCC accumulation; hence, *acd2-9*, which is significantly diminished in RCCR but does not accumulate RCC, does not show the phenotype (see Supplemental Figures 1 and 2 online). Furthermore, spontaneous cell death was age-dependent, always occurring first in older leaves (Greenberg et al., 1994; Mach et al., 2001), and involved the activation of PAO. It can be argued that parallel pathways of cell death induction, either through RCC (chloroplast-dependent) or protoporphyrin IX (mitochondria-dependent), might exist in *acd2-2*. At present, the mechanism(s) of cell death formation remains elusive. A loss of the mitochondrial membrane potential has been implicated as an early marker of protoporphyrin IX–induced cell death (Yao et al., 2004), through the accumulation of mitochondria-derived H_2O_2 and a subsequent mitochondrial oxidative burst (Yao and Greenberg, 2006). It had been speculated that light absorption by RCC causes the production of singlet oxygen (Hörtensteiner, 2006), which has been shown to trigger cell death caused by chloroplast-dependent protochlorophyllide accumulation (op den Camp et al., 2003) through a signaling pathway involving EXECUTER1 (EX1) (Wagner et al., 2004). Indeed, upon light exposure, singlet oxygen, as determined by fluorescence quenching of DanePy (Hideg et al., 1998; Kálai et al., 1998), was produced rapidly in *acd2-2* leaves in which chlorophyll breakdown (i.e., the formation of RCCs) had been induced by dark incubation (Figure 4). It seems likely that, in analogy with the *flu/ex1* system, in RCCR-deficient lines RCC-dependent production of singlet

oxygen triggers cell death signaling via EX1. To analyze this notion in more detail, we started to produce *acd2-2 ex1* double mutants.

In RCCR Mutants, RCC Is Modified and Transported to the Vacuole

During dark-induced senescence, four different types of RCC were identified in RCCR-deficient lines. Noteworthy, in *C. prototothecoides*, which is devoid of a reductase with the function of RCCR, the breakdown of chlorophyll has been shown to end in the production of several RCC-like compounds, which also differ from each other by peripheral modifications, particularly at the methoxycarbonyl group at C13 (Engel et al., 1991, 1996). Thus, one major chlorophyll breakdown product in *C. prototothecoides* is $C13^2$-demethyl RCC, which is identical to At-RCC-1. This pigment, together with its decarboxylation product (Engel et al., 1991), At-RCC-2, was (partially) localized to the vacuolar fraction. By contrast, RCC (At-RCC-3) or its isomer (At-RCC-4) was not found in the vacuole. This finding indicated that RCC was transported from the plastid, its site of production by PAO, to the vacuole and that modification of RCC occurred before vacuolar import (i.e., in the plastid or cytosol). It can be concluded that in respective mutants the absence of RCCR causes the accumulation of RCC, which is in part metabolized similar to pFCC, the first identifiable product of porphyrin cleavage in wild-type plants (Mühlecker et al., 1997, Pružinská et al., 2005). In wild-type plants, RCC is rapidly converted to pFCC (i.e., probably before release from PAO [see below] and export from the plastid could occur). Furthermore, chlorophyll catabolite-modifying enzymes and transporters seem to work in a rather unspecific manner. Pheophorbidase, an enzyme that catalyzes the C13 demethylation of pheides *a* and *b*, has been identified and cloned recently by Shioi and coworkers (Shioi et al., 1996; Suzuki et al., 2006), and preliminary results from our laboratory indicate that the same enzyme can use pFCC as a substrate (S. Aubry, A. Pružinská, and S. Hörtensteiner, unpublished data). Thus, it is possible that RCC (At-RCC-3) also is demethylated by this activity to give rise to At-RCC-1. Export of FCCs from the plastid has been shown to involve an active process (Matile et al., 1992), but the nature of the transporter has not been elucidated. Transport of chlorophyll catabolites across the tonoplast probably requires the activity of members of the multidrug resistance–associated protein subfamily of ATP binding cassette transporters, which exhibit a rather broad substrate specificity (Martinoia et al., 2000, Klein et al., 2006). Thus, At-MRP2 and At-MRP3 are able to transport NCCs in vitro (Lu et al., 1998; Tommasini et al., 1998), although FCCs have been indicated to be the natural substrates for vacuolar uptake (Kräutler, 2003; Oberhuber et al., 2003). Likely, these transporters are responsible for the transmembrane transport of RCC-like pigments in the mutants.

The Biochemical Function of RCCR

RCCR is widely distributed among higher plants, but RCCR sequences and activity are not found in green algae or photosynthesizing prokaryotes (Hörtensteiner et al., 2000b; Wüthrich et al., 2000). This is in agreement with its role in RCC reduction: when *C. prototothecoides* is grown under heterotrophic conditions and low nitrogen in the dark, RCC and RCC-like chlorophyll catabolites are excreted into the medium (Engel et al., 1996). Likewise, a red bilin pigment has been described as the final degradation product of chlorophyll metabolism in *C. reinhardtii* (Doi et al., 1997). Higher plants have to cope with chlorophyll catabolites internally, and it has been argued that the invention of RCCR required for the removal of potentially phototoxic RCC was a prerequisite for land colonization by plants (Matile et al., 1999). It seems likely that RCCR of higher plants evolved from bilin reductases of cyanobacteria that catalyze the Fd-dependent reduction of biliverdin to phycobilins. RCCR is distantly related to these bilin reductases and to phytochromobilin reductase (HY2) of higher plants (Frankenberg et al., 2001). Therefore, the similarity is restricted to a few highly conserved amino acids, including Phe-218, which defines the C1 stereospecificity of At-RCCR. Interestingly, different bilin reductases specifically produce the 3*Z* isomers of their respective products, although the thermodynamically more stable 3*E* isomers are substrates for incorporation of the respective holoproteins. The nature of 3*Z*/3*E* isomerization remains elusive (Frankenberg et al., 2001). The stereospecificity of RCCR is irrelevant for functionality, as demonstrated by the complementation of *acd2-2* with RCCRs exhibiting different stereospecificities; hence, it does not affect plant development or senescence. Nevertheless, the importance of RCCR is evident from the cell-death phenotype of RCCR mutants (see above).

The analysis of chlorophyll catabolites found in RCCR-deficient lines showed that in addition to the accumulation of RCCs, downstream catabolites of RCCR action (i.e., FCCs and NCCs) accumulate, although with an apparent loss of C1 stereospecificity. This finding, together with a cell-protective role, which is independent of chlorophyll (Yao and Greenberg, 2006), raised doubts regarding the catalytic activity of RCCR and its involvement in chlorophyll catabolism. By complementation of *acd2-2* with type-1 and type-2 RCCRs, we now confirm the in vivo participation of RCCR in chlorophyll breakdown.

If RCCR mutants are able to reduce RCC, what might be the mechanism involved and what is the catalytic activity of RCCR in this reaction? Preliminary data indicate that HY2 cannot be used for RCC reduction in vitro (A. Pružinská and S. Hörtensteiner, unpublished data). This finding corroborates the known distinct substrate preferences of the members of the HY2 family of ferredoxin-dependent bilin reductases (Frankenberg et al., 2001). Furthermore, it excludes a functional substitution by a related enzyme but leaves open the possibility of an unrelated activity taking over RCCR function in the mutants. As shown for the bilin reductase, phycocyanobilin:ferredoxin oxidoreductase (PcyA) (Frankenberg and Lagarias, 2003), RCCR is devoid of cofactors that are required for electron transfer to RCC (J. Berghold, I. Primožič, S. Hörtensteiner, and B. Kräutler, unpublished data). A reduction mechanism by electron transfer from Fd might be active in RCC reduction by RCCR (Oberhuber and Kräutler, 2002). A similar radical mechanism involving direct electron transfer from Fd has been postulated for PcyA (Tu et al., 2004). Indeed, by purely nonenzymatic, electrochemical means, RCC has been converted to roughly equal ratios of both pFCC-1 and its C1 epimer (Oberhuber and Kräutler, 2002; M. Oberhuber,

J. Berghold, and B. Kräutler, unpublished data). This raises the possibility that in the mutants the redox conditions inside the chloroplast enable a (slow) reduction of the accumulating RCC(s) without the involvement of proteins. Pheide *a* oxygenation by PAO is limited in vitro (Rodoni et al., 1997), probably through product (RCC) inhibition of the enzyme, and only after reduction to pFCC by RCCR is the catabolite released from PAO (Hörtensteiner et al., 1998; Kräutler, 2003). This view is supported by biochemical data suggesting a catalytic cooperation between PAO and RCCR (Rodoni et al., 1997; Wüthrich et al., 2000) and implies a physical interaction. Here, we provide further evidence for such a PAO–RCCR interaction. First, the absence of RCCR in RCCR mutants affects PAO activity and protein abundance, indicating that RCCR may be required for the stabilization of PAO. Nevertheless, PAO levels were sufficient to prevent the accumulation of pheide *a* in RCCR mutants, unlike *pao1*, in which cell death has been attributed to pheide *a* accumulation (Pružinská et al., 2005). Second, the PAO–RCCR interaction could be demonstrated in a bacterial two-hybrid system. It has been argued that RCCR might not be a reductase itself but rather could accelerate the RCC-to-pFCC conversion in the chlorophyll catabolic pathway by enhancing electron transfer reactions and defining a regioselective and stereoselective reduction of RCC at C1 (Kräutler, 2002, 2003; Oberhuber and Kräutler, 2002; Hörtensteiner, 2004, 2006), but preliminary coupled PAO/RFF/RCCR assays (Pružinská et al., 2005) using RCC as substrate did not produce pFCCs, questioning the possibility of a direct electron transfer via PAO (A. Pružinská and S. Hörtensteiner, unpublished data).

Thus, it can be concluded that RCCR is a protein factor that, besides a possible direct function in protection from cellular death (Yao and Greenberg, 2006), is truly involved in chlorophyll breakdown. Its importance is manifested by the cell-death phenotype of RCCR mutants and the accumulation of RCCs, which likely triggers cell death. The biochemical function of RCCR in the reduction of RCC to pFCC remains to be confirmed, but data obtained here and elsewhere (Rodoni et al., 1997; Wüthrich et al., 2000) indicate that RCCR is not a reductase itself but rather functions as a kind of chaperone (Oberhuber and Kräutler, 2002; Kräutler, 2003), promoting the catalytic conversion of RCC to pFCC.

METHODS

Plant Material and Senescence Induction

As wild types of *Arabidopsis thaliana*, ecotypes Col-0, C24, and Ws were used. Seeds of *acd2-2* (Greenberg et al., 1994) were kindly provided by J.T. Greenberg (University of Chicago). *acd2-9* (Ws background) was isolated from the Wisconsin Knockout Facility (Krysan et al., 1999) using the *RCCR/ACD2* (At4g37000)–specific primer AtKO3 (5′-TAGCGTGTACAACACGGGAGGAAACTTCT-3′) and the T-DNA left border primer JL202 (5′-CATTTTATAATAACGCTGCGGACATCTAC-3′). PCR products were analyzed by DNA gel blot analysis (Hörtensteiner et al., 2000a) using a digoxygenin-labeled (Dig High Prime; Roche) *RCCR* probe. In two subsequent rounds, positive signals were obtained in pools of 2025 (#16) and pools of 225 (#142; CSH142) (Krysan et al., 1999). Seed stock CSH142, containing seeds from 25 pools of 9 were obtained through the ABRC, and a *RCCR* T-DNA insertion was identified in a pool of 9 (#26; CSJ3526). One of the individual lines from seed stock CSJ3526 was renamed *acd2-9*, and homozygous siblings were used for further analysis. The presence of the T-DNA insertion within the *RCCR* gene in *acd2-9* was confirmed by sequencing the PCR product generated from genomic DNA with the gene-specific primer At-RCCR7 (5′-AGGAGTTGTGATTGGAGGCG-3′) and JL202. For the relative locations of primers, see Supplemental Figure 1 online.

Plants were grown on soil either in short-day (8 h/16 h) or long-day (16 h/8 h) growth rooms under fluorescent light of 60 to 120 μmol photons·m^{-2}·s^{-1} at 22°C. For senescence induction, leaves from 3- to 4-week-old (long-day) or 8-week-old (short-day) plants were excised and incubated in permanent darkness on wet filter paper for up to 7 d at ambient temperature. Alternatively, individual attached leaves were wrapped with aluminum foil (Pružinská et al., 2005). For the induction of cell death in seedlings, seeds were surface-sterilized and grown on Murashige and Skoog agar plates without sucrose for 7 d under long-day conditions. Plates were then wrapped in aluminum foil for 7 d and analyzed after reexposure to light for 1 d.

Canola (*Brassica napus*) was grown on soil, and senescence of cotyledons was induced by dark incubation of 10-d-old seedlings in the dark (Hörtensteiner et al., 1995). Based on publicly available RCCR sequences (see Supplemental Figure 4 online), seeds or leaf material from respective species were obtained from the Botanical Gardens of Bern and Zürich, Switzerland, or from local garden shops. Seeds from diploid and tetraploid *Triticum* and *Aegilops* species were a gift from B. Keller (University of Zürich). For a few species, plant material could not be obtained, and following the assumption that RCCR stereospecificity is conserved within genera (Hörtensteiner et al., 2000b), a different species of the same genus was used instead.

Biocomputational Methods and Data Sources

Homologs of At-RCCR were searched for and identified with the BLAST neighborhood search algorithm (Altschul et al., 1997) through database searches with the National Center for Biotechnology Information, the *Chlamydomonas reinhardtii* genomic database, Chlamy Center (http://www.chlamy.org/chlamydb.html), and the CyanoBase (http://www.kazusa.or.jp/cyano/cyano.html). Protein sequences were derived from conceptual translation of cDNA sequences or overlapping ESTs. RCCR homologs were aligned (Figure 6) using the programs DIALIGN (Morgenstern, 2004) and GENEDOC (http://www.psc.edu/biomed/genedoc). For the phylogenetic tree shown in Supplemental Figure 4 online, RCCR protein sequences were aligned using ClustalW and the tree was calculated using neighbor joining with the program MEGA3.1 (Kumar et al., 2004). Accession numbers for the sequences used are indicated in the figure legends.

Constructs and Production of Transgenic Plants

RCCR Cosuppression

Arabidopsis line 68-13-1, in which the expression of the endogenous RCCR is cosuppressed, was obtained during the attempt to overexpress RCCR in C24. For this, full-length *Arabidopsis RCCR* (At-*RCCR*) was cloned behind the cauliflower mosaic virus 35S promoter containing a double enhancer element (35SDE). The open reading frame of At-*RCCR* was amplified from pGEM-At-RCCR (Wüthrich et al., 2000) with primers At-RCCR6 (5′-*GGATCC*ATGGCGATGATATTTTGCAACAC-3′) and At-RCCR3 (5′-*TGATC*ATAATCTAGAGAACACCGAAAGC-3′) (restriction sites in italics) and recloned into pGEM-T Easy (Promega), yielding pSC1a. A *Sph*I/*Bgl*II fragment of pER30 (E. van der Graaff, personal communication) containing 35SDE was ligated to *Sph*I/*Bam*HI-restricted pSC1a, yielding pSC2a. Subsequently, the *uidA* gene of the binary vector pGPTV-KAN (Becker et al., 1992) was replaced by the 35SDE-At-*RCCR*

fragment of pSC2a to give pSC4. *Arabidopsis* plants (C24) were transformed using the flower dip method (Sidler et al., 1998). Thirty kanamycin-resistant plants were analyzed for levels of RCCR by immunoblot analysis. After isolation of homozygous siblings, line 68-13-1, which showed strong reduction of RCCR levels (Figure 1D), was analyzed further.

RCCR RNA Interference Plants

Primer combinations SIL4 (5′-*CTCGAGCCATGG*ATAGGAAGTTGGATACATTGC-3′)/SIL5 (5′-*GGTACC*ATCTCTCAATATCTCCTCC-3′) and SIL6 (5′-*GGATCC*ATAGGAAGTTGGATACATTGC-3′)/SIL7 (5′-*ATCGAT*GATCTCTCAATATCTCC-3′) were used to amplify by PCR two 420-bp fragments of At-*RCCR* from pGEM-RCCR (Wüthrich et al., 2000). Appropriate restriction sites linked to the primers enabled a two-step cloning of the PCR products in opposite directions into pHannibal (Wesley et al., 2001). After digestion with *Not*I, the RNA interference construct was introduced into *Not*I-restricted pGreen0029 (Hellens et al., 2000) to produce pCSIL. *Arabidopsis* plants (Col-0 or Ws) were transformed (Sidler et al., 1998), and homozygous kanamycin-resistant T2 plants (Col-0+pCSIL#2-2, Col-0+pCSIL#7-1, Ws+pCSIL#5-4, and Ws+pCSIL#7-1) were isolated for further analysis.

Complementation of acd2-2

Full-length At-*RCCR* was amplified by PCR using primers At-RCCR8 (5′-GC*TCTAGACATATG*GCGATGATATTTTGCAACAC-3′) and At-RCCR9 (5′-*GAATTCTGCAG*AGAACACCGAAAGCTTC-3′) and, after *Xba*I/*Eco*RI digestion, cloned into *Xba*I/*Eco*RI-restricted p35S-2 (Hellens et al., 2000). The 35S-At-*RCCR* terminator–containing *Eco*RV fragment was cloned into *Eco*RV/*Stu*I-restricted pGreen0029 (Hellens et al., 2000), yielding pGr-At-RCCR. To complement *acd2-2* with a type-2 RCCR (protein X = At-RCCR-X; Figure 6D), an *Nco*I/*Pst*I fragment of pGr-At-RCCR encoding amino acids 40 to 319 of At-RCCR was replaced by the respective fragment of pX (see Supplemental Table 2 online), to yield pGr-At-RCCR-X. *acd2-2* was transformed with pGr-At-RCCR and pGr-At-RCCR-X (Figure 7A), and transgenic lines (*acd2-2*+At-RCCR and *acd2-2*+At-RCCR-X, respectively) were selected as described above.

Engineering of Tomato and Arabidopsis *RCCRs*

Chimeric *RCCR* sequences encoding fragments of predicted mature forms of Le-RCCR from tomato (*Solanum lycopersicum*) and At-RCCR (Figure 6) were produced by PCR according to the scheme shown in Supplemental Table 2 online using the primers listed in Supplemental Table 1 online. As cDNA sources, pGEM-RCCR (Wüthrich et al., 2000) and pLe-RCCR (GenBank accession number AM233528) were used. Chimeric PCR products were restricted with *Bam*HI/*Pst*I and cloned in-frame to the His_6 tag of pQE30 (Qiagen). The fidelity of the constructs was confirmed by sequencing. After expression in *Escherichia coli* JM109, proteins were extracted as described (Wüthrich et al., 2000; Pružinská et al., 2005) and used in enzyme assays (see below). Expression of engineered RCCRs was confirmed by immunoblot analysis.

BacterioMatch Two-Hybrid System

The BacterioMatch two-hybrid system (Stratagene) was used for the analysis of interaction between PAO and RCCR. Truncated At-PAO missing the predicted N-terminal transit peptide and the two C-terminal transmembrane domains was produced from a full-length cDNA clone (pda07874) (Seki et al., 2002) by PCR using primers R4LP-Not (5′-GAT*GCGGCCGC*GCCGCCGTCTGTACC-3′) and R4RPsol-Xho (5′-GAC*CTCGAG*GATTTGGAAACTGTTGTAAG-3′). After *Not*I/*Xho*I digestion, the fragment was cloned into *Not*I/*Xho*I-restricted pTRG to yield pTRG-PAO. Likewise, At-*RCCR* missing the transit peptide sequence was amplified from pAt-RCCR (see Supplemental Table 2 online) with primers At-RCCRLP-Not (5′-GAT*GCGGCCGC*CATGGAAGACCACGACG-3′) and At-RCCRRP-Bam (5′-CG*GGATCC*TAGAGAACACCGAAAGCTTC-3′) and cloned into pBT (pBT-RCCR). pBT-LGF2 and pTRG11 were used as control plasmids. Cotransformation into the BacterioMatch reporter strain (Stratagene) and analysis of protein interaction were performed according to the manufacturer's instructions.

Analysis of Chlorophyll and Chlorophyll Catabolites

Chlorophyll

Chlorophyll was isolated from leaf tissue by homogenization in liquid nitrogen and subsequent threefold extraction into 80% (v/v) acetone containing 1 μM KOH. After centrifugation (2 min at 16,000*g*), supernatants were combined and chlorophyll concentrations were determined spectrophotometrically (Strain et al., 1971).

Red and Colorless Chlorophyll Catabolites

Tetrapyrrolic chlorophyll catabolites (RCCs, FCCs, and NCCs) were extracted into methanol as described (Pružinská et al., 2005) and analyzed either directly or after concentration on a C18 SepPak cartridge (Waters) (Mühlecker et al., 1997) by HPLC as described (Pružinská et al., 2005), except that the following elution program was used: 35 to 75% solvent B (20% [v/v] 25 mM potassium phosphate buffer, pH 7.0, in methanol) in solvent A (50 mM potassium phosphate, pH 7.0) over 60 min, 75 to 100% solvent B over 10 min, and 100% solvent B for 8 min. RCCs were identified by their absorption properties (Hörtensteiner, 1999) and/or by cochromatography with a RCC standard (Kräutler et al., 1997) or with extracts of degreened *Chlorella protothecoides* cultures (Engel et al., 1991, 1996; Hörtensteiner et al., 2000a). Pyrrole ring B together with the C5-formyl group in RCCs and FCCs is responsible for the absorption maxima at 316 to 320 nm, as is the case for NCCs (Kräutler et al., 1991). Peak areas of RCC and FCC fractions were estimated with a standard NCC, Cj-NCC-1 (Oberhuber et al., 2001), at defined concentrations (log $\varepsilon_{315nm} = 4.2$) (Kräutler et al., 1991). For the identification of FCCs and NCCs, HPLC runs were performed under identical conditions using extracts from either senescent Col-0 leaves containing a defined set of catabolites (Pružinská et al., 2005) or from in vitro PAO/RCCR assays containing both pFCC-1 and pFCC-2 (Rodoni et al., 1997).

UV/Vis Spectral and Mass Spectrometric Data

For on-line liquid chromatography/electrospray ionization (LC/ESI) mass spectrometric experiments, C18 SepPak–concentrated extracts were separated on an Ultimate Nano HPLC system with diode array detection (LC Packings; flow rate, 900 μL/min; column, Hypersil ODS 5 μm, 10 cm, 100-μm inner diameter; solvent A, 0.02% HCOOH in acetonitrile; solvent B, 0.02% HCOOH in water; gradient started at 15% A and was increased to 90% A within 155 min). The HPLC was connected to a Finnigan MAT 95-S mass spectrometer (positive-ion mode) using a Picoview nanospray source (New Objective; spray voltage, 2.2 kV).

ESI-MS: m/z (percent relative intensity) of At-NCCs. At-NCC-1: 815 (10, $[M+Na]^+$), 793 (100, $[M+H]^+$), 749 (65, $[M-CO_2+H]^+$), 619 (40, [M-glucosyl+H]$^+$). C1-*epi*-At-NCC-5: 615 (100, $[M+H]^+$), 571 (40, $[M-CO_2+H]^+$), 492 (10, [M-ring A+H]$^+$). At-NCC-5: 615 (100, $[M+H]^+$), 571 (40, $[M-CO_2+H]^+$), 492 (10, [M-ring A+H]$^+$), 448 (10, $[M-CO_2$-ring A+H]$^+$). At-NCC-2: 631 (100, $[M+H]^+$), 587 (30, $[M-CO_2+H]^+$), 508 (10, [M-ring A+H]$^+$). At-NCC-3: 631 (100, $[M+H]^+$), 587 (35, $[M-CO_2+H]^+$), 508 (10, [M-ring A+H]$^+$). The latter two At-NCCs are isomers and are named here as established previously (Ginsburg and Matile, 1993); however, assignment of these two NCCs to one of the possible four isomers

At-NCC-2, C1-*epi*-At-NCC-2, At-NCC-3, or C1-*epi*-At-NCC-3 was not successful (Table 1).

For the analysis of At-RCCs by UV/Vis spectra and ESI–mass spectrometry with nozzle-skimmer collision-induced dissociation (ESI-MS/CID), C18 SepPak–concentrated extracts were separated by HPLC (Agilent HP 1100; diode array detection) as described elsewhere (Berghold et al., 2002). After collection, RCC fractions were concentrated in vacuo to remove methanol. The four pure RCC fractions were analyzed by LC-MS using the Ultimate Nano HPLC-MS system described above. The gradient started at 15% A and was increased to 50% A within 50 min.

UV/Vis spectra of At-RCCs (λ_{max}, acetonitrile:water 1:1 [v/v], relative absorbance; sh, shoulder). At-RCC-1: 236 (0.55), 272.5 (0.62), 317 (1.00), 346 (sh, 0.53), 459 (sh, 0.31), 484 (0.35), 526 (sh, 0.26). At-RCC-2: 232 (0.55), 270 (0.62), 316.5 (1.00), 346 (sh, 0.53), 456 (sh, 0.26), 485 (0.35), 523 (sh, 0.29). At-RCC-3: 235 (0.29), 272 (0.55), 316.5 (1.00), 346 (sh, 0.47), 456 (sh, 0.29), 485 (0.34), 523 (sh, 0.26). At-RCC-4: 233 (0.29), 270 (0.55), 316.5 (1.00), 346 (sh, 0.50), 456 (sh, 0.25), 485 (0.32), 523 (sh, 0.26).

ESI-MS and ESI-MS/CID data (60-V nozzle skimmer) of At-RCCs (m/z, percent relative intensity). At-RCC-1: ESI-MS, 613 (30, $[M+H]^+$), 569 (100, $[M-CO_2+H]^+$); ESI-MS/CID, 1137 (25, $[2(M-CO_2)+H]^+$), 613 (30, $[M+H]^+$), 607 (20, $[M-CO_2+K]^+$), 569 (100, $[M-CO_2+H]^+$), 432 (85, $[M-CO_2$-ring B$+H]^+$), 420 (20). At-RCC-2: ESI-MS, 1137 (20, $[2M+H]^+$), 607 (10, $[M+K]^+$), 569 (100, $[M+H]^+$), 432 (10, [M-ring B$+H]^+$); ESI-MS/CID, 1137 (10, $[2M+H]^+$), 607 (15, $[M+K]^+$), 569 (100, $[M+H]^+$), 432 (95, [M-ring B$+H]^+$), 420 (25). At-RCC-3: ESI-MS, 627 (100, $[M+H]^+$), 595 (10, $[M-CH_3OH+H]^+$), 490 (10, [M-ring B$+H]^+$); ESI-MS/CID, 627 (100, $[M+H]^+$), 595 (35, $[M-CH_3OH+H]^+$), 569 (10, $[M-CH_3OH-CO+H]^+$), 490 (90, [M-ring B$+H]^+$). At-RCC-4: ESI-MS, 627 (100, $[M+H]^+$), 569 (90, $[M-CH_3OH-CO+H]^+$); ESI-MS/CID, 627 (25, $[M+H]^+$), 569 (90, $[M-CH_3OH-CO+H]^+$), 490 (10, [M-ring B$+H]^+$), 432 (100, $[M-CH_3OH$-CO-ring B$+H]^+$), 420 (25).

Isolation of Protoplasts, Vacuoplasts, and Evacuolated Protoplasts

Arabidopsis protoplasts were isolated from leaves of 3-week-old *acd2-2* plants that were incubated in the dark for 4 d to induce senescence. After careful injury of the adaxial leaf surface using sandpaper (SIA 1913; Hager), cell walls were digested for 2 h in 0.5 M sorbitol, 10 mM MES-imidazole, pH 5.8, 1 mM $CaCl_2$, 1% cellulase, and 0.5% macerozyme. Protoplasts were liberated and purified via Percoll density gradient centrifugation as described (Hinder et al., 1996). Subcellular fractionation of protoplasts into evacuolated protoplasts and vacuoplasts was performed by ultracentrifugation according to published procedures (Hörtensteiner et al., 1992, 1994). Cell numbers were quantified with a Neubauer chamber. For HPLC analysis of nongreen chlorophyll catabolites, equal numbers of cells were lysed by the addition of 25% (v/v) 20 mM potassium phosphate, pH 7.0, in methanol, and extracts were clarified by centrifugation.

Protein Extraction and Immunoblot Analysis

Soluble proteins were extracted from leaf tissues and used either directly or after precipitation with ammonium sulfate (Rodoni et al., 1997; Wüthrich et al., 2000; Pružinská et al., 2003) for protein determination according to Bradford (1976) and/or for assaying RCCR (Pružinská et al., 2005). PAO was isolated from canola or *Arabidopsis* chloroplast membranes by Triton X-100 solubilization according to standard procedures (Hörtensteiner et al., 1995; Pružinská et al., 2005).

After separation by SDS-PAGE, proteins were transferred to nitrocellulose membranes according to standard procedures. Proteins were labeled with antibodies against *Arabidopsis* RCCR (1:1000) (Wüthrich et al., 2000), PAO (monoclonal, 1:500; polyclonal, 1:2000) (Gray et al., 2004), or as outlined in Supplemental Figure 3 online, and thereafter with alkaline phosphatase–conjugated secondary antibodies, and visualized using bromochloroindolyl phosphate/nitroblue tetrazolium as substrate.

Enzyme Assays

PAO and RCCR activities were assessed in an assay according to published procedures (Hörtensteiner et al., 1995; Wüthrich et al., 2000; Pružinská et al., 2005). Briefly, assays (total volume of 50 μL) contained different combinations of PAO (equivalent to 0.5 g of tissue), *E. coli* (50 μg) protein extracts as a source of RFF (Pružinská et al., 2005), and purified His_6-At-RCCR (2.9 μg) (Pružinská et al., 2005) or proteins extracted from different plant species (equivalent to 50 mg of tissue) or from RCCR-expressing *E. coli* cells (corresponding to 0.2 mL of culture at $OD_{600} = 1.5$) as a source of RCCR. The assays were supplemented with 0.5 mM pheide *a* (Hörtensteiner et al., 1995), 10 μg of Fd, and a Fd-reducing system consisting of 2 mM glucose-6-phosphate, 1 mM NADPH, 50 milliunits of glucose-6-phosphate dehydrogenase, and 5 milliunits of ferredoxin NADPH oxidoreductase. After 1 h of incubation at 25°C, reactions were terminated by the addition of 80 μL of methanol. Formation of pFCC-1 was followed by reverse-phase HPLC with 36% (v/v) 50 mM potassium phosphate buffer, pH 7.0, in methanol as solvent. Activities were determined as integrated fluorescence units (320/450 nm) of pFCC-1 or pFCC-2 (FU_{pFCC}). Identities of pFCC-1 and pFCC-2 were confirmed with authentic standards (Mühlecker et al., 1997, 2000).

Ion Leakage

For ion conductivity analysis, senescence was induced in detached leaves that were incubated in the dark for up to 8 d. Eight leaf discs (1 cm in diameter) were excised and transferred to six-well cell culture plates (Sarstedt) containing 5 mL of water. After reexposure to light (150 μmol photons·m^{-2}·s^{-1}) for up to 8 h, ion leakage from the leaf discs as a measure of cellular damage was determined by measuring the conductivity of the solution with a CDH-42 conductivity meter (Omega Engineering).

Singlet Oxygen Determination

Singlet oxygen was detected in leaves by DanePy fluorescence quenching according to Hideg et al. (1998). For this, detached dark-incubated leaves of 4-week-old plants were exposed to light (150 μmol photons·m^{-2}·s^{-1}) for up to 10 min, before leaf discs (5 mm in diameter) were excised and infiltrated with either 2 mM DanePy (dissolved in 1% ethanol) or 1% ethanol under green safelight. Fluorescence was immediately determined using a Fluorolite 1000 plate fluorometer (Dynatech Laboratories) with excitation at 365 nm and emission at 520 ± 10 nm.

Accession Numbers

cDNA and genomic sequences encoding RCCRs have been deposited in the GenBank/EMBL data libraries under accession numbers AM233528 (*Solanum lycopersicum* RCCR), AM233529 (*Brassica napus* RCCR), AM233530 (*Citrullus lanatus* RCCR), AM233531 (*Marchantia polymorpha* RCCR), AM233532 (*Pinus taeda* RCCR), and AM237454 (*Festuca pratensis* RCCR).

Supplemental Data

The following materials are available in the online version of this article.

Supplemental Table 1. Primers Used for the Construction of Chimeric RCCR Proteins.

Supplemental Table 2. PCR Strategies for the Construction of Chimeric RCCR Proteins.

Supplemental Figure 1. Characterization of *acd2-9*.

Supplemental Figure 2. HPLC Analysis of Chlorophyll Catabolites from RCCR-Deficient Lines.

Supplemental Figure 3. Characterization of Subcellular Fractions of *acd2-2* Protoplasts.

Supplemental Figure 4. Phylogenetic Tree and Stereospecificity of RCCR Proteins.

Supplemental Figure 5. Alignment of a Stereospecificity-Defining Domain of RCCR Proteins.

ACKNOWLEDGMENTS

This article is dedicated to Philippe Matile on the occasion of his 75th birthday. We thank Jean T. Greenberg (University of Chicago) for *acd2-2*; Tamás Kálai and Kálmán Hideg (Pécs University, Hungary) for DanePy; Éva Hideg (Hungarian Academy of Sciences, Szeged, Hungary) for her help with the determination of singlet oxygen; Eric van den Graaff (University of Freiburg, Germany) for pER30; and Beat Keller (University of Zürich, Switzerland) for diploid and tetraploid *Triticum* and *Aegilops* species. For the supply of antibodies, we thank John Gray (University of Toledo) for PAO/ACD1; Shimon Gepstein (Israel Institute of Technology) for LSU; Masayoshi Maeshima (Nagoya University, Japan) for BIP, γ-TIP, and PAQ; and Tom Elthon (University of Nebraska, Lincoln) for AOX. EST clones encoding RCCRs were kindly provided from Clemson University (GenBank accession number AW039958), by Chang-Muk Lee (Pohang University of Science and Technology, Korea) (accession number HO7443), Katsuyuki Thomas Yamato (Kyoto University, Japan) (accession number C96086), Jeong-Sheop Shin (Korea University, Korea) (accession number AI563045), and Ross W. Whetten (North Carolina State University) (accession number AA556973). We thank Jean T. Greenberg (University of Chicago) and Helen Ougham and Howard Thomas (Institute of Grassland and Environmental Research, Aberystwyth, Wales) for helpful discussions and Rebecca Alder and Christopher Ball for taking care of plants. This project was funded by grants from the Swiss National Science Foundation (3100-063628 and 3100A0-105389), the National Center of Competence in Research Plant Survival, and the research program of the Swiss National Science Foundation to S.H. and by the Austrian National Science Foundation (P-16097) to B.K.

Received May 29, 2006; revised November 22, 2006; accepted December 5, 2006; published January 19, 2007.

REFERENCES

Altschul, S.F., Madden, T.L., Schaffer, A.A., Zhang, J.H., Zhang, Z., Miller, W., and Lipman, D.J. (1997). Gapped BLAST and PSI-BLAST: A new generation of protein database search programs. Nucleic Acids Res. **25:** 3389–3402.

Becker, D., Kemper, E., Schell, J., and Masterson, R. (1992). New plant binary vectors with selectable markers located proximal to the left T-DNA border. Plant Mol. Biol. **20:** 1195–1197.

Berghold, J., Breuker, K., Oberhuber, M., Hörtensteiner, S., and Kräutler, B. (2002). Chlorophyll breakdown in spinach: On the structure of five nonfluorescent chlorophyll catabolites. Photosynth. Res. **74:** 109–119.

Bradford, M.M. (1976). A rapid and sensitive method for the quantitation of microgram quantities of protein utilizing the principle of protein-dye binding. Anal. Biochem. **72:** 248–254.

Doi, M., Shima, S., Egashira, T., Nakamura, K., and Okayama, S. (1997). New bile pigment excreted by a *Chlamydomonas reinhardtii* mutant: A possible breakdown catabolite of chlorophyll *a*. J. Plant Physiol. **150:** 504–508.

Eckhardt, U., Grimm, B., and Hörtensteiner, S. (2004). Recent advances in chlorophyll biosynthesis and breakdown in higher plants. Plant Mol. Biol. **56:** 1–14.

Emanuelsson, O., Nielsen, H., and Von Heijne, G. (1999). ChloroP, a neural network-based method for predicting chloroplast transit peptides and their cleavage sites. Protein Sci. **8:** 978–984.

Engel, N., Curty, C., and Gossauer, A. (1996). Chlorophyll catabolism in *Chlorella prototheocoides*. VIII. Facts and artefacts. Plant Physiol. Biochem. **34:** 77–83.

Engel, N., Jenny, T.A., Mooser, V., and Gossauer, A. (1991). Chlorophyll catabolism in *Chlorella prototheocoides*. Isolation and structure elucidation of a red bilin derivative. FEBS Lett. **293:** 131–133.

Frankenberg, N., and Lagarias, J.C. (2003). Phycocyanobilin:ferredoxin oxidoreductase of *Anabaena* sp. PCC 7120. J. Biol. Chem. **278:** 9219–9226.

Frankenberg, N., Mukougawa, K., Kohchi, T., and Lagarias, J.C. (2001). Functional genomic analysis of the HY2 family of ferredoxin-dependent bilin reductases from oxygenic photosynthetic organisms. Plant Cell **13:** 965–978.

Ginsburg, S., and Matile, P. (1993). Identification of catabolites of chlorophyll porphyrin in senescent rape cotyledons. Plant Physiol. **102:** 521–527.

Gray, J., Close, P.S., Briggs, S.P., and Johal, G.S. (1997). A novel suppressor of cell death in plants encoded by the *Lls1* gene of maize. Cell **89:** 25–31.

Gray, J., Wardzala, E., Yang, M., Reinbothe, S., Haller, S., and Pauli, F. (2004). A small family of LLS1-related non-heme oxygenases in plants with an origin amongst oxygenic photosynthesizers. Plant Mol. Biol. **54:** 39–54.

Greenberg, J.T., and Ausubel, F.M. (1993). *Arabidopsis* mutants compromised for the control of cellular damage during pathogenesis and aging. Plant J. **4:** 327–341.

Greenberg, J.T., Guo, A., Klessig, D.F., and Ausubel, F.M. (1994). Programmed cell death in plants: A pathogen-triggered response activated coordinately with multiple defense functions. Cell **77:** 551–563.

Hellens, R., Edwards, E.A., Leyland, N.R., Bean, S., and Mullineaux, P.M. (2000). pGreen: A versatile and flexible binary Ti vector for *Agrobacterium*-mediated plant transformation. Plant Mol. Biol. **42:** 819–832.

Hideg, É., Kálai, T., Hideg, K., and Vass, I. (1998). Photoinhibition of photosynthesis in vivo results in singlet oxygen production detection via nitroxide-induced fluorescence quenching in broad bean leaves. Biochemistry **37:** 11405–11411.

Hinder, B., Schellenberg, M., Rodoni, S., Ginsburg, S., Vogt, E., Martinoia, E., Matile, P., and Hörtensteiner, S. (1996). How plants dispose of chlorophyll catabolites. Directly energized uptake of tetrapyrrolic breakdown products into isolated vacuoles. J. Biol. Chem. **271:** 27233–27236.

Hörtensteiner, S. (1999). Chlorophyll breakdown in higher plants and algae. Cell. Mol. Life Sci. **56:** 330–347.

Hörtensteiner, S. (2004). The loss of green color during chlorophyll degradation—A prerequisite to prevent cell death? Planta **219:** 191–194.

Hörtensteiner, S. (2006). Chlorophyll degradation during senescence. Annu. Rev. Plant Biol. **57:** 55–77.

Hörtensteiner, S., Chinner, J., Matile, P., Thomas, H., and Donnison, I.S. (2000a). Chlorophyll breakdown in *Chlorella prototheocoides*: Characterization of degreening and cloning of degreening-related genes. Plant Mol. Biol. **42:** 439–450.

Hörtensteiner, S., Martinoia, E., and Amrhein, N. (1992). Reappearance of hydrolytic activities and tonoplast proteins in the regenerated vacuole of evacuolated protoplasts. Planta **187:** 113–121.

Hörtensteiner, S., Martinoia, E., and Amrhein, N. (1994). Factors affecting the re-formation of vacuoles in evacuolated protoplasts and the expression of the two vacuolar proton pumps. Planta **192:** 395–403.

Hörtensteiner, S., Rodoni, S., Schellenberg, M., Vicentini, F., Nandi, O.I., Qiu, Y.-L., and Matile, P. (2000b). Evolution of chlorophyll degradation: The significance of RCC reductase. Plant Biol. **2:** 63–67.

Hörtensteiner, S., Vicentini, F., and Matile, P. (1995). Chlorophyll breakdown in senescent cotyledons of rape, *Brassica napus* L.: Enzymatic cleavage of phaeophorbide *a in vitro*. New Phytol. **129:** 237–246.

Hörtensteiner, S., Wüthrich, K.L., Matile, P., Ongania, K.-H., and Kräutler, B. (1998). The key step in chlorophyll breakdown in higher plants. Cleavage of pheophorbide *a* macrocycle by a monooxygenase. J. Biol. Chem. **273:** 15335–15339.

Hu, G., Yalpani, N., Briggs, S.P., and Johal, G.S. (1998). A porphyrin pathway impairment is responsible for the phenotype of a dominant disease lesion mimic mutant of maize. Plant Cell **10:** 1095–1105.

Ishikawa, A., Okamoto, H., Iwasaki, Y., and Asahi, T. (2001). A deficiency of coproporphyrinogen III oxidase causes lesion formation in *Arabidopsis*. Plant J. **27:** 89–99.

Isidore, E., Scherrer, B., Chalhoub, B., Feuillet, C., and Keller, B. (2005). Ancient haplotypes resulting from extensive molecular rearrangements in the wheat A genome have been maintained in species of three different ploidy levels. Genome Res. **15:** 526–536.

Kálai, T., Hideg, É., Vass, I., and Hideg, K. (1998). Double (fluorescent and spin) sensors for detection of reactive oxygen species in the thylakoid membrane. Free Radic. Biol. Med. **24:** 649–652.

Kleffmann, T., Russenberger, D., von Zychlinski, A., Christopher, W., Sjolander, K., Gruissem, W., and Baginsky, S. (2004). The *Arabidopsis thaliana* chloroplast proteome reveals pathway abundance and novel protein functions. Curr. Biol. **14:** 354–362.

Klein, M., Burla, B., and Martinoia, E. (2006). The multidrug resistance-associated protein (MRP/ABCC) subfamily of ATP-binding cassette transporters in plants. FEBS Lett. **580:** 1112–1122.

Kräutler, B. (2002). Unravelling chlorophyll catabolism in higher plants. Biochem. Soc. Trans. **30:** 625–630.

Kräutler, B. (2003). Chlorophyll breakdown and chlorophyll catabolites. In The Porphyrin Handbook, K.M. Kadish, K.M. Smith, and R. Guilard, eds (Amsterdam: Elsevier Science), pp. 183–209.

Kräutler, B., and Hörtensteiner, S. (2006). Chlorophyll catabolites and the biochemistry of chlorophyll breakdown. In Chlorophylls and Bacteriochlorophylls: Biochemistry, Biophysics, Functions and Applications, B. Grimm, R. Porra, W. Rüdiger, and H. Scheer, eds (Dordrecht, The Netherlands: Springer-Verlag), pp. 237–260.

Kräutler, B., Jaun, B., Bortlik, K.-H., Schellenberg, M., and Matile, P. (1991). On the enigma of chlorophyll degradation: The constitution of a secoporphinoid catabolite. Angew. Chem. Int. Ed. Engl. **30:** 1315–1318.

Kräutler, B., and Matile, P. (1999). Solving the riddle of chlorophyll breakdown. Acc. Chem. Res. **32:** 35–43.

Kräutler, B., Mühlecker, W., Anderl, M., and Gerlach, B. (1997). Breakdown of chlorophyll: Partial synthesis of a putative intermediary catabolite. Helv. Chim. Acta **80:** 1355–1362.

Krysan, P.J., Young, J.C., and Sussman, M.R. (1999). T-DNA as an insertional mutagen in *Arabidopsis*. Plant Cell **11:** 2283–2290.

Kumar, S., Tamura, K., and Nei, M. (2004). MEGA3: Integrated software for molecular evolutionary genetics analysis and sequence alignment. Brief. Bioinform. **5:** 150–163.

Lorrain, S., Vailleau, F., Balaqué, C., and Roby, D. (2003). Lesion mimic mutants: Keys for deciphering cell death and defense pathways in plants? Trends Plant Sci. **8:** 263–271.

Lu, Y.-P., Li, Z.-S., Drozdowicz, Y.-M., Hörtensteiner, S., Martinoia, E., and Rea, P.A. (1998). AtMRP2, an *Arabidopsis* ATP binding cassette transporter able to transport glutathione *S*-conjugates and chlorophyll catabolites: Functional comparisons with AtMRP1. Plant Cell **10:** 267–282.

Mach, J.M., Castillo, A.R., Hoogstraten, R., and Greenberg, J.T. (2001). The *Arabidopsis* accelerated cell death gene *ACD2* encodes red chlorophyll catabolite reductase and suppresses the spread of disease symptoms. Proc. Natl. Acad. Sci. USA **98:** 771–776.

Martinoia, E., Klein, M., Geisler, M., Sánchez-Fernández, R., and Rea, P.A. (2000). Vacuolar transport of secondary metabolites and xenobiotics. In Vacuolar Compartments. Annual Plant Reviews, D.G. Robinson and J.C. Rogers, eds (Sheffield, UK: Sheffield Academic Press), pp. 221–253.

Matile, P., Hörtensteiner, S., and Thomas, H. (1999). Chlorophyll degradation. Annu. Rev. Plant Physiol. Plant Mol. Biol. **50:** 67–95.

Matile, P., Schellenberg, M., and Peisker, C. (1992). Production and release of a chlorophyll catabolite in isolated senescent chloroplasts. Planta **187:** 230–235.

Meskauskiene, R., Nater, M., Goslings, D., Kessler, F., op den Camp, R., and Apel, K. (2001). FLU: A negative regulator of chlorophyll biosynthesis in *Arabidopsis thaliana*. Proc. Natl. Acad. Sci. USA **98:** 12826–12831.

Morgenstern, B. (2004). DIALIGN: Multiple DNA and protein sequence alignment at BiBiServ. Nucleic Acids Res. **32:** W33–W36.

Mühlecker, W., and Kräutler, B. (1996). Breakdown of chlorophyll: Constitution of nonfluorescing chlorophyll catabolites from senescent cotyledons of the dicot rape. Plant Physiol. Biochem. **34:** 61–75.

Mühlecker, W., Kräutler, B., Moser, D., Matile, P., and Hörtensteiner, S. (2000). Breakdown of chlorophyll: A fluorescent chlorophyll catabolite from sweet pepper (*Capsicum annuum*). Helv. Chim. Acta **83:** 278–286.

Mühlecker, W., Ongania, K.-H., Kräutler, B., Matile, P., and Hörtensteiner, S. (1997). Tracking down chlorophyll breakdown in plants: Elucidation of the constitution of a 'fluorescent' chlorophyll catabolite. Angew. Chem. Int. Ed. Engl. **36:** 401–404.

Müller, T., Moser, S., Ongania, K.-H., Pružinská, A., Hörtensteiner, S., and Kräutler, B. (2006). A divergent path of chlorophyll breakdown in the model plant *Arabidopsis thaliana*. ChemBioChem **7:** 40–42.

Oberhuber, M., Berghold, J., Breuker, K., Hörtensteiner, S., and Kräutler, B. (2003). Breakdown of chlorophyll: A nonenzymatic reaction accounts for the formation of the colorless ''nonfluorescent'' chlorophyll catabolites. Proc. Natl. Acad. Sci. USA **100:** 6910–6915.

Oberhuber, M., Berghold, J., Mühlecker, W., Hörtensteiner, S., and Kräutler, B. (2001). Chlorophyll breakdown—On a nonfluorescent chlorophyll catabolite from spinach. Helv. Chim. Acta **84:** 2615–2627.

Oberhuber, M., and Kräutler, B. (2002). Breakdown of chlorophyll: Electrochemical bilin reduction provides synthetic access to fluorescent chlorophyll catabolites. ChemBioChem **3:** 104–107.

op den Camp, R.G., Przybyla, D., Ochsenbein, C., Laloi, C., Kim, C., Danon, A., Wagner, D., Hideg, E., Gobel, C., Feussner, I., Nater, M., and Apel, K. (2003). Rapid induction of distinct stress responses after release of singlet oxygen in *Arabidopsis*. Plant Cell **15:** 2320–2332.

Pružinská, A., Anders, I., Tanner, G., Roca, M., and Hörtensteiner, S. (2003). Chlorophyll breakdown: Pheophorbide *a* oxygenase is a Rieske-type iron-sulfur protein, encoded by the *accelerated cell death 1* gene. Proc. Natl. Acad. Sci. USA **100:** 15259–15264.

Pružinská, A., Tanner, G., Aubry, S., Anders, I., Moser, S., Müller, T., Ongania, K.-H., Kräutler, B., Youn, J.-Y., Liljegren, S.J., and Hörtensteiner, S. (2005). Chlorophyll breakdown in senescent Arabidopsis leaves: Characterization of chlorophyll catabolites and of chlorophyll catabolic enzymes involved in the degreening reaction. Plant Physiol. **139:** 52–63.

Rodoni, S., Mühlecker, W., Anderl, M., Kräutler, B., Moser, D., Thomas, H., Matile, P., and Hörtensteiner, S. (1997). Chlorophyll breakdown in senescent chloroplasts. Cleavage of pheophorbide *a* in two enzymic steps. Plant Physiol. **115:** 669–676.

Seki, M., et al. (2002). Functional annotation of a full-length *Arabidopsis* cDNA collection. Science **296:** 141–145.

Shioi, Y., Watanabe, K., and Takamiya, K. (1996). Enzymatic conversion of pheophorbide *a* to a precursor of pyropheophorbide *a* in leaves of *Chenopodium album*. Plant Cell Physiol. **37:** 1143–1149.

Sidler, M., Hassa, P., Hasan, S., Ringli, C., and Dudler, R. (1998). Involvement of an ABC transporter in a developmental pathway regulating hypocotyl cell elongation in the light. Plant Cell **10:** 1623–1636.

Strain, H.H., Cope, B.T., and Svec, W.A. (1971). Analytical procedures for the isolation, identification, estimation and investigation of the chlorophylls. Methods Enzymol. **23:** 452–476.

Suzuki, Y., Amano, T., and Shioi, Y. (2006). Characterization and cloning of the chlorophyll-degrading enzyme pheophorbidase from cotyledons of radish. Plant Physiol. **140:** 716–725.

Suzuki, T., and Shioi, Y. (2002). Re-examination of Mg-dechelation reaction in the degradation of chlorophylls using chlorophyllin *a* as substrate. Photosynth. Res. **74:** 217–223.

Takamiya, K., Tsuchiya, T., and Ohta, H. (2000). Degradation pathway(s) of chlorophyll: What has gene cloning revealed? Trends Plant Sci. **5:** 426–431.

Thomas, H., Ougham, H.J., Wagstaff, C., and Stead, A.D. (2003). Defining senescence and death. J. Exp. Bot. **54:** 1127–1132.

Tommasini, R., Vogt, E., Fromenteau, M., Hörtensteiner, S., Matile, P., Amrhein, N., and Martinoia, E. (1998). An ABC transporter of *Arabidopsis thaliana* has both glutathione-conjugate and chlorophyll catabolite transport activity. Plant J. **13:** 773–780.

Tu, S.L., Gunn, A., Toney, M.D., Britt, R.D., and Lagarias, J.C. (2004). Biliverdin reduction by cyanobacterial phycocyanobilin: ferredoxin oxidoreductase (PcyA) proceeds via linear tetrapyrrole radical intermediates. J. Am. Chem. Soc. **126:** 8682–8693.

Wagner, D., Przybyla, D., op den Camp, R., Kim, C., Landgraf, F., Lee, K.P., Würsch, M., Laloi, C., Nater, M., Hideg, E., and Apel, K. (2004). The genetic basis of singlet oxygen-induced stress responses of *Arabidopsis thaliana*. Science **306:** 1183–1185.

Wesley, S.V., et al. (2001). Construct design for efficient, effective and high-throughput gene silencing in plants. Plant J. **27:** 581–590.

Wüthrich, K.L., Bovet, L., Hunziker, P.E., Donnison, I.S., and Hörtensteiner, S. (2000). Molecular cloning, functional expression and characterisation of RCC reductase involved in chlorophyll catabolism. Plant J. **21:** 189–198.

Yao, N., Eisfelder, B.J., Marvin, J., and Greenberg, J.T. (2004). The mitochondrion—An organelle commonly involved in programmed cell death in *Arabidopsis thaliana*. Plant J. **40:** 596–610.

Yao, N., and Greenberg, J.T. (2006). *Arabidopsis* ACCELERATED CELL DEATH2 modulates programmed cell death. Plant Cell **18:** 397–411.

Zhang, S.P., Zhao, J.Q., and Jiang, L.J. (2000). Photosensitized formation of singlet oxygen by phycobiliproteins in neutral aqueous solutions. Free Radic. Res. **33:** 489–496.

11. Conclusion and outlook

During the three years I worked on chl catabolism, I investigated several aspects of a basic plant problem: how to get rid of the extremely phototoxic chl derivatives once chl gets started to be degraded during senescence. Catabolites and enzymes involved in porphyrin degradation were already well described when I started this work. Questions were open regarding the transport processes implicated in chl detoxification and its regulation during leaf senescence.

A major "black" point, still remaining to be determined is which step controls the pathway. Limits of our understanding of chl breakdown regulation are set by our weak knowledge of the degradation of chl apoproteins, two processes intimately associated. Recent studies on mutants of SGR (section 7) or chlases (S. Hörtensteiner and S. Schelbert, personal communication) show a tightly joint mechanism of photosystem/chl degradation. A detailed elucidation of antenna degradation, where most of the chl is located, as well as of PS core degradation would improve a lot our understanding of the limitation of chl degradation. Matile et al. (1999) already pointed to a lack of information concerning the mechanism of photosystem degradation, and converging interests from "pigment and protein researchers" would help understanding these mechanisms. A first report from Kusaba et al. (2007) suggested that the overall degradation might start with a destabilization of the antennas by the conversion of chl *b* to *a*. Even if this hypothesis is correct, the processes of chl conversion from *b* to *a*, as well as the degradation of the antennas, to the dephytylation of chl by a chlase are still poorly described.

In this context, knowledge on the function of SGR or elucidation of SGR-interacting partners would bring critical information on early chl degradation. Regulation might also occur as often suggested at the PAO level (Chung et al., 2006). *pao1* expression analysis by microarray technology might add more information about genes which are regulated in response to accumulation of pheide. It has been shown that *SGR* expression is downregulated in a *pao1* background upon dark-induced senescence, whereas it is upregulated in WT (Park et al., 2007). The mechanism by which PAO absence leads to a down-regulation of *SGR* would highlight an interesting feature of a probable regulation of part of the senescence activated genes via pheide accumulation (Fig. 30). On the other hand, silencing of *SGR* in *pao1* does prevent accumulation of

pheide, suggesting SGR to be upstream of PAO in the pathway (Aubry et al., 2008). A feedback mechanism of degradation, avoiding pheide accumulation by stopping further photosystem degradation might exist. Infiltrating pheide into plants or an inducible PAO silencing system would help to understand the exact regulation mechanism between SGR and PAO.

Of the chl catabolic reactions PAO remains to date the only step of chl breakdown which if absent entirely stops the process. All other steps are either not well described or involve reactions, whose absence only cause a partial retention of chl or its catabolites. PAO confers one of the few proofs of an unique pathway in the chloroplast to detoxify chl. Occurrence of an other pathway as suggested in the past (Takamiya et al., 2000) is really unlikely based on actual data.

Besides the enzymatic reactions taking place, which are in most known cases encoded by single copy genes, it is clear that transport of chl catabolites across the chloroplast envelope and the tonoplast in both cases involves a set of different transporters. Still it is likely that individual transporters (*At*WBC23 for the chlp, *At*MRP2 for the tonoplast) are major contributors to overall transport. The known broad substrate specificity of ABC transporters might be understood more as a selective advantage than a consequence of unspecificity. Chl derivatives are occurring mainly during senescence, and transport has to happen in a fast way in order not to slow-down the detoxification process. In *Arabidopsis*, within about three days, almost all of the 1 mg chl/g fresh weight present in green leaves is translocated to the vacuole. Knowing that 1 mg leaf material corresponds to 1.10^7 cells, one can roughly calculate that every cell has to convert 0.1 pmol chl in 3 days, meaning roughly 2.10^5 molecules of chl per second have to be exported from the chloroplast and sent to the vacuole. These amounts are most probably traces in comparison to the degradation products of the photosystem complex proteins. However a rather quick and efficient transporter system is needed for catabolite transport not to induce phototoxic effects. In the special case of the HR response, where chl is degraded in localized areas, PAO with a whole set of other genes is known to trigger the response, and it would be interesting to check HR response in *wbc23* mutants for example.

In the biosynthetic pathways of some secondary metabolites, it has been shown that all the enzymes involved are working in complexes to channel the substrates and to avoid loss of intermediates (Jorgensen et al., 2005). The proof of an interaction of PAO and RCCR is rather weak (Pružinská et al., 2007) but it could be imagined that

chlide is also taken through a MCS-PAO-RCCR complex which might even interact with WBC23 to directly export pFCC from the plastid. Channelling of the chl intermediates would allow a safer processing of the phototoxins and may also facilitate a regulation of degradation.

As described all along this study, chl breakdown during senescence is rather well understood. However, at the steady-state level, *i.e.* before senescence, parts of photosystems get recycled and chl biosynthesis genes keep basal expression levels, indicating basal chl biosynthesis. From an other point of view, plants are adapting to different light conditions by changing the size of their antennas, and this in some situation might also need a degradation of chl-protein complexes (Ballottari et al., 2007). Partial degradation/recycling of photosystems, either the cores or the antennas, requires a mechanism by which chl is degraded/recycled, but which is not senescence-associated. So far, no evidence has been reported for an involvement of the PAO pathway in this process, or not even than such a process is going on. NCCs were not yet detected in green tissues. However, the severity of the *pao1* lesion-mimic phenotype seems correlated with the age of the tissue, suggesting minimal pheide accumulation before senescence, maybe due to a premature initiation of early chl degradation. Experiments correlating pheide accumulation with the age of the plants in *pao1* should be performed to confirm such an hypothesis. Chl degradation in green tissue is a physiological need, as anabolism and catabolism are coexisting. Conflicting results of chl half-life times in *Synechocystis* (more than 200 h) or higher plants (6 to 80 h) would need some more experiments to evaluate the real impact of chl turnover for the whole porphyrin metabolism regulation (Stobart and Hendry, 1984; Hendry and Stobart, 1986; Vavilin and Vermaas, 2007).

In conclusion, chl and photosystems allow plants to convert light energy to chemical energy during photosynthesis, the basic process for all life on earth. However the photoreactive property of chl is a sword of Damocles (Timaeus of Tauromenium, 350 BC), and soon turns into a threat when chl is released from its apoproteins. The complexity of the chl detoxification process underlines major selective advantage it gives to a photosynthesizing organisms to carefully degrade pigments.

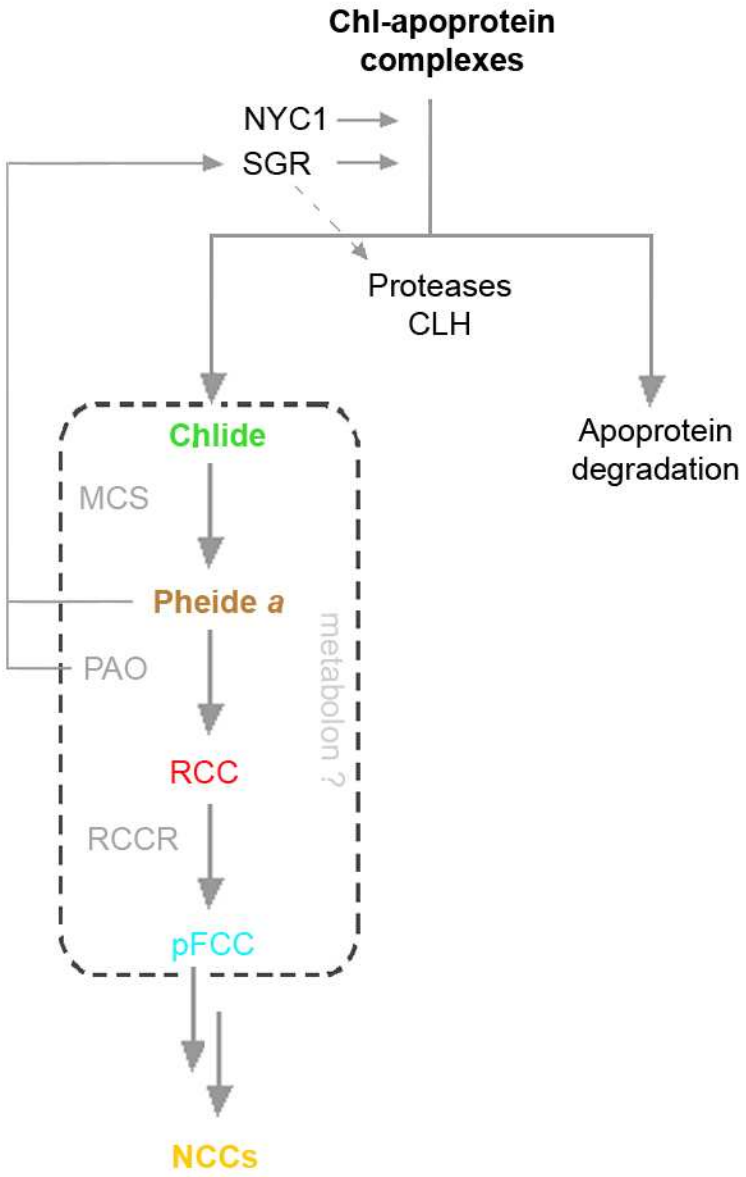

Figure 30. Proposed model for regulation of Chl breakdown. The scheme is based on available data from mutants defective in *SGR* (Park et al., 2007, Aubry et al., 2008) and *NYC* (Kusaba et al., 2007). For abbreviations, see text.

12. References

Abbott BL (2003) ABCG2 (BCRP) expression in normal and malignant hematopoietic cells. Hematol. Oncol. **21:** 115-130

Adam Z, Clarke AK (2002) Cutting edge of chloroplast proteolysis. Trends Plant Sci. **7:** 451-456

Adamska I, Lindahl M, RoobolBoza M, Andersson B (1996) Degradation of the light-stress protein is mediated by an ATP-independent, serine-type protease under low-light conditions. Eur. J. Biochem. **236:** 591-599

Ajioka RS, Phillips JD, Weiss RB, Dunn DM, Kushner JP (2006) HAMP and HVJ as candidate modifier genes in typel hereditary hemochromatosis with high iron burden and in porphyria cutanea tarda (PCT). Blood **108:** 444A

Ankele E, Kindgren P, Pesquet E, Strand A (2007) *In vivo* visualization of Mg-protoporphyrinIX, a coordinator of photosynthetic gene expression in the nucleus and the chloroplast. Plant Cell **19:** 1964-1979

Apel K, Hirt H (2004) Reactive oxygen species: Metabolism, oxidative stress, and signal transduction. Annu. Rev. Plant Biol. **55:** 373-399

Armstead I, Donnison I, Aubry S, Harper J, Hörtensteiner S, James C, Mani J, Moffet M, Ougham H, Roberts L, Thomas A, Weeden N, Thomas H, King I (2006) From crop to model to crop: identifying the genetic basis of the staygreen mutation in the *Lolium*/*Festuca* forage and amenity grasses. New Phytol. **172:** 592-597

Armstead I, Donnison I, Aubry S, Harper J, Hörtensteiner S, James C, Mani J, Moffet M, Ougham H, Roberts L, Thomas A, Weeden N, Thomas H, King I (2007) Cross-species identification of Mendel's *I* locus. Science **315:** 73

Asada K (2006) Production and scavenging of reactive oxygen species in chloroplasts and their functions. Plant Physiol. **141:** 391-396

Aubry S, Mani J, Hörtensteiner S (2008) Stay-green protein, defective in Mendel's green cotyledon mutant, acts independent and upstream of pheophorbide a oxygenase in the chlorophyll catabolic pathway. Plant Mol. Biol. **PMID: 18301989**

Baena-Gonzalez E, Aro EM (2002) Biogenesis, assembly and turnover of photosystem II units. Phil. Trans. R. Soc. Lond. B **357:** 1451-1459

Bahmaei M, Sabbaghian ES, Farzadkish E (2005) Development of a method for chlorophyll removal from canola oil using mineral acids. J. Am. Oil Chem. Soc. **82:** 679-684

Ballottari M, Dall'Osto L, Morosinotto T, Bassi R (2007) Contrasting behavior of higher plant photosystem I and II antenna systems during acclimation. J. Biol. Chem. **282:** 8947-8958

Benedetti CE, Costa CL, Turcinelli SR, Arruda P (1998) Differential expression of a novel gene in response to coronatine, methyl jasmonate, and wounding in the *coi1* mutant of *Arabidopsis*. Plant Physiol. **116:** 1037-1042

Bollivar DW, Beale SI (1996) The chlorophyll biosynthetic enzyme Mg-protoporphyrin IX monomethyl ester (oxidative) cyclase characterization and partial purification from *Chlamydomonas reinhardti*i and *Synechocystis* sp. PCC 6803). Plant Physiol. **112:** 105-114

Brehelin C, Kessler F, van Wijk KJ (2007) Plastoglobulies: versatile lipoprotein particles in plastids. Trends Plant Sci. **12:** 260-266

Buchanan-Wollaston V, Earl S, Harrison E, Mathas E, Navabpour S, Page T, Pink D (2003) The molecular analysis of leaf senescence - a genomics approach. Plant Biotech. J. **1:** 3-22

Buchanan-Wollaston V, Page T, Harrison E, Breeze E, Lim PO, Nam HG, Lin JF, Wu SH, Swidzinski J, Ishizaki K, Leaver CJ (2005) Comparative transcriptome analysis reveals significant differences in gene expression and signalling pathways between developmental and dark/starvation-induced senescence in *Arabidopsis*. Plant J. **42:** 567-585

Chen QJ, Zhou HM, Chen J, Wang XC (2006) A Gateway-based platform for multigene plant transformation. Plant Mol. Biol. **62:** 927-936

Chen S, Sanchez-Fernandez R, Lyver ER, Dancis A, Rea PA (2007) Functional characterization of *At*ATM1, *At*ATM2, and *At*ATM3, a subfamily of *Arabidopsis* half-molecule ATP-binding cassette transporters implicated in iron homeostasis. J. Biol. Chem. **282:** 21561-21571

Chung DW, Pružinská A, Hörtensteiner S, Ort DR (2006) The role of pheophorbide *a* oxygenase expression and activity in the canola green seed problem. Plant Physiol. **142:** 88-97

Csere P, Lill R, Kispal G (1998) Identification of a human mitochondrial ABC transporter, the functional orthologue of yeast Atm1p. FEBS Lett. **441:** 266-270

Di Bartolo ND, Booth P, Locher K, Hvorup R, Findlay H (2006) In vitro folding and assembly of the ABC transporter, BtuCD. FASEB J. **20:** A1368-A1368

Egner R, Kuchler K (1996) The yeast multidrug transporter Pdr5 of the plasma membrane is ubiquitinated prior to endocytosis and degradation in the vacuole. FEBS Lett. **378:** 177-181

Emborg TJ, Walker JM, Noh B, Vierstra RD (2006) Multiple heme oxygenase family members contribute to the biosynthesis of the phytochrome chromophore in *Arabidopsis*. Plant Physiol. **140:** 856-868

Engel N, Jenny TA, Mooser V, Gossauer A (1991) Chlorophyll catabolism in *Chlorella prototheco*ides. Isolation and structure elucidation of a red bilin derivative. FEBS Lett. **293:** 131-133

Forsberg J, Strom J, Kieselbach T, Larsson H, Alexciev K, Engstrom A, Akerlund HE (2005) Protease activities in the chloroplast capable of cleaving an LHCII N-terminal peptide. Physiol. Plant. **123:** 21-29

Frankenberg N, Mukougawa K, Kohchi T, Lagarias JC (2001) Functional genomic analysis of the HY2 family of ferredoxin-dependent bilin reductases from oxygenic photosynthetic organisms. Plant Cell **13:** 965-978

Fryer MJ, Oxborough K, Mullineaux PM, Baker NR (2002) Imaging of photo-oxidative stress responses in leaves. J. Exp. Bot. **53:** 1249-1254

Funamoto Y, Yamauchi N, Shigyo M (2006) Control of isoperoxidases involved in chlorophyll degradation of stored broccoli (*Brassica oleracea*) florets by heat treatment. J. Plant Physiol. **163:** 141-146

Gadsby DC, Vergani P, Csanady L (2006) The ABC protein turned chloride channel whose failure causes cystic fibrosis. Nature **440:** 477-483

Gan S, Amasino RM (1997) Making sense of senescence. Molecular genetic regulation and manipulation of leaf senescence. Plant Physiol. **113:** 313-319

Gan SS, Amasino RM (1995) Inhibition of leaf senescence by autoregulated production of cytokinin. Science **270:** 1986-1988

Garcia O, Bouige P, Forestier C, Dassa E (2004) Inventory and comparative analysis of rice *Arabidopsis* ATP-binding cassette (ABC) systems. J. Mol. Biol. **343:** 249-265

Gaude N, Brehelin C, Tischendorf G, Kessler F, Dörmann P (2007) Nitrogen deficiency in *Arabidopsis* affects galactolipid composition and gene expression and results in accumulation of fatty acid phytyl esters. Plant J. **49:** 729-739

Gray J, Janick-Bruckner D, Bruckner B, Close PS, Johal GS (2002) Light-dependent death of maize *lls1* cells is mediated by mature chloroplasts. Plant Physiol. **130:** 1894-1907

Gray J, Wardzala E, Yang M, Reinbothe S, Haller S, Pauli F (2004) A small family of LLS1-related non-heme oxygenases in plants with an origin amongst oxygenic photosynthesizers. Plant Mol. Biol. **54:** 39-54

Greenberg JT, Ausubel FM (1993) *Arabidopsis* mutants compromised for the control of cellular damage during pathogenesis and aging. Plant J. **4:** 327-341

Greenberg JT, Guo A, Klessig DF, Ausubel FM (1994) Programmed cell death in plants: a pathogen-triggered response activated coordinately with multiple defense functions. Cell **77:** 551-563

Hardwick LJA, Velamakanni S, van Veen HW (2007) The emerging pharmacotherapeutic significance of the breast cancer resistance protein (ABCG2). Brit. J. Pharm. **151:** 163-174

Harpaz-Saad S, Azoulay T, Arazi T, Ben-Yaakov E, Mett A, Shiboleth YM, Hörtensteiner S, D. G, Gal-On A, Goldschmidt EE, Eyal Y (2007) Chlorophyllase is a rate-limiting enzyme in chlorophyll catabolism and is posttranslationally regulated. Plant Cell **19:** 1007-1022

Hayashi Y, Hayashi M, Hayashi H, Hara-Nishimura I, Nishimura M (2001) Direct interaction between glyoxysomes and lipid bodies in cotyledons of the *Arabidopsis thaliana* ped1 mutant. Protoplasma **218:** 83-94

Heddad M, Adamska I (2002) The evolution of light stress proteins in photosynthetic organisms. Comp. Func. Gen. **3:** 504-510

Heddad M, Noren H, Reiser V, Dunaeva M, Andersson B, Adamska I (2006) Differential expression and localization of early light-induced proteins in *Arabidopsis*. Plant Physiol. **142:** 75-87

Helmerhorst E, Stokes GB (1980) Microcentrifuge desalting - a rapid, quantitative method for desalting small amounts of protein. Anal. Biochem. **104:** 130-135

Hendry GAF, Houghton JD, Brown SB (1987) Chlorophyll degradation. A biological enigma. New Phytol. **107:** 255-302

Hendry GAF, Stobart AK (1986) Chlorophyll turnover in greening barley. Phytochemistry **25:** 2735-2737

Hilditch P, Thomas H, Rogers LJ (1986) Two processes for the breakdown of the Q_B protein of chloroplasts. FEBS Lett. **208:** 313-316

Hilditch PI, Thomas H, Thomas BJ, Rogers LJ (1989) Leaf senescence in a non-yellowing mutant of *Festuca pratensis*: proteins of photosystem II. Planta **177:** 265-272

Himelblau E, Amasino RM (2001) Nutrients mobilized from leaves of *Arabidopsis thaliana* during leaf senescence. J. Plant Phys. **158:** 1317-1323

Hinder B, Schellenberg M, Rodoni S, Ginsburg S, Vogt E, Martinoia E, Matile P, Hörtensteiner S (1996) How plants dispose of chlorophyll catabolites. Directly energized uptake of tetrapyrrolic breakdown products into isolated vacuoles. J. Biol. Chem. **271:** 27233-27236

Hoober JK, Eggink LL, Chen M (2007) Chlorophylls, ligands and assembly of light-harvesting complexes in chloroplasts. Photosynth. Res. **94:** 387-400

Horn R, Paulsen H (2004) Early steps in the assembly of light-harvesting chlorophyll *a*/*b* complex - Time-resolved fluorescence measurements. J. Biol. Chem. **279:** 44400-44406

Hörtensteiner S (1998) NCC malonyltransferase catalyses the final step of chlorophyll breakdown in rape (*Brassica napus*). Phytochemistry **49:** 953-956

Hörtensteiner S (1999) Chlorophyll breakdown in higher plants and algae. Cell. Mol. Life Sci. **56:** 330-347

Hörtensteiner S (2004) The loss of green color during chlorophyll degradation - a prerequisite to prevent cell death? Planta **219:** 191-194

Hörtensteiner S (2006) Chlorophyll degradation during senescence. Annu. Rev. Plant Biol. **57:** 55-77

Hörtensteiner S, Chinner J, Matile P, Thomas H, Donnison IS (2000) Chlorophyll breakdown in *Chlorella protothecoides*: characterization of degreening and cloning of degreening-related genes. Plant Mol. Biol. **42:** 439-450

Hörtensteiner S, Feller U (2002) Nitrogen metabolism and remobilization during senescence. J. Exp. Bot. **53:** 927-937

Hörtensteiner S, Vicentini F, Matile P (1995) Chlorophyll breakdown in senescent cotyledons of rape, *Brassica napus* L.: enzymatic cleavage of phaeophorbide *a* *in vitro*. New Phytol. **129:** 237-246

Hörtensteiner S, Wüthrich KL, Matile P, Ongania K-H, Kräutler B (1998) The key step in chlorophyll breakdown in higher plants. Cleavage of pheophorbide *a* macrocycle by a monooxygenase. J. Biol. Chem. **273:** 15335-15339

Horton P, Ruban AV, Walters RG (1996) Regulation of light harvesting in green plants. Annu. Rev. Plant Physiol. Plant Mol. Biol. **47:** 655-684

Hu G, Yalpani N, Briggs SP, Johal GS (1998) A porphyrin pathway impairment is responsible for the phenotype of a dominant disease lesion mimic mutant of maize. Plant Cell **10:** 1095-1105

Hvorup RN, Goetz BA, Niederer M, Hollenstein K, Perozo E, Locher KP (2007) Asymmetry in the structure of the ABC transporter-binding protein complex BtuCD-BtuF. Science **317:** 1387-1390

Ischebeck T, Zbierzak AM, Kanwischer M, Dörmann P (2006) A salvage pathway for phytol metabolism in *Arabidopsis*. J. Biol. Chem. **281:** 2470-2477

Jacob-Wilk D, Holland D, Goldschmidt EE, Riov J, Eyal Y (1999) Chlorophyll breakdown by chlorophyllase: isolation and functional expression of the Chlase1 gene from ethylene-treated Citrus fruit and its regulation during development. Plant J. **20:** 653-661

Jiang CZ, Rodermel SR, Shibles RM (1993) Photosynthesis, Rubisco activity and amount, and their regulation by transcription in senescing soybean leaves. Plant Physiol. **101:** 105-112

Jiang HW, Li MR, Liang NB, Yan HB, Wei YL, Xu X, Liu JF, Xu Z, Chen F, Wu GJ (2007) Molecular cloning and function analysis of the stay green gene in rice. Plant J. **52:** 197-209

Jonker JW, Buitelaar M, Wagenaar E, van der Valk MA, Scheffer GL, Scheper RJ, Plösch T, Kuipers F, Oude Elferink RPJ, Rosing H, Beijnen JH, Schinkel AH (2002) The breast cancer resistance protein protects against a major chlorophyll-derived dietary phototoxin and protoporphyria. Proc. Natl. Acad. Sci. USA **99:** 15649-15654

Jorgensen K, Rasmussen AV, Morant M, Nielsen AH, Bjarnholt N, Zagrobelny M, Bak S, Moller BL (2005) Metabolon formation and metabolic channeling in the biosynthesis of plant natural products. Curr. Opin. Plant Biol. **8:** 280-291

Kariola T, Brader G, Li J, Palva ET (2005) Chlorophyllase 1, a damage control enzyme, affects the balance between defense pathways in plants. Plant Cell **17:** 282-294

Kemp S, Wanders RJA (2007) X-linked adrenoleukodystrophy: Very long-chain fatty acid metabolism, ABC half-transporters and the complicated route to treatment. Mol. Gen. Metab. **90:** 268-276

Keskitalo J, Bergquist G, Gardestrom P, Jansson S (2005) A cellular timetable of autumn senescence. Plant Physiol. **139:** 1635-1648

Kim DY, Bovet L, Noh EW, Martinoia E, Lee Y (2007) AtATM3 is involved in heavy metal resistance in *Arabidopsis*. Plant Physiol. **145:** 290-290

Kim J, Eichacker LA, Rüdiger W, Mullet JE (1994) Chlorophyll regulates accumulation of the plastid-encoded chlorophyll proteins P700 and D1 by increasing apoprotein stability. Plant Physiol. **104:** 907-916

Kingston-Smith AH, Thomas H, Foyer CH (1997) Chlorophyll *a* fluorescence, enzyme and antioxidant analyses provide evidence for the operation of alternative electron sinks during leaf senescence in a *stay-green* mutant of *Festuca pratensis*. Plant Cell Environ. **20:** 1323-1337

Klein M, Burla B, Martinoia E (2006) The multidrug resistance-associated protein (MRP/ABCC) subfamily of ATP-binding cassette transporters in plants. FEBS Lett. **580:** 1112-1122

Klein M, Geisler M, Suh SJ, Kolukisaoglu HU, Azevedo L, Plaza S, Curtis MD, Richter A, Weder B, Schulz B, Martinoia E (2004) Disruption of *AtMRP4*, a guard cell plasma membrane ABCC-type ABC transporter, leads to deregulation of stomatal opening and increased drought susceptibility. Plant J. **39:** 219-236

Klein M, Martinoia E, Weissenböck G (1998) Directly energized uptake of beta-estradiol 17-(beta-D-glucuronide) in plant vacuoles is strongly stimulated by glutathione conjugates. J. Biol. Chem. **273:** 262-270

Komenda J, Barker M, Kuvikova S, de Vries R, Mullineaux CW, Tichy M, Nixon PJ (2006) The FtsH protease slr0228 is important for quality control of photosystem II in the thylakoid membrane of *Synechocystis* sp PCC 6803. J. Biol. Chem. **281:** 1145-1151

Kräutler B, Jaun B, Bortlik K-H, Schellenberg M, Matile P (1991) On the enigma of chlorophyll degradation: the constitution of a secoporphinoid catabolite. Angew. Chem. Int. Ed. Engl. **30:** 1315-1318

Kräutler B, Mühlecker W, Anderl M, Gerlach B (1997) Breakdown of chlorophyll: partial synthesis of a putative intermediary catabolite. Helv. Chim. Acta **80:** 1355-1362

Kreuz K, Tommasini R, Martinoia E (1996) Old enzymes for a new job. Herbicide detoxification in plants. Plant Physiol. **111:** 349-353

Krishnamurthy P, Schuetz JD (2005) The ABC transporter ABCG2/BCRP: role in hypoxia mediated survival. Biometals **18:** 349-358

Krishnamurthy P, Schuetz JD (2006) Role of ABCG2/BCRP in biology and medicine. Annu. Rev. Pharmacol. Toxicol. **46:** 381-410

Krishnamurthy P, Xie T, Schuetz JD (2007) The role of transporters in cellular heme and porphyrin homeostasis. Pharmacol. Ther. **114:** 345-358

Kruse E, Mock HP, Grimm B (1995) Reduction of coproporphyrinogen oxidase level by antisense RNA synthesis leads to deregulated gene expression of plastid proteins and affects the oxidative defense system. EMBO J. **14:** 3712-3720

Küchler M, Decker S, Hörmann F, Soll J, Heins L (2002) Protein import into chloroplasts involves redox-regulated proteins. EMBO J. **21:** 6136-6145

Kusaba M, Ito H, Morita R, Iida S, Sato Y, Fujimoto M, Kawasaki S, Tanaka R, Hirochika H, Nishimura M, Tanaka A (2007) Rice NON-YELLOW COLORING1 is involved in light-harvesting complex II and grana degradation during leaf senescence. Plant Cell **19:** 1362-1375

Kushnir S, Babiychuk E, Storozhenko S, Davey MW, Papenbrock J, De Rycke R, Engler G, Stephan UW, Lange H, Kispal G, Lill R, Van Montagu M (2001) A mutation of the mitochondrial ABC transporter Sta1 leads to dwarfism and chlorosis in the *Arabidopsis* mutant starik. Plant Cell **13:** 89-100

Latunde-Dada G, Laftah A, Shayeghi M, Simpson R, McKie A (2007) Expression and regulation of HCP1 and ABCG2 in mice tissues and human cultured cells. Am. J. Hematol. **82:** 570-570

Lee K (1999) Benzene-induced uncoupling of naphthalene dioxygenase activity and enzyme inactivation by production of hydrogen peroxide. J. Bacteriol. **181:** 2719-2725

Liao Y, An K, Zhou X, Chen WJ, Kuai BK (2007) AtCLH2, a typical but possibly distinctive chlorophyllase gene in *Arabidopsis*. J. Integ. Plant Biol. **49:** 531-539

Lill R, Diekert K, Kaut A, Lange H, Pelzer W, Prohl C, Kispal G (1999) The essential role of mitochondria in the biogenesis of cellular iron-sulfur proteins. Biol. Chem. **380:** 1157-1166

Lim PO, Woo HR, Nam HG (2003) Molecular genetics of leaf senescence in *Arabidopsis*. Trends Plant Sci. **8:** 272-278

Lin JF, Wu SH (2004) Molecular events in senescing *Arabidopsis* leaves. Plant J. **39:** 612-628

Lorrain S, Vailleau F, Balaqué C, Roby D (2003) Lesion mimic mutants: keys for deciphering cell death and defense pathways in plants? Trends Plant Sci. **8:** 263-271

Lu Y-P, Li Z-S, Drozdowicz Y-M, Hörtensteiner S, Martinoia E, Rea PA (1998) AtMRP2, an *Arabidopsis* ATP binding cassette transporter able to transport glutathione *S*-conjugates and chlorophyll catabolites: functional comparisons with AtMRP1. Plant Cell **10:** 267-282

Mach JM, Castillo AR, Hoogstraten R, Greenberg JT (2001) The *Arabidopsis*-accelerated cell death gene ACD2 encodes red chlorophyll catabolite reductase and suppresses the spread of disease symptoms. Proc. Natl. Acad. Sci. USA **98:** 771-776

Mach JMG, J.T. (2004) Free Radicals and Oxidative Stress. *In* LD Nooden, ed, Plant Cell Death Processes. Elsevier, pp 203-214

Mackenzie SM, Howells AJ, Cox GB, Ewart GD (2000) Sub-cellular localisation of the White/Scarlet ABC transporter to pigment granule membranes within the compound eye of Drosophila melanogaster. Genetica **108:** 239-252

Mannucci L, Guardamagna O, Bertucci P, Pisciotta L, Liberatoscioli L, Bertolini S, Irace C, Gnasso A, Federici G, Cortese C (2007) Beta-sitosterolaemia: a new nonsense mutation in the ABCG5 gene. European Journal of Clinical Investigation **37:** 997-1000

Matile P (1997) The vacuole and cell senecence. *In* JA Callow, ed, Advances in Botanical Research, Vol 25
Academic Press, New York, pp 87-112

Matile P, Ginsburg S, Schellenberg M, Thomas H (1988) Catabolites of chlorophyll in senescing barley leaves are localized in the vacuoles of mesophyll cells. Proc. Natl. Acad. Sci. USA **85:** 9529-9532

Matile P, Hörtensteiner S, Thomas H (1999) Chlorophyll degradation. Annu. Rev. Plant Physiol. Plant Mol. Biol. **50:** 67-95

Matile P, Schellenberg M (1996) The cleavage of pheophorbide *a* is located in the envelope of barley gerontoplasts. Plant Physiol. Biochem. **34:** 55-59

Matile P, Schellenberg M, Peisker C (1992) Production and release of a chlorophyll catabolite in isolated senescent chloroplasts. Planta **187:** 230-235

Mentewab A, Stewart CN (2005) Overexpression of an *Arabidopsis thaliana* ABC transporter confers kanamycin resistance to transgenic plants. Nature Biotech. **23:** 1177-1180

Meyer A, Eskandari S, Grallath S, Rentsch D (2006) AtGAT1, a high affinity transporter for gamma-aminobutyric acid in *Arabidopsis thaliana*. J. Mol. Biol. **281:** 7197-7204

Mochizuki N, Brusslan JA, Larkin R, Nagatani A, Chory J (2001) *Arabidopsis genomes uncoupled 5* (*GUN5*) mutant reveals the involvement of Mg-chelatase H subunit in plastid-to-nucleus signal transduction. Proc. Natl. Acad. Sci. USA **98:** 2053-2058

Mock HP, Grimm B (1997) Expression of uroporphyrinogen decarboxylase antisense RNA in tobacco leads to reduction of UROD protein, but also affects activities of other enzymes involved in tetrapyrrole biosynthesis. Plant Physiol. **113:** 1101-1112

Molina A, Volrath S, Guyer D, Maleck K, Ryals J, Ward E (1999) Inhibition of protoporphyrinogen oxidase expression in *Arabidopsis* causes a lesion-mimic phenotype that induces systemic acquired resistance. Plant J. **17:** 667-678

Mortz E, Krogh TN, Vorum H, Gorg A (2001) Improved silver staining protocols for high sensitivity protein identification using matrix-assisted laser desorption/ionization-time of flight analysis. Proteomics **1:** 1359-1363

Moser D, Matile P (1997) Chlorophyll breakdown in ripening fruits of *Capsicum annuum*. J. Plant Physiol. **150:** 759-761

Moulin M, Smith AG (2005) Regulation of tetrapyrrole biosynthesis in higher plants. Biochem. Soc. Trans. **33:** 737-742

Müller T, Moser S, Ongania K-H, Pružinská A, Hörtensteiner S, Kräutler B (2006) A divergent path of chlorophyll breakdown in the model plant *Arabidopsis thaliana*. ChemBioChem **7:** 40-42

Murgia I, Tarantino D, Vannini C, Bracale M, Carravieri S, Soave C (2004) *Arabidopsis thaliana* plants overexpressing thylakoidal ascorbate peroxidase show increased resistance to paraquat-induced photooxidative stress and to nitric oxide-induced cell death. Plant Physiol. **38:** 940-953

Nelson N, Yocum CF (2006) Structure and function of photosystems I and II. Ann. Rev. Plant Biol. **57:** 521-565

Oberhuber M, Berghold J, Breuker K, Hörtensteiner S, Kräutler B (2003) Breakdown of chlorophyll: a nonenzymatic reaction accounts for the formation of the colorless "nonfluorescent" chlorophyll catabolites. Proc. Natl. Acad. Sci. USA **100:** 6910-6915

Otsu CT, daSilva I, de Molfetta JB, da Silva LR, de Almeida-Engler J, Engler G, Torraca PC, Goldman GH, Goldman MHS (2004) NtWBC1, an ABC transporter gene specifically expressed in tobacco reproductive organs. J. Exp. Bot. **55:** 1643-1654

Ougham HJ, Morris P, Thomas H (2005) The colors of autumn leaves as symptoms of cellular recycling and defenses against environmental stresses. *In* Current Topics Development Biology, Vol 66, pp 135-160

Panikashvili D, Savaldi-Goldstein S, Mandel T, Yifhar T, Franke RB, Hofer R, Schreiber L, Chory J, Aharoni A (2007) The *Arabidopsis* DESPERADO/AtWBC11 transporter is required for cutin and wax secretion. Plant Physiol. **145:** 1345-1360

Papenbrock J, Mishra S, Mock HP, Kruse E, Schmidt EK, Petersmann A, Braun HP, Grimm B (2001) Impaired expression of the plastidic ferrochelatase by antisense RNA synthesis leads to a necrotic phenotype of transformed tobacco plants. Plant J. **28:** 41-50

Park SY, Yu JW, Park JS, Li J, Yoo SC, Lee NY, Lee SK, Jeong SW, Seo HS, Koh HJ, Jeon JS, Park YI, Paek NC (2007) The senescence-induced staygreen protein regulates chlorophyll degradation. Plant Cell **19:** 1649-1664

Parthier B (1988) Gerontoplasts - The yellow end in ontogenesis of chloroplasts. Endocyt. C. Res. **5:** 163-190

Paterson JK, Shukla S, Black CM, Tachiwada T, Garfield S, Wincovitch S, Ernst DN, Agadir A, Li X, Ambudkar SV, Szakacs G, Akiyama SI, Gottesman

MM (2007) Human ABCB6 localizes to both the outer mitochondrial membrane and the plasma membrane. Biochemistry **46:** 9443-9452

Pighin JA, Zheng HQ, Balakshin LJ, Goodman IP, Western TL, Jetter R, Kunst L, Samuels AL (2004) Plant cuticular lipid export requires an ABC transporter. Science **306:** 702-704

Pružinská A, Anders I, Aubry S, Schenk N, Tapernoux-Lüthi E, Müller T, Kräutler B, Hörtensteiner S (2007) In vivo participation of red chlorophyll catabolite reductase in chlorophyll breakdown. Plant Cell **19:** 369-387

Pružinská A, Anders I, Tanner G, Roca M, Hörtensteiner S (2003) Chlorophyll breakdown: pheophorbide *a* oxygenase is a Rieske-type iron-sulfur protein, encoded by the *accelerated cell death 1* gene. Proc. Natl. Acad. Sci. USA **100:** 15259-15264

Pružinská A, Tanner G, Aubry S, Anders I, Moser S, Müller T, Ongania K-H, Kräutler B, Youn J-Y, Liljegren SJ, Hörtensteiner S (2005) Chlorophyll breakdown in senescent *Arabidopsis* leaves: characterization of chlorophyll catabolites and of chlorophyll catabolic enzymes involved in the degreening reaction. Plant Physiol. **139:** 52-63

Rea PA (2005) A farewell to bacterial ARMs? Nature Biotech. **23:** 1085-1087

Rea PA (2007) Plant ATP-binding cassette transporters. Annu. Rev. Plant Biol. **58:** 347-375

Rea PA, Li Z-S, Lu Y-P, Drozdowicz YM, Martinoia E (1998) From vacuolar GS-X pumps to multispecific ABC transporters. Annu. Rev. Plant Physiol. Plant Mol. Biol. **49:** 727-760

Reinbothe S, Quigley F, Gray J, Schemenewitz A, Reinbothe C (2004) Identification of plastid envelope proteins required for import of protochlorophyllide oxidoreductase A into the chloroplast of barley. Proc. Natl. Acad. Sci. USA **101:** 2197-2202

Ren GD, An K, Liao Y, Zhou X, Cao YJ, Zhao HF, Ge XC, Kuai BK (2007) Identification of a novel chloroplast protein AtNYE1 regulating chlorophyll degradation during leaf senescence in *Arabidopsis*. Plant Physiol. **144:** 1429-1441

Robey RW, Steadman K, Polgar O, Morisaki K, Blayney M, Mistry P, Bates SE (2004) Pheophorbide a is a specific probe for ABCG2 function and inhibition. Cancer Res. **64:** 1242-1246

Rodoni S, Mühlecker W, Anderl M, Kräutler B, Moser D, Thomas H, Matile P, Hörtensteiner S (1997) Chlorophyll breakdown in senescent chloroplasts. Cleavage of pheophorbide *a* in two enzymic steps. Plant Physiol. **115:** 669-676

Rodoni S, Vicentini F, Schellenberg M, Matile P, Hörtensteiner S (1997) Partial purification and characterization of red chlorophyll catabolite reductase, a stroma protein involved in chlorophyll breakdown. Plant Physiol. **115:** 677-682

Rommens CM (2006) Kanamycin resistance in plants: an unexpected trait controlled by a potentially multifaceted gene. Trends in Plant Science **11:** 317-319

Rossini S, Casazza AP, Engelmann ECM, Havaux M, Jennings RC, Soave C (2006) Suppression of both ELIP1 and ELIP2 in *Arabidopsis* does not affect tolerance to photoinhibition and photooxidative stress. Plant Physiol. **141:** 1264-1273

Rubio V, Shen YP, Saijo Y, Liu YL, Gusmaroli G, Dinesh-Kumar SP, Deng XW (2005) An alternative tandem affinity purification strategy applied to Arabidopsis protein complex isolation. Plant J. **41:** 767-778

Rüdiger W (2002) Biosynthesis of chlorophyll *b* and the chlorophyll cycle. Photosynth. Res. **74:** 187-193

Sanchez-Fernandez R, Davies TGE, Coleman JOD, Rea PA (2001) The *Arabidopsis thaliana* ABC protein superfamily, a complete inventory. J. Biol. Chem. **276:** 30231-30244

Sato Y, Morita R, Nishimura M, Yamaguchi H, Kusaba M (2007) Mendel's green cotyledon gene encodes a positive regulator of the chlorophyll-degrading pathway. Proc. Natl. Acad. Sci. USA **104:** 14169-14174

Satoh H, Nakayama K, Okada M (1998) Molecular cloning and functional expression of a water-soluble chlorophyll protein, a putative carrier of chlorophyll molecules in cauliflower. J. Biol. Chem. **273:** 30568-30575

Schenk N, Schelbert S, Kanwischer M, Goldschmidt EE, Dormann P, Hortensteiner S (2007) The chlorophyllases AtCLH1 and AtCLH2 are not essential for senescence-related chlorophyll breakdown in *Arabidopsis thaliana*. FEBS Lett. **581:** 5517-5525

Schmitz G, Langmann T, Heimerl S (2001) Role of ABCG1 and other ABCG family members in lipid metabolism. J Lipid Res. **42:** 1513-1520

Shayeghi M, Latunde-Dada GO, Oakhill JS, Laftah AH, Takeuchi K, Halliday N, Khan Y, Warley A, McCann FE, Hider RC, Frazer DM, Anderson GJ, Vulpe CD, Simpson RJ, McKie AT (2005) Identification of an intestinal heme transporter. Cell **122:** 789-801

Sheptovitsky YG, Brudvig GW (1996) Isolation and characterization of spinach photosystem II membrane-associated catalase and polyphenol oxidase. Biochemistry **35:** 16255-16263

Shevchenko A, Wilm M, Vorm O, Mann M (1996) Mass Spectrometric Sequencing of Proteins from Silver-Stained Polyacrylamide Gels. Anal Chem. **68:** 850-858

Solomon EI, Brunold TC, Davis MI, Kemsley JN, Lee SK, Lehnert N, Neese F, Skulan AJ, Yang YS, Zhou J (2000) Geometric and electronic structure/function correlations in non-heme iron enzymes. Chem. Rev. **100:** 235-349

Stengel A, Benz P, Balsera M, Soll J, Bolter B (2008) TIC62 - Redox-regulated translocon composition and dynamics. J. Biol. Chem. **PMID: 18180301** M706719200

Stobart AK, Hendry GAF (1984) The turnover of chlorophyll in greening wheat leaves. Phytochemistry **23:** 27-30

Strain HH, Cope BT, Svec WA (1971) Analytical procedures for the isolation, identification, estimation and investigation of the chlorophylls. Methods Enzymol. **23:** 452-476

Suzuki T, Shioi Y (2002) Re-examination of Mg-dechelation reaction in the degradation of chlorophylls using chlorophyllin *a* as substrate. Photosynth. Res. **74:** 217-223

Suzuki Y, Shioi Y (1999) Detection of chlorophyll breakdown products in the senescent leaves of higher plants. Plant Cell Physiol. **40:** 909-915

Takamiya K, Tsuchiya T, Ohta H (2000) Degradation pathway(s) of chlorophyll: what has gene cloning revealed? Trends Plant Sci. **5:** 426-431

Tamura A, Wakabayashi K, Onishi Y, Takeda M, Ikegami Y, Sawada S, Tsuji M, Matsuda Y, Ishikawa T (2007) Re-evaluation and functional classification of non-synonymous single nucleotide polymorphisms of the human ATP-binding cassette transporter ABCG2. Cancer Sci. **98:** 231-239

Tanaka A, Tanaka R (2006) Chlorophyll metabolism. Curr. Opin. Plant Biol. **9:** 248-255

Tanaka R, Tanaka A (2005) Effects of chlorophyllide a oxygenase overexpression on light acclimation in *Arabidopsis thaliana*. Photosynth. Res. **85:** 327-340

Terpstra W (1981) Identification of chlorophyllase as a glycoprotein. FEBS Lett. **126:** 231-235

Terry MJ, Linley PJ, Kohchi T (2002) Making light of it: the role of plant haem oxygenases in phytochrome chromophore synthesis. Biochem. Soc. Trans. **30:** 604-609

Thomas H (1987) *Sid*: a Mendelian locus controlling thylakoid membrane disassembly in senescing leaves of *Festuca pratensis*. Theor. Appl. Genet. **73:** 551-555

Thomas H, Evans C, Thomas HM, Humphreys MW, Morgan G, Hauck B, Donnison I (1997) Introgression, tagging and expression of a leaf senescence gene in *Festulolium*. New Phytol. **137:** 29-34

Thomas H, Howarth CJ (2000) Five ways to stay green. J. Exp. Bot. **51:** 329-337

Thomas H, Ougham HJ, Davies TGE (1992) Leaf senescence in a non-yellowing mutant of *Festuca pratensis*. Transcripts and translation products. J. Plant Physiol. **139:** 403-412

Tommasini R, Vogt E, Fromenteau M, Hörtensteiner S, Matile P, Amrhein N, Martinoia E (1998) An ABC transporter of *Arabidopsis thaliana* has both glutathione-conjugate and chlorophyll catabolite transport activity. Plant J. **13:** 773-780

Tsuchiya T, Ohta H, Okawa K, Iwamatsu A, Shimada H, Masuda T, Takamiya K (1999) Cloning of chlorophyllase, the key enzyme in chlorophyll degradation: finding of a lipase motif and the induction by methyl jasmonate. Proc. Natl. Acad. Sci. USA **96:** 15362-15367

Tziveleka LA, Argyroudi-Akoyunoglou JH (1998) Implications of a developmental-stage-dependent thylakoid-bound protease in the stabilization of the light-harvesting pigment-protein complex serving photosystem II during thylakoid biogenesis in red kidney bean. Plant Physiol. **117:** 961-970

Tzvetkova-Chevolleau T, Franck F, Alawady AE, Dall'Osto L, Carriere F, Bassi R, Grimm B, Nussaume L, Havaux M (2007) The light stress-induced protein ELIP2 is a regulator of chlorophyll synthesis in *Arabidopsis thaliana*. Plant J. **50:** 795-809

Unno M, Matsui T, Ikeda-Saito M (2007) Structure and catalytic mechanism of heme oxygenase. Nat. Prod. Rep. **24:** 553-570

Valentin HE, Lincoln K, Moshiri F, Jensen PK, Qi Q, Venkatesh TV, Karunanandaa B, Baszis SR, Norris SR, Savidge B, Gruys KJ, Last RL (2006) The *Arabidopsis vitamin E pathway gene5-1* mutant reveals a critical role for phytol kinase in seed tocopherol biosynthesis. Plant Cell **18:** 212-224

Vavilin D, Brune DC, Vermaas W (2005) N-15-labeling to detennine chlorophyll synthesis and degradation in *Synechocystis* sp PCC 6803 strains lacking one or both photosystems. Biochem. Biophys. Acta **1708:** 91-101

Vavilin D, Vermaas W (2007) Continuous chlorophyll degradation accompanied by chlorophyllide and phytol reutilization for chlorophyll synthesis in Synechocystis sp PCC 6803. Biochem. Biophys. Acta **1767:** 920-929

Vavilin D, Yao D, Vermaas W (2007) Small cab-like proteins retard degradation of photosystem II-associated chlorophyll in *Synechocystis* sp PCC 6803 - Kinetic

analysis of pigment labeling with N-15 and C-13. J. Biol. Chem. **282:** 37660-37668

Vila-Carriles WH, Zhao GL, Bryan J (2007) Defining a binding pocket for sulfonylureas in ATP-sensitive potassium channels. FASEB J. **21:** 18-25

von Wettstein D, Gough S, Kannangara CG (1995) Chlorophyll biosynthesis. Plant Cell **7:** 1039-1057

Wagner D, Przybyla D, op den Camp R, Kim C, Landgraf F, Lee KP, Würsch M, Laloi C, Nater M, Hideg E, Apel K (2004) The genetic basis of singlet oxygen-induced stress responses of *Arabidopsis thaliana*. Science **306:** 1183-1185

Wakabayashi K, Nakagawa H, Tamura A, Koshiba S, Hoshijima K, Komada M, Ishikawa T (2007) Intramolecular disulfide bond is a critical check point determining degradative fates of ATP-binding Cassette (ABC) transporter ABCG2 protein. Drug Metab Pharmacokinet. **282:** 27841-27846

Wang N, Yvan-Charvet L, Lutjohann D, Mulder M, Vanmierlo T, Kim T-W, Tall AR (2007) ATP-binding cassette transporters G1 and G4 mediate cholesterol and desmosterol efflux to HDL and regulate sterol accumulation in the brain. FASEB J. **PMID: 18039927**

Willstätter R, Stoll A (1913) Die Wirkungen der Chlorophyllase. *In* R Willstätter, A Stoll, eds, Untersuchungen über Chlorophyll. Verlag Julius Springer, Berlin, pp 172-187

Woo HR, Kim JH, Nam HG, Lim PO (2004) The delayed leaf senescence mutants of Arabidopsis, ore1, ore3, and ore9 are tolerant to oxidative stress. Plant Cell Physiol. **45:** 923-932

Wood CS, Koepke JI, Teng H, Boucher KK, Katz S, Chang P, Terlecky LJ, Papanayotou I, Walton PA, Terlecky SR (2006) Hypocatalasemic fibroblasts accumulate hydrogen peroxide and display age-associated pathologies. Traffic **7:** 97-107

Wüthrich KL, Bovet L, Hunziker PE, Donnison IS, Hörtensteiner S (2000) Molecular cloning, functional expression and characterisation of RCC reductase involved in chlorophyll catabolism. Plant J. **21:** 189-198

Xu XM, Adams S, Chua NH, Moller SG (2005) AtNAP1 represents an atypical SufB protein in Arabidopsis plastids. J. Biol. Chem. **280:** 6648-6654

Yang M, Wardzala E, Johal GS, Gray J (2004) The wound-inducible *Lls1* gene from maize is an orthologue of the *Arabidopsis Acd1* gene, and the LLS1 protein is present in non-photosynthetic tissues. Plant Mol. Biol. **54:** 175-191

Yao N, Eisfelder BJ, Marvin J, Greenberg JT (2004) The mitochondrion - an organelle commonly involved in programmed cell death in *Arabidopsis thaliana*. Plant J. **40:** 596-610

Yao N, Greenberg JT (2006) *Arabidopsis* ACCELERATED CELL DEATH2 modulates programmed cell death. Plant Cell **18:** 397-411

Zelisko A, Garcia-Lorenzo M, Jackowski G, Jansson S, Funk C (2005) AtFtsH6 is involved in the degradation of the light-harvesting complex II during high-light acclimation and senescence. Proc. Natl. Acad. Sci. USA **102:** 13699-13704

Zhu YQ, Xu KX, Luo B, Wang JW, Chen XY (2003) An ATP-binding cassette transporter GhWBC1 from elongating cotton fibers. Plant Physiol. **133:** 580-588

Zimmermann P, Hirsch-Hoffmann M, Hennig L, Gruissem W (2004) GENEVESTIGATOR. Arabidopsis microarray database and analysis toolbox. Plant Physiol. **136:** 2621-2632

13. Acknowledgements

My first and main thanks go to Stefan who managed my PhD in a perfect way all along this very enjoyable period. I am extremely thankful for all those hours and days trying to dig into plants mysterious.

I would like to thanks Enrico who take us on the boat in the middle of my PhD and with his constantly coming tips and ideas. Thanks H. Thomas and B. Keller for having accepted correcting my work.

My “lab” thanks to Adriana and Silvia which were perfect lab mate. Thanks to Jan for his brilliant work on the SGR story. Thanks to Iwona and Kathrin for nice technical help.

All the thanks to previous lab members, as well as the french-connexion in Bern.

Thanks my far-away-but-not-so-far family and Evelyne for supporting me time after time and making all the life even more enjoyable.

This work was supported by the Swiss National Science Foundation (grants 3100A0-105389 and 3100A0-117940) and the National Center of Competence in Research Plant Survival, research program of the Swiss National Science Foundation.

14. Curriculum vitae

CURRICULUM VITAE

AUBRY Sylvain
PhD Plant Physiology
University of Zürich. Switzerland

AUBRY Sylvain
Date of Birth : 13/09/81
Place of Birth : Marseille. France

Education

2004-2008	**PhD Thesis.** 2 first years University of Bern. Institute of Plant Science Last year at University of Zürich. Institute of Plant Biology *Chlorophyll degradation in higher plants*
2003-2004.	**Master 2** in Science. Genetic, Adaptation and Crops Engineering. University of Rennes I and National Superior Agronomic School from Rennes (E.N.S.A.R.) **Placement: University of Bern.** *Role of ABC-type transporters in chlorophyll degradation*
2002-2003	**Master 1** in Cell Biology and Physiology. Option Plant Physiology. University of Rennes I
2001-2002.	**Bachelor** in Cell Biology and Physiology. University of Rennes I
1999	Baccalauréat scientifique. Lycée St Louis. Lorient. France

Research Experiences

2004. University of Bern. 7 months placement. Characterization of an ABC transporter involved in chlorophyll catabolism in *Arabidopsis thaliana*.

2003. Mediterranean and tropical symbiosis laboratory. Montpellier. France. 4 months placement. UMR ENSAM, CIRAD, IRD, INRA. Montpellier. Functional characterization of two transcription factor PpsR involved in photosynthetic regulation in *Rhodopseudomonas palustris.*

2002. University of Bern. 2 months placement. Biochemical characterization of the red chlorophyll catabolite reductase in *Arabidopsis thaliana* and tomato.

- **Aubry SJ**, Jonker JW, Kräutler B, Hörtensteiner S. Chlorophyll Degradation: Analysis of WBC23 involved in FCC export from the chloroplast. In preparation

- **Aubry SJ**, Mani J. and Hörtensteiner S. Stay-green protein, defective in Mendel's green cotyledon mutant, acts independent and upstream of PAO pathway in chlorophyll catabolic pathway. *Plant Mol Biol.* 2008. Published on-line.

- Pruzinska A, Anders I, **Aubry SJ**, Schenk N, Tapernoux-Luthi E, Muller T, Krautler B, Hortensteiner S. In vivo participation of red chlorophyll catabolite reductase in chlorophyll breakdown. *Plant Cell*. 2007;19(1):369-87

- Armstead I, Donnison I, **Aubry SJ**, Harper J, Hörtensteiner S, James C, Mani J, Moffet M, Ougham H, Roberts L, Thomas A, Weeden N, Thomas H, King I. Cross-species identification of Mendel's I locus. *Science*. 2007;315(5808):73.

- Armstead I, Donnison I, **Aubry SJ**, Harper J, Hörtensteiner S, James C, Mani J, Moffet M, Ougham H, Roberts L, Thomas A, Weeden N, Thomas H, King I.From crop to model to crop: identifying the genetic basis of the staygreen mutation in the Lolium/Festuca forage and amenity grasses. *New Phytol.* 2006;172(4):592-7.

- Pruzinská A, Tanner G, **Aubry SJ**, Anders I, Moser S, Müller T, Ongania KH, Kräutler B, Youn JY, Liljegren SJ, Hörtensteiner S. Chlorophyll breakdown in senescent *Arabidopsis* leaves. Characterization of chlorophyll catabolites and of chlorophyll catabolic enzymes involved in the degreening reaction. *Plant Physiol*. 2005;139(1):52-63